2014

LOBELANE ANALOGS WITH VARIOUS METHYLENE LINKER LENGTHS AND ACYCLIC LOBELANE ANALOGS AS POTENTIAL PHARMACOTHERAPIES TO TREAT METHAMPHETAMINE ABUSE

Zheng Cao
University of Kentucky, i_caozheng@hotmail.com

STUDENT AGREEMENT:

I represent that my thesis or dissertation and abstract are my original work. Proper attribution has been given to all outside sources. I understand that I am solely responsible for obtaining any needed copyright permissions. I have obtained needed written permission statement(s) from the owner(s) of each third-party copyrighted matter to be included in my work, allowing electronic distribution (if such use is not permitted by the fair use doctrine) which will be submitted to UKnowledge as Additional File.

I hereby grant to The University of Kentucky and its agents the irrevocable, non-exclusive, and royalty-free license to archive and make accessible my work in whole or in part in all forms of media, now or hereafter known. I agree that the document mentioned above may be made available immediately for worldwide access unless an embargo applies.

I retain all other ownership rights to the copyright of my work. I also retain the right to use in future works (such as articles or books) all or part of my work. I understand that I am free to register the copyright to my work.

REVIEW, APPROVAL AND ACCEPTANCE

The document mentioned above has been reviewed and accepted by the student's advisor, on behalf of the advisory committee, and by the Director of Graduate Studies (DGS), on behalf of the program; we verify that this is the final, approved version of the student's thesis including all changes required by the advisory committee. The undersigned agree to abide by the statements above.

Zheng Cao, Student

Dr. Linda P. Dwoskin, Major Professor

Dr. Jim R. Pauly, Director of Graduate Studies

LOBELANE ANALOGS WITH VARIOUS METHYLENE LINKER LENGTHS AND ACYCLIC LOBELANE ANALOGS AS POTENTIAL PHARMACOTHERAPIES TO TREAT METHAMPHETAMINE ABUSE

DISSERTATION

A dissertation submitted in partial fulfillment of the requirements for the degree of Doctor of Philosophy in the College of Pharmacy at the University of Kentucky

By

Zheng Cao

Lexington, Kentucky

Director: Dr. Linda Dwoskin, Professor of Pharmaceutical Sciences

Lexington, Kentucky

2014

ABSTRACT OF DISSERTATION

LOBELANE ANALOGS WITH VARIOUS METHYLENE LINKER LENGTHS AND ACYCLIC LOBELANE ANALOGS AS POTENTIAL PHARMACOTHERAPIES TO TREAT METHAMPHETAMINE ABUSE

Methamphetamine interacts with vesicular monoamine transporter-2 (VMAT2) to inhibit dopamine (DA) uptake and promotes DA release from presynaptic vesicles, increasing cytosolic DA available for methamphetamine-induced reverse transport by DA transporters. By inhibiting VMAT2, lobelane, a defunctionalized, saturated lobeline analog, decreases methamphetamine-evoked DA release and methamphetamine self-administration in rats. In this dissertation structure-activity relationships around the lobelane structure were investigated on racemic lobelane analogs with varying methylene linker lengths at central piperidine ring. Affinity for dihydrotetrabenazine (DTBZ) sites on VMAT2 and for inhibition of VMAT2 function was determined to be 0.88-63 and 0.024-4.6 µM, respectively, and positively correlated. The most potent and selective analog, (±)-cis-2-benzyl-6-(3-phenylpropyl)piperidine [(±)-GZ-730B], for VMAT2 uptake was identified as the lead. The ability of (±)-GZ-730B to inhibit methamphetamine-evoked [^{3}H]DA release from striatal synaptic vesicles and endogenous DA release from striatal slices was determined. The lead analog-induced inhibition of methamphetamine-evoked vesicular [^{3}H]DA release did not translate to inhibition of methamphetamine-evoked DA release in the more intact striatal slices. Moreover, poor water solubility of these lobelane analogs prohibited further *in vivo* work. Subsequent work focused on analogs with the C-3 and C-4 carbons in the piperidine ring eliminated to afford racemic acyclic lobelane analogs. Generally, acyclic analogs exhibited greater water solubility and less lipophilicity compared to lobelane. Acyclic analogs exhibited affinities (K_i = 0.096-17 µM) for [^{3}H]DTBZ sites that correlated positively with affinity (K_i = 3.3-300 nM) for inhibition of [^{3}H]DA uptake. Pure enantiomers of potent racemic analogs were synthesized, and found to potently, selectively, and competitively inhibit [^{3}H]DA uptake at VMAT2 and to release vesicular [^{3}H]DA in a biphasic

manner. Lead enantiomer (R)-N-(1-phenylpropan-2-yl)-3-phenylpropan-1-amine [(R)-GZ-924] inhibited methamphetamine-evoked [^{3}H]DA release from striatal synaptic vesicles, but not from the more intact striatal slices. Surprisingly, (R)-GZ-924 inhibited nicotine-evoked [^{3}H]DA overflow from striatal slices, revealing nonspecific effects. Importantly, (R)-GZ-924 inhibited methamphetamine self-administration in rats. However, the analog also inhibited food-maintained responding, revealing a lack of specificity. The lead analog will not be pursued further as a pharmacotherapy due to the lack of specificity. Further evaluation of the pharmacophore is needed to discover analogs which specifically inhibit the neurochemical and behavioral effect of methamphetamine.

KEYWORDS: Lobeline, Lobelane, Methamphetamine, Vesicular Monoamine Tranporter-2, (R)-GZ-924

Zheng Cao

Student's Signature

03/15/14

Date

LOBELANE ANALOGS WITH VARIOUS METHYLENE LINKER LENGTHS AND ACYCLIC LOBELANE ANALOGS AS POTENTIAL PHARMACOTHERAPIES TO TREAT METHAMPHETAMINE ABUSE

by

Zheng Cao

Dr. Linda P. Dwoskin
Director of Dissertation

Dr. Jim R. Pauly
Director of Graduate Studies

December 4, 2012

Acknowledgement

I would like to thank my advisor Dr. Linda Dwoskin for the support and guidance that help my scientific career. In addition, I would like to thank my committee members: Dr. Michael Bardo, Dr. Kimberly Nixon, and Dr. Kyung-Bo Kim for their time and advice. I would like to thank Dr. Lawrence Gottlob for agreeing to be my outside examiner. I would like to thank former and current members in Dr. Dwoskin's lab: Dr.Justin Nickell, Dr. Kiran Babu Siripurapu, Agripina Deaciuc, Dr. Andrew Smith, Dr. Mahesh Darna, Dr. David Horton, Dr. Vidya Narayanaswami, and Dr. Sucharita Sen Somkuwar. Their frequent discussion with me improved my English speaking and the understanding of their and my own project. I would like to thank Dr. Peter Crooks and Dr. Guangrong Zheng for synthesis of the compounds and their expertise on chemistry. I would like to thank members in Dr. Bardo's lab: Dr. Josh Beckmann, Dr. Carrie Wilmouth and Emily Denehy for performing the behavior study and their expertise. I would like to thank Catina Rossoll and Charolette Garland for their assistance and coordination. This research was supported by NIH DA13519 and UL1TR000117. The University of Kentucky holds patents on lobeline and the analogs described in the current work. A potential royalty stream to LPD, GZ and PAC may occur consistent with University of Kentucky policy.

I would like to thank my parents, Hongzhi Cao and Weimin Hu, for years of support and love. You are the best parents. I would like to thank my wife,

Xiaoyan Zhang, for your love and patience and I could never finish this dissertation without you.

Table of Contents

List of Tables

List of Figures

CHAPTER 1 Introduction

1.1 Methamphetamine

1.1.1 Physicochemical Characteristics

Methamphetamine (N-methyl-1-phenylpropan-2-amine; Figure 1.1) is a central nervous system stimulant and N-methyl derivative of amphetamine (Figure1.1). Methamphetamine is a white, odorless, bitter-tasting crystalline powder that easily dissolves in water or alcohol and can be taken orally, intranasally, by needle injection, or by smoking. The structure of methamphetamine constitutes a phenyl ring connected to a secondary amine by an ethyl side chain with a methyl group on the α-carbon. Methamphetamine is soluble in water (0.93 m/l; Log S value = -2.09) and is lipophilic (Log P value = 2.20) (Tetko et al., 2005). Methamphetamine exists in two stereoisomers with the d-isomer [also denoted as S (+)-methamphetamine, the S-enantiomer form of methamphetamine] and the l-isomer [also denoted as D (+)-methamphetamine, the R-enantiomer form of methamphetamine]. The d-methamphetamine is responsible for the psychostimulant effects of the drug and the l-isomer is inactive in the central nervous system (CNS) (Logan, 2002).

1.1.2 History and Background

Amphetamine was first synthesized by Lazar Edeleanu, a Romanian chemist, at the University of Berlin in 1887, and the clinical use of amphetamine was initiated in the 1930s (MacKenzie and Heischober, 1997). In 1932, an

amphetamine-based inhaler was marketed by Smith, Kline & French Laboratories as the first amphetamine product to treat nasal and bronchial congestion (Snyder, 1986). Amphetamines were prescribed to treat asthma and narcolepsy in 1930s (Prinzmetal, 1935).

Methamphetamine was synthesized from ephedrine in Japan in 1893 and was found to alleviate fatigue and produce feelings of alertness and well-being (Lineberry and Bostwick, 2006). Methamphetamine and amphetamine were given to German, English, American, and Japanese military personnel during World War II to promote energy and enhance performance (Logan, 2002). After World War II, Large amount of methamphetamine was dumped to civilian markets by the Japanese military (Matsumoto, 2002). In 1950s methamphetamine was prescribed to treat obesity (Anglin et al., 2000) and narcolepsy (Mitler et al., 1993). Truckers, homemakers, college students and athletes used methamphetamine for non-medical purposes to stay awake or keep active (Anglin et al., 2000; Logan, 2002).

In the 1970s, methamphetamine was regulated by the Controlled Substances Act, and the availability of illicit methamphetamine was restricted greatly (MacKenzie and Heischober, 1997). In the1980s, methamphetamine was produced mostly by neighborhood clandestine labs and was trafficked by motorcycle gangs in the United States (Brouwer et al., 2006). Methamphetamine abuse was reported to be increased among people exhibiting risky sexual behavior, as well as among homosexual men (Ruf et al., 2006; Stall et al., 2000).

In the 1990s, rural locations in the United States became ideal for methamphetamine manufacturing due to the geographic isolation, available supply of ephedrine, pseudoephedrine and anhydrous ammonia (Booth et al., 2006). Methamphetamine was also produced in Mexico and brought to the United States through the northern border of Mexico (Brouwer et al., 2006). In 1996, the Comprehensive Methamphetamine Control Act was passed by congress, which regulated transactions involving precursor chemicals such as pseudoephedrine, phenylpropanolamine, and combination ephedrine drug products (Drug Enforcement Administration, 2002). Despite substantial efforts to reduce the supply of precursor chemicals, increasing amount of clandestine methamphetamine labs was seized in the United States. In 2000, over 6,300 illegal clandestine methamphetamine labs were seized and the number increased by 25% from 2001 to 2005 (Crime, 2007; Sulzer et al., 2005).

Increasing abuse of methamphetamine emerged throughout the country. In 2004, methamphetamine became the number1 drug threat in the United States (NDTS, 2008). In 2005, national assessment of the economic burden of methamphetamine abuse was $23.4 billion, including cost attributed to health care, crime and reduced productivity (Justice, 2008; Statistics, 2009). Based on the 2006 National Association of Counties reports (NACO, 2006), there were more methamphetamine-related emergency room visits than for any other controlled prescription drug (NACO, 2006). Forty-seven percent of 200 responding hospitals reported that methamphetamine was the top illicit drug involved in emergency room presentations at their hospitals (NACO, 2006).

Seventy-three percent of hospital officials reported that emergency room presentations involving methamphetamine had increased over the last 5 years (NACO, 2006). Fifty-six percent of hospitals reported that costs had increased at their facilities because of the growing use of methamphetamine (NACO, 2006). Between 2008 and 2010, emergency room visits involving amphetamines/methamphetamine increased by 50 percent. In 2010 amphetamine and methamphetamine were the primary causes of over 137,000 emergency room admissions (Network, 2010). Thus, methamphetamine abuse is a great health concern in the United States.

Ten million people used methamphetamine at least once in the United States and the number of people who used methamphetamine continued to escalate each year with 133, 000 new methamphetamine users in 2011 (NSDUH, 2011). The average age of new methamphetamine users was decreasing from 22.2 to 17.8 years from 2006 to 2011 (NSDUH, 2011). The increase in methamphetamine use was primarily due to its stimulant properties and enhancement of sexual pleasure (Human, 2012). Methamphetamine use is associated with risky sexual behavior and is highly prevalent in people infected with human immunodeficiency virus (HIV; Yamamoto et al., 2010). Methamphetamine abuse is a great economic burden and health concern in the United States. Methamphetamine abuse was also reported in England, Australia, Sweden, South America, Asia, and Africa (MacKenzie and Heischober, 1997). Methamphetamine is used by 15-16 million people in a global estimation (Cruickshank and Dyer, 2009; Krasnova and Cadet, 2009). An estimated

production of more than 2.9 billion doses of methamphetamine (100 mg) was reported world-widely in 2005 (Crime, 2007). Thus, methamphetamine abuse is a world-wide health concern. Currently, no medical treatments are available for methamphetamine abuse.

1.1.3 Pharmacokinetics

Following oral intake, methamphetamine is absorbed into the bloodstream and the peak plasma concentration is reached in approximately 3 to 6 hours after administration. Peak plasma concentration of the major metabolite, amphetamine, is reached at 10 to 24 hours after oral administration (Schep et al., 2010). After intranasal administration of methamphetamine, the peak plasma concentration is achieved approximately 3 to 4 hours after administration (Harris et al., 2003). After inhalation of vapor methamphetamine, the peak concentration is reached at approximately 2.5 hours (Perez-Reyes et al., 1991b). After absorption, methamphetamine is widely distributed throughout the body. Methamphetamine crosses the blood brain barrier due to the high lipophilicity and has effects in the central nervous system (Schep et al., 2010). Methamphetamine is metabolized into amphetamine and 4-hydroxymethamphetamine by the cytochrome P450 isoenzyme, CYP2D6 (Lin et al., 1997). Methamphetamine is excreted via the kidneys, and the rate of excretion into the urine is dependent on urinary pH. In alkaline urine, methamphetamine is not charged due to its weak base property and a large amount of methamphetamine will be reabsorbed back into the blood by passive

diffusion across membranes due to its lipophilic property. In acidic urine, methamphetamine will be ionized and can not be reabsorbed. Subsequently, the ionized methamphetamine will be excreted in the urine (Beckett and Rowland, 1965). The average plasma half-life of methamphetamine is 9-12 hours in humans and 3 hours in rodents (Schep et al., 2010).

1.1.4 Clinical Pharmacology

The effect of methamphetamine is complex, and involves both peripheral and central actions (Logan, 2002). Peripheral effects of methamphetamine are caused mainly by release of norepinephrine (NE). Methamphetamine is capable of inducing mydriasis, bronchial muscle dilation, vasoconstriction, coronary dilatation, and bladder contraction through NE activation of adrenergic receptors (Perez-Reyes et al., 1991b). Methamphetamine can also produce arrhythmia, anorexia, flushed skin, excessive sweating, dry mouth, rapid breathing, high body temperature, diarrhea, constipation, insomnia, palpitations, tremors, increase of heart rate, blood pressure and glucose levels (Cruickshank and Dyer, 2009). In the male, increase in libido and intensity of orgasm associated with the use of this drug has been found, however, at higher doses the drug resulted in failure to achieve orgasm and loss of interest in sexual activity (Logan, 2002).

Psychological effects of methamphetamine are caused mainly by release of several neurotransmitters including NE, dopamine (DA), epinephrine, and serotonin (5-HT), and the subsequent activation of the receptors of the neurotransmitters. Psychological effects associated with methamphetamine use

include euphoria, alertness, anxiety, paranoia, agitation, and psychosis (Lineberry and Bostwick, 2006).

Chronic abuse of methamphetamine leads to withdrawal symptoms, including fatigue, depression, and decreased appetite, and may last for days, weeks or months (McGregor et al., 2005). Severity and length of withdrawal symptoms are dependent on the length of time and the amount of methamphetamine used (McGregor et al., 2005). Other withdrawal symptoms including anxiety, irritability, agitation, narcolepsy, and suicidal ideation may occur (McGregor et al., 2005).

Tolerance of both central and peripheral effects of methamphetamine has been reported (Gygi et al., 1996; Perez-Reyes et al., 1991a). Acute tolerance has been reported also in a smoking/intravenous study (Cook et al., 1992; Logan, 2002). The extent of tolerance and the rate at which it develops is highly dependent on methamphetamine dosage, duration of use, and frequency of administration (Graham et al., 2008; McFadden et al., 2012a; McFadden et al., 2012b). However, awakening effect of methamphetamine is not subject to tolerance development (Comer et al., 2001), making methamphetamine suitable for the treatment of narcolepsy (Logan, 2002; Mitler et al., 1993). Specifically, methamphetamine at a single morning dose of 40-60 mg for 28 days decreases sleep tendency during daytime and improves performance in narcoleptics comparable to those of unmedicated controls (Mitler et al., 1993). In addition, due to its ability to decrease impulsivity (Richards et al., 1999), methamphetamine

hydrochloride is prescribed as a pharmacotherapy for the treatment of attention deficit-hyperactivity disorder (ADHD) under the trade name Desoxyn (Akhondzadeh et al., 2003). Despite of use in clinical practice, methamphetamine has limited published studies on ADHD and most of the published studies on stimulants to treat ADHD focus on amphetamine and methylphenidate (Babcock et al., 2012; Elia et al., 1999). Generally, methylphenidate and d-amphetamine with daily dose of 60 and 40 mg, respectively, were able to reduce ADHD symptoms of 70-80% of patients (Elia et al., 1999). However, abuse potential has been found for the stimulants after repeated administration to children and adolescents (Manchikanti, 2007; Sweeney et al., 2013).

1.2 DA and Reward

1.2.1 DA Biosynthesis, Metabolism and Storage

DA belongs to the catecholamine family and is a monoamine neurotransmitter. DA is mainly synthesized within neural cells and the medulla of the adrenal glands (Von Bohlen und Halbach and Dermietzel, 2002). First , L-tyrosine is converted into L-3,4-dihydroxyphenylalanine (L-DOPA) by tyrosine hydroxylase (TH). Cofactors including $Fe^{2+,}$ O_2, and tetrahydropteridine are required by the enzyme to hydrolyze L-tyrosine to L-DOPA. Subsequently, L-DOPA is converted into DA by aromatic L-amino acid decarboxylase with pyridoxal phosphate (vitamin B6) as the cofactor and in the cytoplasm of the axon terminals.

Following biosynthesis, monoamines are stored in vesicles, and three pools of vesicles have been reported (Rizzoli and Betz, 2005). The readily releasable pool is defined as a pool of synaptic vesicles that are immediately available upon physiological stimulation and can be depleted within seconds. These vesicles are generally thought to be close to the presynaptic terminals and are readily releasable (Richards et al., 2003). The recycling pool is defined as the pool of vesicles that is responsible for release on moderate (physiological) stimulation and 5-20% of all vesicles are in this pool (Rizzoli and Betz, 2005). This pool of vesicles is released more slowly than the readily releasable pool (Richards et al., 2003). The reserve pool is defined as a depot of synaptic vesicles and release is only caused by intense stimulation and 80-90% of vesicles within presynaptic terminals are stored in this pool (Delgado et al., 2000). Vesicles in this pool are probably never recruited upon physiological stimulation (Richards et al., 2003). Depletion of vesicles in the recycling pool cause the recruiting and release of vesicles in the reserve pool; however, the underlying molecular mechanisms are not understood (Rizzoli and Betz, 2005).

DA is metabolized by two enzymes, monoamine oxidase (MAO) and catechol-O-methyltransferase (COMT) (Von Bohlen und Halbach and Dermietzel, 2002). Within presynaptic terminals, DA is mainly converted into 3,4-dihydroxyphenylacetaldehyde (DOPAL) by MAO. Subsequently, DOPAL is converted into 3,4-dihydroxyphenylacetic acid (DOPAC) by the aldehyde dehydrogenase (ALDH). Finally, DOPAC is converted into homovanillic acid (HVA) by COMT, and HVA is then excreted in urine. In the synaptic cleft, DA also

can be metabolized into 3-methoxytyramine (3-MT) by COMT. Subsequently, 3-MT is metabolized to HVA by MAO and is excreted in urine as well.

1.2.2 DA Receptors

DA receptors belong to G protein-coupled receptors (GPCRs) and contain five receptor subtypes, D1, D2, D3, D4, and D5 receptors (Sokoloff and Schwartz, 1995). D1 receptors are found to be located primarily in the striatum and cortex; D5 receptors are located primarily in the thalamus, hypothalamus and hippocampus; D2 receptors are located primarily in the striatum and cortex; D3 receptors are located primarily in the island of Calleja, nucleus accumbens (NAc), and olfactory tubercle; D4 receptors are located primarily in cortex (Hurley and Jenner, 2006; Sokoloff and Schwartz, 1995). The five receptor subtypes are categorized into D1-like and D2-like subfamilies based on the respective functions and properties. The D1-like subfamily includes D1 and D5 receptors and are coupled to stimulatory G protein (or Gs protein). Receptor activation elevates cyclic adenosine monophosphate (cAMP) concentrations by activating adenylate cyclase. The cAMP acts as secondary messenger that activates cAMP-dependent protein kinase (PKA) and initiates subsequent signal transduction (Chio et al., 1994a; Chio et al., 1994b; Sokoloff and Schwartz, 1995). The D2-like subfamily includes D2, D3, and D4 receptors and are coupled to inhibitory G protein (or Gi protein). Receptor activation decreases cAMP concentration by inhibiting adenylate cyclase. Decrease of cAMP results in lack of PKA activation and subsequent inhibition of signal transduction (Chio et al.,

1994a; Chio et al., 1994b; Sokoloff and Schwartz, 1995). D1 receptors are more widespread in the brain than the D3, D4, and D5 receptors. Expression of D2 receptors in brain is very similar to that of D1 receptors, except for the presynaptic D2 receptors on the terminals of dopaminergic neurons. The presynaptic D2 receptors are autoreceptors and activation of the receptor decreases DA synthesis, release and neurotransmission through a negative feedback mechanism (Fasano et al., 2008) .

1.2.3 Dopaminergic Pathways

Dopaminergic pathways are neural pathways in the brain through which DA is transmitted from one region of the brain to another. The mesolimbic pathway transmits DA from the VTA to NAc, ventral palladium and amygdala. The mesocortical pathway transmits DA from the VTA to the frontal cortex. Those two pathways together are involved in motivation, reward, emotion and cognition (Di Chiara and Imperato, 1988; Pierce and Kumaresan, 2006; Simon et al., 1980; Wise, 1978). The nigrostriatal pathway transmits DA from the substantia nigra (SN) to striatum and this pathway regulates motor function (Robertson and Robertson, 1989). Psychostimulants including methamphetamine, cocaine and nicotine activate the mesolimbic, mesocortical, and nigrostriatal pathway to elicit the reward and reinforcing effects (Everitt and Robbins, 2005; Wise, 2009).

1.2.4 DA Transporter (DAT)

DAT contains 12 putative transmembrane domains (TMD) spanning the plasma membrane (Torres et al., 2003b). DAT is mainly expressed in brain regions involved in the mesolimbic and mesocortical DA pathways, including striatum, NAc, olfactory tubercle, cingulated cortex, frontal cortex, lateral habenula, and on cell bodies in the VTA and SN (Ciliax et al., 1995). DAT is responsible for taking up DA back into presynaptic terminals from synaptic cleft. DA in the synaptic cleft is released through exocytosis via fusion of synaptic vesicles with presynaptic terminal membranes. The extracellular DA concentrations are the net result of release through exocytosis and uptake through DAT (Torres et al., 2003b).

DAT uptakes DA back into presynaptic terminals in a sodium-and chloride-dependent manner. One DA molecule is co-transported with one Cl^- and two Na^+, which follow the Na^+ gradient generated by Na^+/K^+ ATPase (Krueger, 1990). “Alternating access model” is applied to explain the process of DA transportation (Gnegy, 2003; Jardetzky, 1966). In such models, DAT faces outward towards the synaptic cleft, and initially the DA and co-substrates (ions) bind to the outward facing transporter. Subsequently, the conformation of the transporter changes and the transporter faces toward the cytosol with the bound DA and ions facing the cytosol accordingly. DA and ions are released into the cytosol and the transporter faces outward again and continues to transport DA.

In addition, electrophysiological investigations of DAT suggested that the transporter exhibits characteristics similar to that of ion channels. Similar to ion channels, current is generated and measured by patch clamp simultaneously with the transportation of DA and is inhibited by transporter inhibitors (Galli et al., 1996; Mager et al., 1994; Sonders et al., 1997). Considered as ion channels, DAT exists in two conformations including one similar to closed ion channels and the other similar to open ion channels. Open channels allow the passage of DA and ions through the membrane and the presence of DA and ions increases the probability of channel opening (Sonders and Amara, 1996).

DAT consists of 620 amino acid residues, with N and C termini both located on the interior side of the plasma membrane facing the cytoplasm (Torres et al., 2003b). The highest conserved regions of amino acid sequences are within the putative TMDs, while the least conserved regions are within the amino and carboxyl termini. The role of TMD3 in DA uptake has been reported (Lee et al., 1998) and mutation of a phenylalanine in TMD3 decreases transporter affinity for DA (Chen et al., 2001). In addition, mutation of an aspartic acid in TMD1 abolishes DA uptake activity, without alteration of the expression of the mutant protein on the cell surface (Kitayama et al., 1992). Potential N-glycosylation sites for post-translational modification are found in the large putative extracellular loop between TMD3 and TMD4. This loop in the DAT protein is involved in the conformational change of DAT during transportation of DA (Chen et al., 2000; Ferrer and Javitch, 1998) and tyrosine residue mutation in this loop diminishes uptake activity of the transporter (Loland et al., 2002). Based on the crystal

structure of *Aquifex aeolicus* leucine transporter (LeuTAa), a homologous protein to monoamine transporters, a 3-D model of DAT was constructed (Indarte et al., 2008; Yamashita et al., 2005). This novel structure contained a leucine binding pocket formed by TMD1, TMD3, TMD6 and TMD8 (Indarte et al., 2008; Yamashita et al., 2005). Models based on LeuTAa are a more rational approach to further determine the monoamine transporter-ligand complexes. Recently, two substrate binding sites have been found on DAT, S1, the site lodged in the interior of the transporter, and S2, the other site located in the "extracellular vestibule" (Manepalli et al., 2012). DAT substrates such as DA and amphetamine bind both sites and DAT inhibitors such as cocaine and methylphenidate bind the S2 site to block transport of substrates (Manepalli et al., 2012).

The role of phosphorylation in transporter function has been extensively studied due to the presence of sites for protein kinase phosphorylation by cAMP-dependent protein kinase, protein kinase C (PKC) and Ca^{2+}/calmodulin-dependent protein kinase (Torres et al., 2003b). For instance, PKC activation down-regulates transporter activity (Vaughan et al., 1997). Interestingly, down-regulation of transporter function is largely due to protein trafficking from the cell surface to the cytosol, without alternation of the transport activity (Torres et al., 2003b). Activation of PKC leads to internalization of DAT in a way that closely resembles the internalization of G protein-coupled receptors (Daniels and Amara, 1999). PKC-induced internalization of DAT is also mediated by ubiquitination of the amino terminus of DAT (Miranda et al., 2007). In addition, a very important role of protein-protein interactions has been found in the life cycle of monoamine

transporters (Sager and Torres, 2011). The role of N-linked glycosylation in the third loop between TMD3 and TMD4 has also been investigated using site-directed mutagenesis and N-linked glycosylation appears to be essential for the normal expression of DAT at the cell surface. However, such glycosylation does not alter ligand binding or translocation of DA (Nguyen and Amara, 1996; Tate and Blakely, 1994; Torres et al., 2003a). Interestingly, glycosylated DAT expression and function are significantly higher for nigrostriatal neurons compared to mesolimbic neurons, showing that the effect of glycosylation on the transporter is brain region dependent (Afonso-Oramas et al., 2009).

DAT knockout mice provide an opportunity to investigate the role of these proteins in vivo. DAT knockout in mice reduced striatal DA content by 95%, but increased the extracellular DA concentration (Giros et al., 1996). In DAT knock mice, the persistence of extracellular DA was 300-fold longer compared to wild type mice (Giros et al., 1996; Jones et al., 1998a). DAT knockout mice exhibited increased locomotor activity compared to wild type mice, associated with increased concentrations of extracellular DA (Giros et al., 1996). Interestingly, DAT knockout mice exhibited 90% lower TH levels, but increased TH activity, compared to wild type mice (Jones et al., 1998a). In addition, DAT knockout mice exhibited less D2 receptor expression compared to wild type mice, and the decrease in D2 autoreceptors might be responsible for the increase of TH activity (Giros et al., 1996; Jones et al., 1999). DAT knockout mice also exhibited an increase of COMT activity compared to wild type mice, indicating a compensation effect for the elevated concentration of extracellular DA (Jones et al., 1998a). In

addition, DAT knockout mice were used to study the mechanism of action of amphetamine and methamphetamine (Gainetdinov, 2008). Despite the absence of DAT, amphetamine increased the extracellular DA in the NAc and developed conditioned place preference (Budygin et al., 2004; Gainetdinov, 2008). Methamphetamine did not increase extracellular DA in striatum (Fumagalli et al., 1998) and methamphetamine-induced dopaminergic neurotoxicity was reduced in DAT knock mice (Fumagalli et al., 1998; Numachi et al., 2007).

Similar to the DAT, the 5-HT transporter (SERT) is a plasma membrane transporter, composed of 630 amino acid residues in 12 TMDs with both N and C termini located in the cytosol (Rothman and Baumann, 2003). SERT uptakes 5-HT into presynaptic terminals in a sodium- and chloride-dependent manner and one 5-HT molecule is co-transported with one sodium ion and one chloride ion (Gu et al., 1998). Among the 12 TMDs, TMD 1, 3, 6 and 8 are involved in substrate binding and translocation and interaction of inhibitors with the transporter (Rudnick, 2006). In the brain, SERT is expressed on 5-HT neurons in the dorsal and medial raphe nucleus, SN, VTA, hypothalamus, striatum, cortex and hippocampus (Hoffman et al., 1998). SERT is responsible for uptake of 5-HT from the synaptic cleft into the presynaptic terminals. In the cytosol, 5-HT is metabolized or transported into synaptic vesicles by VMAT2 for storage and subsequent release. In the brain, 5-HT is responsible for regulation of mood, appetite, memory, sleep, thyroid function, gastrointestinal function, and sexual drive (Jacobs and Azmitia, 1992). SERT inhibitors, such as fluoxetine,

paroxetine, and sertraline have been prescribed to treat depression (Rudnick, 2006).

Similar to the DAT and SERT, the NE transporter (NET) is a plasma membrane transporter, composed of 617 amino acid residues in 12 TMDs with both N and C termini located in the cytosol (Torres et al., 2003a). TMDs 1-5 and 9-12 are involved in substrate translocation, while TMDs 6-8 are responsible for interaction with inhibitors (Giros et al.,1994). In the brain, NET is expressed on the noradrenergic neurons in locus coeruleus, hippocampus, and cortex (Torres et al., 2003a). NET is responsible for uptake of NE from the extracellular space into presynaptic terminals. In the brain, NE regulates learning, attention, mood arousal, memory, and autonomic functioning (Zapata et al., 2007). NET inhibitors such as atomoxetine, reboxetine, desipramine, and mazindol have been prescribed to treat depression, ADHD, and drug abuse (Zhou, 2004).

1.2.5 Vesicular Monoamine Transporter (VMAT)

Similar to DAT, VMAT contains 12 putative TMDs and the apparent molecular weight is 70kDa. VMATs are responsible for uptake of cytosolic monoamines [DA, 5-HT, epinephrine and NE] into vesicles for storage and subsequent release. Two VMAT isoforms, VMAT1 and VMAT2, have been reported (Erickson and Eiden, 1993). In humans, VMAT2 is mainly expressed in monoaminergic neurons in the CNS and postganglionic neurons in sympathetic nervous system. VMAT1 is mainly expressed in neuroendocrine cells including chromaffin and enterochromaffin cells (Peter et al., 1995). VMAT1 and VMAT2

are coexpressed in chromaffin cells of the adrenal medulla. Interestingly, the distribution of VMAT1 and VMAT2 is dependent on species (Hansson et al., 1998). Exclusive expression of VMAT1 is observed in rat adrenal medulla, while VMAT2 is the major transporter in bovine chromaffin granules (Henry et al., 1998; Howell et al., 1994).

Bovine adrenal chromaffin granules have been used extensively to study the bioenergetics and the substrate selectivity of VMAT. Kinetics studies have been done and the uptake efficiencies were determined to be in the order of 5-HT>DA> epinephrine>NE (Wimalasena, 2011). Package of monoamines into vesicles was not favorable since transport was against the concentration gradient and a large amount of energy was required. For instance, Kirshner reported that catecholamine uptake into bovine chromaffin granules by VMAT was ATP-dependent and reserpine sensitive (Kirshner, 1962). The inside of vesicle was acidic and the monoamine transport was driven by a transmembrane proton gradient generated by the vesicular H^+-ATPase. One cytosolic amine inward transport was associated with two protons efflux (Knoth et al., 1981b; Parsons, 2000). The efflux of the first proton from the granules resulted in a conformational change in the transporter and a high-affinity amine-binding site on VMAT was generated with the concurrent binding of the amine to VMAT. The efflux of the second proton resulted in a second conformational change of VMAT, leading to transport of the amine molecule from the cytosol into granules and decrease of the amine-binding affinity with concurrent dissociation of the amine (Parsons, 2000).

Tetrabenazine (TBZ, Figure 1.1), a benzoquinoline compound, and reserpine (Figure 1.1), an indole alkaloid, interacted with chromaffin granule VMAT to inhibit uptake of the monoamines (Scherman and Henry, 1984). Specifically, binding of [^{3}H]reserpine to chromaffin granule VMAT was biphasic, and pH sensitive. Two classes of sites on VMAT were reported: a high affinity site (B_{max} = 7 pmole/mg of protein and K_D = 0.7 nM), and a low affinity site (B_{max} = 60 pmole/mg of protein and K_D = 25 nM). The High affinity site was TBZ-resistant, while the low affinity site was suggested to be equivalent to [^{3}H]dihydrotetrabenazine (DTBZ) binding site (Scherman and Henry, 1984). Reserpine binding kinetics was accelerated by addition of ATP, the energy source of the granule membrane proton pump. In the presence of ATP, the reserpine binding curve became monophasic and was comparable to that of [^{3}H]DTBZ (Scherman and Henry, 1984). Reserpine VMAT binding rate was accelerated also by the transmembrane pH gradient (Scherman and Henry, 1984). In addition, substrate NE at micromolar concentrations was capable of replacing reserpine binding to chromaffin granule VMAT. However, the pH gradient and NE had no effect on VMAT [^{3}H]DTBZ binding kinetics. Such differences suggested that VMAT might exist in two conformations: an active conformation with high- and low-affinity sites for reserpine and an inactive conformation with only the low-affinity site for TBZ. Substrates bound to the high affinity site of the active conformation VMAT in a pH gradient and ATP dependent manner (Scherman and Henry, 1984).

Heterologous expression systems have been used to study characteristic of substrate and inhibitor for the two transporters. VMAT1 and VMAT2 have been expressed using CV-1 cells derived from *Cercopithecus aethiops* monkey kidneys. 5-HT has a similar affinity for both transporters and DA, NE, and epinephrine have a 3-5 fold higher affinity for VMAT2 (Erickson et al., 1996; Yelin and Schuldiner, 2002). However, the two isoforms of VMAT exhibit completely different affinity for histamine. The affinity of histamine for VMAT2 is much higher than that for VMAT1 (Erickson et al., 1996). In addition, the ability of reserpine to inhibit VMAT2 function is equivalent to its ability to inhibit VMAT1 function, while affinity of TBZ for VMAT2 function is much greater than that for VMAT1 (Peter et al., 1994; Yelin and Schuldiner, 2002). Additionally, although heterologous VMAT expression systems are utilized extensively to obtain the K_i or K_m parameters to measure the affinity of various substrates and inhibitors for VMAT, such systems lack the complex interactions of VMAT with other synaptic vesicle proteins. Thus, the K_i or K_m parameters determined in such system may not reflect directly the affinities of the ligands for VMAT under physiological conditions.

Studies on DA uptake parameters using synaptic vesicles from rat brain have also been performed (Nickell et al., 2011b; Slotkin et al., 1978; Teng et al., 1998). The affinity of DA, NE and 5-HT for rat brain VMAT2 was 0.14 ± 0.014, 0.41 ± 0.07, and 0.12 ± 0.006 µM (Nickell et al., 2011b; Slotkin et al., 1978); The affinity of DA, NE and 5-HT for bovine adrenal chromaffin granules expressed VMAT2 was 25 ± 7, 92 ± 11, and 19 ± 4 µM (Knoth et al., 1981a; Wimalasena and Wimalasena, 2004; Wimalasena, 2011); The affinity of DA, NE and 5-HT for

CV-1 cells expressed human VMAT2 was 1.4 ± 0.2, 3.4 ± 0.5 and 0.9 ± 0.1 μM (Erickson et al., 1996; Wimalasena, 2011). Thus, rat brain VMAT2 exhibited higher affinity for monoamine, including DA, NE and 5-HT, compared to bovine adrenal chromaffin granules expressed VMAT2 and CV-1 cell expressed human VMAT2. The affinity of [^{3}H]DTBZ for rat brain VMAT2 was 1.67 nM (Teng et al., 1998), while the affinity of [^{3}H]DTBZ for bovine adrenal chromaffin granules expressed VMAT2 and CV-1 cells expressed human VMAT2 was 1.3 and 97 nM, respectively (Scherman and Henry, 1984; Teng et al., 1998). Thus, the affinity of [^{3}H]DTBZ for rat brain VMAT2 was approximately the same as bovine adrenal chromaffin granules expressed VMAT2, but higher compared to the CV-1 cell expressed human VMAT2.

In addition, heterologous expression systems have been used extensively to study the structure-function relationships of VMAT. VMAT1 and VMAT2, although expressed from two different genes, exhibit overall sequence homology of 60% (Erickson et al., 1996). Although the crystallographic structures of VMAT have not been resolved, the sequence of each protein has been reported and suggested to be transmembrane proteins with 12 TMDs (Wimalasena, 2011). Rat VMAT2 isolated by expression cloning in CV-1 cell lines indicates that both C- and N-terminals of the transporter face the cytosol (Erickson et al., 1992). Studies using photoaffinity-labeling techniques to characterize VMAT2-specific ligands suggest that the C-terminal half of the VMAT2 molecule interacts with the substrate (DA, NE and 5-HT), whereas the N-terminal half of the protein interacts with reserpine and TBZ (Sievert and Ruoho, 1997). Reserpine is hypothesized to

bind to the high affinity site on VMAT2 as a substrate; however, the compound can neither be transported nor released due to the relative bulkiness compared to the monoamines. The high affinity of reserpine for VMAT2 and the bulkiness of the analog lead to the irreversible binding of this inhibitor at VMAT2 (Rudnick et al., 1990).

Mutagenesis studies have been performed and His419 is involved in coupling ATPase generated energy to transport monoamines by facilitating the first proton-dependent conformational change of the transporter, generating the high-affinity amine-binding site on VMAT1 (Shirvan et al., 1994). The Asp431 residue is responsible for substrate transport and the proposed second conformational change in the protein, leading to transport of the amine molecule from the cytosol into the vesicles (Steiner-Mordoch et al., 1996). In addition, four aspartic acid residues and one Lys residue in the VMAT2 sequence are highly conserved and may be responsible for recognition of the substrate (Wimalasena, 2011).

Post-translational modifications of VMAT2 including glycosylation and phosphorylation have been reported. However, mutant VMAT transporters devoid of all three glycosylation sites are still capable of taking up 5-HT and of binding reserpine. Thus, glycosylation is not essential for regulation of transporter function (Yelin et al., 1998). Phosphorylation is ubiquitous in regulating protein activity and also is involved in regulating VMAT function. A protein kinase inhibitor, K252a, increases VMAT function, while a protein phosphatase inhibitor,

okadaic acid, has the opposite effect (Nakanishi et al., 1995). Rat VMAT2, but not VMAT1, is constitutively phosphorylated by the acidotropic kinases casein kinase I and casein kinase II, and serine 512 and 514 at the carboxyl terminus of VMAT2 are the phosphorylation sites (Krantz et al., 1997). However, simultaneous replacement of Ser-512 and Ser-514 with Ala did not change transporter function (Krantz et al., 1997). Thus, phosphorylation may not regulate VMAT function directly.

VMAT2 knockout mice models have been generated to study the physiological effects of VMAT2. Homozygous (VMAT2-/-) mice are smaller, hypoactive, feed poorly, and die a few days after birth. Significantly reduced monoamine content is observed in brains from VMAT2-/- animals (Fon et al., 1997; Wang et al., 1997). However, monoamine metabolites of VMAT2-/- mice are not different compared to wild type. Results indicate that monoamines in VMAT2 -/- mice brain are not stored in synaptic vesicles and are metabolized rapidly. Thus, vesicular transport of monoamine into vesicles protects newly synthesized neurotransmitter from metabolism.

Recent studies classified VMAT2-containing vesicles into two groups: vesicles that co-fractionate with synaptosomal membranes after osmotic lysis, and vesicles that do not. VMAT2 localized on vesicles that co-fractionate with synaptosomal membranes are defined as VMAT2M, while the VMAT2 on the vesicles that do not co-fractionate with synaptosomal membranes are defined as VMAT2C (Fleckenstein et al., 2008). No evidence indicates that the VMAT2M

and VMAT2C are different or interconvertible proteins. Interestingly, different kinetics of these two transporters have been reported using the respective transporter-associated vesicles (Volz et al., 2007).

DA uptake into the VMAT2C containing vesicles is ATP- and temperature-dependent and obeys Michaelis-Menten kinetics (Volz et al., 2006). In contrast, DA uptake into the VMAT2M containing vesicles does not display Michaelis-Menten kinetics. DA uptake by VMAT2M fits a sigmoidal curve, in which uptake rate is dramatic affected over the concentration range spanning the “steepest” portion of the curve (Volz et al., 2007). The different kinetic profiles of VMAT2M and VMAT2C might result in different physiological roles and distinct therapeutic opportunities. However, in a subsequent study from Dr. Fleckenstein’s lab (Chu et al., 2010), the sigmoidal curve was not replicated. Different methods used in the studies might be responsible for the contradictory results. Rotating disk voltammetry was employed in the studies in 2007 (Volz et al., 2007), while [^{3}H]DA uptake kinetic study optimized from our lab (Hong et al, 1998) was used in the later study (Chu et al., 2010).

1.3 Methamphetamine Mechanism of Action

Methamphetamine and amphetamine exhibit no differences to induce DA release in striatum, no difference in elimination rates, or other pharmacokinetic properties (Sulzer and Pothos, 2000), and equal doses of the two drugs are not

differentiated in human studies (Lamb and Henningfield, 1994). However, the effect of the two drugs on memory and behavioral tolerance are different probably due to a subtly greater DA release evoked by amphetamine in the prefrontal cortex (Shoblock et al., 2003a; Shoblock et al., 2003b). In addition, the synthesis process of methamphetamine is easier compared to amphetamine, which contributes to more methamphetamine available on the illicit market (Cho, 1990).

1.3.1 Methamphetamine on DA biosynthesis

Amphetamine, in a concentration-dependent manner, enhanced the rate of DA synthesis in a study using striatal synaptosome preparations from adult rats (Costa et al.,1972). The rate of DA synthesis was dependent on the rate of tyrosine hydroxylation. The increase of synthesis rate reached a peak (70% increase) at 0.015 mM amphetamine, while increasing the concentration of amphetamine decreased the synthesis rate and 0.5 mM amphetamine abolished the increase of synthesis completely (Fung and Uretsky, 1982). Free calcium ions in striatum was suggested to be responsible for the enhancement of DA synthesis by amphetamine (Fung and Uretsky, 1982). The following study determining TH activity supported the critical role of calcium in the process of tyrosine hydroxylation by facilitating phosphorylation of serine residues on TH (Griffiths and Marley, 2001). The mechanism underlying the effect of a high concentration amphetamine to inhibit TH has been suggested to be due to the feedback inhibition caused by an increase in cytosolic DA (Harris and

Baldessarini, 1975). Similarly, methamphetamine at 0.01 mM enhanced DA synthesis by up-regulating activity of TH activity, increasing DA in the cytosol in mouse midbrain neuronal cultures (Larsen et al., 2002). However, a toxic regimen of methamphetamine pretreatment (4 injections; 10 mg/kg/injection; 2 h intervals) decreased TH activity in studies using male rats. In such case, TH was readily nitrated by both nitric oxide and peroxynitrite produced by high doses of methamphetamine (Kuhn et al., 1999). Additionally, decreased DA content in rat brain was due to the toxic effects of methamphetamine. In such a case, methamphetamine-induced elevation of cytosolic DA was readily oxidized to form reactive oxygen species and quinones, leading to increases in oxidative stress (Yamamoto et al., 2010).

1.3.2 Methamphetamine on DA metabolism

Under physiological conditions, DA in the cytosol is metabolized by MAO located on the outer mitochondrial membrane. Amphetamine inhibits the activity of the enzyme by blocking the consumption of oxygen otherwise used to oxidize substrates (Sulzer and Pothos, 2000). However, MAO inhibitors alone do not increase DA release, while a VMAT2 inhibitor reserpine and MAO inhibitor pargyline together induce a profound increase in DA release similar to amphetamine (Mosharov et al., 2003). Interestingly, the relatively low affinity of amphetamine (K_i = 0.01 mM) and methamphetamine (K_i = 0.1 mM) for MAO have been reported (Mantle et al., 1976; Robinson, 1985). Since amphetamine can enter the presynaptic terminal via transport or lipophilic diffusion, it may

accumulate in the presynaptic terminals to a concentration that inhibits MAO function (Sulzer and Pothos, 2000). However, MAO was collected from rat liver in the above studies and MAO in the brain could exhibit different affinity for amphetamine and methamphetamine.

1.3.3 Methamphetamine on Plasma Membrane Transporters

Amphetamine induces the release of monoamines including NE, 5-HT, and DA among which DA is primarily responsible for amphetamine-induced reinforcing and rewarding effects (Sulzer et al., 2005). Mechanisms of amphetamine-mediated DA release have been studied. DAT uptake inhibitors, nomifensine and cocaine, inhibit amphetamine-induced DA release, indicating that DA release is DAT mediated (Fleckenstein et al., 2007; Raiteri et al., 1979). In addition, other monoamine transporters such as SERT and NET are also regulated by amphetamine and methamphetamine, and are involved in the action of these two stimulants (Budygin et al., 2004; Gainetdinov, 2008).

Amphetamine inhibits [^{3}H]monoamine uptake into rat synaptosomes via an action at plasma membrane transporters including SERT, NET and DAT (Coyle and Snyder, 1969; Ross and Renyi, 1964; Ross and Renyi, 1966). Amphetamine acts as a substrate for monoamine transporters and is co-transported with Na^+/Cl^- similar to monoamines (Bonisch, 1984). Facilitated exchange diffusion model was suggested in which extracellular amphetamine was transported into cells by DAT and displaced DA on the inner binding site on DAT, and the DA was transported reversely into extracellular space (Fischer and Cho, 1979).

A further study demonstrated that amphetamine accumulated in a saturable, temperature-dependent, and ouabain (an inhibitor of sodium-potassium ATPase)-sensitive manner in striatal synaptosomes, indicating that amphetamine was a substrate for DAT (Zaczek et al., 1991). An electrophysiology study demonstrated that both amphetamine and methamphetamine elicited DA-like transporter-associated currents (Sonders et al., 1997), indicating that amphetamine and methamphetamine act as substrate at DAT and are transported by DAT into the cytosol, and that cytosolic DA is transported to extracellular space. Subsequently, a concentration-dependent dual mechanism of amphetamine-induced DA release was proposed. Specifically, extracellular amphetamine at a low concentration substituted for cytosolic DA via an interaction with DAT, while amphetamine at higher concentrations diffused into presynaptic terminals and displaced DA from intraneuronal binding sites (Liang and Rutledge, 1982). In addition to the amphetamine-induced transporter-like DA release, an amphetamine-induced faster channel-like DA release via DAT was reported (Kahlig et al., 2005). In such channel-like DA release, DAT acts like a channel instead of a transporter and can not transport DA against the concentration gradient. Amphetamine was responsible for the activation of this channel-like state of DAT, while DA inhibited this state of the transporter (Kahlig et al., 2005). The study demonstrated that 10% of amphetamine-induced DA release was via the channel-like state of DAT (Kahlig et al., 2005).

Amphetamine and methamphetamine pretreatment decreased DAT function. The extension and duration of transporter function loss depended on the regimen of administration of the drug. A single injection of methamphetamine (15 mg/kg, s.c.) down-regulated DAT function by around 50%, while function loss was capable of recovering within 24 hours (Fleckenstein et al., 1997). Whereas multiple injections (4 injections; 10 mg/kg/injection; 2 h intervals) resulted in DAT function down-regulation by around 50% for up to 9 days after cessation (Eisch et al., 1996; Fleckenstein et al., 1997). Studies indicated that the down-regulation of DAT function was not associated with loss of the transporter protein, but due to a modification of the protein including phosphorylation and internalization, or dysregulation of DAT function by reactive species formation (Fleckenstein et al., 2007).

1.3.4 Effect of Methamphetamine on VMAT2

In addition to plasma membrane uptake transporters like DAT, monoamine secretory/synaptic vesicles play an important role in the action of amphetamine. Burn and Rand showed that effects of amphetamine were abolished by a VMAT2 inhibitor, reserpine, indicating the involvement of vesicular DA on amphetamine action (Burn and Rand, 1958). Consistent with Burn and Rand's study, amphetamine-induced NE release was inhibited by reserpine in most studies (Fitzgerald and Reid, 1993; Florin et al., 1995; Kalisker et al., 1975). Little or no effect of reserpine on amphetamine-induced DA release has been demonstrated *in vivo* experiments measuring effects of reserpine and

amphetamine on DA release (Arbuthnott et al., 1990; Callaway et al., 1989; Niddam et al., 1985). However, the inhibitory effect of reserpine has been reported in *in vitro* studies using neuronal cultures (Parker and Cubeddu, 1986; Parker and Cubeddu, 1988). Contradictory results of the effect of reserpine on amphetamine-induced DA release have been found in studies using synaptosomes as well (Bagchi et al., 1980; Masuoka et al., 1982). The explanation for the different findings between NE and DA was that NE was mainly synthesized from DA within synaptic vesicles, and the concentration of NE in vesicles would be expected to be higher than that in the cytosol. Thus, the effect of VMAT2 inhibition by reserpine on amphetamine-induced release was expected to be greater for NE than DA. The explanation for the conflicting findings measuring DA release was that TH activity could be upregulated by reserpine, producing an increase of cytosolic DA (Pasinetti et al., 1990). However, in the studies measuring DA in ventral midbrain neuronal cultures, shorter-term exposure of reserpine (90 min) did not upregulate TH activity (Sulzer et al., 1996). Such short-term exposure of reserpine depleted vesicular DA and inhibited amphetamine-induced DA release by around 75% (Larsen et al., 2002; Sulzer et al., 1996).

Genetic manipulations have been used to study the role of synaptic vesicles in amphetamine action. DAT and VMAT2 were expressed using COS cells respectively or together (Pifl et al., 1995). Despite lacking synaptic vesicles, the cells contained other acidic organelles, possibly including endosomes and lysosomes which expressed VMAT2, providing a means to accumulate DA.

Amphetamine-evoked DA release occurred in cells that expressed DAT alone, while greater release was observed for cells that coexpressed VMAT2 and DAT. Amphetamine-induced DA release from cells that expressed DAT alone reached a peak and quickly dropped back to baseline release (Pifl et al., 1995). However, amphetamine-induced DA release was sustained in COS cells that coexpressed DAT and VMAT2 (Pifl et al., 1995). The above evidence indicates that cytosol DA and vesicular DA were two components in amphetamine-induced DA release and both were essential for the action of the drug.

In addition to COS cells that expressed VMAT2 and DAT, VMAT2 and DAT knockout mice have been used to study the role of VMAT2 in amphetamine-induced DA release. DAT knockout mice did not exhibit amphetamine-induced DA release (Giros et al., 1996; Jones et al., 1998b). VMAT2 knockout mice died soon after birth, while neuronal cultures collected from VMAT2 knockout mice survived (Fon et al., 1997; Takahashi et al., 1997). Interestingly, amphetamine-induced DA release from ventral midbrain neurons collected from VMAT2 knockout mice was decreased by 65% (Fon et al., 1997), indicating the important role of vesicular component of DA in amphetamine-induced DA release.

Except for knockout mouse mutants, it is impossible to distinguish DA in cytosol versus vesicles until a means to measure cytosolic catecholamines has been introduced (Sulzer et al., 1995). An intracellular carbon fiber electrode was used to determine free cytosolic DA in a giant DA neuron in the pond snail *Planorbis corneus*. An increase of cytosolic DA in the presence of amphetamine

was found using the above method, supporting the hypothesis that amphetamine redistributed DA from the vesicles to the cytosol. In a following study to determine the cytosolic catecholamine concentrations, intracellular patch electrochemistry was developed (Mosharov et al., 2003), in which a carbon fiber electrode was placed inside a patch electrode inserted into the whole chromaffin cells. Amphetamine at 0.01 mM increased cytosolic DA by 15-fold within 10-15 min. Using carbon fiber electrodes, the amount of DA that was released per secretory vesicle fusion, i.e., the ‘‘quantal size’’, was determined in the presence of amphetamine. Amphetamine at 10 μM decreased quantal size by 50% in 10 min periods in PC12 cells (Sulzer et al., 1995). Thus, all of the above evidence indicates that amphetamine redistributed DA from synaptic vesicles to the cytosol.

In conclusion, amphetamine redistributes vesicular DA to the cytosol in mutated COS cell lines and mice, and neuronal cultures determined by electrochemical detection techniques. Later, in a study using fast scan cyclic voltammetry (Jones et al., 1998b), the real time changes of DA in the extracellular fluid of striatal slices was determined. In brain slices from wild-type mice, amphetamine increased extracellular DA gradually over a 30 min period with a simultaneous disappearance of DA available for depolarization-evoked release. In contrast, in slices from DAT mutant mice, amphetamine did not increase extracellular DA, but the similar disappearance of DA for depolarization-evoked release occurred. The above evidence suggested that most amphetamine-induced DA release from the presynaptic terminals was originally

redistributed from vesicles into the cytosol (Jones et al., 1998b). In addition, a concentration-dependent response of amphetamine action has been found, in which low concentrations of amphetamine preferentially released cytosolic DA, while higher concentrations of the drug redistributed vesicular DA to the cytosol (Seiden et al., 1993).

Further studies suggested that amphetamine and amphetamine derivatives act as VMAT2 substrates (Partilla et al., 2006). Such substrate-type ligands once bound to VMAT2 were transported subsequently into synaptic vesicles and promoted monoamine release. In contrast, VMAT2 uptake inhibitors, including reserpine and TBZ (Scherman and Henry, 1984), once bound to VMAT2, were not transported. These inhibitors elevated transmitter concentrations in the cytosol by blocking VMAT2 uptake of transmitter from the cytosol. Two assays, inhibition of [^{3}H]DHTBZ binding and inhibition of [^{3}H]DA uptake, have been developed to differentiate VMAT2 substrates from VMAT2 inhibitors. Binding assays measure the affinity of analogs for the DTBZ binding site on VMAT2, and uptake assays measure the ability of analogs to inhibit [^{3}H]DA transport across the vesicular membranes. Previous studies demonstrated that VMAT2 inhibitors had similar potencies in both types of assays, while VMAT2 substrates had much greater potency in the functional assay than the binding assay (Partilla et al., 2006). For instance, VMAT2 uptake inhibitors (TBZ and reserpine) had similar potencies in both assays (Partilla et al., 2006), while methamphetamine inhibited [^{3}H]DHTBZ binding with a 80 µM K_i value and inhibited [^{3}H]DA uptake with a 0.1 µM K_i value (Nickell et al., 2010).

Similar results have been demonstrated in the studies using substrates, including DA and NE, in which the substrates inhibited VMAT2 function at the micromolar range, but had much lower affinity for the DTBZ binding site on VMAT2 (Partilla et al., 2006). In our previous study, vesicles preloaded with [^{3}H]DA spontaneously released transmitter and this release was prevented by reserpine (Horton et al., 2013; Teng et al., 1998), further indicating reserpine is an inhibitor of VMAT2. In contrast, vesicles preloaded with [^{3}H]DA were depleted in the presence of methamphetamine (Nickell et al., 2011b), confirming that the action of methamphetamine on vesicular DA was different from reserpine. Thus, similar to the action of amphetamine on DAT, the facilitated exchange diffusion model could be used to explain the action of amphetamine on VMAT2, however, the mechanism underlying the reverse transport was not clear (Sulzer et al., 2005). No direct evidence was provided to show that amphetamine competed with catecholamines as an actual substrate for VMAT2, and the role of amphetamine competition with catecholamines was not clearly differentiated from the drug's week base effect on the proton gradient associated transport (Sulzer et al., 2005). Later studies indicated that methamphetamine elicited DA release by two proposed mechanisms: 1) inhibition of VMAT2 function (Gonzalez et al., 1994), and 2) depletion of vesicular DA by degrading the pH gradient that generated energy for the transporter (Sulzer and Rayport, 1990).

Although it is difficult to test whether amphetamine and derivatives are actually substrates for VMAT2, it is reasonable that transmitters and amphetamine compete for a common site on VMAT2. Binding studies using

amphetamine and its derivatives have measured the affinity of the drugs for VMAT. Affinity of amphetamine for VMAT2 is around 10-fold higher than that for VMAT1 in the studies using transfected fibroblasts that express either VMAT1 or VMAT2 (Erickson et al., 1996). Affinity of S-(+)-amphetamine for both VMAT isoforms is around 5-fold more potent than that of the R-(-)-isomer, as has also been demonstrated with DAT. Consistently, affinity of methamphetamine for VMAT2 is 10-fold higher than that of VMAT1, when transfected CHO cells expressing either VMAT1 or VMAT2 were employed; and the S-(+)-isomer of methamphetamine is 3-fold more potent at VMAT2 (Peter et al., 1994). Competition at the VMAT2 binding site between methamphetamine and reserpine has been demonstrated, and the results suggest that these two drugs bind to the same site on VMAT2 (Peter et al., 1994). Since reserpine is suggested to bind to the same site that the monoamines and methamphetamine bind, methamphetamine might bind the same site that the monoamines bind. Amphetamine and methamphetamine both displace [^{3}H]DTBZ binding at VMAT2 (Gonzalez et al., 1994; Nickell et al., 2010). Since TBZ and reserpine are suggested to bind to different sites on VMAT, the underlying mechanism of amphetamine to displace DTBZ and reserpine is still not fully understood.

Methamphetamine is a weak base with a pKa value of 9.9 and is capable of decreasing the proton gradient provided by secretory vesicles. Using acridine orange, a weak base vital dye, real time vesicular pH gradients were determined in chromaffin vesicles and secretory organelles of midbrain DA neuronal culture (Sulzer and Rayport, 1990). Amphetamine at 50 μM decreased 50% of the

chromaffin vesicle proton gradient. Interestingly, amphetamine-induced collapse of chromaffin vesicle pH gradients was not stereo-specific, indicating that amphetamine molecule entered the vesicles via lipophilic diffusion. Meanwhile, the effect of amphetamine was not blocked by reserpine, further suggesting that the entry of the molecule into the isolated vesicle preparation was due to lipophilic diffusion instead of VMAT transport. Also, if the effect of amphetamine was due to its weak base property, any weak base compounds would be expected to abolish the vesicular acidic pH gradient. A further study demonstrated that ammonium chloride and chloroquine, agents which have been long used to disrupt pH gradients, released DA from DA neuronal culture (Sulzer et al., 1993). Thus, weak base compounds were capable of decreasing vesicular pH gradients and the subsequent lack of energy decreased vesicular DA transport (Mundorf et al., 1999; Pothos et al., 2002). However, a straightforward relationship between change of pH gradients and accumulation of monoamine has not been established (Reith and Coffey, 1994). The ability of amphetamine to abolish pH gradient was less efficient than that to release monoamine. That is, amphetamine at 3 μM was capable of depleting 70% of vesicular DA, but only decreasing 12% of proton gradient using isolated synaptic vesicles from rat whole brain. In contrast, at 100 μM, amphetamine was capable of inducing correlated level of vesicular alkalinization with DA release (Reith and Coffey, 1994). Bafilomycin, not a VMAT substrate, was demonstrated to induce proton pump inhibition and reduce the pH gradient 2 times more than amphetamine, but

release DA at only half of the rate (Floor and Meng, 1996). These results suggest that alkalization is not sufficient to explain vesicular DA release.

Finally, the most convincing evidence of the incompleteness of the weak base theory for explaining effects of amphetamine on vesicular DA release was that the S-(+)- amphetamine was more effective than the R-(-)-isomer in depleting vesicular DA content. The two isomers exhibited the same ability to abolish the proton gradient and the S-(+)-isomer preferentially bound to the transporter (Peter et al., 1994). Such results suggested a role of amphetamine-induced inhibition of VMAT function in regulating vesicular DA content (Erickson et al., 1996; Peter et al., 1994).

In addition, effects of methamphetamine injection on VAMT2 have been studied (Brown et al., 2000; Hogan et al., 2000). Multiple injections of methamphetamine (four injections, 10 mg/kg per injection, s.c., 2-h intervals) decrease striatal VMAT2 uptake and DTBZ binding, and the drug-induced inhibition persists at least 24 hours in mice and rats. Consistent with the binding study, multiple injections of methamphetamine decreased VMAT2 immunoreactivity 24 hours after treatment (Eyerman and Yamamoto, 2005; Riddle et al., 2002). All of the above studies on VMAT2 function and expression were performed using VMAT2C containing vesicles. For VMAT2M containing vesicles, multiple injections of methamphetamine (four injections, 10 mg/kg per injection, s.c., 2-h intervals) decreased VMAT2M immunoreactivity 24 hours after the last treatment (Eyerman and Yamamoto, 2005), but did not alter VMAT2M

expression 1 hour after the treatment in rats (Riddle et al., 2002). The effect of the same dosing regimen of methamphetamine on DA uptake by VMAT2M and on VMAT2M immunoreactivity persisted up to seven days after treatment (Eyerman and Yamamoto, 2005; Eyerman and Yamamoto, 2007). A similar inhibitory effect of the same dosing regimen of methamphetamine on DA uptake and transporter immunoreactivity was also found using VMAT2C containing vesicles from rat striatum (Brown et al., 2000; Chu et al., 2008; Eyerman and Yamamoto, 2005; Eyerman and Yamamoto, 2007). In addition, a single methamphetamine administration (15 mg/kg s.c.) decreased DA uptake at VMAT2M 1 hour after treatment, and transporter function recovered 24 hours after the treatment (Chu et al., 2010). The effect of single methamphetamine injection on VMAT2 function and immunoreactivity was proposed to be due to drug-induced trafficking of the transporter (Chu et al., 2010). However, methamphetamine-induced decreases in VMAT2C expression was not accompanied by an increase of VMAT2M expression (Chu et al., 2010). Thus, mechanisms beyond redistribution of vesicles underly the acute effects of methamphetamine challenge (Chu et al., 2010).

1.4 Methamphetamine Neurotoxicity

Damage to dopaminergic and serotonergic nerve terminals in rat brain has been reported after methamphetamine and amphetamine administration (Fleckenstein et al., 2009; Yamamoto et al., 2010). Specifically, methamphetamine administration resulted in a long-term decrease of TH activity,

monoamine content, and monoamine transporter function (Hotchkiss et al., 1979; Ricaurte et al., 1980; Wagner et al., 1980). In addition, methamphetamine produced hyperthermia that played an important role in producing the long-term damage to the dopaminergic and serotonergic nerve terminals (Hotchkiss and Gibb, 1980). In addition, methamphetamine administration decreased 5-HT content and SERT function in prefrontal cortex, hippocampus, and striatum in rats (Ricaurte et al., 1980). Methamphetamine-induced decrease of 5-HT content, and function of DAT and SERT lasted up to 4 years after the last administration of drug in nonhuman primates (Woolverton et al., 1989). Meanwhile, methamphetamine-induced decrease of DAT density lasted up to 3 years or more in abstinent humans (McCann et al., 1998).

Methamphetamine-induced neurotoxicity was accompanied by the production of reactive oxygen and reactive nitrogen species that contributed to the induction of oxidative stress (Stephans and Yamamoto, 1994). Excessive extracellular DA can be oxidized to produce DA quinones and reactive oxygen species, leading to increases in oxidative stress (Michel and Hefti, 1990). The involvement of oxidative stress in methamphetamine-induced neurotoxicity was further supported by studies showing that free radical scavengers and antioxidants reduced the neurotoxic effects of methamphetamine (Fukami et al., 2004; Wagner et al., 1980). Reactive radicals were responsible for the production of lipid peroxides and oxidization of proteins in nerve terminals. Besides reactive oxygen species, reactive nitrogen species seem to be involved in mediating methamphetamine-induced neurotoxicity. The role of reactive nitrogen species in

methamphetamine-induced toxicity was supported by the fact that nitric oxide synthase inhibition was neuroprotective against methamphetamine-induced long-term DA depletion in mice (Itzhak and Ali, 1996). In addition, methamphetamine administration potentiated the formation of peroxynitrite nitrotyrosine, which elicited the nitration of tyrosine residues on various proteins including TH and vesicular monoamine transporters (Kuhn et al., 2002). Overall, methamphetamine administration resulted in lipid peroxidation and protein oxidation or nitration, contributing the toxic effects on DA and 5-HT terminals.

Involvement of glutamate excitotoxicity also was suggested in the neurotoxic effects of methamphetamine (Battaglia et al., 2002). Glutamate-induced excitotoxicity is mediated by the over activation of glutamate receptors and the subsequent elevation of intracellular Ca^{2+} levels. Such increase of Ca^{2+} activates several kinases, lipases, and proteases, which leads to cytoskeletal protein damage, free radicals generation, DNA damage, and ultimately neurodegeneration (Lipton and Rosenberg, 1994; Sattler and Tymianski, 2000). Metabotropic glutamate inhibitors prevented methamphetamine-induced DA depletions in mice, without altering methamphetamine-induced hyperthermia, suggesting that activation of glutamate receptor was responsible for the DA depletions (Battaglia et al., 2002). Administration of a toxic regimen of methamphetamine increased extracellular glutamate concentrations in rat striatum, which was thought to result in the excitotoxicity (Stephans and Yamamoto, 1994). In addition, elevation of intracellular calcium led to reactive nitrogen species generation, as well as nitric oxide synthase activation, which in

turn resulted in reactive nitrogen species generation (Schmidt et al., 1996). Thus, methamphetamine-induced excitotoxicity could synergize with methamphetamine-induced oxidative stress.

In addition to oxidative stress and excitotoxicity, alteration in mitochondrial function was produced by methamphetamine resulting in toxic effects (Brown et al., 2005; Burrows et al., 2000). In addition, mitochondrial function was inhibited by methamphetamine when the rats were maintained normothermic, suggesting that such an inhibitory effect was not due to methamphetamine-induced hyperthermia. Interestingly, the glutamate receptor antagonist MK-801 and the peroxynitrite decomposition catalyst Fe-TPPS attenuated methamphetamine-induced inhibition of mitochondrial function (Brown et al., 2005). Thus, the convergence of methamphetamine-induced excitotoxicity and inhibition of mitochondrial function appears to exist (Quinton and Yamamoto, 2006).

1.5 Review of Potential Treatment and Therapeutic Targets for Methamphetamine Abuse

1.5.1 Behavioral Therapy

No pharmacotherapy has been approved by the FDA to be an effective treatment of methamphetamine abuse, even though a number of clinical trials have been conducted. Several behavioral treatments have been developed for the treatment of methamphetamine abuse (Carroll and Onken, 2005). Among which, contingency management, motivational interviewing, and cognitive

behavioral therapy are the three behavioral therapies with the strongest level of empirical support in clinical trials (Sofuoglu et al., 2013). Contingency management is a type of treatment used in which abstinence or adherence to program rules are reinforced with incentives (Higgins et al., 1991). This behavioral task employs operant conditioning in which a certain behavior (drug abstinence in this situation) is reinforced. In such a behavior treatment, monetary reward is usually provided and contingency management is moderately effective in reducing methamphetamine abuse (Shoptaw et al., 2006b). Motivational interviewing is a type of treatment in which a specific, nonjudgmental interviewing style is used to motivate the patient to achieve their goals (Hettema et al., 2005; Miller, 2005). Warmth, genuine empathy, and unconditioned positive regard are useful for the improvement of treatment efficacy (Hettema et al., 2005). Patients are guided to think differently about their behavior and to consider the benefits through change (drug abstinence in this case) (Hettema et al., 2005). Cognitive behavioral therapy is a type of therapy in which specific strategies and skills are introduced to reduce substance use (Carroll et al., 1994). It has been noted that methamphetamine addicts show significant cognitive impairments, especially in attention, working memory and response inhibition functions (Sofuoglu, 2010). Cognitive impairments are generally associated with addiction and the possible relevance of these cognitive deficits as predictors of treatment outcome in addiction has been proposed. Cognitive behavioral therapy, treatment targeting cognitive-enhancement strategies for methamphetamine abuse, has been reported to achieve cognitive improvement in the drug addicted populations

(Kiluk et al., 2010). However, few studies have been performed to directly assess the ability of cognitive enhancing treatments to improve substance use outcomes. Thus, the efficacy of such an approach needs to be determined in future clinical research (Sofuoglu et al., 2013). Despite the limited success of contingency management, motivational interviewing, and cognitive behavioral therapy, behavior therapies are not efficacious for all methamphetamine addict populations (Sofuoglu et al., 2013). For instance, cognitive behavioral therapy was suggested not to treat patients who are not medically stable. In addition, one of the primary limitations of behavioral treatment is that high level of motivation and cooperation are required from the patients, and behavioral therapy is limited to compliant individuals (Ronen, 2004). Psychotherapy alone as treatment for drug abuse was criticized by Dr. George Woody, and was suggested to be used as a secondary treatment (Woody, 2003). Thus, pharmacotherapies for the treatment of methamphetamine abuse are in demand.

1.5.2 Replacement Therapy

A replacement therapy model has been developed using stimulants to treat methamphetamine abuse (Moeller et al., 2008). D-amphetamine is capable of reducing intravenous and oral administration of illicit amphetamine in a clinical study on amphetamine abusing patients (White, 2000). Methylphenidate, a DAT blocker, has been suggested also as a potential treatment for methamphetamine addiction, and is well tolerated and effective for alleviating symptoms of depression in amphetamine abstinence (Laqueille et al., 2005). Furthermore, the

amount of amphetamine uses by patients with severe dependence is significantly decreased by methylphenidate (Tiihonen et al., 2007). The above studies suggest that methylphenidate could be a potential treatment for amphetamine addiction. However, potential for abuse liability of methylphenidate is a major concern of this approach (Manchikanti, 2007; Sweeney et al., 2013).

1.5.3 5-HT Receptors as a Therapeutic Target

5-HT receptors are a group of GPCRs and ligand-gated ion channels widely distributed in both the central and peripheral systems (Hoyer et al., 1994). 5-HT receptors mediate various biological and neurological processes including aggression, anxiety and appetite. 5-HT receptors are targets of various pharmacotherapies, including many antidepressants, antipsychotics, and gastroprokinetic agents. Activation of these receptors by 5-HT regulates both excitatory and inhibitory neurotransmission (Nichols and Nichols, 2008). Seven main subtypes of 5-HT receptors have been characterized, among which 5-HT_1 and 5-HT_5 receptors are coupled to the inhibitory Gi/Go-protein. 5-HT_3 receptors are ligand-gated ion channels. 5-HT_2, 5-HT_4, 5-HT_6, 5-HT_7 receptors are the excitatory receptors coupled to the GqG_{11}- and Gs-protein (Hoyer et al., 1994; Nichols and Nichols, 2008).

Serotonergic systems may regulate effects of psychostimulants by increasing DA release in NAc and VTA (Guan and McBride, 1989; Parsons and Justice, 1993). Activation of the 5-$HT_{2a/2c}$ receptor alters methamphetamine drug discrimination, indicating the involvement of serotonergic system in

methamphetamine-induced behaviors (Munzar et al., 1999). The 5-HT_{1a} receptor agonist, 7-(Dipropylamino)-5,6,7,8-tetrahydronaphthalen-1-ol (8-OH-DPAT), inhibits amphetamine-induced elevation of extracellular DA in NAc, striatum and mPFC (Ichikawa et al., 1995; Kuroki et al., 1999). The 5-HT_{1a} receptor antagonist, N-[2-[4-(2-methoxyphenyl)-1-piperazinyl]-ethyl]-N-(2-pyridinyl)cyclohexanecarboxamide (WAY-100635), reverses the inhibitory effects of 8-OH-DPAT on amphetamine. In contrast, 5-HT_{1a} receptor agonist, osemozotan, does not inhibit methamphetamine-induced elevation of extracellular DA levels in the PFC in mice (Ago et al., 2006). Mirtazapine, an FDA approved antidepressant inhibiting 5-HT_{2a} and 5-HT_3 receptors, reverses methamphetamine-induced behavioral sensitization in rats (McDaid et al., 2007). In addition, mirtazapine prevents methamphetamine-induced conditioned place preference in rats (Herrold et al., 2009). However, mirtazapine has no effect on methamphetamine withdrawal symptoms in clinical trials (Cruickshank et al., 2008), and no effective therapies for the treatment of methamphetamine addiction have been generated using 5-HT receptors as the target.

1.5.4 Immunotherapy

Immunotherapies have been developed to reduce the amount of methamphetamine entering the brain by administering anti-methamphetamine antibodies (Kosten and Owens, 2005). The antibodies could be used in the hospital to treat intoxicated patients, used during abstinence to prevent drug-induced relapse, or used in a patient who intends to be drug resistant. Anti-

methamphetamine antibodies are capable of protecting patients for several weeks due to the long half-life of immunoglobulin. Pre-treatment with a mouse monoclonal anti-methamphetamine antibody decreased methamphetamine self-administration (McMillan et al., 2004) and drug-induced locomotor activity in rats (Gentry et al., 2004) by protecting the brain from methamphetamine exposure. In addition, the antibody inhibits the discriminative stimulus effects of methamphetamine in pigeons (Daniels et al., 2006). Immunotherapy as a treatment for substance abuse is promising, and clinical trials are necessary to further determine the efficacy of this type of therapeutic.

1.5.5 Gamma-aminobutyric Acid (GABA) Receptors as Therapeutic Targets

GABA receptors are a group of receptors which GABA interacts with, and the activation of the receptors produces inhibitory neurotransmission in the CNS (Kuffler and Edwards, 1958). GABA receptors are the targets of pharmacotherapies such as sedative and hypnotic medicines. Two classes of GABA receptors have been characterized: $GABA_A$ and $GABA_B$ receptors. $GABA_A$ receptors are ligand-gated ion channels, while $GABA_B$ receptors are G protein-coupled receptors (Kuffler and Edwards, 1958).

Activation of GABA neurons inhibits DA transmission in the NAc and VTA in rat brain (Gong et al., 1998), which inhibits the reinforcing effects of psychostimulants. Thus, studies have been performed to investigate GABA receptor agonists as potential treatments for methamphetamine abuse. However, baclofen, a GABA receptor agonist, did not reduce depressive symptoms,

craving for methamphetamine, or methamphetamine-positive urine samples in drug-dependent outpatients (Heinzerling et al., 2006). In addition, Gamma-Vinyl GABA (GVG), a GABA-transaminase inhibitor, increases GABA transmission by inhibiting GABA metabolism (Gerasimov et al., 1999). The subsequent activation of GABA receptors decreases cocaine and methamphetamine-induced elevation of DA in NAc (Gerasimov et al., 1999). However, no convincing positive results have been found in clinical studies in methamphetamine abusers (Brodie et al., 2005).

1.5.6 Sigma Receptors as Therapeutic Targets

Sigma receptors (σ-1 and σ-2) are non-opioid proteins and are involved in various neurological disorders (Narayanan et al., 2011). Activation of σ receptors may result in hypertonia, tachypnea, and mydriasis. Agonists for the receptors include cocaine, morphine, fluvoxamine, methamphetamine, dextromethorphan. Recently, σ receptors have been studied as a target in the treatment of depression and psychotic (Leonard, 2004). The σ-1 receptor subtype is a chaperon protein widely expressed in the brain and peripheral tissues. These receptors regulate K^+ and Ca^{2+} dependent signaling cascades at the endoplasmic reticulum and neurotransmission in CNS (Narayanan et al., 2011).

Pharmacologically relevant concentrations of methamphetamine interact with σ-1 receptors (Xu et al., 2012), indicating a potential site for pharmacologic interaction. Methamphetamine significantly elevated σ-1 receptor expression in the VTA and SN (Hayashi et al., 2010), indicating an involvement of the receptor

in methamphetamine addiction. Recently, σ-1 receptors have been studied as targets in the discovery of treatment of substance abuse. Preclinical studies demonstrate that σ-1 receptor ligands attenuate behavioral effects of methamphetamine (Seminerio et al., 2012). Specifically, pretreatment with σ-1 receptor antagonist, 3-(4-(4-cyclohexylpiperazin-1-yl)pentyl)-6-flourobenzo[*d*]thiazol-2(3*H*)-one (AZ66), inhibited methamphetamine-induced acute locomotor stimulatory effects, and expression and development of behavioral sensitization in Swiss Webster mice. In addition, the σ-1 receptor antagonist, AZ66, ameliorate methamphetamine-induced striatal DA depletions in Swiss Webster mice (Seminerio et al., 2013). Together, the results suggest that activation of σ-1 receptors is involved in addictive properties of methamphetamine and methamphetamine-induced toxicity. Additional studies need to determine the role of σ-1 receptor as a potential target for the treatment of methamphetamine abuse.

1.5.7 DA Receptors as Therapeutic Targets

Since activation of DA receptors plays an important role in the stimulant properties of methamphetamine, DA receptor antagonists have been studied as the target in treatment of methamphetamine abuse (Newman et al., 2012). However, the D2 receptor antagonist, haloperidol, did not reduce the stimulant-like effects of methamphetamine in healthy volunteers (Wachtel et al., 2002). Another D2 receptor antagonist, quetiapine, decreases the self-reported craving severity induced by methamphetamine (Sattar et al., 2004). However, poor

experimental design including very small sample size and lack of subject blinding preclude any convincing conclusions from this study. The above studies suggest that D2 receptor antagonists do not block the stimulant properties of methamphetamine in humans.

DA receptor partial agonists have been studied as potential therapies to ameliorate altered brain DA homeostasis in stimulant abusers (Lile et al., 2005). Specifically, the partial agonist stimulates receptors during abstinence when dopaminergic tone is reduced, but antagonizes receptors during relapse when dopaminergic tone is increased. The above approach is supported by several studies. For instance, the DA D2 receptor partial agonist, aripiprazole, decreases amphetamine and cocaine self-administration in rats (Pulvirenti et al., 1998), and inhibits the discriminative effects of d-amphetamine in human volunteers (Lile et al., 2005). Decrease of goodness feeling, drug liking and willingness to take the drug again are reported by volunteers administered d-amphetamine with the D2 receptor partial agonist aripiprazole (Lile et al., 2005). However, subsequent Phase II studies demonstrate that aripiprazole increases amphetamine use by addicts and such results prevent further investigation (Tiihonen et al., 2007).

In addition to DA D2 receptors, the D3 receptor has been studied as a potential target for discovery of pharmacotherapy for the treatment of methamphetamine abuse (Newman et al., 2012). Exposure to psychostimulants, including cocaine and methamphetamine, results in an increase in expression and function of D3 receptors (Caine and Koob, 1993; Heidbreder and Newman,

2010; Neisewander et al., 2004). In addition, upregulation of D3 receptors is found via positron emission tomography (PET) studies in methamphetamine polydrug abusers (Boileau et al., 2012). The D3 receptor antagonist, N-[trans-4-[2-(6-cyano-3,4-dihydroisoquinolin-2(1H)-yl)ethyl]cyclohexyl]quinoline-4-carboxamide (SB-277011A), significantly decreases breakpoints of methamphetamine self-administration in rats (Higley et al., 2011; Xi et al., 2005), and dose dependently decreases methamphetamine self-administration in rats. Additionally, buspirone, a high affinity ligand at both D3 and D4 receptors, decreases methamphetamine self-administration in rats, suggesting the role of D3 receptor ligand as potential therapy for the treatment of methamphetamine abuse (Newman et al., 2012). However, buspirone has high affinity for the 5-HT_{1A} receptor which has been suggested to mediate the stimulant properties of methamphetamine (Muller et al., 2007). Thus, buspirone inhibition of methamphetamine effects could be due to action at the 5-HT_{1A} receptor. No successful pharmacotherapies have been generated by the above approach and the effect of selective D3 receptor antagonists and partial agonists needs to be evaluated in human methamphetamine abusers (Newman et al., 2012).

1.5.8 Plasma Membrane Transporters as Therapeutic Target

Methamphetamine reverses DAT to elevate extracellular DA that results in its subsequent rewarding effect. In addition to DAT, NET and SERT are also regulated by methamphetamine (Budygin et al., 2004; Gainetdinov, 2008). The antidepressant drug, bupropion, which inhibits both NET and DAT, has been

proposed to decrease the craving for methamphetamine in early abstinence and to prevent relapse by inhibiting the reinforcing effects of methamphetamine (Berigan and Russell, 2001). Bupropion has been shown to be safe in Phase I clinical trials (Newton et al., 2005). In addition, bupropion has been shown to decrease the subjective effects of methamphetamine and reduce drug craving in a Phase II clinical trial (Newton et al., 2006). However, bupropion did not decrease methamphetamine use in participants following a 12-week treatment program (Shoptaw et al., 2008). Inhibitors for the plasma membrane monoamine transporters have been evaluated in discovery of treatment for methamphetamine abuse. However, no successful pharmacotherapies have been generated.

Serotonergic systems are involved in the effects of psychostimulants, as activation of 5-HT receptors by 5-HT released in response to methamphetamine is involved in its rewarding effects (Chiu and Schenk, 2012). 5-HT reuptake inhibitors (SSRI) increase extracellular 5-HT concentrations, and have been studied as potential treatment of methamphetamine abuse (Shoptaw et al., 2006a). SSRIs decrease the rewarding effects of psychostimulants (Takamatsu et al., 2006). Specifically, pre-treatment with the SSRI, fluoxetine, inhibits methamphetamine-induced locomotor sensitization and conditioned place preference in mice. However, fluoxetine does not reduce methamphetamine use in clinical trials (Batki et al., 2000). Moreover, another SSRI, sertraline, does not decrease methamphetamine use in a clinical trial (Rawson et al., 2004). The

above results suggest that SSRIs are not effective treatments for methamphetamine addiction (Shoptaw et al., 2006a).

1.5.9 Acetylcholine Neurotransmitter System

In the central nervous system, acetylcholine plays an important role in plasticity, arousal and reward (Eglen, 2006; Yakel, 2013). Damage to the cholinergic system in the brain has been associated with memory deficits in Alzheimer's disease (Tabet, 2006). Cholinergic receptors include two main types of receptors, i.e., the nicotinic receptor, a ligand gated ion channel and the muscarinic receptor, a G-protein-coupled receptor. Activation of nicotinic receptor ion channels and the subsequent inward flux of Ca^{2+} results in the fusion of the synaptic vesicles with the presynaptic terminals and the release of the neurotransmitter into the synaptic cleft (Anand et al., 1991). Muscarinic receptors are coupled to G proteins, and receptor activation regulates secondary messengers and the subsequent signal transduction (Eglen, 2006).

Acetylcholine neurotransmission has been suggested to be involved in methamphetamine-induced reinforcement and locomotor activation. Regulation of acetylcholinesterase, the enzyme which metabolizes acetylcholine, may mediate methamphetamine seeking behavior as suggested by the finding that the acetylcholinesterase inhibitor donepezil inhibits reinstatement of methamphetamine-seeking behavior (Hiranita et al., 2006). The above inhibitory effect on reinstatement of methamphetamine may be due to activation of nicotinic, but not of muscarinic, cholinergic receptors in the NAc core, prelimbic

cortex, amygdala and hippocampus (Hiranita et al., 2006). Rivastigmine, an inhibitor for both butyrylcholinesterase and acetylcholinesterase (Williams et al., 2003), decreases methamphetamine-induced craving and anxiety, and methamphetamine-induced positive subjective effects in an experimental model of intravenous self-administration in human volunteers (De La Garza et al., 2008). However, total choices for methamphetamine over a monetary alternative were not reduced among abusers (De La Garza et al., 2008). Additional clinical trials are required to determine efficacy of cholinesterase inhibitors as a treatment for methamphetamine abuse.

1.5.10 Opioid Receptors as Therapeutic Targets

An opioid is a chemical that binds to opioid receptors, which are distributed in both the central and peripheral nervous system. Opioids have analgesic effects and their side effects include sedation, respiratory depression, constipation, and euphoria (Benyamin et al., 2008). Opioid-induced euphoria is well known, and responsible for the recreational use. Repeated use of opioids leads to dependence, tolerance, and abstinence which is accompanied by a withdrawal syndrome (Benyamin et al., 2008). Opioid receptors are a group of G protein-coupled receptors and there are four major subtypes of opioid receptors, including the δ-opioid receptor, κ-opioid receptor, mu-opioid receptor, and the nociceptin receptor (Paterson et al., 1983).

Endogenous opioids are increased by acute administration of methamphetamine (Olive et al., 2001). Opioid agonists activate the firing rate of

DA neurons (Matthews and German, 1984) and elevate DA concentration (Klitenick et al., 1992) in VTA. Pretreatment of opioid receptor antagonist naloxone inhibits methamphetamine-induced conditioned place preference in rats (Trujillo et al., 1991). In addition, naloxone decreases both amphetamine-induced elevation of extracellular DA and locomotor activity (Hooks et al., 1992). Similar to amphetamine, methamphetamine-induced behavioral sensitization and reinstatement are inhibited by naloxone (Chiu et al., 2005). In addition to preclinical studies, naltrexone reduces the subjective response of patients to amphetamine in clinical studies employing amphetamine-addicted individuals (Jayaram-Lindstrom et al., 2004). Thus, naltrexone appears to be a highly promising pharmacotherapy for methamphetamine dependence. However, total amphetamine intake was not measured in Jayaram-Lindstrom's study and further clinical studies are necessary to determine the effect of naltrexone on the reinforcing effect of amphetamine and methamphetamine.

1.5.11 Nicotinic Receptors as Therapeutic Targets

Nicotinic receptors, members of the Cys-loop family of ligand-gated ion channel receptors, consist of pentameric transmembrane proteins with various subunits (Anand et al., 1991; Millar and Gotti, 2009). The presence of nine nicotinic receptor subunit genes (α2–α7, β2–β4) in mammalian brain suggests an extraordinary diversity of nicotinic receptors (Dani and Bertrand, 2007).

d-Amphetamine increases choice of cigarette smoking over monetary reinforcement in human addicts and this effect is caused by a drug-produced

enhancement in the reinforcing effects of smoking (Tidey et al., 2000). Individuals who abuse amphetamine use nicotine more than people who are only addicted to nicotine (Barrett et al., 2006). Acute doses of amphetamine increase smoking related behaviors and responses (Cousins et al., 2001; Henningfield and Griffiths, 1981; Schoffelmeer et al., 2002; Tidey et al., 2000). Neurochemical studies indicate that nicotine-induced DA efflux from rat striatum is potentiated by acute amphetamine, suggesting that potentiation of nicotine response by amphetamine is via elevated DA (Jutkiewicz et al., 2008). Additionally, a low dose of methamphetamine potentiates nicotine self-administration in rats (Rauhut et al., 2003). Nicotine and methamphetamine share discriminative stimulus effects in rats (Gatch et al., 2008), and interchangeable use of these stimulants in human users is also observed (Barrett et al., 2006). Chronic methamphetamine results in cross-sensitization to nicotine in mice (Kuribara, 1999), which may be the consequence of elevated nicotine-evoked DA release. Taken together, these results indicate that nicotine-evoked DA release is potentiated by methamphetamine and amphetamine pretreatment, and there is a pharmacological basis for the elevated DA release. However, the mechanism for the elevation of nicotine-evoked DA release by amphetamine or methamphetamine pretreatment is not clear.

Previous studies have suggested that amphetamine and its derivatives bind to nicotinic receptors. d-Amphetamine has been suggested to activate α7 nicotinic receptors, resulting in calcium increase in bovine adrenal chromaffin cells and [^{3}H]NE release from the cell (Liu et al., 2003). Moreover, d-

amphetamine inhibits α-bungarotoxin binding, an α7 nicotinic receptor ligand, to rat and mouse diaphragms (Skau and Gerald, 1978). These results suggest that amphetamine and methamphetamine bind to and activate α7 nicotinic receptors. Interestingly, recent studies show that methamphetamine binds to α7 and α4β2* nicotinic receptors on membranes from both cell lines and mouse brain, and methamphetamine is expected to exhibit agonistic or positive allosteric effect at these receptors (Garcia-Rates et al., 2007). Local infusion of an α3β4 nicotinic receptor antagonist, 18-methoxycoronaridine, into medial habenula, the interpeduncular area or the basolateral amygdala decreases methamphetamine self-administration by indirectly regulating the dopaminergic mesolimbic pathway (Glick et al., 2008). Thus, selective α3β4 nicotinic receptor antagonists may be potential treatments for methamphetamine abuse. However, no clinical studies have been performed on 18-methoxycoronaridine (Pace et al., 2004) or any specific nicotinic receptor antagonists to determine the efficacy to treat methamphetamine abuse.

1.6 VMAT2 as Therapeutic Target

VMAT2, located on vesicles within presynaptic terminals, transports cytosolic DA into the vesicles for storage and subsequent release into the extracellular space (Section 1.2.5). Methamphetamine inhibits DA uptake and promotes DA release at VMAT2, consequently increasing cytosolic DA available to DAT for reverse transport (Section 1.3.4). VMAT2 has been studied as a target to discover pharmacotherapies to treatment methamphetamine abuse (Dwoskin and Crooks, 2002; Zheng et al., 2006). Lobeline, targeting VMAT2, have been

studied in our lab as potential pharmacotherapies to treat methamphetamine abuse (Dwoskin and Crooks, 2002).

1.6.1 Lobeline

1.6.1.1 Background and Historical Use

Lobeline (Figure 1.1) is a major alkaloid from *Lobelia inflata,* an herb named after the famous French botanist Matthias de Lobel (1570–1616) (Millspaugh, 1974). *Lobelia inflata* grows in dry fields in North America. The plant tastes like tobacco and produces effects like nicotine and the dried leaves of the plant was smoked by American Indians to obtain the CNS effects. In addition, a tobacco-like sensation is generated after chewing the plant leaves. Thus, the plant is commonly called Indian tobacco. *Lobelia inflata* was first reported in the 1700s as an emetic and application for sore eyes. In the 1800s, *Lobelia inflata* was applied as a treatment for asthma (Dwoskin and Crooks, 2002). Extracts of *Lobelia inflata* were first reported in 1838 and used as an expectorant, emetic, anti-asthmatic, anti-spasmodic, respiratory stimulant (Millspaugh, 1974). *Lobelia inflata* seeds were found to contain the highest level of lobeline which was the pharmacologically active ingredient (Dwoskin and Crooks, 2002). The availability of pure lobeline accelerated studies discovering the pharmacological properties of the alkaloid (Dwoskin and Crooks, 2002).

1.6.1.2 Lobeline Physicochemical Characteristics and Pharmacology

The lobeline molecule contains a central piperidine ring with two phenylethyl substituents at the C-2 and C-6 position of the central piperidine ring. One hydroxyl moiety is connected at the 8-position, and a keto moiety is connected at the 10-position of the phenylethyl substituents. Three chiral centers at the 8-position on the side chain, and the C-2 and C-6 position of the piperidine ring are included in the structure of the molecule. Lobeline is predicted to exhibit a Log S value of -4.01 (29.8 mg/L) and a Log P value of 3.75 (Tetko et al., 2005).

Lobeline was used as a smoking cessation agent in 1936 to alleviate nicotine withdrawal symptoms, but this result was not replicated in later studies (Davison and Rosen, 1972). Recently, lobeline has been studied again. A sublingual formulation with improved bioavailability was developed to determine the efficacy of lobeline in smoking cessation (Glover et al., 2010). However, sublingual formulation of lobeline does not reduce smoking in people who are addicted to cigarettes.

Lobeline has many nicotine-like effects and has been considered a nicotinic receptor agonist (Stead and Hughes, 2012). However, nicotine is self-administered by rats (Corrigall et al., 1994), while lobeline does not support self-administration in rats (Harrod et al., 2001). Chronic nicotine administration increases locomotor activity (Clarke and Kumar, 1983), and generates conditioned place preference in rats (Fudala et al., 1985), but chronic lobeline does not (Fudala and Iwamoto, 1986). Initially, lobeline is not differentiated from

nicotine by rats in drug discrimination studies (Geller et al., 1971), but the result is not replicated in latter studies (Romano and Goldstein, 1980; Schechter and Rosecrans, 1972). Thus, different behavioral effects of lobeline and nicotine suggest that different mechanisms are involved in the drug-induced behavioral effect.

Lobeline inhibits [^{3}H]nicotine binding with high affinity (K_i = 4-30 nM) (Yamada et al., 1985), and the subtypes of the receptors to which lobeline binds have been studied. Lobeline displaces α4β2* nicotinic receptor ligands in PET studies using mouse brain (Horti et al., 1997). In addition, lobeline has high affinity for β2-containing nicotinic receptors, independent of the α-subtype in the combination (Parker et al., 1998). Meanwhile, lobeline displaces (K_i = 6.6 μM) [^{3}H]methyllycaconitine (an α7 selective ligand) binding to rat whole brain membranes (Miller et al., 2004), suggesting an interaction with α7 nicotinic receptors. Interestingly, nicotinic receptors are up-regulated by chronic nicotine in different brain regions (Collins et al., 1990), while up-regulation is not found following chronic lobeline (Auta et al., 1999; Bhat et al., 1991). Although lobeline has been considered a nicotinic receptor agonist, antagonist effects of lobeline at α7 nicotinic receptors has been reported at wild-type human receptors expressed in *Xenopus* oocytes (Briggs and McKenna, 1998).

In addition to the above binding studies, a functional assay was used to determine effects of lobeline on DA release from presynaptic dopaminergic terminals. Both nicotine and lobeline evoked [^{3}H]DA overflow from rat striatal

slices (Giorguieff-Chesselet et al., 1979; Teng et al., 1997), however, lobeline-evoked release was not antagonized by mecamylamine (a nicotinic receptor channel blocker that inhibits nicotine-evoked [^{3}H]DA release), suggesting that lobeline-evoked release was not mediated by nicotinic receptors. Thus, lobeline-regulated dopaminergic neurotransmission was not by activating nicotinic receptors. In addition, lobeline inhibited nicotine-evoked [^{3}H]DA overflow from rat striatal slices (Miller et al., 2000). The above results indicated that lobeline inhibited the neurochemical effect of nicotine, but evoked [^{3}H]DA overflow from presynaptic terminals that was not mediated by nicotinic receptors.

In addition to the studies using [^{3}H]DA, the ability of lobeline to release endogenous DA from rat striatal slices was determined and lobeline evoked DOPAC rather than DA overflow (Teng et al., 1998; Teng et al., 1997). However, endogenous DA was released in the presence of the highest concentration (100 μM) of lobeline. The above results determined that lobeline increased cytosolic DA, which was metabolized into DOPAC (Teng et al., 1997). Furthermore, lobeline-induced DOPAC overflow suggested that lobeline did not inhibit MAO function (Dwoskin and Crooks, 2002). In a microdialysis study using rats, lobeline did not release DA or DOPAC from NAc core, but inhibited nicotine-evoked DA and DOPAC overflow (Benwell and Balfour, 1998). In a subsequent microdialysis study (Meyer et al., 2013), lobeline did not release DA release from NAc shell, but increased DOPAC release, indicating the metabolism of DA. The above results indicated that lobeline evoked endogenous DOPAC overflow without inhibition of MAO (Dwoskin and Crooks, 2002).

The following studies have been performed to determine the mechanism by which lobeline regulates DA transmission. Lobeline inhibited DA uptake into synaptic vesicles and promoted DA release into the cytosol within presynaptic dopaminergic terminals, and the redistributed DA was subsequently metabolized to DOPAC by MAO (Miller et al., 2000; Teng et al., 1997). Lobeline inhibited (IC_{50} = 0.90 μM) [^{3}H]DTBZ binding on VMAT2 using vesicular membrane preparation (Teng et al., 1998; Teng et al., 1997). DTBZ is a VMAT2 inhibitor and binds to VMAT2 with high affinity at the site that is different from the substrate site that reserpine binds (Section 1.2.5). The above results indicate that lobeline binds to DTBZ sites on VMAT2 to inhibit vesicular DA uptake by the transporter, which contributes to the elevated DA in cytosol and subsequent metabolism of the transmitter.

Further studies have been performed to investigate the effect of lobeline on methamphetamine-induced neurochemical and behavioral changes. Lobeline inhibited methamphetamine-evoked endogenous DA release from rat striatal slices (Nickell et al., 2011). In a microdialysis study using rats, in NAc shell, lobeline did not alter the effects of methamphetamine on DA; however, lobeline enhanced the duration of the methamphetamine-induced decrease in extracellular DOPAC (Meyer et al., 2013). The alternation of TH activity was suggested to be responsible for such effect of lobeline on methamphetamine-induced decrease in extracellular DOPAC. The reason why methamphetamine-evoked DA release is not inhibited in the microdialysis study is not fully understood. Lobeline pretreatment inhibited the discriminatory effect of

methamphetamine, methamphetamine-induced elevation of locomotor activity (Miller et al., 2001), and methamphetamine self-administration in rats (Harrod et al., 2001). In addition, the effect of lobeline to decrease methamphetamine self-administration was not overcome by higher lobeline doses, indicating that the effect of lobeline is noncompetitive. Since lobeline was not self-administered by rats (Harrod et al., 2001), these results are taken to suggest that the alkaloid does not possess abuse liability.

In summary, lobeline acts as an inhibitor that binds to the DTBZ site on the synaptic VMAT2 to inhibit DA uptake, leading to an elevation in cytosolic DA that is subsequently metabolized to DOPAC by MAO. As such, the redistribution of DA storage decreases the cytosolic DA available for methamphetamine-induced reverse transport by DAT. Thus, the rewarding effect of methamphetamine is inhibited by decreasing extracellular DA. Together, these results suggest that lobeline could be a potential treatment for methamphetamine abuse. The above studies also suggest that VMAT2 is a promising target for discovering pharmacotherapies to treat methamphetamine abuse.

In this regard, lobeline has been tested in Phase Ib clinical trials and has been found to be safe in methamphetamine addicted individuals. Lobeline has no significant side-effects, other than an extremely bitter taste (Jones, 2007). Furthermore, lobeline has high affinity for α4β2* nicotinic receptors and moderate affinity for α7 nicotinic receptor (Damaj et al., 1997; Harrod et al., 2004; Miller et al., 2004), leading to the potential for several side effect including nausea,

vomiting, and diarrhea. Thus, additional studies have been performed to discover lobeline analogs with improved selectivity for VMAT2.

1.6.2 Lobelane Physicochemical Characteristics and Pharmacology

In order to increase the selectivity of lobeline at VMAT2, lobelane (Figure 1.1), a defunctionalized, saturated analog of lobeline has been generated. Lobelane is predicted to exhibit a Log S value of -5.46 (7.25 mg/L) and a Log P value of 5.74 (Tetko et al., 2005). Lobelane shows higher affinity for VMAT2, lower affinity for α4β2* and α7* nicotinic receptors, and higher affinity (K_i = 40 nM) to inhibit vesicular DA uptake in comparison to that (K_i = 0.4 μM) of lobeline (Miller et al., 2004). Furthermore, lobelane decreases methamphetamine-evoked DA release from striatal slices and methamphetamine self-administration without influence on sucrose-maintained responding (Neugebauer et al., 2007; Nickell et al., 2010). However, the effect of lobelane is tolerated after repeated treatment (Neugebauer et al., 2007). Thus, more structure activity relationship studies have been performed to discover drug candidates for the treatment of methamphetamine abuse.

1.7 Drug-likeness

The Rule-of-five (RO5) (Lipinski et al., 2001) is based on a distribution of calculated properties of several thousand drugs that passed Phase 2 clinical trial. The original RO5 is based on the properties of orally active compounds and defined by four physicochemical parameter ranges (molecular weight ≤ 500, logP

≤ 5, H-bond donors ≤ 5, H-bond acceptors ≤ 10). Acceptable water solubility, intestinal permeability, first steps in oral bioavailability are obtained from compounds with the above parameters. Compounds that fail the RO5 will probably not be orally active. The goal of RO5 is to guide chemists to avoid making compounds with poor physicochemical properties (Lipinski et al., 2001). Lobeline met RO5 and no difficulties were found when determining the effect of the compound in rats. Lobelane met RO5 except that the logP value was larger than 5. Consistent with RO5, lobelane possessed low water solubility but were still active after subcutaneous injection in rats.

CNS drugs need to penetrate the blood-brain-barrier and more restrictive physicochemical properties are required. P-glycoprotein (PGP) is a transporter that effluxes compounds out of the CNS and a major barrier for compounds to enter the CNS (Mahar Doan et al., 2002). Affinity for PGP efflux transporter should be considered when CNS drugs are generated. Two simple rules are capable of predicting CNS activity: N + O (the number of nitrogen and oxygen atoms) ≤ 5; log P > (N + O). Compounds with the above parameters have a greater chance to be CNS active (Norinder and Haeberlein, 2002). Lobeline and lobelane meets the requirement and are supposed to be CNS active.

1.8 Hypothesis and Specific Aims

To further refine the structure-activity relationships, lobelane analogs with varying methylene linker lengths at the C-2 and C-6 position of the central piperidine ring and acyclic lobelane analogs have been evaluated for their affinity

for DTBZ binding site on VMAT2, ability to inhibit VMAT2 function and methamphetamine-evoked [^{3}H]DA release from synaptic vesicles, as well as the mechanism of inhibition. Furthermore, the ability of (±)-GZ-729C, (±)-GZ-730B, and (R)-GZ-924 to inhibit methamphetamine-evoked DA release was determined. In the end, methamphetamine self-administration was performed to determine the ability of (R)-GZ-924 to inhibit the reinforcing effect of the drug.

Hypothesis 1: Lobelane analogs with varying methylene linker lengths will inhibit VMAT2 binding and function, and potent and selective analogs for VMAT2 function will inhibit methamphetamine-evoked [^{3}H]DA release from synaptic vesicles and endogenous DA release from striatal slices.

Specific Aims:

1) Determine the ability of lobelane analogs to inhibit VMAT2 binding and function.

2) Determine the ability of potent and selective lobelane analogs to inhibit methamphetamine-evoked [^{3}H]DA release from synaptic vesicles.

3) Determine the ability of potent and selective lobelane analogs to inhibit methamphetamine-evoked endogenous DA release from rat striatal slices.

Hypothesis 2: Acyclic lobelane analogs will inhibit VMAT2 binding and function, and potent and selective analogs for VMAT2 function will inhibit

methamphetamine-evoked [^{3}H]DA release from synaptic vesicles and DA release from striatal slices, as well as methamphetamine self-administration in rats.

Specific Aims:

1) Determine the ability of acyclic lobelane analogs to inhibit VMAT2 binding and function.

2) Determine the ability of potent and selective acyclic lobelane enantiomers to inhibit methamphetamine-evoked [^{3}H]DA release from synaptic vesicles.

3) Determine the ability of potent and selective acyclic lobelane enantiomers to inhibit methamphetamine-evoked DA release from striatal slices.

4) Determine the ability of (R)-GZ-924 to inhibit methamphetamine self-administration in rats.

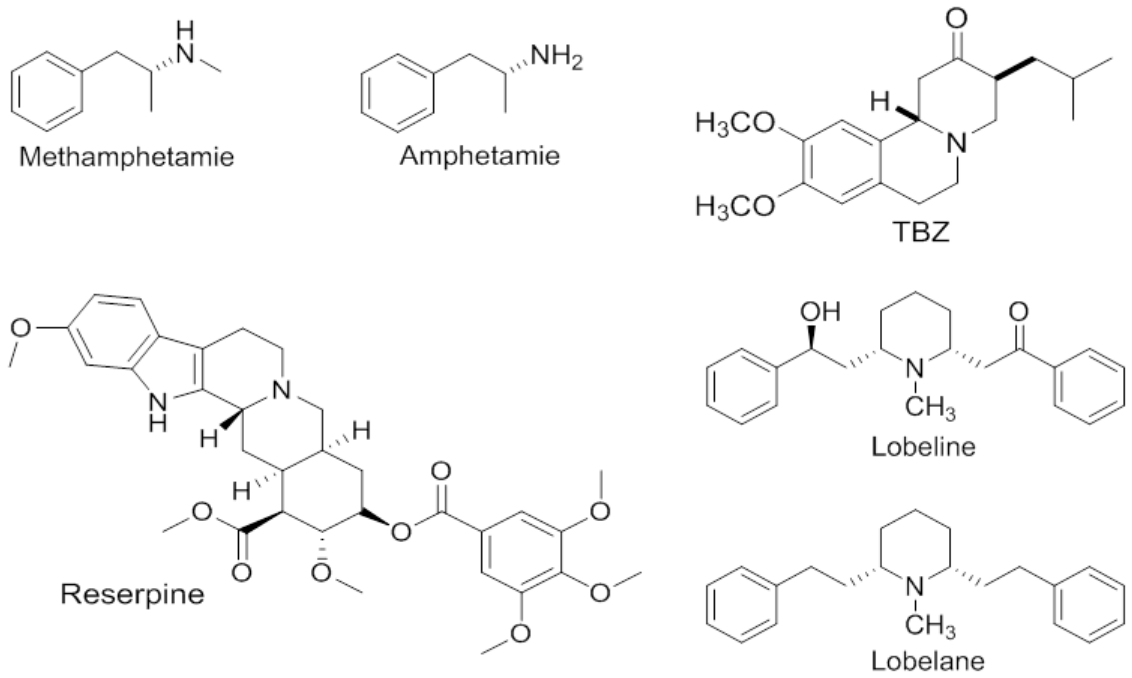

Figure 1.1. Chemical structures of methamphetamine, amphetamine, TBZ, reserpine, lobeline, and lobelane.

TBZ is a benzoquinolizine compound and VMAT2 inhibitor interacting with the site distinct from the DA uptake site on VMAT2. RO4-1284 is also a benzoquinolizine compound that inhibits VMAT2 in a similar manner. Lobeline is the principal alkaloid from *lobelia inflata*. Lobelane is a defunctionalized, saturated analog of lobeline.

CHAPTER 2 Lobelane analogs with varying methylene linker lengths as novel ligands that interact with vesicular monoamine transporter-2

2.1 Introduction

Methamphetamine inhibits dopamine (DA) uptake and promotes DA release from presynaptic vesicles by interacting with the vesicular monoamine transporter-2 (VMAT2), contributing to increased DA within presynaptic terminals (Brown et al., 2000; Pifl et al., 1995; Sulzer et al., 1995). Cytosolic DA concentrations are further increased by methamphetamine-induced inhibition of monoamine oxidase (MAO), the mitochondrial enzyme that is responsible for the metabolism of cytosolic DA (Mantle et al., 1976). The elevated cytosolic DA is released into the synaptic cleft by methamphetamine through reverse transport at DA transporter (DAT) (Sulzer et al., 1995). Interaction of methamphetamine with DAT and VMAT2 leads to elevated extracellular DA concentrations that contribute to its rewarding and reinforcing effects. Currently, no efficacious medicinal treatments are available to treat methamphetamine abuse. Recently, VMAT2 has been suggested to be a promising target, and recent studies focusing on VMAT2 as a therapeutic target have been performed (Dwoskin and Crooks, 2002; Zheng et al., 2006).

Lobeline (Figure 2.1), a major alkaloid from *Lobelia inflata*, is currently being evaluated in a phase 1b clinical trials as a novel therapeutic for the treatment of methamphetamine abuse (Jones, 2007). Lobeline inhibits vesicular DA uptake and promotes vesicular DA release, resulting in redistributed

cytoplasmic DA that is metabolized by MAO intraneuronally (Dwoskin and Crooks, 2002). It has been reported that lobeline inhibits methamphetamine-induced release of DA from rat striatal slices, as well as hyperactivity and self-administration of methamphetamine in rats (Harrod et al., 2001; Miller et al., 2001; Nickell et al., 2010). Meanwhile lobeline does not support self-administration in rats, indicating a lack of abuse liability (Harrod et al., 2003). VMAT2 is responsible for the uptake of cytoplasmic DA into synaptic vesicles for storage and subsequent release (Dwoskin and Crooks, 2002). *In vitro* studies indicate that lobeline decreases the amount of methamphetamine-evoked DA release from presynaptic terminals via an interaction with VMAT2 at the dihydrotetrabenazine (DTBZ) binding site (Teng et al., 1998; Zheng et al., 2007). However, previous studies have shown that lobeline can bind α4β2* and α7 nicotinic acetylcholine receptors (nAChRs) as well (Damaj et al., 1997; Miller et al., 2004). In order to increase the selectivity of lobeline at VMAT2, lobelane (Figure 2.1), a defunctionalized, saturated analog of lobeline has been generated. Lobelane shows higher affinity for the DTBZ binding site on VMAT2, lower affinity for α4β2* and α7 nAChRs, and higher affinity to inhibit vesicular DA uptake in comparison to lobeline (Miller et al., 2004). Furthermore, lobelane decreases methamphetamine-evoked DA release from striatal slices and methamphetamine self-administration without altering sucrose-maintained responding (Neugebauer et al., 2007; Nickell et al., 2010). However, the effect of lobelane is tolerated after repeated treatment (Neugebauer et al., 2007). Thus, more structure activity relationship work has been performed to discover a drug candidate for the

treatment of methamphetamine abuse.

Recently, several antipsychotics have been withdrawn or had restricted labelling due to the potential cardiac side effects (Haddad and Anderson, 2002). These antipsychotics drugs may prolong the ventricular action potential duration (APD, *i.e.* the QT interval of the electrocardiogram) and cause a polymorphic ventricular tachycardia, known as Torsades de Pointes (TdP), and sudden death (Tamargo, 2000). Drug-induced TdP are associated with blockage of the rapidly activating, delayed rectifier potassium current I_{Kr} channel coded by the human *ether-a-go-go*-related gene (hERG). This channel plays a major role in repolarization of ventricular myocytes and analogs with high affinity for such hERG channel have potential to possess cardiac toxicity (Sanguinetti et al., 1995; Trudeau et al., 1995).

In the current study, lobelane analogs with varying methylene linker lengths have been evaluated for their affinity for the DTBZ site on VMAT2 and for their potency to inhibit VMAT2 function. Affinity at DAT was evaluated to assess potential abuse liability, and affinity at hERG channels was evaluated to assess potential cardiac toxicity. The most potent and selective analog for VMAT2 function over DAT and hERG channels was identified as lead. The lead analog was evaluated for its ability to inhibit methamphetamine-evoked [^{3}H]DA release from synaptic vesicles, as well as methamphetamine-evoked endogenous DA release from striatal slices.

2.2 Methods

2.2.1 Animals

Male Sprague-Dawley rats (200–250 g) were purchased from Harlan (Indianapolis, IN) and were housed in the Division of Laboratory Animal Resources at the College of Pharmacy at the University of Kentucky (Lexington, KY). Food and water were available ad libitum. Experimental protocols were according to the National Institutes of Health Guide for the Care and Use of Laboratory Animals and were approved by the Institutional Animal Care and Use Committee at the University of Kentucky.

2.2.2 Materials

[^{3}H]DA (dihydroxyphenylethylamine, 3,4-[7-^{3}H]; specific activity, 28 Ci/mmol) was purchased from PerkinElmer, Inc. (Boston, MA, USA). [^{3}H]DTBZ ((±)-α-[O-methyl-3H]dihydrotetrabenazine; specific activity, 79.0 Ci/mmol) was a gift from Dr. Michael R. Kilbourn (Department of Internal Medicine and Neurology, University of Michigan, Ann Arbor, MI). Bovine serum albumin, disodiumethylenediamine (EDTA), ethyleneglycoltetraacetate (EGTA), L-(+) tartaric acid, N-[2-hydroxyethyl]piperazine-N'-[2-ethanesulfonic acid] (HEPES), sucrose, magnesium sulfate, polyethyleneimine, adenosine 5'-triphosphate magnesium salt, 3-hydroxytyramine (DA), d-methamphetamine hydrochloride (methamphetamine), sodium chloride, and magnesium sulfate were purchased from Sigma-Aldrich (St. Louis, MO). L-Ascorbic acid and monobasic potassium

phosphate were purchased from AnalaR-BHD Ltd. (Poole, UK) and Mallinckrodt (St. Louis, MO) respectively. (2R,3S,11bS)-2-Ethyl-3-isobutyl-9,10-dimethoxy-2,2,4,6,7,11b-hexahydro-1Hpyrido[2,1-a]isoquinolin-2-ol (RO4-1284) and tetrabenazine (TBZ) were gifts from Hoffman-La Roche Ltd. (Basel, Switzerland). Lobeline hemisulfate was purchased from ICN Biomedicals Inc. (Costa Mesa, CA). All other commercial chemicals were purchased from Fisher Scientific Co. (Pittsburgh, PA). The lobelane and lobelane analogs were synthesized by Dr. Guangrong Zheng (Zheng et al., 2008) and their structures are illustrated in Figure 2.1 and Figure 2.2. All racemics are cis-analogs and each contains same amount of two enantiomers. Lobelane analogs include 1-methyl-2,6-cis-dibenzylpiperidine (GZ-709C); 2,6-cis-dibenzylpiperidine (GZ-709B); 1-methyl-2,6-cis-di(3-phenylpropyl)piperidine (GZ-712C); 2,6-cis-di(3-phenylpropyl)piperidine (GZ-712B); 1-methyl-2,6-cis-diphenylpiperidine (GZ-632A); (±)-1-methyl-cis-2-phenyl-6-benzylpiperidine [(±)-GZ-731B]; (±)-cis-2-phenyl-6-benzylpiperidine [(±)-GZ-731A]; (±)-1-methyl-cis-2-phenyl-6-(2-phenethyl)piperidine [(±)-GZ-725A]; (±)-cis-2-phenyl-6-(2-phenethyl)piperidine [(±)-GZ-713A]; (±)-1-methyl-cis-2-phenyl-6-(3-phenylpropyl)piperidine [(±)-GZ-726A]; (±)-cis-2-phenyl-6-(3-phenylpropyl)piperidine [(±)-GZ-714A]; (±)-1-methyl-cis-2-benzyl-6-(2-phenethyl)piperidine [(±)-GZ-729C]; (±)-cis-2-benzyl-6-(2-phenethyl)piperidine [(±)-GZ-729B]; (±)-1-methyl-cis-2-benzyl-6-(3-phenylpropyl)piperidine [(±)-GZ-730C]; (±)-cis-2-benzyl-6-(3-phenylpropyl)piperidine [(±)-GZ-730B]; (±)-1-methyl-cis-2-(2-phenethyl)-6-(3-phenylpropyl)piperidine [(±)-GZ-644C]; (±)-cis-2-(2-phenethyl)-6-(3-

phenylpropyl)piperidine [(±)-GZ-644B]; (±)-1-methyl-cis-2-cyclohexyl-6-(2-phenethyl)piperidine [(±)-GZ-725B]; (±)-cis-2-cyclohexyl-6-(2-phenethyl)piperidine [(±)-GZ-713B]; (±)-1-methyl-cis-2-cyclohexyl-6-(3-phenylpropyl)piperidine [(±)-GZ-726B]; (±)-cis-2-cyclohexyl-6-(3-phenylpropyl)piperidine [(±)-GZ-714B].The structures of the analogs were verified by ^{1}H and ^{13}C NMR spectroscopy, mass spectrometry, and, in some instances, X-ray crystallography.

2.2.3 [^{3}H]DTBZ Binding

Lobelane- and lobelane analogs-induced inhibition of [^{3}H]DTBZ binding were determined using a previously described method (Horton et al., 2011a). The whole brain (excluding cerebellum) from rats was homogenized in 20 ml of ice-cold sucrose solution (0.32 M) with seven up-and-down strokes of a Teflon pestle homogenizer (clearance ≈ 0.003 inch). Homogenates were centrifuged (1000g for 12 min at 4°C), and the resulting supernatants were again centrifuged (22,000g for 10 min at 4°C). Resulting pellets were incubated in 18 ml of ice-cold water for 5 min, followed by adding 2 ml of HEPES (25 mM) and potassium tartrate (100 mM) solution. Samples were centrifuged (20,000g for 20 min at 4°C), followed by adding 20 µl of $MgSO_4$ (1 mM) solution to the supernatants. Solutions were centrifuged (100,000g for 45 min at 4°C) and resulting pellets were resuspended in ice-cold assay buffer (25 mM HEPES, 100 mM potassium tartrate, 5 mM $MgSO_4$, 0.1 mM EDTA, and 0.05 mM EGTA, pH 7.4). Assays were performed in duplicate using 96-well plates. Aliquots of vesicular suspension (15

μg of protein in 100 μl) were added to wells containing 5 nM [^{3}H]DTBZ, 50 μl of analog (0.1 nM to 1 mM), and 50 μl of buffer. Nonspecific binding was determined in the presence of RO4-1284 (20 μM). Reactions were terminated by filtration (Packard Filtermate harvester; PerkinElmer Life and Analytical Sciences) onto Unifilter-96 GF/B filter plates (presoaked in 0.5% polyethyleneimine). Filters were subsequently washed five times with 350 μl of ice-cold buffer (25 mM HEPES, 100 mM potassium tartrate, 5 mM $MgSO_4$, and 10 mM NaCl, pH 7.4). Filter plates were dried at 48°C and bottom-sealed, and each well was filled with 40 μl of scintillation cocktail (MicroScint 20; PerkinElmer Life and Analytical Sciences). Radioactivity on the filters was determined by liquid β-scintillation spectrometry (TopCount NXT; PerkinElmer Life and Analytical Sciences).

2.2.4 Vesicular [^{3}H]DA Uptake

Lobelane- and lobelane analogs-induced inhibition of [^{3}H]DA uptake were determined using a previously described method (Horton et al., 2011a). Rat striata were homogenized with 10 up-and-down strokes of a Teflon pestle homogenizer (clearance ≈ 0.003 inch) in 14 ml of 0.32 M sucrose solution. Homogenates were centrifuged (2000g for 10 min at 4°C), and the resulting supernatants were centrifuged again (10,000g for 30 min at 4°C). Pellets were resuspended in 2 ml of 0.32 M sucrose solution and subjected to osmotic shock by adding 7 ml of ice-cold water to the preparation, followed by the immediate restoration of osmolarity by adding 900 μl of 0.25 M HEPES buffer and 900 μl of

1.0 M potassium tartrate solution. Samples were centrifuged (20,000g for 20 min at 4°C), and the resulting supernatants were centrifuged again (55,000g for 1 h at 4°C), followed by the addition of 100 µl of 10 mM MgSO4, 100 µl of 0.25 M HEPES, and 100 µl of 1.0 M potassium tartrate solution before the final centrifugation (100,000g for 45 min at 4°C). Final pellets were resuspended in 2.4 ml of assay buffer (25 mM HEPES, 100 mM potassium tartrate, 50 µM EGTA, 100 µM EDTA, 1.7 mM ascorbic acid, 2 mM ATP-Mg^{2+}, pH 7.4). Aliquots of the vesicular suspension (100 µl) were added to tubes containing assay buffer, various concentrations of analog (0.1 nM to 0.1 mM) and 0.1 µM [^{3}H]DA to give a final volume of 500 µl. Nonspecific uptake was determined in the presence of RO4-1284 (10 µM). Reactions were terminated by filtration, and radioactivity retained by the GF/B filters (presoaked for 2 h in assay buffer) was determined by liquid β-scintillation spectrometry.

2.2.5 Synaptosomal [^{3}H]DA Uptake

Lobelane analogs inhibition of [^{3}H]DA uptake into rat striatal synaptosomes was evaluated according to previously published methods (Teng et al., 1997). Rat striata were homogenized in ice-cold sucrose (pH 7.4), with 15 up-and-down strokes of a Teflon pestle homogenizer (clearance ≈ 0.005 inch). Homogenates were centrifuged (2000g for 10 min at 4 °C), and resulting supernatants were centrifuged again (20,000g for 17 min at 4 °C). Resulting pellets were resuspended in 2.4 ml of assay buffer (125 mM NaCl, 5 mM KCl, 1.5 mM MgSO4, 1.25 mM $CaCl_2$, 1.5 mM KH_2PO4, 10 mM α-D-glucose, 25 mM

HEPES, 0.1 mM EDTA, 0.1 mM pargyline, 0.1 mM ascorbic acid, saturated with 95% 0_2/5% CO_2, pH 7.4). Aliquots of the synaptosomal suspension (25 µl) were added to tubes containing assay buffer and a range of concentrations of analog (1 nM –100 µM), and incubated at 34 °C for 5 min. Samples were then placed on ice, and 50 µl [^{3}H]DA added to each tube (final concentration 0.1 µM), and incubated for 10 min at 34 °C. Assays were performed in duplicate in a total volume of 500 µl. Nonspecific uptake was determined in the presence of nomifensine (10 µM). Reactions were terminated by addition of 3 ml of ice-cold assay buffer and subsequent filtration. Radioactivity retained by the filters (presoaked for 2 hr in 0.5% PEI) was determined as previously described.

2.2.6 Vesicular [^{3}H]DA Release

(±)-GZ-729C and (±)-GZ-730B, the most potent analogs to inhibit VMAT2 function, were evaluated for their ability to release [^{3}H]DA from synaptic vesicles using previously described methods (Nickell et al., 2011a). Synaptic vesicle suspensions from rat striatum were prepared as previously described. The final pellets were resuspended in 2.7 ml of cold assay buffer and were preloaded with 300 µl of 0.3 µM [^{3}H]DA solution. After incubation at 37°C for 8 min, samples containing the vesicle suspension were centrifuged (100,000 g for 1 hour at 4°C), and the resulting pellet was resuspended in a final volume of 4.2 ml of assay buffer. Aliquots of [^{3}H]DA-preloaded vesicular suspensions (180 µl) were added to tubes in the absence or presence of various concentrations of inhibitors (1 nM-1 mM), and incubated at 37°C for 8 min. Reactions were terminated by adding

2.5 ml of ice-cold assay buffer and followed by rapid filtration. [^{3}H]DA remaining in the vesicles following exposure to analogs was retained by the filters. Analog-evoked [^{3}H]DA release for each concentration was determined by subtracting the radioactivity remaining in the presence of analog from the amount of radioactivity on the filter in the absence of analog (control).

To determine if (±)-GZ-729C and (±)-GZ-730B inhibit methamphetamine-induced [^{3}H]DA release from striatal synaptic vesicles, [^{3}H]DA-preloaded synaptic vesicles (180 µl) were added to duplicate tubes containing a range of concentrations (100 nM – 2 mM) of methamphetamine in the absence and presence of (±)-GZ-729C (10 nM – 1 µM) or (±)-GZ-730B (10 nM - 1µM), and incubated (final volume, 200 µl) for 8 min at 37 ºC. Samples were processed as previously described.

2.2.7 [^{3}H]Dofetilide Binding Assay to HERG Channels Expressed in HEK-293 Cells Membranes

The HEK-293 cell line stably expressing the human ERG (ether-a-go-go related gene) potassium channel (accession number U04270) was obtained at passage 11 (P11) from Millipore (CYL3006, lot 2, Billerica, MA). hERG-HEK cells were cultured according to the protocol provided by Millipore and were

(obtained from Life Technologies, Carlsbad, CA). Cells were incubated at 37 °C in a humidified atmosphere with 5% CO_2. Frozen aliquots of cells were transferred into T-75 cm^2 flasks and allowed to adhere for 4-8 h, after which the medium was replaced. The medium was replaced every 2 or 3 days, and routine passages were carried out every 6 or 7 days using 0.05% Trysin-EDTA (1X) with phenol (Life Technologies, Carlsbad, CA). Dissociated cells were seeded into new 150x25 mm culture dishes (surface area: 151.9 cm^2) obtained from BD Biosciences/Fisher Scientific (Florence, KY) at 2-3x10^6 cells per dish. Cells were passaged at least 3 times after thawing and were placed at 30 °C, 5% CO_2, for 40-48 hrs prior to membrane preparation. Cell membrane preparations were obtained 6 or 7 days after the last passage, at passages 20 or 21. Cells were at about 70-90% confluence.

Cell membrane were prepared based on previously described methods (Erickson et al., 1990; Fieber and Adams, 1991; Finlayson et al., 2001; Nooney et al., 1992) using cells grown from two different batches provided by Millipore. Cells were rinsed with pre-warmed (37 °C) HBSS (Life Technologies, Carlsbad, CA). Cells were then collected by scraping the 150 mm dishes using 13 ml plus 5 mL ice-cold 0.32 M sucrose with a Corning® cell scrapers blade L 1.8 cm (Sigma-Aldrich, St. Louis, MO). Harvested cell suspensions were poured into centrifuge tubes and homogenized on ice with a Teflon pestle using a Maximal Digital homogenizer (Fisher Scientific). Cells were then pelleted by centrifugation at 300 g and 800 g for 4 min each at 4 °C. Pellets were resuspended in 9 mL of ice-cold Milli-Q water. Osmolarity was restored by the addition of 1 mL of 500

mM Tris buffer (pH 7.4) and homogenization. Cellular suspensions were centrifuged again at 20,000 g for 30 min at 4 °C. Resulting pellets were homogenized in ~2 mL assay buffer composed of 50 mM Tris, 10 mM KCl, 1 mM $MgCl_2$ (pH 7.4), prepared the day prior to plasma membrane preparation and kept at 4 °C. Homogenization was performed using Pasteur glass pipettes and 2 ml tissue grinders (Kimble Chase, Vineland, NJ), and aliquots of cell membranes were stored at -80 °C. Cell membranes were thawed prior to assay, and protein content was determined using a Bradford Protein Assay (Bradford, 1976) and albumin from bovine serum (Sigma, St. Louis, MO, A2153) as the standard.

The potassium channel I_{Kr} coded by hERG plays a major role in phase 3 repolarization of ventricular myocytes by opposing the depolarizing Ca^{2+} influx during the plateau phase (Sanguinetti et al., 1995). Analogs with high affinity for this channel have potential to possess cardiac toxicity. Dofetilide, an antiarryhtmic agent, has been shown to preferentially block open (or activated) hERG transfected in HEK-293 cells (Snyders and Chaudhary, 1996). [^{3}H]Dofetilide binding assays were utilized to determine the affinity of analogs for this channel. [^{3}H]Dofetilide binding assays were performed at room temperature in a Tris buffer (50 mM Tris, 10 mM KCl, 1 mM $MgCl_2$; pH 7.4) as previously reported (Nooney et al., 1992). Buffer was prepared less than 48 h before the assay and kept at 4 °C. The reaction protocol was as follows: cell membrane suspension (4-10 µg) was added to tubes containing assay buffer, 25 µl of test compound or the corresponding vehicle and 25 µl of [^{3}H]dofetilide (5 nM, final concentration) for a final volume of 250 µl. Nonspecific binding was determined in

the presence of amitriptyline (1 mM). Amitriptyline has been reported to induce QT prolongation by blocking the current of heterologously expressed hERG potassium channels (Jo et al., 2000; Teschemacher et al., 1999). Assays were performed in duplicate. Reactions proceeded for 60 min at room temperature and were terminated by rapid filtration in a Brandel M-48 cell/membrane harvester using GF/B Glass Fiber FP-105 filters (Brandel Inc., Gaithersburg, MD) pre-soaked in 0.25% polyethylenimine solution (PEI, Fluka/Sigma-Aldrich, St. Louis, M) overnight. Filters were then washed three times with ~1 ml of ice-cold assay buffer. Filter discs that match the filter grids of the Brandel harvester were transferred into vials, and 5 ml scintillation cocktail (Research Products International Corporation, Mount Prospect, IL) was added. Radioactivity was determined by liquid scintillation spectrometry.

2.2.8 Inhibition of Methamphetamine-Evoked Endogenous DA Release

To determine if analogs inhibition of methamphetamine-induced DA release from vesicles translated to inhibition of methamphetamine-induced DA release from the intact striatal slice preparation, a previously described slice superfusion methodology was modified and employed (Gerhardt et al., 1989). In the endogenous release study, striatal slices (0.5 mm thickness) were prepared and incubated for 60 min in Krebs' buffer (118 mM NaCl, 4.7 mM KCl, 1.2 mM $MgCl_2$, 1.0 mM NaH_2PO_4, 1.3 mM $CaCl_2$, 11.1 mM α-D-glucose, 25 mM $NaHCO_3$, 0.11 mM L-ascorbic acid, and 0.004 mM EDTA, pH 7.4, saturated with 95% O_2/5% CO_2) at 34 °C in a metabolic shaker. Each slice was transferred to a glass

superfusion chamber and superfused with Krebs' buffer at 1 ml/min for 60 min prior to sample collection. Samples (1 ml) were collected for 1 min every 5 min during the 80 min superfusion period. Initially, two samples were collected in the absence of analog to determine basal DA outflow. Each slice was superfused for 30 min with a single concentration of (±)-GZ-729C (0, 0.1-10 μM) or (±)-GZ-730B (0, 0.1-30 μM) to determine analog-evoked fractional release. Then, methamphetamine (5 μM) was added to the buffer with analogs for 15 min, followed by an additional 25 min of superfusion with analogs alone. In each experiment, duplicate control slices were superfused with methamphetamine in the absence of analogs. Methamphetamine concentration (5 μM) and exposure time (15 min) were chosen to provide reliable DA release of sufficient quantity to allow evaluation of inhibition by analogs (Horton et al., 2011b). Samples (1 ml) were kept on ice. Perchloric acid (0.1 M; 50 μl) was added to each sample. Upon assay, 20 μl ascorbate oxidase (168 U/mg reconstituted to 81 U/ml) was added to a 500 μl aliquot of each sample. Samples were vortexed for 30 s and an aliquot (100 μl) was injected into the HPLC-EC system to determine amounts of DA and DOPAC in the superfusate samples.

The HPLC-EC system consisted of a pump (model 126; Beckman Coulter, Fullerton, CA), autosampler (model 508; Beckman Coulter), an ODS Ultrasphere C18 reverse-phase 80 × 4.6 mm, 3 μm column, and a Coulometric-II detector with guard cell (model 5020) maintained at + 0.60 V and analytical cell (model 5011) with E1 and E2 set at −150 mV and +350 mV, respectively (ESA Inc., Chelmsford, MA). HPLC mobile phase (flow rate, 1.2 ml/min) consisted of 0.07 M

citrate/0.1 M acetate buffer, containing 175 mg/L octylsulfonic acid sodium salt and 650 mg/L NaCl (pH 4.2) and 7% methanol. Separations were performed at room temperature, and 5 to 6 min was required to process each sample. Retention times of DA and DOPAC standards were used to identify respective peaks. Peak heights were used to quantify the detected amounts of DA and DOPAC based on standard curves. Detection limit for DA and DOPAC was 1 to 2 pg/100 µl.

2.2.9 Data analysis

For studies using vesicles, synaptosomes, and hERG-HEK-293 cell membranes, specific [^{3}H]DTBZ binding, [^{3}H]DA uptake, and [^{3}H]dofetilide binding were determined by subtracting the nonspecific binding or uptake from the total. Non-specific [^{3}H]DTBZ binding and vesicular [^{3}H]DA uptake were determined in the presence of RO4-1284. Non-specific synaptosomal [^{3}H]DA uptake and [^{3}H]dofetilide binding were determined in the presence of nomifensine and amitriptyline, respectively. Concentrations of analogs that produced 50% inhibition of maximal binding or uptake (IC_{50} values) or evoked 50% of [^{3}H]DA release (EC_{50} values) were determined from the concentration-response curves via an iterative curve-fitting program (Prism 5.0; GraphPad Software Inc., San Diego, CA). Inhibition constants (K_i values) were determined using the Cheng-Prusoff equation (Cheng and Prusoff, 1973). To determine if the structural changes to the lobelane molecule increased affinity for the VMAT2 binding site, the VMAT2 uptake site and for DAT, two-tailed t tests were performed to

compare the log K_i value for each analog to that obtained for lobelane, the parent compound, in each assay. To assess if analog affinity at the DTBZ site on VMAT2 was associated with analog affinity at the [^{3}H]DA uptake on VMAT2, Spearman correlation of the K_i values for the [^{3}H]DTBZ binding and K_i values for the vesicular [^{3}H]DA uptake was conducted. For vesicular [^{3}H]DA release assay, F test was performed to compare the fits of two equations, the one-site binding model and the two-site binding model. Analogs inhibition of methamphetamine-evoked vesicular [^{3}H]DA release was analyzed by two-way repeated-measures ANOVA, with concentration of analogs and methamphetamine as repeated measure factors. If a significant analogs x methamphetamine interaction was found, one-way ANOVAs followed by Dunnetts's tests were performed at each methamphetamine concentration to determine the analog concentrations that decreased methamphetamine-evoked [^{3}H]DA release. To further elucidate the mechanism of analogs inhibition of methamphetamine-evoked [^{3}H]DA release, a Lew and Angus plot of the pEC_{50} values as a function of log analog concentration was generated, and the data underwent linear regression analysis using Prism 5.0 (GraphPad Software Inc.). Difference from unity of the regression slope (95% confidence intervals) revealed if the interaction was at the same site, i.e., orthosteric; or at two different sites, i.e., allosteric (Kenakin, 2006b).

For the methamphetamine-evoked endogenous DA release, DA and DOPAC concentrations in each superfusate sample were divided by the respective striatal slice weight to obtain fractional release. Basal endogenous DA and DOPAC were determined as the average fractional release in the two

superfusate samples collected just before addition of analog to the buffer. To determine if the analog in a concentration and time dependent manner evoked fractional DA and DOPAC release, two-way repeated-measures ANOVA was performed on release in samples obtained prior to addition of methamphetamine to the buffer. If concentration × time interactions were found, one-way ANOVAs were performed at each time point to determine the analog concentrations that evoked fractional DA and DOPAC release. To determine if the analog in a concentration and time dependent manner inhibited the effect of methamphetamine on fractional DA and DOPAC release, two-way repeated-measures ANOVA was performed on release data in samples after the addition of methamphetamine to the buffer. If concentration × time interactions were found, one-way ANOVAs were performed at each time point to determine the analog concentrations that inhibited methamphetamine-evoked release.

2.3 Results

2.3.1 Inhibition of [^{3}H]DTBZ binding at VMAT2

In order to determine analogs affinity for the DTBZ site on VMAT2, [^{3}H]DTBZ binding inhibition assay was performed. Concentration-response curves for the series of lobelane analogs, and for the standards lobelane, lobeline, and RO4-1284 to inhibit [^{3}H]DTBZ binding to whole brain membranes are illustrated in Figure 2.3. K_i and I_{max} values from the concentration-response curves are provided in Table 2.1. The standard compounds, RO4-1284, lobelane and lobeline had K_i values of 0.016 ± 0.0013, 0.97 ± 0.19 and 3.5 ± 1.0 μM,

consistent with previous results (Nickell et al., 2011b). All compounds inhibited [^{3}H]DTBZ binding within the concentration range utilized (0.1 nM -1 mM) except for GZ-632A (K_i > 100 μM), an analog afforded by removing methylene linkers at both C-6 and C-2 position of the piperidine ring. All the other compounds showed affinity for VMAT2 in the concentration range of 0.88-62.5 μM. The results indicate that to maintain high binding affinity at VMAT2, lobelane analogs with the methyl substituent at the N atom should contain one to three methylene units at the C-6 linker and two or three methylene units at the C-2 linker, nor-lobelane analog should contain one and three methylene units at the C-6 and C-2 linker, respectively.

The symmetrical lobelane analogs exhibited affinity either not different from or lower than that for lobelane (Figure 2.3, top panel). GZ-709C, the symmetrical N-methylated lobelane analog with one methylene unit on each side of the piperidine ring, exhibited 11-fold lower affinity (K_i = 10.5 ± 3.36 μM, p < 0.01) compared to lobelane. The corresponding nor-analog of GZ-709C, GZ-709B, exhibited 7-fold lower affinity (K_i = 7.68 ± 1.44 μM, p < 0.05) compared to lobelane. GZ-712C, the other symmetrical N-methylated analog with three methylene units exhibited affinity (K_i = 1.00 ± 0.23 μM) that was not different from lobelane. The corresponding nor-analog of GZ-712C, GZ-712B, exhibited 4-fold lower affinity (K_i = 4.50 ± 1.02 μM, p < 0.05) compared to lobelane.

The non-symmetrical lobelane analogs exhibited affinity either not different from or lower than that for lobelane (Figure 2.3, middle panel). The non-

symmetrical N-methylated lobelane analogs with no methylene linker at the C-6 position of the piperidine ring [(±)-GZ-731B, (±)-GZ-725A, and (±)-GZ-726A] exhibited 14-, 17-, and 64-fold lower affinity (K_i = 13.6 ± 8.1 µM, 16.1 ± 4.1 µM, and 62.5 ± 16.6 µM, respectively) compared to lobelane ($p < 0.05$ for all). The corresponding nor-analogs [(±)-GZ-731A, (±)-GZ-713A, and (±)-GZ-714A] exhibited 24-, 29-, and 29-fold lower affinity (K_i = 24.1 ± 6.1 µM, 28.4 ± 7.3 µM, and 28.6 ± 2.4 µM, respectively) compared to lobelane ($p < 0.05$ for all). Other non-symmetrical N-methylated analogs [(±)-GZ-730C, (±)-GZ-729C, and (±)-GZ-644C] with 1-2 and 2-3 methylene units at the C-6 and C-2 position of the piperidine ring showed affinity (K_i = 1.62 ± 0.39 µM, 2.77 ± 1.77 µM, and 0.88 ± 0.30 µM, respectively) not different from lobelane. The corresponding nor-analog of (±)-GZ-730C, (±)-GZ-730B, showed affinity (K_i = 1.13 ± 0.28 µM) not different from lobelane. The corresponding nor-analogs of (±)-GZ-729C and (±)-GZ-644C, (±)-GZ-729B and (±)-GZ-644B, exhibited 12- and 4-fold lower affinity (K_i = 12.2 ± 0.2 µM and 4.60 ± 0.56 µM, respectively) compared to lobelane ($p < 0.05$ for both).

2.3.2 Inhibition of [^{3}H]DA uptake at VMAT2

In order to determine analogs affinity for the DA translocation site on VMAT2, vesicular [^{3}H]DA uptake inhibition assay was performed. Concentration-response curves of lobelane analogs and the standards lobelane, lobeline, and RO4-1284 are illustrated in Figure 2.4. K_i and I_{max} values are provided in Table 2.1. The standard compounds, RO4-1284, lobelane and lobeline had K_i values for inhibition of [^{3}H]DA uptake of 0.041 ± 0.008, 0.040 ± 0.004, and 0.56 ± 0.03

µM, consistent with previous results (Nickell et al., 2010). All compounds inhibited VMAT2 function completely within the concentration range utilized (0.1 nM-100 µM) except for GZ-632A (I_{max} = 74.6%), a compound afforded by removing the methylene linkers on both sides of the piperidine ring. The range of K_i values for the series of racemic analogs was 0.024 to 4.55 µM. The results indicated that to maintain high affinity to inhibit VMAT2 function, lobelane analogs with the methyl substituent at the N atom should contain one or two methylene units at the C-6 linker and one to three methylene units at the C-2 linker, nor-lobelane analogs should contain one or three methylene units at both C-6 and C-2 linker.

The symmetrical lobelane analogs exhibited affinity either not different from or lower than that for lobelane (Figure 2.4, top panel). GZ-632A, the N-methylated analog with no methylene unit, showed 114-fold lower affinity (K_i = 4.55 ± 0.96 µM, $p < 0.05$) in comparison with lobelane. GZ-712C, the N-methylated analog with 3 methylene units in both linkers exhibited 2-fold lower affinity (K_i = 0.078 ± 0.013 µM, $p < 0.01$) compared to lobelane. The corresponding nor-analog of GZ-712C, GZ-712B, exhibited affinity (K_i = 0.049 ± 0.010 µM) not different from lobelane. GZ-709C, the N-methylated analog with 1 methylene in both linkers exhibited affinity (K_i = 0.046 ± 0.007 µM) not different from lobelane. The corresponding nor-analog of GZ-709C, GZ-709B, exhibited affinity (K_i = 0.036 ± 0.007 µM) not different from lobelane.

The non-symmetrical lobelane analogs exhibited a wide range of affinity

(0.024-1.42 µM) for the DA translocation site on VMAT2 (Figure 2.4, middle (Figure 2.4, middle panel). The non-symmetrical N-methylated lobelane analogs [(±)-GZ-731B, (±)-GZ-725A and (±)-GZ-726A], compounds afforded by removing the methylene unit at the C-6 position of the piperidine ring, exhibited 6-, 36- and 10-fold lower affinity (K_i = 0.25 ± 0.05 µM, 1.42 ± 0.11 µM, and 0.41 ± 0.03 µM, respectively) compared to lobelane ($p < 0.05$). The corresponding nor-analogs [(±)-GZ-731A, (±)-GZ-713A, and (±)-GZ-714A] exhibited 13-, 24- and 6-fold lower affinity (K_i = 0.52 ± 0.05 µM, 0.97 ± 0.18 µM, and 0.24 ± 0.03 µM, respectively) compared to lobelane ($p < 0.05$). Non-symmetric N-methylated analogs [(±)-GZ-730C and (±)-GZ-644C] with 1,3 and 2,3 methylene units in the linkers on each side of the piperidine exhibited affinity (K_i = 0.036 ± 0.003 µM and 0.062 ± 0.005 µM) not different from lobelane. The corresponding nor-analog of (±)-GZ-730C, (±)-GZ-730B, exhibited the highest affinity [K_i = 0.024 ± 0.002 µM, $t_{(6)} = 4.38$, $p < 0.01$] and was different from that for lobelane. The corresponding nor-analog of (±)-GZ-644C, (±)-GZ-644B, exhibited 2-fold lower affinity (K_i = 0.067 ± 0.005 µM) compared to lobelane ($p < 0.05$). (±)-GZ-729C, the non-symmetrical N-methylated lobelane analog with 1,2 methylene units in the linkers, exhibited 2-fold higher affinity [K_i = 0.025 ± 0.003 µM, $t_{(6)} = 3.44$, $p < 0.05$] compared to lobelane. The corresponding nor-analog of (±)-GZ-729C, (±)-GZ-729B, exhibited 2-fold lower affinity (K_i = 0.093 ± 0.009 µM) compared to lobelane.

For the non-symmetrical lobelane analogs with the cyclohexane substituent (Figure 2.4, bottom panel), (±)-GZ-725B, the N-methylated analog with 0,2 methylene units in the linkers exhibited 7-fold higher affinity [K_i = 0.22 ±

0.02 µM, $t_{(6)}$ = 14.2, p < 0.0001] compared to (±)-GZ-725A, the corresponding analog with a phenyl substituent. The corresponding nor-analog of (±)-GZ-725B, (±)-GZ-713B, exhibited 5-fold higher affinity [K_i = 0.20 ± 0.01 µM, $t_{(6)}$ = 7.26, p < 0.001] compared to (±)-GZ-713A (K_i = 0.97 ± 0.18 µM), the corresponding analog with a phenyl substituent. The cyclohexane substituent did not increase affinity for (±)-GZ-726B, the N-methylated analog with 0,3 methylene units in the linkers, or its corresponding nor-analog, (±)-GZ-714B.

Most of the compounds in this series exhibited affinity to inhibit vesicular [^{3}H]DA uptake at an order of magnitude greater than the respective binding affinity, while RO4-1284 exhibited affinity not different between binding and uptake assays. The K_i values for the lobelane analogs in these two assays were positively correlated (Spearman r = 0.68; p < 0.01, Figure 2.5).

2.3.3 Selectivity of (±)-GZ-729C, and (±)-GZ-730B for VMAT2 over DAT and hERG channel

In order to determine analogs selectivity at VMAT2 over DAT and hERG channels, DAT [^{3}H]DA uptake inhibition assay and [^{3}H]dofetilide binding inhibition assay was performed. Concentration-response of (±)-GZ-729C and (±)-GZ-730B, and IC_{50} values to inhibit specific [^{3}H]DTBZ binding, [^{3}H]dofetilide binding and [^{3}H]DA uptake are illustrated in the top and bottom panels in Figure 2.6, respectively. Both (±)-GZ-729C and (±)-GZ-730B inhibited [^{3}H]DTBZ binding, [^{3}H]dofetilide binding and [^{3}H]DA uptake completely within the concentration range utilized (0.1 nM-100 µM). IC_{50} value of (±)-GZ-729C (0.050 ± 0.0018 µM,

top panel in Figure 2.6) to inhibit [^{3}H]DA uptake at VMAT2 was 112-fold lower than that for [^{3}H]DTBZ binding, 22-fold lower than that for [^{3}H]dofetilide binding, and 20-fold lower than that for [^{3}H]DA uptake at DAT. IC_{50} value of (±)-GZ-730B (0.048 ± 0.0038 μM, bottom panel in Figure 2.6) to inhibit [^{3}H]DA uptake at VMAT2 was 47-fold lower than that for [^{3}H]DTBZ binding, 50-fold lower than that for [^{3}H]dofetilide binding, and 102-fold lower than that for [^{3}H]DA uptake at DAT.

2.3.4 Release of [^{3}H]DA from striatal synaptic vesicles

In order to determine analogs ability to redistribute DA from synaptic vesicles to cytosol, vesicular [^{3}H]DA release assay was performed. Two analogs with the highest affinity in the vesicular [^{3}H]DA uptake assay were evaluated for their ability to evoke [^{3}H]DA release from striatal synaptic vesicles. Concentration-response curves and EC_{50} and E_{max} values for lobelane, lobeline, methamphetamine, (±)-GZ-729C, and (±)-GZ-730B to evoke [^{3}H]DA release from synaptic vesicles are provided in Figure 2.7. EC_{50} values of lobelane, lobeline, and methamphetamine were 0.26 ± 0.031, 13 ± 7.4, and 19 ± 4.1 μM, respectively (top panel in Figure 2.7), consistent with previous results (Nickell et al., 2011b). The EC_{50} value for lobelane was 50-fold lower than that for lobeline [$t_{(6)} = 3.86$, $p < 0.01$], and 35-fold lower than that for methamphetamine [$t_{(6)} = 11.1$, $p < 0.001$]. Both analogs released [^{3}H]DA from the synaptic vesicles in a biphasic manner [$F_{(2, 39)} = 4.50$ for (±)-GZ-729C, $p < 0.05$; $F_{(2, 39)} = 8.22$ for (±)-GZ-730B, $p < 0.01$; bottom panel in Figure 2.7]. No difference of the High EC_{50} [60 ± 40 nM for (±)-GZ-729C, 110 ± 63 nM for (±)-GZ-730B], or the Low EC_{50} [13 ± 6.2

μM for (±)-GZ-729C, 15 ± 7.9 μM for (±)-GZ-730B] was found between (±)-GZ-729C and (±)-GZ-730B. Similarly, no difference of the High E_{max} [24 ± 3.4 for (±)-GZ-729C, 27± 4.7 for (±)-GZ-730B], or the Low E_{max} [63 ± 4.8 for (±)-GZ-729C, 65 ± 5.6 for (±)-GZ-730B] was found between (±)-GZ-729C and (±)-GZ-730B.

2.3.5 (±)-GZ-729C and (±)-GZ-730B inhibited methamphetamine-evoked [^{3}H]DA release from striatal synaptic vesicles

To determine the ability of (±)-GZ-729C and (±)-GZ-730B to inhibit effect of methamphetamine at synaptic vesicles, methamphetamine-evoked vesicular [^{3}H]DA release was determined in the presence of the analogs. The concentration response of methamphetamine-evoked vesicular [^{3}H]DA release in the presence of (±)-GZ-729C and (±)-GZ-730B is illustrated in the top and bottom panels, respectively, in Figure 2.8. For (±)-GZ-729C, two-way repeated measures ANOVA revealed main effects of methamphetamine [$F_{(10, 120)} = 886$, $p < 0.001$] and (±)-GZ-729C [$F_{(3, 12)} = 50.9$, $p < 0.001$], and a methamphetamine × (±)-GZ-729C interaction [$F_{(30, 120)} = 13.0$, $p < 0.001$]. (±)-GZ-729C inhibited methamphetamine-evoked [^{3}H]DA release at 0.1 μM [$F_{(3, 12)} = 5.04$, $p < 0.05$], 1 μM [$F_{(3, 12)} = 4.84$, $p < 0.05$], 3 μM [$F_{(3, 12)} = 8.06$, $p < 0.01$], 10 μM [$F_{(3, 12)} = 56.3$, $p < 0.0001$], 30 μM [$F_{(3, 12)} = 63.8$, $p < 0.0001$], 100 μM [$F_{(3, 12)} = 103$, $p < 0.0001$], 200 μM [$F_{(3, 12)} = 51.0$, $p < 0.0001$], 500 μM [$F_{(3, 12)} = 44.0$, $p < 0.0001$], and 1 mM [$F_{(3, 12)} = 26.5$, $p < 0.0001$]. Post hoc analyses revealed that (±)-GZ-729C at 100 nM and 1 μM decreased [^{3}H]DA release induced by 0.1-1000 μM methamphetamine. From the methamphetamine concentration-response curves,

EC_{50} and E_{max} values in the absence and presence of (±)-GZ-729C were generated and provided in Table 2.2. EC_{50} and E_{max} values for methamphetamine alone were 9.0 ± 2.9 µM and 83 ± 1.4%, respectively, consistent with a previous study (Nickell et al., 2010). Increasing concentrations of (±)-GZ-729C contributed to a rightward shift of methamphetamine concentration-response curve with no inhibition of maximum release. (±)-GZ-729C (100 nM and 1 µM) increased the log EC_{50} values by 5- and 19-fold, respectively, [$F_{(3,12)} = 13.6$, $p < 0.001$]. Lew and Angus analysis revealed a linear fit ($R^2 = 0.95$, $p < 0.0001$) with a slope of -0.62 and a 95% confidence interval of -0.72 and -0.52, which did not overlap with unity (inset in top panel in Figure 2.8), suggesting that (±)-GZ-729C inhibited methamphetamine-evoked [^{3}H]DA release in a surmountable, allosteric manner (Kenakin, 2006).

For (±)-GZ-730B, two-way repeated measures ANOVA revealed main effects of methamphetamine [$F_{(10, 110)} = 156$, $p < 0.001$] and (±)-GZ-730B [$F_{(3, 11)} = 9.99$, $p < 0.01$], and a methamphetamine × (±)-GZ-730B interaction [$F_{(30, 110)} = 3.81$, $p < 0.001$]. (±)-GZ-730B inhibited methamphetamine at 3 µM [$F_{(3, 11)} = 4.54$, $p < 0.05$], 10 µM [$F_{(3, 11)} = 19.3$, $p < 0.0001$], 30 µM [$F_{(3, 11)} = 8.02$, $p < 0.01$], 100 µM [$F_{(3, 11)} = 71.0$, $p < 0.0001$], 200 µM [$F_{(3, 11)} = 7.88$, $p < 0.01$] and 1 mM [$F_{(3, 11)} = 7.13$, $p < 0.01$]. (±)-GZ-730B at 100 nM and 1 µM inhibited [^{3}H]DA release induced by methamphetamine at 10-100 µM and 3-1000 µM concentration ranges, respectively. From the methamphetamine concentration-response curves, EC_{50} and E_{max} values in the absence and presence of (±)-GZ-730B were generated and provided in Table 2.2. EC_{50} and E_{max} values for methamphetamine

alone were 5.8 ± 1.0 µM and 79 ± 3.7%, respectively, consistent with a previous study (Nickell et al., 2010). Increasing concentrations of (±)-GZ-730B contributed to a rightward shift of the methamphetamine concentration-response curve with no inhibition of the maximum release like (±)-GZ-729C. (±)-GZ-730B (1 µM) increased the log EC_{50} values by 40-fold [$F_{(3,11)} = 48.3$, $p < 0.001$]. Lew and Angus analysis revealed a linear fit ($R^2 = 0.94$, $p < 0.0001$) with a slope of -0.63 and a 95% confidence interval of -0.74 and -0.53, which did not overlap with unity (inset in bottom panel in Figure 2.8), suggesting that (±)-GZ-730B inhibited methamphetamine-evoked [^{3}H]DA release in a surmountable, allosteric manner (Kenakin, 2006).

2.3.6 Lack of (±)-GZ-729C inhibition of methamphetamine-evoked endogenous fractional DA release from striatal slices

To determine the ability of (±)-GZ-729C to inhibit effect of methamphetamine at striatal slices, methamphetamine-evoked endogenous DA release from striatal slices was determined in the presence of the analog. The time course of the concentration-dependent effect of (±)-GZ-729C alone on fractional DA release across the first 15-40 min of superfusion is illustrated in the top panel of Figure 2.9. Two-way repeated measures ANOVA revealed main effects of (±)-GZ-729C [$F_{(5,13)} = 10.6$, $p < 0.0001$] and time [$F_{(5,9)} = 5.36$, $p < 0.05$]. The interaction of concentration × time was not significant. (±)-GZ-729C (10 µM) released DA at 30 min [$F_{(5,20)} = 8.23$, $p < 0.001$] and 35 min [$F_{(5,20)} = 5.65$, $p < 0.01$]. Analysis of fractional DA release following the addition of

methamphetamine to the superfusion buffer 45-55 min in the absence and presence of (±)-GZ-729C revealed that the concentration effect and the concentration × time interaction were not significant; however a main effect of time [$F_{(2, 16)} = 13.9$; $p < 0.0001$] was found. Thus, methamphetamine increased fractional DA release from superfused striatal slices across the 15 min exposure period in the absence and presence of (±)-GZ-729C; however, (±)-GZ-729C did not inhibit the effect of methamphetamine to release DA.

The time course of the concentration-dependent effect of (±)-GZ-729C alone on fractional release of DOPAC across the first 15-40 min of superfusion is illustrated in bottom panel of Figure 2.9. The main effect of (±)-GZ-729C and time were significant [$F_{(5, 20)} = 5.34$, $p < 0.01$; $F_{(5, 16)} = 23.7$, $p < 0.0001$, respectively], and the interaction of concentration × time was not significant. (±)-GZ-729C increased fractional release of DOPAC at 25 min [$F_{(5, 21)} = 3.85$, $p < 0.05$], 30 min [$F_{(5, 21)} = 15.5$, $p < 0.0001$], 35 min [$F_{(5, 21)} = 7.59$, $p < 0.001$], and 40 min [$F_{(5, 20)} = 6.41$, $p < 0.01$]. (±)-GZ-729C at 3 and 10 µM increased release of DOPAC at 40 min and 25-40 min, respectively. The time course of the concentration-dependent effect of (±)-GZ-729C on fractional release of DOPAC across the 45-50 min of superfusion in the presence of methamphetamine is illustrated in bottom panel of Figure 2.9 as well. The main effect of (±)-GZ-729C was significant [$F_{(5, 21)} = 8.41$, $p < 0.0001$], and time and interaction of concentration × time were not significant. (±)-GZ-729C increased fractional release of DOPAC at 45 min [$F_{(5, 21)} = 5.10$, $p < 0.01$], 50 min [$F_{(5, 21)} = 10.2$, $p < 0.0001$], and 55 min [$F_{(5, 21)} = 6.91$, $p < 0.001$].

(±)-GZ-729C at 3 and 10 μM increased release of DOPAC 50-80 min, 45-80 min, respectively.

2.3.7 Lack of (±)-GZ-730B inhibition of methamphetamine-evoked endogenous fractional DA release from striatal slices

To determine the ability of (±)-GZ-730B to inhibit effect of methamphetamine at striatal slices, methamphetamine-evoked endogenous DA release from striatal slices was determined in the presence of the analog. The time course of concentration-dependent effect of (±)-GZ-730B alone on fractional DA release across the first 15-40 min of superfusion is illustrated in the top panel of Figure 2.10. The effects of (±)-GZ-730B, time, and the interaction of concentration × time were not significant. Analysis of fractional DA release following the addition of methamphetamine to the superfusion buffer 45-55 min in the absence and presence of (±)-GZ-730B revealed that the concentration effect and the concentration × time interaction were not significant; however a main effect of time [$F_{(2, 33)} = 41.2$; $p < 0.0001$] was found. Thus, methamphetamine increased fractional DA release from superfused striatal slices across the 15 min exposure period in the absence and presence of (±)-GZ-730B; however, similar to (±)-GZ-729C, (±)-GZ-730B did not inhibit the effect of methamphetamine to release DA.

The time course of concentration-dependent effect of (±)-GZ-730B alone on fractional release of DOPAC across the first 15-40 min of superfusion is illustrated in bottom panel of Figure 2.10. The main effect of (±)-GZ-730B and

time were significant [$F_{(5, 29)} = 114$, $p < 0.0001$; $F_{(5, 25)} = 9.12$, $p < 0.0001$, respectively], and the interaction of concentration × time was not significant. (±)-GZ-730B increased fractional release of DOPAC at 30 min [$F_{(5, 33)} = 3.65$, $p < 0.01$], 35 min [$F_{(5, 33)} = 5.65$, $p < 0.001$], and 40 min [$F_{(5, 33)} = 8.01$, $p < 0.0001$]. (±)-GZ-730B at 10 and 30 µM increased release of DOPAC 35-40 min and 30-40 min, respectively. The time course of the concentration-dependent effect of (±)-GZ-730B on fractional release of DOPAC across the 45-50 min of superfusion in the presence of methamphetamine is illustrated in bottom panel of Figure 2.10 as well. The main effect of (±)-GZ-730B was significant [$F_{(5, 33)} = 9.76$, $p < 0.0001$], and time and interaction of concentration × time were not significant. (±)-GZ-730B increased fractional release of DOPAC at 45 min [$F_{(5, 33)} = 6.59$, $p < 0.001$], 50 min [$F_{(5, 33)} = 9.00$, $p < 0.0001$], and 55 min [$F_{(5, 33)} = 12.3$, $p < 0.0001$]. (±)-GZ-730B at 10 and 30 µM increased release of DOPAC 45-80 min.

2.4 Discussion

The objective of this study was to modify the length of the methylene linkers of the lobelane molecule to afford a series of analogs in the search for potent ligands at VMAT2 as the target to inhibit methamphetamine action at this site and prevent methamphetamine-evoked [^{3}H]DA and endogenous DA release. Importantly, all the asymmetrical analogs in this series are racemic containing same amount of enantiomers. The enantiomers of the racemic compounds might exhibit different affinities to inhibit VMAT2 function and methamphetamine-evoked [^{3}H]DA release from striatal synaptic vesicles and endogenous DA

release from striatal slices. The results indicate that the linkers between the central piperidine and the phenyl rings of the lobelane analogs that contain one methylene units at the C-6 position and one or three methylene units at the C-2 position of the piperidine ring maintain high affinity at VMAT2 to inhibit binding and function. Introducing a cyclohexane substituent at the C-6 position of the piperidine ring improved affinity of one analog [(±)-GZ-725A], the analog with 0,2 methylene units in the linkers, in the VMAT2 binding and uptake assay. A positive correlation was found between the K_i values in the [^{3}H]DTBZ binding and [^{3}H]DA uptake assays, as would be expected if analogs inhibition of VMAT2 function were due to binding to the DTBZ site on VMAT2. However, GZ-632A, the analog with no linkers, inhibited VMAT2 function but exhibited complete loss of affinity at the DTBZ site on VMAT2, suggesting an interaction with the substrate translocation site instead of the DTBZ binding site on VMAT2 (Nickell et al., 2011a; Scherman and Henry, 1984). Among all analogs, (±)-GZ-730B was the most potent and selective analog to inhibit VMAT2 function and was identified as the lead. Furthermore, (±)-GZ-730B inhibited methamphetamine-evoked [^{3}H]DA release from the vesicle preparation via a surmountable allosteric interaction with VMAT2. However, (±)-GZ-730B did not inhibit methamphetamine-evoked endogenous DA release from striatal slices. Different tissue preparation, striatal synaptic vesicles versus slices, and different label, [^{3}H]DA versus endogenous DA, might contribute to the contradictory results. In addition, poor water solubility of the lead analog prevented further investigation *in vivo* in behavioral studies using rats.

The [^{3}H]DTBZ binding assay provides important information regarding the affinity of the analogs at the DTBZ site on VMAT2. N-methylated analogs with one to three methylene units at the C-6 and two or three methylene units at the C-2 position of the piperidine ring [(±)-GZ-712C, (±)-GZ-729C, (±)-GZ-730C, and (±)-GZ-644C] exhibited affinity that was not different compared to that of lobelane. For N-methylated analogs, removing the methylene linker at the C-6 position [(±)-GZ-731B, (±)-GZ-725A, and (±)-GZ-726A] contributed to a decreased affinity and removing both linkers [(±)-GZ-632A] resulted in complete loss of affinity at the DTBZ site on VMAT2. Thus, when the methylene linker between the phenyl ring and the piperidine ring was removed, this structural change afforded a more rigid structure which appeared detrimental for the affinity at the DTBZ site on VMAT2. For N-methylated analogs, a cyclohexane substituent at C-6 position of the piperidine ring provided a 13-fold increased affinity for an analog with three methylene units at the C-2 position [(±)-GZ-726B], but only 2-fold increase for the analog with two methylene units [(±)-GZ-725B]. Thus, when the phenyl substituent was replaced by the cyclohexane, this afforded a more flexible structure providing a higher affinity at the DTBZ site on VMAT2 for N-methylated analogs with longer methylene linkers.

All nor-analogs except for (±)-GZ-730B (the nor-analog with 1,3 methylene units in the linkers) exhibited lower affinity compared to lobelane, suggesting that the methyl substituent at the N atom is important for maintaining analog affinity at the DTBZ site on VMAT2. Similar to the N-methylated analogs, removing the methylene linker at the C-6 position of the piperidine ring in nor-analogs [(±)-GZ-

731A, (±)-GZ-713A, and (±)-GZ-714A] contributed to a decreased affinity for the DTBZ site on VMAT2, suggesting a similar detrimental effect of the more rigid structure. However, the cyclohexane substituent at C-6 position did not improve the affinity of the nor-analogs [(±)-GZ-713B and (±)-GZ-714B] for the DTBZ site on VMAT2.

Affinity for the substrate translocation site on VMAT2 which is responsible for DA uptake provides important information related to transporter function. Similar to the binding assay, for N-methylated analogs, a more rigid structure afforded by removing the methylene linker [(±)-GZ-731B, (±)-GZ-725A, and (±)-GZ-726A] was detrimental for affinity for the substrate translocation site on VMAT2. A cyclohexane substituent at C-6 position of the piperidine ring provided a 7-fold increased affinity for an N-methylated analog with two methylene units at the C-2 position [(±)-GZ-725B], but no increase for the N-methylated analog with three methylene units [(±)-GZ-726B]. Thus, when the phenyl substituent was replaced by the cyclohexane, in contrast to the binding study, this afforded a more flexible structure providing a higher affinity at the substrate translocation site on VMAT2 for the N-methylated analogs with short methylene linkers.

For nor-analogs, similar to the N-methylated analogs, removing the methylene linker at the C-6 position [(±)-GZ-731A, (±)-GZ-713A, and (±)-GZ-714A] contributed to a decreased affinity for the substrate translocation site on VMAT2, suggesting a similar detrimental effect of the more rigid structure. Similar to the N-methylated analogs, a cyclohexane substituent at C-6 position of the

piperidine ring provided a 5-fold increased affinity for an nor-analog with two methylene units at the C-2 position [(±)-GZ-713B], but no increase for the nor-analog with three methylene units [(±)-GZ-714B]. Thus, similar to the N-methylated analogs, replacing phenyl substituent with the cyclohexane also afforded a more flexible structure providing a higher affinity at the substrate translocation site on VMAT2 for the nor-analogs with short methylene linkers.

Binding affinity of N-1,2-dihydroxypropyl lobelane analogs, meso-transdiene analogs, and phenyl ring-substituted lobelane analogs at the [^{3}H]DTBZ site on VMAT2 has been shown to not be associated with the affinity for the translocation site on the transporter evaluated by inhibition of function, such that no correlation between inhibition of binding and function was found (Horton et al., 2011a; Horton et al., 2011b; Nickell et al., 2011a). However, a positive correlation was found between the binding affinity and functional affinity in the current study, indicating that inhibition of VMAT2 function might be due to inhibition of binding at the DTBZ site on VMAT2. DTBZ is a noncompetitive inhibitor at VMAT2 and interacts with a site that is different from the DA translocation site on the transporter (Scherman and Henry, 1984). Thus, for this series of analogs, the interaction with the DTBZ binding site on VMAT2 may be responsible for the inhibition of DA uptake (VMAT2 function), i.e., through an allosteric effect. Interestingly, binding affinity for RO4-1284 was not different from its affinity in the functional assay, suggesting that inhibitors at the DTBZ site on VMAT2 were equipotent in the binding and the functional assay. Lobeline and nor-lobelane exhibited 5-fold greater affinity in the functional assay relative to the

binding assay, suggesting that lobeline and lobelane might inhibit VMAT2 function via a mechanism different from TBZ analog RO4-1284. In the current study, all lobelane analogs in this study exhibited at least 10-fold greater affinity in the functional assay relative to the binding assay. In general, compounds interacting with VMAT2 can be classified as either uptake inhibitors or substrates. In terms of substrates, higher potencies were observed in VMAT2 functional assays relative to binding assays, while equivalent potencies were observed in both assays for uptake inhibitors (Andersen, 1987; Nickell et al., 2011a; Partilla et al., 2006). All the analogs in this study exhibited higher affinities in the VMAT2 functional assay in relative to the binding assay, suggesting that they are substrates for VMAT2. In addition, GZ-632A inhibited VMAT2 function but exhibited complete loss of affinity for the DTBZ site on VMAT2, suggesting an interaction of the analog with the substrate translocation site on VMAT2. Thus, lobelane analogs in the current study might bind the substrate site at which DA is transported into synaptic vesicles to inhibit DA uptake.

Inhibition of DAT has been associated with abuse liability (Howell and Wilcox, 2001). To identify lead compounds, selectivity for VMAT2 versus DAT was determined for the two most potent analogs in the uptake assay, (±)-GZ-729C and (±)-GZ-730B. The selectivity of (±)-GZ-729C and (±)-GZ-730B for VMAT2 over DAT was 20 and 102-fold, respectively, indicating that these compounds would be predicted to not have abuse liability. The selectivity of (±)-GZ-729C and (±)-GZ-730B for VMAT2 over the hERG channel was determined to be 22 and 50-fold, indicating that these leads would be predicted to not

possess cardiac toxicity. Thus, the most potent and selective analog at VMAT2 were demonstrated to be selective over both DAT and the hERG channel. Since selectivity was greatest with (±)-GZ-730B, this compound was selected for lead compound status.

(±)-GZ-729C and (±)-GZ-730B were evaluated in the vesicular [^{3}H]DA release assay to determine their ability to redistribute presynaptic DA by interacting with VMAT2. (±)-GZ-729C and (±)-GZ-730B evoked [^{3}H]DA release from synaptic vesicles in a biphasic manner, indicating an interaction of the analogs with two different sites (a high-affinity release site and a low-affinity release site) on VMAT2. Our group has suggested that inhibition of methamphetamine at VMAT2 could contribute to the inhibition in methamphetamine self-administration in rats (Horton et al., 2012). Thus, (±)-GZ-729C and (±)-GZ-730B were evaluated for their ability to inhibit methamphetamine-evoked [^{3}H]DA release form synaptic vesicles. (±)-GZ-729C and (±)-GZ-730B produced a rightward shift of the methamphetamine concentration response with no influence alteration in the amount of DA release at maximum. The Lew and Angus regression revealed a slope different from unity, indicating an allosteric interaction. Thus, (±)-GZ-729C and (±)-GZ-730B inhibited methamphetamine-evoked [^{3}H]DA release via an interaction with VMAT2 by surmountable allosteric mechanism (Kenakin, 2006a). Thus, binding of (±)-GZ-729C and (±)-GZ-730B to a site different from the methamphetamine binding site on VMAT2 resulted in a conformational change in the transporter to decrease affinity for methamphetamine, but did not alter the efficacy of

methamphetamine to release DA (Figure 2.11). Four different sites on VMAT2 have been suggested by our results: an extravesicular DTBZ binding site, an extravesicular DA uptake site and two intravesicular high and low affinity DA release sites. Methamphetamine interacts with the low affinity intravesicular site to evoke vesicular DA release (Horton et al., 2012). Thus, as allosteric inhibitors, (±)-GZ-729C and (±)-GZ-730B may interact with the extravesicular DTBZ binding site, the extravesicular DA uptake site and the intravesicular high affinity DA release site to inhibit methamphetamine effect (Figure 2.11).

The next critical step in our drug discovery approach was to determine whether (±)-GZ-729C and (±)-GZ-730B inhibited methamphetamine-evoked endogenous DA release from striatal slices. Despite inhibiting methamphetamine-evoked [^{3}H]DA release from synaptic vesicles, neither lead compounds inhibited methamphetamine-evoked endogenous DA release from striatal slices, but increased DOPAC release significantly in the absence of methamphetamine. Such lack of inhibition on methamphetamine-evoked DA release but increase of DOPAC release from NAc shell has been reported using lobeline in a microdialysis study (Meyer et al., 2013). Increase of DOPAC release suggested that the (±)-GZ-729C and (±)-GZ-730B redistributed DA into the cytosol and the DA was metabolized into DOPAC by MAO. However, it was not fully understood why GZ-729C and (±)-GZ-730B inhibited methamphetamine-evoked [^{3}H]DA release from striatal vesicles but not endogenous DA release from striatal slices. Different tissue preparation, striatal synaptic vesicles versus

slices, and different label, [^{3}H]DA versus endogenous DA, might contribute to the contradictory results.

In conclusion, current findings indicate that the length of the methylene linker is critical for maintaining high affinity of the analog for the VMAT2 binding and uptake sites. A positive correlation was found between the K_i values for these two sites, indicating the analogs inhibition of VMAT2 function may be due at least in part to binding at the DTBZ site on VMAT2. All of the analogs acted like VMAT2 substrates with much higher affinity for the substrate translocation site relative to the DTBZ binding site on VMAT2. The most potent and selective analog for VMAT2, (±)-GZ-730B, inhibited methamphetamine-evoked vesicular [^{3}H]DA release via VMAT2 by a surmountable allosteric mechanism. However, this inhibitory effect of (±)-GZ-730B at VMAT2 did not translate to evaluation using striatal slices probably due to different tissue and label prepared in the respective experiment. Behavioral studies using rats were not performed due to the poor water solubility of (±)-GZ-730B. Further structural modification of lobelane to afford potent and selective VMAT2 inhibitors with better water solubility are needed and were studied in the following chapter of this thesis.

Table 2.1. K_i and I_{max} values in the [^{3}H]DTBZ binding and vesicular [^{3}H]DA uptake assays.

Compound	[^{3}H]DTBZ binding		[^{3}H]DA uptake		Binding/Uptake K_i Ratio
	K_i (μM)	Imax (%)	K_i (μM)	Imax (%)	
RO4-1284	0.028 ± 0.003 [a]	93 ± 7	0.041 ± 0.008	100	0.68
lobeline	2.76 ± 0.64	91 ± 0.3	0.56 ± 0.03	100	5
lobelane	0.97 ± 0.19	98 ± 2	0.040 ± 0.004	100	24
nor-lobelane	2.31 ± 0.21	98 ± 1	0.43 ± 0.008	99 ± 1	5
Symmetrical analogs					
GZ-709C	10.5 ± 3.36 *	73 ±6	0.046 ± 0.007	100	228
GZ-709B	7.68 ± 1.44 *	94 ± 3	0.036 ± 0.007	100	213
GZ-712C	1.00 ± 0.23	98 ± 2	0.078 ± 0.013 *	100	13
GZ-712B	4.50 ± 1.02 *	100	0.049 ± 0.010	100	92
GZ-632A	> 100	10 ± 3	4.55 ± 0.96 *	75 ± 3	N/A
Asymmetrical analogs					
(±)-GZ-731B	13.6 ± 8.1 *	63 ± 11	0.25 ± 0.05 *	98 ± 1	54
(±)-GZ-731A	24.1 ± 6.1 *	86 ± 4	0.52 ± 0.05 *	97 ± 1	46
(±)-GZ-725A	16.1 ± 4.1 *	63 ± 2	1.42 ± 0.11 *	96 ± 2	11
(±)-GZ-713A	28.4 ± 7.3 *	99 ±1	0.97 ± 0.18 *	96 ± 2	29
(±)-GZ-726A	62.5 ± 16.6 *	100	0.41 ± 0.03 *	97 ± 1	152
(±)-GZ-714A	28.6 ± 2.4 *	72 ± 2	0.24 ± 0.03 *	97 ± 2	119
(±)-GZ-729C	2.77 ± 1.77	93 ± 7	0.025 ± 0,003 *	97 ± 2	111
(±)-GZ-729B	12.2 ± 0.2 *	95 ± 1	0.093 ± 0.009 *	100	131
(±)-GZ-730C	1.62 ± 0.39	99 ±1	0.036 ± 0.003	100	45
(±)-GZ-730B	1.13 ± 0.28	100	0.024 ± 0.002 *	99 ± 1	47
(±)-GZ-644C	0.88 ± 0.30	100	0.062 ± 0.005 *	99 ± 1	14
(±)-GZ-644B	4.60 ± 0.56 *	98 ± 1	0.067 ± 0.005 *	99 ± 1	69
Asymmetrical analogs with cyclohexane substituent					
(±)-GZ-725B	9.35 ± 4.47 *	93 ± 4	0.22 ± 0.02 *	100	43
(±)-GZ-713B	39.6 ± 6.86 *	67 ± 0.1	0.20 ± 0.01 *	96 ± 4	198
(±)-GZ-726B	4.84 ± 0.60 *	84 ± 13	0.35 ± 0.03 *	95 ± 0.1	14
(±)-GZ-714B	48.9 ± 19.0 *	83 ±5	0.13 ± 0.03 *	100	376

[a] K_i and I_{max} values are mean (± SEM); n = 3-4 experiments/analog. * $p < 0.05$ different from lobelane.

Table 2.2. Summary of EC_{50} and E_{max} for methamphetamine-evoked [^{3}H]DA release in the absence and presence of (±)-GZ-729C or (±)-GZ-GZ930B.

	EC_{50} (μM)	E_{max} (%)
(±)-GZ-729C on methamphetamine-evoked [^{3}H]DA release		
(±)-GZ-729C (0 nM)	9.0 ± 2.9 [a]	83 ± 1.4 [a]
(±)-GZ-729C (10 nM)	11 ± 1.8	83 ± 0.6
(±)-GZ-729C (100 nM)	48 ± 6.6 *	72 ± 3.2
(±)-GZ-729C (1 μM)	179 ± 17 *	70 ± 2.7
(±)-GZ-730B on methamphetamine-evoked [^{3}H]DA release		
(±)-GZ-730B (0 nM)	5.8 ± 1.0	79 ± 3.7
(±)-GZ-730B (10 nM)	18 ± 7.1	73 ± 8.5
(±)-GZ-730B (100 nM)	51 ± 5.3	70 ± 2.6
(±)-GZ-730B (1 μM)	233 ± 60 *	63 ± 5.0

[a] EC_{50} and E_{max} values are mean (± SEM). * $p < 0.05$ different from [^{3}H]DA release in the presence of methamphetamine alone. n = 4 experiments/analog.

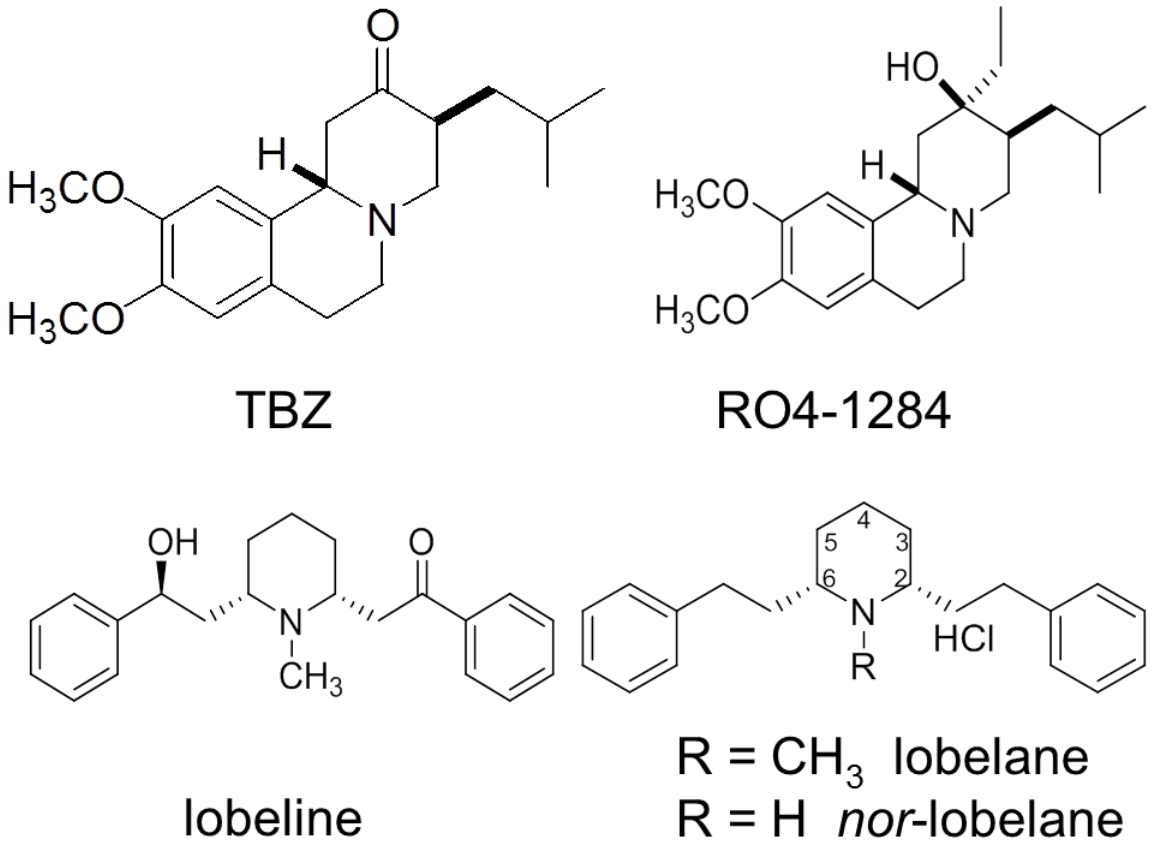

Figure 2.1. Chemical structures of TBZ, RO4-1284, lobeline and lobelane/*nor*-lobelane.

TBZ is a benzoquinolizine compound and VMAT2 inhibitor interacting with the site distinct from the DA uptake site on VMAT2. RO4-1284 is also a benzoquinolizine compound that inhibits VMAT2 in a similar manner. Lobeline is the principal alkaloid from *lobelia inflata*. Lobelane is a defunctionalized, saturated analog of lobeline and nor-lobelane is the N-demethylated analog of lobelane.

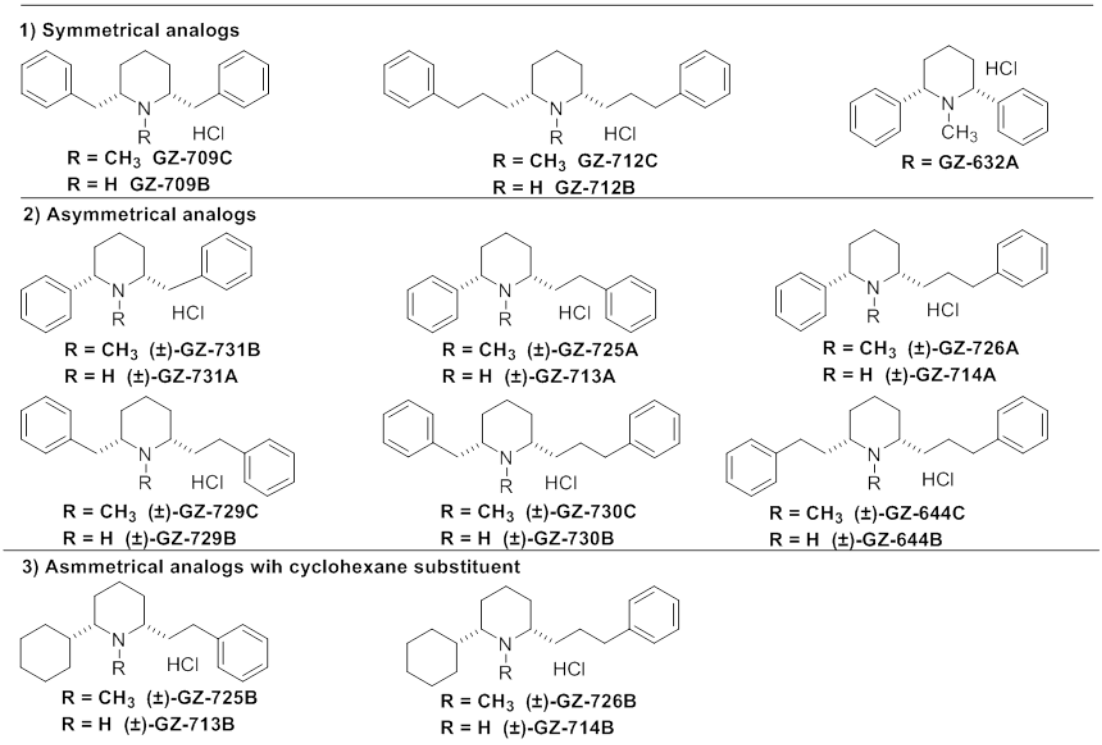

Figure 2.2. Chemical structures of lobelane analogs and their corresponding nor-analogs.

Analogs are grouped according to structural similarity: 1) symmetrical analogs with the same length of methylene linker on both side of the piperidine ring; 2) asymmetrical analogs with different length of the linkers on each side of the piperidine ring; 3) analogs with cyclohexane substituent at the C-6 position of the piperidine ring.

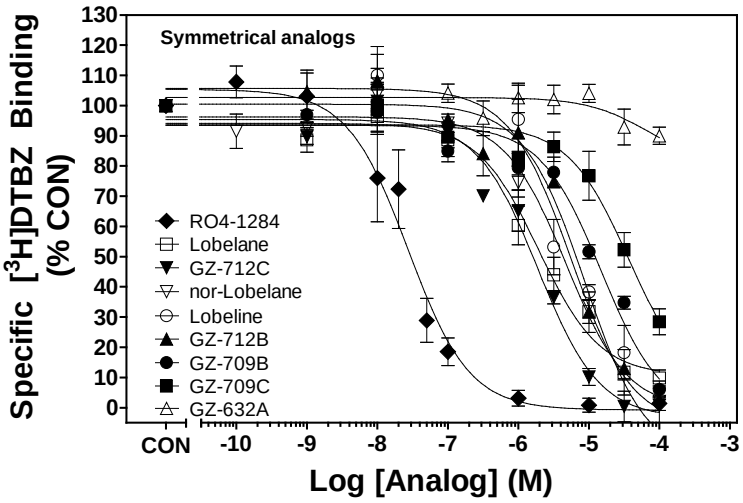
Symmetrical analogs
Specific [3H]DTBZ Binding (% CON)
RO4-1284
Lobelane
GZ-712C
nor-Lobelane
Lobeline
GZ-712B
GZ-709B
GZ-709C
GZ-632A
CON
Log [Analog] (M)

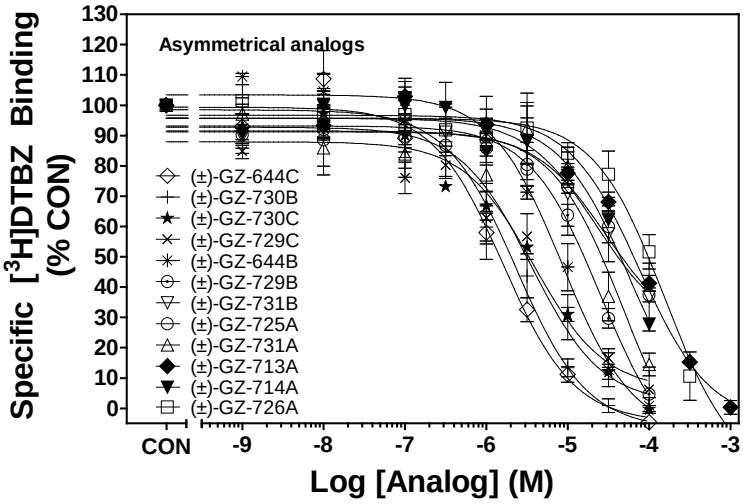
Asymmetrical analogs
Specific [3H]DTBZ Binding (% CON)
(±)-GZ-644C
(±)-GZ-730B
(±)-GZ-730C
(±)-GZ-729C
(±)-GZ-644B
(±)-GZ-729B
(±)-GZ-731B
(±)-GZ-725A
(±)-GZ-731A
(±)-GZ-713A
(±)-GZ-714A
(±)-GZ-726A
CON
Log [Analog] (M)

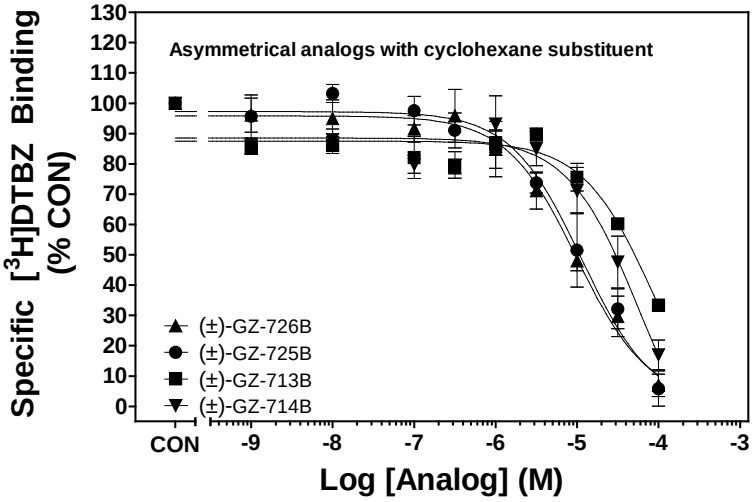
Asymmetrical analogs with cyclohexane substituent
Specific [3H]DTBZ Binding (% CON)
(±)-GZ-726B
(±)-GZ-725B
(±)-GZ-713B
(±)-GZ-714B
CON
Log [Analog] (M)

Figure 2.3. RO4-1284, lobeline, lobelane and lobelane analogs inhibit [^{3}H]DTBZ binding to whole brain vesicles.

The first panel of the figure contains K_i values for RO4-1284, lobeline, lobelane, symmetrical lobelane analogs and their corresponding *nor*-analogs. The second panel of the figure contains K_i values for asymmetrical lobelane analogs and their corresponding *nor*-analogs. The third panel of the figure contains K_i values for asymmetrical lobelane analogs with a cyclohexane substituent directly attached to the C-6 position of the piperidine ring and their corresponding *nor*-analogs. K_i values of all the analogs and their corresponding *nor*-analogs are presented in the legend in order from the most potent to the least potent. Control represents specific [^{3}H]DTBZ binding in the absence of analogs. Data are mean (± SEM) specific [^{3}H]DTBZ binding presented as a percentage of the respective control (1.99 ± 0.07 pmol/mg, n = 3-4 experiments/analog).

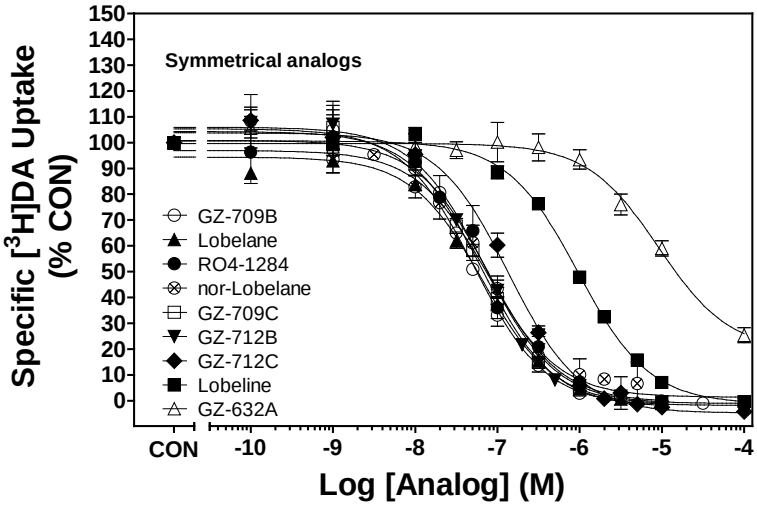
Symmetrical analogs
Specific [3H]DA Uptake (% CON)
GZ-709B
Lobelane
RO4-1284
nor-Lobelane
GZ-709C
GZ-712B
GZ-712C
Lobeline
GZ-632A
CON
Log [Analog] (M)

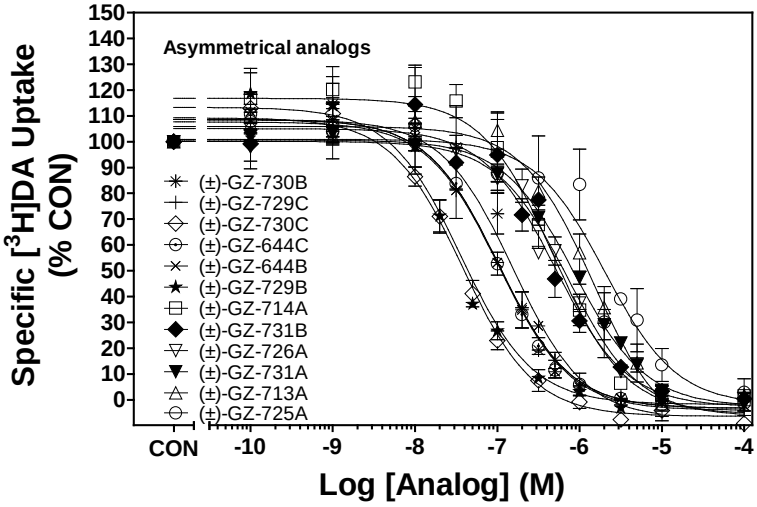
Asymmetrical analogs
Specific [3H]DA Uptake (% CON)
(±)-GZ-730B
(±)-GZ-729C
(±)-GZ-730C
(±)-GZ-644C
(±)-GZ-644B
(±)-GZ-729B
(±)-GZ-714A
(±)-GZ-731B
(±)-GZ-726A
(±)-GZ-731A
(±)-GZ-713A
(±)-GZ-725A
CON
Log [Analog] (M)

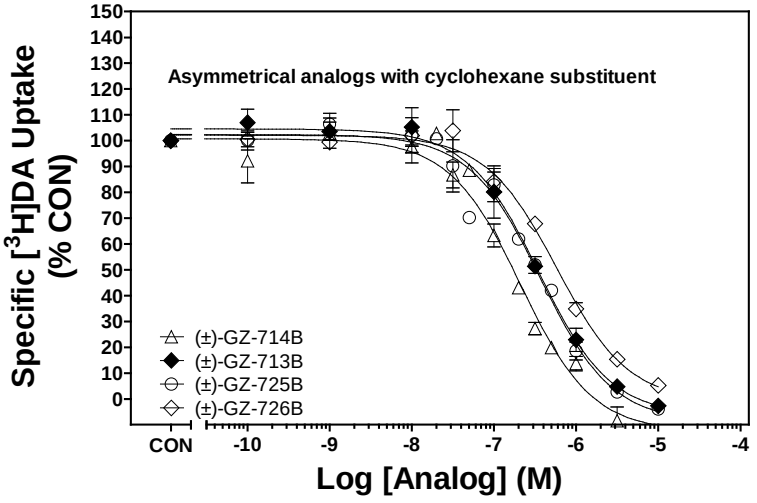
Asymmetrical analogs with cyclohexane substituent
Specific [3H]DA Uptake (% CON)
(±)-GZ-714B
(±)-GZ-713B
(±)-GZ-725B
(±)-GZ-726B
CON
Log [Analog] (M)

Figure 2.4. RO4-1284, lobeline, lobelane and lobelane analogs inhibit [^{3}H]DA uptake to striatal synaptic vesicles.

The first panel of the figure contains K_i values for RO4-1284, lobeline, lobelane, symmetrical lobelane analogs and their corresponding *nor*-analogs. The second panel of the figure contains K_i values for asymmetrical lobelane analogs and their corresponding *nor*-analogs. The third panel of the figure contains K_i values for asymmetrical lobelane analogs with a cyclohexane substituent directly attached to the C-6 position of the piperidine ring and their corresponding *nor*-analogs. K_i values of all the analogs and their corresponding *nor*-analogs are presented in the legend in the order from the most potent to the least potent. Control represents specific [^{3}H]DA uptake in the absence of analogs. Data are mean (± SEM) specific [^{3}H]DA uptake presented as a percentage of the respective control (24.7 ± 2.2 pmol/min/mg, n = 4 experiments/analog).

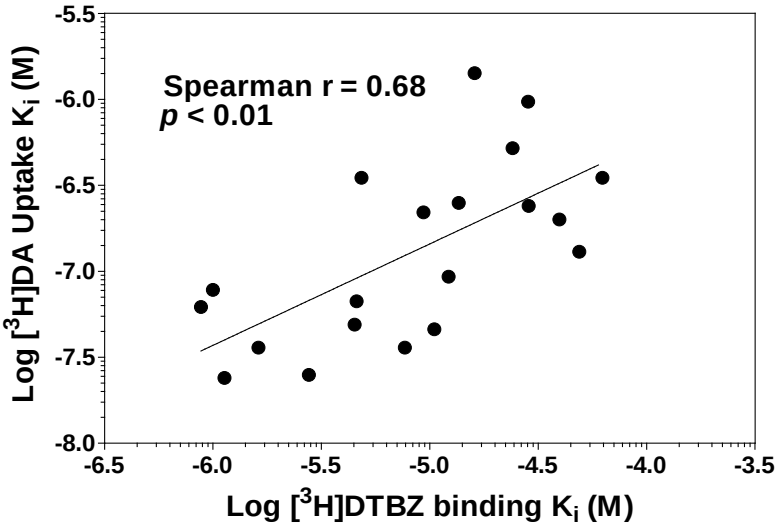

Figure 2.5. Vesicular [^{3}H]DA uptake and [^{3}H]DTBZ binding affinity correlation.

Affinity for [^{3}H]DTBZ binding site on VMAT2 and affinity to inhibit VMAT2 function are positively correlated (Spearman r = 0.68; $p < 0.01$). GZ-632A is not included in the correlation because it has no affinity for the DTBZ binding site at VMAT2.

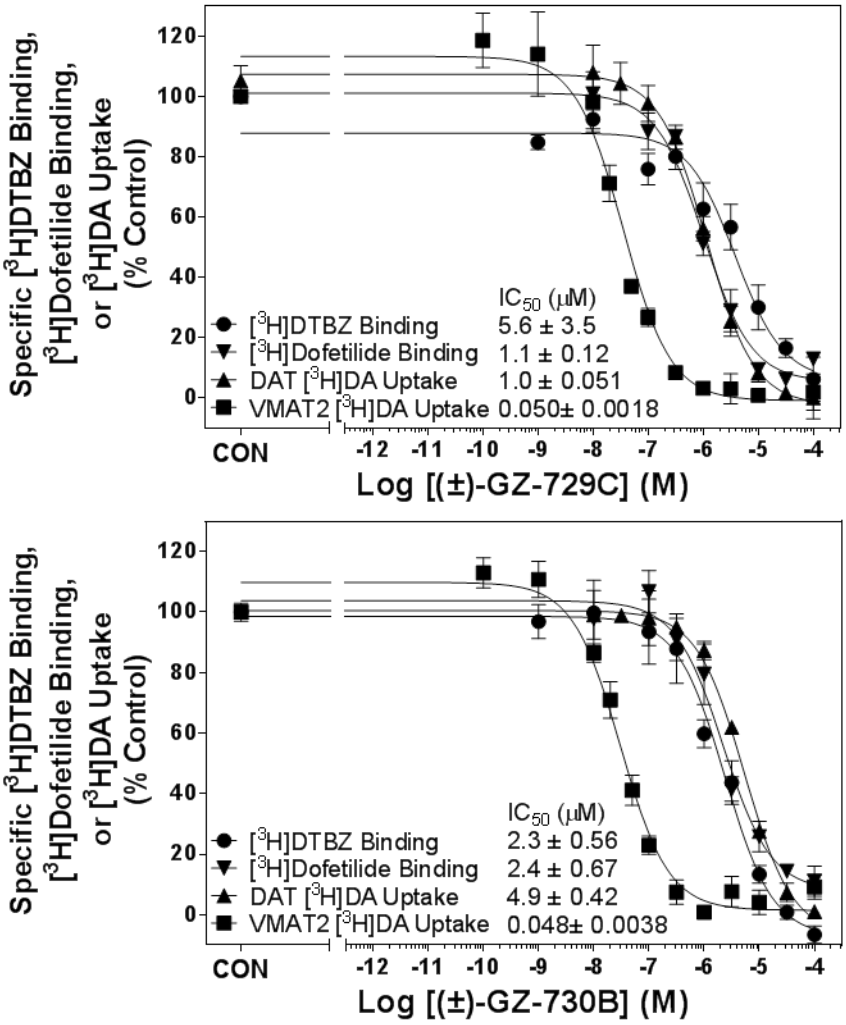

Figure 2.6. (±)-GZ-729C and (±)-GZ-730B are selective for VMAT2 over DAT and hERG channel.

IC_{50} values and concentration-response of (±)-GZ-729C and (±)-GZ-730B to inhibit specific [^{3}H]DTBZ binding, [^{3}H]dofetilide binding and [^{3}H]DA uptake are illustrated in the top and bottom panels, respectively. Data are mean (± SEM) specific binding or uptake presented as a percentage of the respective control ([^{3}H]DTBZ binding: 2341 ± 201 fmol/mg for (±)-GZ-729C, 1508 ± 240 fmol/mg for (±)-GZ-730B; [^{3}H]dofetilide binding: 27.3 ± 7.52 fmol/min/mg for (±)-GZ-729C, 27.4 ± 8.77 fmol/min/mg for (±)-GZ-730B; DAT [^{3}H]DA uptake: 9.96 ± 1.62 pmol/min/mg for (±)-GZ-729C, 13.9 ± 2.64 pmol/min/mg for (±)-GZ-730B. VMAT2

[^{3}H]DA uptake: 32.4 ± 8.25 pmol/min/mg for (±)-GZ-729C, 23.9 ± 2.95 pmol/min/mg for (±)-GZ-730B). n = 3-4 experiments/analog.

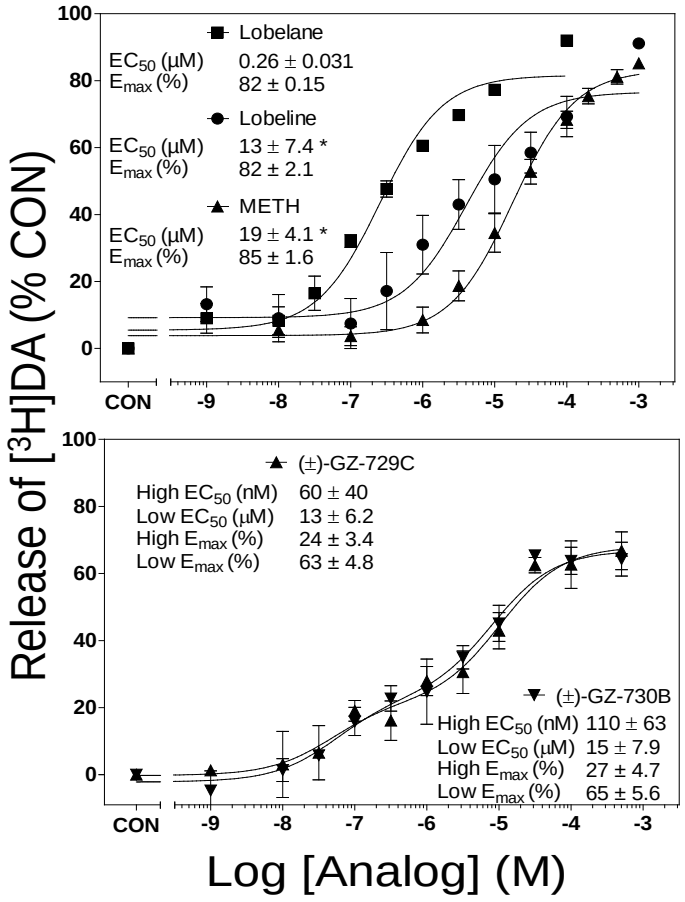

Figure 2.7. (±)-GZ-729C and (±)-GZ-730B evoke [^{3}H]DA release from synaptic vesicles.

Concentration-response curves and EC_{50} and E_{max} values for standards (lobelane, lobeline, methamphetamine), (±)-GZ-729C and (±)-GZ-730B to evoke [^{3}H]DA release from synaptic vesicles are provided in top and bottom panels, respectively. Control represents [^{3}H]DA release in the absence of analogs. METH represents methamphetamine. Release values in the curves are mean (± SEM) [^{3}H]DA release as a percentage of the respective control (3174 ± 778 disintegrations per minute (DPM), n = 4 rats/analog).

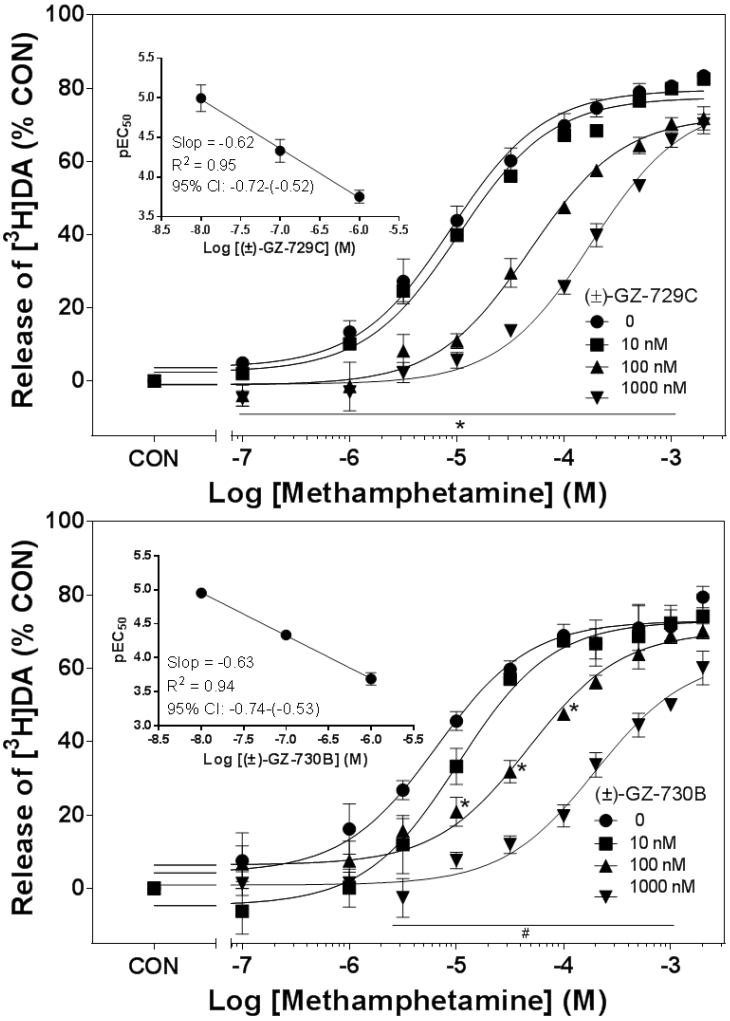

Figure 2.8. (±)-GZ-729C and (±)-GZ-730B inhibit methamphetamine-evoked [^{3}H]DA release from striatal synaptic vesicles.

The concentration response of methamphetamine-evoked vesicular [^{3}H]DA release in the presence of (±)-GZ-729C and (±)-GZ-730B are illustrated in top and bottom panels, respectively. Control represent [^{3}H]DA release in the absence of methamphetamine and (±)-GZ-729C or (±)-GZ-730B. Release values in the curves are mean (± SEM) [^{3}H]DA release as a percentage of the control (3076 ± 573 DPM for (±)-GZ-729C and 3591 ± 363 DPM for (±)-GZ-730B; n = 4 rats/experiment). Inset shows the Lew and Angus analysis in which pEC_{50} values are plotted as a function of log value of (±)-GZ-729C and (±)-GZ-730B

concentration, respectively. In the top panel, * $p < 0.05$ between methamphetamine-evoked release in the presence of 100-1000 nM (±)-GZ-729C and methamphetamine alone. In the bottom panel, * $p < 0.05$ between methamphetamine-evoked release in the presence of 100 nM (±)-GZ-729C and methamphetamine alone, $^{\#}$ $p < 0.05$ between methamphetamine-evoked release in the presence of 1000 nM (±)-GZ-730B and methamphetamine alone.

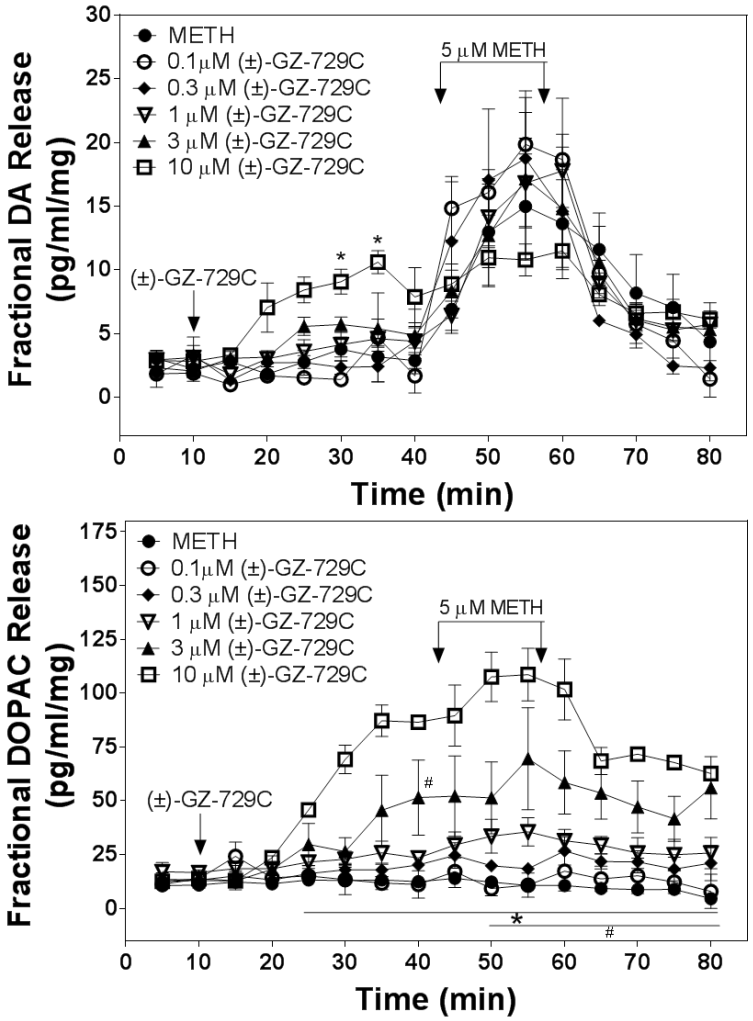

Figure 2.9. (±)-GZ-729C increases DOPAC release with no influence on methamphetamine-evoked fractional DA release**.**

Striatal slices were superfused with a range of concentrations of (±)-GZ-729C (0.1-10 μM). Fractional DA and DOPAC release are amount of DA and DOPAC released in each min sample in the top and bottom panel, respectively. (±)-GZ-729C was added to the buffer following 10 min basal sample collection, indicated by the arrow, and the analog remained in the buffer until the end of the experiment. METH represents methamphetamine. Methamphetamine (5 μM) was added to the buffer for 15 min, indicated by the horizontal bar with two arrows. Fractional release values are expressed as mean (± SEM) pg/ml/mg of the slice weight. n = 6 rats. In the top panel, * $p < 0.05$ compared to control. In the bottom

panel, * $p < 0.05$ between release in the presence of 10 µM (±)-GZ-729C and control. # $p < 0.05$ between release in the presence of 3 µM (±)-GZ-729C and control.

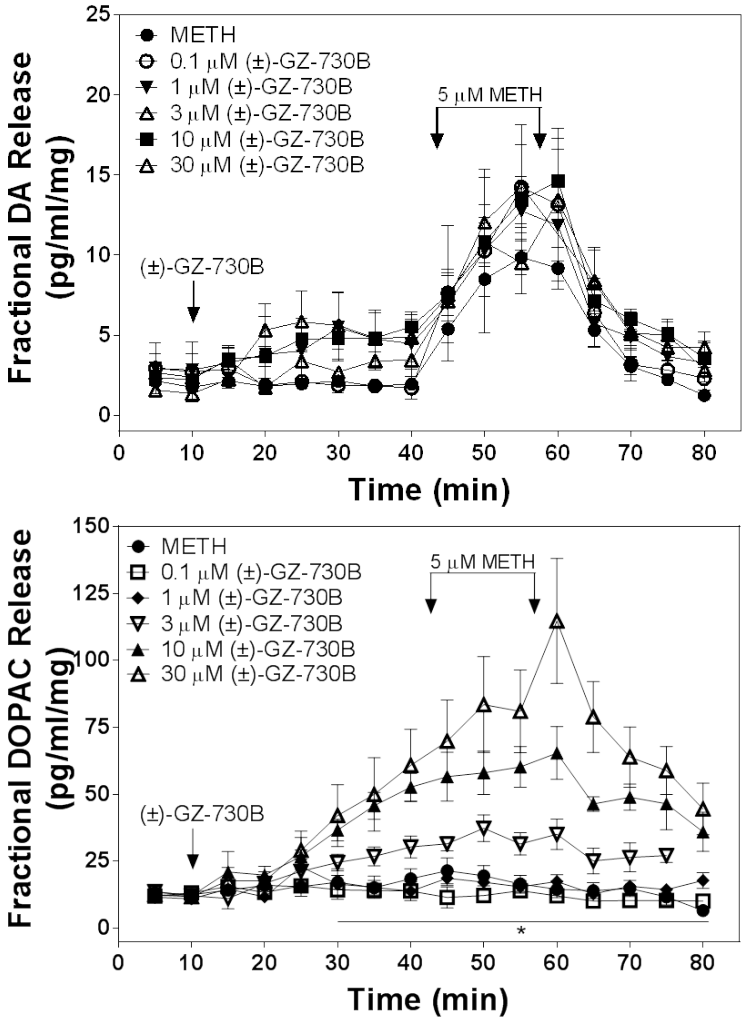

Figure 2.10. (±)-GZ-730B increases DOPAC release with no influence on methamphetamine-evoked fractional DA release.

Striatal slices were superfused with a range of concentrations of (±)-GZ-730B (0.1-30 μM). Fractional DA and DOPAC release are amount of DA and DOPAC released in each min sample in the top and bottom panel, respectively. (±)-GZ-730B was added to the buffer following 10 min basal sample collection, indicated by the arrow, and the analog remained in the buffer until the end of the experiment. METH represents methamphetamine. Methamphetamine (5 μM) was added to the buffer for 15 min, indicated by the horizontal bar with two arrows. Fractional release values are expressed as mean (± SEM) pg/ml/mg of the slice weight. n = 10 rats. In the bottom panel, * $p < 0.05$ between release in the

presence of 30 µM (±)-GZ-730B and control. $^{\#}$ $p < 0.05$ between release in the presence of 10 µM (±)-GZ-730B and control.

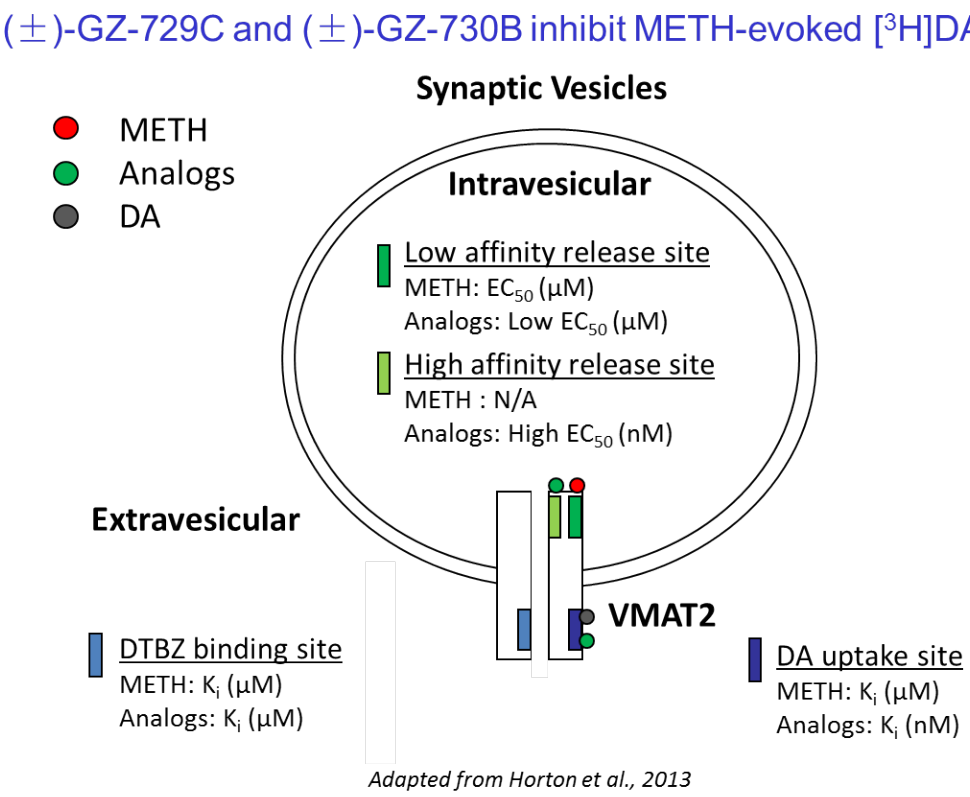

Figure 2.11. (±)-GZ-729C and (±)-GZ-730B interact with the extravesicular [^{3}H]DTBZ binding site, the extravesicular [^{3}H]DA uptake site, and the intravesicular high affinity [^{3}H]DA release site on VMAT2 to inhibit methamphetamine-evoked vesicular [^{3}H]DA release.

METH represents methamphetamine.

CHAPTER 3 Acyclic Lobelane Analogs Inhibit Vesicular Monoamine Transporter-2 Function and Methamphetamine Self-administration in Rats

3.1 Introduction

Pharmacotherapies are not available currently for the treatment of methamphetamine abuse. As a substrate at the presynaptic dopamine transporter (DAT), methamphetamine releases cytosolic dopamine (DA) from the presynaptic terminal into the extracellular space (Sulzer et al., 1995), which leads to its reinforcing properties. Although DAT has been evaluated extensively as a target for the treatment of psychostimulant abuse (Dar et al., 2005; Grabowski et al., 1997; Howell et al., 2007; Tanda et al., 2009), this approach has not been successful thus far. The vesicular monoamine transporter-2 (VMAT2) is an alternative target (Dwoskin and Crooks, 2002; Zheng et al., 2006), since methamphetamine inhibits DA uptake and promotes DA release also at this site, consequently increasing cytosolic DA available to DAT for reverse transport (Brown et al., 2000; Pifl et al., 1995; Sulzer et al., 1995).

VMAT2, located on vesicles within presynaptic terminals, transports cytosolic DA into the vesicles for storage and subsequent release into the extracellular space in response to appropriate physiological signals. In addition, the VMAT2 localized on the vesicles that co-fractionate with synaptosomal membranes are defined as VMAT2M, while the VMAT2 on the vesicles that do not co-fractionate with synaptosomal membranes are defined as VMAT2C (Volz

et al., 2007). [^{3}H]Dihydrotetrabenazine (DTBZ) binding is used to assess interactions with VMAT2 (Scherman and Henry, 1984). Lobeline (Figure 3.1), a major alkaloid from *Lobelia inflata,* displaces [^{3}H]DTBZ from vesicle membrane preparations, inhibits [^{3}H]DA uptake, and promotes [^{3}H]DA release from isolated VMAT2C-associated vesicles (Teng et al., 1998; Teng et al., 1997). In this manner, lobeline redistributes DA from vesicles to the cytosol. However, lobeline does not inhibit monoamine oxidase (MAO); the majority of the redistributed DA is metabolized by MAO to dihydroxyphenylacetic acid (DOPAC) and as such is not available as a substrate for methamphetamine-induced reverse transport by DAT (Dwoskin and Crooks, 2002; Teng et al., 1997). As a result, lobeline, in a concentration-dependent manner, inhibits methamphetamine-evoked DA release from rat striatal slices and, in a dose-dependent manner, decreases methamphetamine self-administration in rats (Harrod et al., 2001; Miller et al., 2001; Nickell et al., 2010). Furthermore, lobeline is not self-administered by rats, indicating a lack of abuse liability (Harrod et al., 2003).

Based on these promising preclinical findings, lobeline was evaluated in Phase 1b clinical trials employing experienced methamphetamine abusers to assess its safety in this population. Lobeline was found to have no significant side-effects, other than an extremely bitter taste and associated nausea (Glover et al., 2010; Jones, 2007). The high affinity of lobeline for α4β2* nicotinic receptors (nAChRs) and moderate affinity for α7 nAChRs (Damaj et al., 1997; Harrod et al., 2004; Miller et al., 2004), together with its bitter taste, led us to

conduct structure-activity studies to identify novel analogs with greater target selectivity, inhibitory potency at VMAT2C and improved druglikeness.

The defunctionalized, saturated lobeline analog, lobelane (Figure 3.1), was found to be more selective and had higher affinity at VMAT2C compared to lobeline (Miller et al., 2004). Lobelane inhibited methamphetamine-evoked DA release from rat striatal slices and specifically decreased methamphetamine self-administration in rats (Neugebauer et al., 2007; Nickell et al., 2010). These data support the idea that VMAT2C is a promising target for the discovery of novel therapeutics for methamphetamine abuse. Unfortunately, upon repeated administration, tolerance developed to the behavioral effects of lobelane (Neugebauer et al., 2007), reducing enthusiasm for this analog.

Recently, several antipsychotics have been withdrawn or warranted restricted labelling by the FDA due to potential cardiac side effects (Haddad and Anderson, 2002). These antipsychotics drugs are predicted to prolong the ventricular action potential duration (APD, *i.e.* the QT interval of the electrocardiogram) and cause a polymorphic ventricular tachycardia, Torsades de Pointes, and sudden death (Tamargo, 2000). Drug-induced ventricular tachycardia is associated with blockage of the rapidly activating, delayed rectifier potassium current I_{Kr} channel coded by the human *ether-a-go-go*-related gene (hERG). This channel plays a major role in repolarization of ventricular myocytes and analogs with high affinity for this hERG channel are predicted to possess cardiac toxicity (Sanguinetti et al., 1995; Trudeau et al., 1995).

The current study describes the pharmacological effects of novel acyclic lobelane analogs, by removing the 3- and 4-carbon atoms in the central piperidine ring of lobelane (Figure 3.1). The majority of the acyclic lobelane analogs were racemic containing same amount of two enantiomers. The enantiomers may exhibit different ability to inhibit VMAT2 binding and function. Thus, several racemic analogs found to be most potent at VMAT2C were synthesized as pure enantiomers. Kinetic analyses of [^{3}H]DA uptake into isolated vesicle preparations were conducted to determine mechanism of action underlying the inhibitory effect of the analogs. Affinity at DAT was evaluated to assess abuse liability and affinity at hERG channels was evaluated to assess cardiac toxicity. Ability of the enantiomers to release [^{3}H]DA from isolated presynaptic VMAT2C, and moreover, to inhibit methamphetamine-evoked [^{3}H]DA release from isolated presynaptic VMAT2M- and VMAT2C-associated vesicles was determined. The ability of the lead analog, (R)-N-(1-phenylpropan-2-yl)-3-phenylpropan-1-amine ((R)-GZ-924), to inhibit methamphetamine-evoked DA release from striatal slices was determined. Ability to inhibit nicotine-evoked DA release from striatal slices was assessed to determine specificity of action. The ability of (R)-GZ-924 to decrease methamphetamine self-administration and food-maintained responding in rats was determined to evaluate the translation from *in vitro* neurochemical findings to whole animal efficacy.

3.2 Methods

3.2.1 Animals

Male Sprague-Dawley rats (200–250 g) were purchased from Harlan Laboratories, Inc. (Indianapolis, IN) and were housed in the Division of Laboratory Animal Resources at the College of Pharmacy at the University of Kentucky (Lexington, KY). For the neurochemical experiments, rats had free access to food and water. For the behavioral experiments, rats were handled for 1 week, and food was restricted to obtain 85% of free-feeding body weight. Experimental protocols were conducted according to the 1996 National Institutes of Health Guide for the Care and Use of Laboratory Animals and were approved by the Institutional Animal Care and Use Committee at the University of Kentucky.

3.2.2 Materials

[^{3}H]DA (specific activity, 28.0 Ci/mmol), [^{3}H]nicotine (L-(–)-[N-methyl-^{3}H]; specific activity, 66.9 Ci/mmol), and Microscint 20 LSC-cocktail were purchased from PerkinElmer Life and Analytical Sciences (Boston, MA). [^{3}H]DTBZ (specific activity, 20 Ci/mmol) and [^{3}H]methyllycaconitine ([^{3}H]MLA; ([1α,4(S),6β,14α,16β]-20-ethyl-1,6,14,16-tetramethoxy-4-[[[2-([3-^{3}H]-methyl-2,5-dioxo-1-pyrrolidinyl) benzoyl]oxy]-methyl]aconitane-7,8-diol; specific activity, 100 Ci/mmol) was obtained from American Radiolabeled Chemicals, Inc. (St. Louis, MO). Bovine serum albumin, disodium ethylenediaminetetraacetate (EDTA),

ethyleneglycoltetraacetate (EGTA), 1-(2-(bis-(4-fluorophenyl)methoxy)ethyl)-4-(3-phenylpropyl)-piperazine (GBR 12909), L-(+)-tartaric acid, sucrose, magnesium sulfate, polyethyleneimine (PEI), adenosine 5'-triphosphate magnesium salt (APT-Mg^{+2}), N-[2-hydroxyethyl]piperazine-N'-[2-ethanesulfonic acid] (HEPES), S(-)nicotine ditartrate (nicotine), 3-hydroxytyramine (dopamine, DA), DOPAC, d-methamphetamine hydrochloride (methamphetamine), sodium chloride, magnesium sulfate, ascorbate oxidase, magnesium chloride, potassium chloride solution and amitriptyline hydrochloride were purchased from Sigma-Aldrich (St. Louis, MO). α-D-Glucose, L-ascorbic acid, and monobasic potassium phosphate were purchased from Aldrich Chemical Co. (Milwaukee, WI), AnalaR-BDH Ltd. (Poole, UK) and Mallinckrodt (St. Louis, MO), respectively. Perchloric acid (70%) was purchased from Mallinckrodt Baker (Phillipsburg, NJ). Lobeline hemisulfate was purchased from ICN Biomedicals Inc. (Costa Mesa, CA). All other commercial chemicals were purchased from Fisher Scientific Co. (Pittsburgh, PA). [2R,3S,11bS]-2-Ethyl-3-isobutyl-9,10-dimethoxy-2,2,4,6,7,11b-hexahydro-1H-pyrido[2,1-a]isoquinolin-2-ol (RO4-1284) was a gift from Hoffman-La Roche Ltd. (Basel, Switzerland). Dofetilide [N-methyl-^{3}H] ([^{3}H]-dofetilide, specific activity: 80 Ci/mmol) was purchased from ARC (St. Louis, MO).

Lobelane and acyclic lobelane analogs were synthesized at the College of Pharmacy at the University of Kentucky and are shown in Figure 3.1. Racemic analogs included (±)-N-(1-(4-bromophenyl)propan-2-yl)-3-phenylpropan-1-amine ((±)-GZ-819A); (±)-N-(1-phenylpropan-2-yl)-3-phenylpropan-1-amine ((±)-GZ-819B); (±)-N-methyl-N-(1-phenylpropan-2-yl)-3-phenylpropan-1-amine ((±)-GZ-

819C); (±)-N-(1-phenylpropan-2-yl)-3-(4-methoxyphenyl)propan-1-amine ((±)-GZ-815A); (±)-N-methyl-N-(1-phenylpropan-2-yl)-3-(4-methoxyphenyl)propan-1-amine ((±)-GZ-815B); (±)-N-(3-phenylpropyl)-4-phenylbutan-2-amine ((±)-GZ-813A); (±)-N-methyl-N-(3-phenylpropyl)-4-phenylbutan-2-amine ((±)-GZ-813B); (±)-N-phenethyl-4-phenylbutan-2-amine ((±)-GZ-814A); (±)-N-methyl-N-phenethyl-4-phenylbutan-2-amine ((±)-GZ-814B); (±)-N-phenethyl-1-(4-methoxyphenyl)propan-2-amine ((±)-GZ-816A); (±)-N-methyl-N-phenethyl-1-(4-methoxyphenyl)propan-2-amine ((±)-GZ-816B); (±)-N-phenethyl-1-phenylpropan-2-amine ((±)-GZ-820B); (±)-N-methyl-N-phenethyl-1-phenylpropan-2-amine ((±)-GZ-820C); (±)-N-phenethyl-1-(4-aminophenyl)propan-2-amine ((±)-GZ-861B); (±)-N-(3-(4-methoxyphenyl)propyl)-4-phenylbutan-2-amine ((±)-GZ-865A); (±)-N-(3-(4-methoxyphenyl)propyl)-4-(4-methoxyphenyl)butan-2-amine ((±)-GZ-865B); (±)-N-(1-(4-methoxyphenyl)propan-2-yl)-3-(4-methoxyphenyl)propan-1-amine ((±)-GZ-865C); (±)-N-(1-phenylpropan-2-yl)-3-(4-methoxyphenyl)propan-1-amine ((±)-GZ-888); (±)-N-(1-(4-bromophenyl)propan-2-yl)-4-phenylbutan-1-amine ((±)-GZ-893A). Racemic analogs were prepared through a reductive amination reaction between an appropriate amine and an appropriate ketone. Chiral pure analogs were prepared through nucleophilic substitution of chiral alcohols with an appropriate amine. Chirally pure analogs included (R)-GZ-924; (S)-N-(1-phenylpropan-2-yl)-3-phenylpropan-1-amine ((S)-GZ-925); (R)-N-(1-(4-methoxyphenyl)propan-2-yl)-3-phenylpropan-1-amine ((R)-GZ-878A); (S)-N-(1-(4-methoxyphenyl)propan-2-yl)-3-phenylpropan-1-amine ((S)-GZ-878B); (R)-N-(1-(4-bromophenyl)propan-2-yl)-3-phenylpropan-1-amine ((R)-GZ-880A); and

(S)-N-(1-(4-bromophenyl)propan-2-yl)-3-phenylpropan-1-amine ((S)-GZ-880B). (R)-GZ-878A and (S)-GZ-878B were pure enantiomers of (±)-GZ-815A, (R)-GZ-880A and (S)-GZ-880B were pure enantiomers of (±)-GZ-819A, and (R)-GZ-924 and (S)-GZ-925 were pure enantiomers of (±)-GZ-819B. Structures and purities of the analogs were verified by ^{1}H and ^{13}C NMR spectroscopy and mass spectrometry.

3.2.3 [^{3}H]DTBZ Binding

Analog inhibition of [^{3}H]DTBZ binding was evaluated using modifications of our published methods (Teng et al., 1998). Briefly, whole rat brain (excluding cerebellum) was homogenized in 20 ml of ice-cold sucrose solution (0.32 M) with 7 up-and-down strokes of a Teflon pestle homogenizer (clearance ≈ 0.003 inch). Homogenates were centrifuged at 1000g for 12 min at 4 °C, and the resulting supernatants were centrifuged again at 22,000g for 10 min at 4 °C. Resulting pellets were incubated in 18 ml of ice-cold water for 5 min, and 2 ml of HEPES (25 mM) and potassium tartrate (100 mM) solution were subsequently added. Samples were centrifuged (20,000g for 20 min at 4 °C), and 20 µl of $MgSO_4$ (1 mM) solution was added to the supernatants. Samples were centrifuged (100,000g for 45 min at 4 °C), and pellets containing the VMAT2C-associated vesicles were resuspended in ice-cold assay buffer (25 mM HEPES, 100 mM potassium tartrate, 5 mM $MgSO_4$, 0.1 mM EDTA, and 0.05 mM EGTA, pH 7.5). Assays were performed in duplicate using 96-well plates. Aliquots of vesicular suspension (15 µg of protein in 100 µl) were added to wells containing 5 nM

[^{3}H]DTBZ, 50 µl of analog (1 nM to 1 mM), and 50 µl of buffer. Nonspecific binding was determined in the presence of RO4-1284 (10 µM). Reactions were terminated by filtration (Packard Filtermate harvester; PerkinElmer Life and Analytical Sciences, Shelton, CT) onto Unifilter-96 GF/B filter plates (presoaked for 2 hr in 0.5% PEI). Filters were subsequently washed 5 times with 350 µl of ice-cold buffer (25 mM HEPES, 100 mM potassium tartrate, 5 mM $MgSO_4$, and 10 mM NaCl, pH 7.5). Filter plates were dried and bottom-sealed, and each well filled with 40 µl of scintillation cocktail (MicroScint 20; PerkinElmer Life and Analytical Sciences). Radioactivity on the filters was determined by liquid β-scintillation spectrometry (TopCount NXT; PerkinElmer Life and Analytical Sciences).

3.2.4 Vesicular [^{3}H]DA Uptake

Analog inhibition of vesicular [^{3}H]DA uptake was evaluated using our previous methods (Nickell et al., 2010). Rat striata were homogenized with 10 up-and-down strokes of a Teflon pestle homogenizer (clearance ≈ 0.008 inch) in 14 ml of 0.32 M sucrose solution. Homogenates were centrifuged (2000g for 10 min at 4 °C), and resulting supernatants were centrifuged again (10,000g for 30 min at 4 °C). Pellets were resuspended in 2 ml of 0.32 M sucrose solution and subjected to osmotic shock by adding 7 ml of ice-cold water, followed by the immediate restoration of osmolarity by adding 900 µl of 0.25 M HEPES buffer and 900 µl of 1.0 M potassium tartrate solution. Samples were centrifuged (20,000g for 20 min at 4 °C), and the resulting supernatants were centrifuged

again (55,000g for 1 hr at 4 °C), followed by the addition of 100 µl of 10 mM MgSO4, 100 µl of 0.25 M HEPES, and 100 µl of 1.0 M potassium tartrate solutions, followed by a final centrifugation (100,000g for 45 min at 4 °C). Final VMAT2C-associated vesicle pellets were resuspended in 2.4 ml of assay buffer (25 mM HEPES, 100 mM potassium tartrate, 50 µM EGTA, 100 µM EDTA, 1.7 mM ascorbic acid, 2 mM ATP-Mg^{+2}, pH 7.4). Aliquots of the vesicular suspension (100 µl) were added to tubes containing assay buffer, a range of analog concentrations (0.1 nM to 10 mM) and 0.1 µM [^{3}H]DA to provide a final volume of 500 µl. Nonspecific uptake was determined in the presence of RO4-1284 (10 µM). Reactions were terminated by filtration, and radioactivity retained by the GF/B filters (presoaked for 2 hr in 0.5% PEI) was determined by liquid β-scintillation spectrometry.

3.2.5 Kinetics of Vesicular [^{3}H]DA Uptake

Kinetic analyses for the chirally pure enantiomers were conducted to determine mechanism of inhibition of DA uptake at VMAT2C. Concentration of analogs used for kinetic analysis was based on K_i values obtained from the vesicular [^{3}H]DA uptake assays. Specifically, concentrations of 40 nM lobelane, 6 nM (R)-GZ-924, 65 nM (S)-GZ-925, 6 nM (R)-GZ-880A, 32 nM (S)-GZ-880B, 45 nM (R)-GZ-878A, and 20 nM (S)-GZ-878B were evaluated in kinetic analyses. Aliquots of 100 µl of vesicular suspensions were added to tubes containing 300 µl assay buffer, 50 µl of analogs and 50 µl of a range of [^{3}H]DA concentrations (0.001-5.0 µM). Nonspecific uptake was determined in the presence of RO4-

1284 (10 μM). After 8 min incubation at 37 °C, [^{3}H]DA uptake was terminated by filtration. Radioactivity remaining on the filters was determined as previously described.

3.2.6 Synaptosomal [^{3}H]DA Uptake

Analog inhibition of [^{3}H]DA uptake into rat striatal synaptosomes was evaluated according to previously published methods (Teng et al., 1997). Rat striata were homogenized in ice-cold sucrose (pH 7.4), with 15 up-and-down strokes of a Teflon pestle homogenizer (clearance ≈ 0.005 inch). Homogenates were centrifuged (2000g for 10 min at 4 °C), and resulting supernatants were centrifuged again (20,000g for 17 min at 4 °C). Resulting pellets were resuspended in 2.4 ml of assay buffer (125 mM NaCl, 5 mM KCl, 1.5 mM MgSO4, 1.25 mM $CaCl_2$, 1.5 mM KH_2PO4, 10 mM α-D-glucose, 25 mM HEPES, 0.1 mM EDTA, 0.1 mM pargyline, 0.1 mM ascorbic acid, saturated with 95% 0_2/5% CO_2, pH 7.4). Aliquots of the synaptosomal suspension (25 μl) were added to tubes containing assay buffer and a range of concentrations of analog (1 nM – 100 μM), and incubated at 34 °C for 5 min. Samples were then placed on ice, and 50 μl [^{3}H]DA added to each tube (final concentration 0.1 μM), and incubated for 10 min at 34 °C. Assays were performed in duplicate in a total volume of 500 μl. Nonspecific uptake was determined in the presence of nomifensine (10 μM). Reactions were terminated by addition of 3 ml of ice-cold assay buffer and subsequent filtration. Radioactivity retained by the filters (presoaked for 2 hr in 0.5% PEI) was determined as previously described

3.2.7 Vesicular [^{3}H]DA Release

Based on the results from the analog-induced inhibition of [^{3}H]DA uptake into vesicles, several of the most potent analogs were chosen to generate pure enantiomers for further evaluation of the ability to induce vesicular [^{3}H]DA release via VMAT2C using published methods (Horton et al., 2013). VMAT2C-associated vesicle pellets from rat striata were prepared as described above in the vesicular [^{3}H]DA uptake assay. Final pellets were resuspended in 2.7 ml of ice-cold assay buffer, to which 300 µl of [^{3}H]DA (final concentration, 0.3 µM) was added (total volume 3.0 ml). After incubation at 37 °C for 8 min, samples containing the vesicle suspension were centrifuged (100,000g for 45 min at 4 °C), and the resulting pellet was resuspended in a final volume of 4.2 ml of ice-cold assay buffer. Aliquots (180 µl) of [^{3}H]DA-preloaded VMAT2C-associated vesicles were added to tubes in the absence (control) or presence of a range of analog concentrations (1 nM-1 mM), and incubated at 37 °C for 8 min. Incubations were terminated by addition of 2.5 ml of ice-cold assay buffer, followed by rapid filtration onto GF/B filters presoaked for 2 hr in 0.5% PEI. [^{3}H]DA remaining in the vesicles following exposure to analog was retained by the filters. [^{3}H]DA release was determined by subtracting the radioactivity remaining in the vesicles in the presence of analog from that in the absence of analog (control).

Further experiments were performed to determine the mechanism of (R)-GZ-924-evoked biphasic release of [^{3}H]DA via VMAT2C. To isolate site(s) on

VMAT2C mediating the biphasic release induced by (R)-GZ-924, ability of TBZ and reserpine to inhibit this effect were determined. Aliquots (180 µl) of [^{3}H]DA-preloaded vesicles were added to duplicate tubes containing (R)-GZ-924 (1 nM-1 mM) in the absence and presence of TBZ (30 nM) or reserpine (50 nM), and incubated in a final volume of 200 µl for 8 min at 37 °C. TBZ and reserpine concentrations were chosen based on previous observations that these concentrations did not evoke [^{3}H]DA release from VMAT2C-associated vesicles (Fieber and Adams, 1991; Horton et al., 2011b). The ability of (R)-GZ-924 to inhibit methamphetamine-evoked [^{3}H]DA release from vesicles via VMAT2C was determined using published method (Horton et al., 2013). [^{3}H]DA-preloaded vesicles (180 µl) were added to duplicate tubes containing methamphetamine (100 nM-1 mM) in the absence and presence of (R)-GZ-924 (3-300 nM). Samples were incubated in a final volume of 200 µl for 8 min at 37ºC and processed as previously described.

In the previous vesicular [^{3}H]DA release study in Chapter 2 (Section 2.2.6), the vesicles collected were VMAT2C vesicles. In the slice release, both VMAT2C and VMAT2M vesicles existed in each intact slice (Figure 3.21). The lead analog in Chapter 2 [(±)-GZ-730B] inhibited methamphetamine-evoked [^{3}H]DA release from synaptic vesicles but endogenous DA release from striatal slices. The incomplete vesicular VMAT2 preparation in the vesicular [^{3}H]DA release study might be responsible for the conflict between those studies. In the current study, the ability of (R)-GZ-924 to inhibit methamphetamine-evoked [^{3}H]DA release from vesicles via VMAT2C and VMAT2M was determined in a

within subject design. Studies on VMAT2M uptake was done at 30 °C in the literature instead of 37 °C (Chu et al., 2010). Thus, all the studies on VMAT2M in this chapter were performed at 30 °C. In order to compare the results between studies using VMAT2C and VMAT2M, inhibition of methamphetamine-evoked [^{3}H]DA release by (R)-GZ-924 via VMAT2C was performed at 30 °C as well.

At a different temperature, function of the transporter might be different and the experiment condition needed to be optimized. Before the inhibition assay at 30 °C, the concentration of [^{3}H]DA and time points at which VMAT2C and VMAT2M vesicles were saturated during the first incubation in the vesicular [^{3}H]DA release study needed to be determined. In order to determine the concentration of [^{3}H]DA utilized in the first incubation in the VMAT2C and VMAT2M [^{3}H]DA release study, [^{3}H]DA uptake kinetic study was required. Furthermore, to perform the above [^{3}H]DA uptake kinetic study, an optimal incubation time needed to be determined by a time course study. Thus, the time points at which VMAT2C and VMAT2M were saturated by 0.1 µM [^{3}H]DA at 30 °C was determined first. 0.1 µM [^{3}H]DA was chosen since the affinity of [^{3}H]DA for VMAT2C was around 0.1 µM (Chu et al., 2010; Nickell et al., 2011b). VMAT2C containing vesicles were isolated as described above. VMAT2M vesicle pellets from rat striata were collected after 20,000 g centrifugation as for the VMAT2C [^{3}H]DA uptake assay. Aliquots of 100 µl of VMAT2C or VMAT2M vesicular suspensions were added to tubes containing 350 µl assay buffer and 50 µl of [^{3}H]DA (0.1 µM final concentration). Total [^{3}H]DA uptake was determined in the absence of drugs. VMAT2C non-specific [^{3}H]DA uptake was determined in

the presence of 10 µM RO4-1284 alone. VMAT2M non-specific [^{3}H]DA uptake was determined in the presence of 10 µM RO4-1284 and 0.1 µM GBR-12909. GBR-12909 was a potent DAT inhibitor (Sai et al., 2008) and was added to block [^{3}H]DA uptake by DAT. Since VMAT2M-containing vesicles were associated with the broken synaptosome membranes, DAT might exist on the membranes in the VMAT2M preparation. DAT may facilitate [^{3}H]DA uptake into the synaptic vesicles (Egana et al., 2009) and GBR-12909 was added to block DAT function. Specific [^{3}H]DA uptake was determined by subtracting the non-specific uptake from the total uptake. After 0.5, 1, 2, 3, 5, 8, and 12 min incubation at 30 °C, [^{3}H]DA uptake for each sample was terminated by filtration. Radioactivity remaining on the filters was determined as previously described. The time at which VMAT2C and VMAT2M vesicles were saturated by 0.1 µM [^{3}H]DA was 8 and 2 min, respectively (Figure 3.10). Thus, [^{3}H]DA uptake kinetics at VMAT2C and VMAT2M were performed using the respective optimal incubation time at 30 °C to determine the optimal concentration of [^{3}H]DA in the first incubation of the vesicular [^{3}H]DA release study. [^{3}H]DA uptake kinetics at VMAT2C at 30 °C was performed as above kinetic study except that the experiment was performed at 30 °C. [^{3}H]DA uptake kinetics at VMAT2M at 30 °C was performed as kinetics study using VMAT2C at 30 °C except that incubation was 2 min and VMAT2M non-specific [^{3}H]DA uptake was determined in the presence of 10 µM RO4-1284 and 0.1 µM GBR-12909. The concentration of [^{3}H]DA at which VMAT2C and VMAT2M vesicles was saturated under respective incubation time at 30 °C was 0.5 µM (Figure 3.11). However, great non-specific [^{3}H]DA uptake was found at

0.5 µM for both VMAT2C and VMAT2M, and 0.3 µM was chosen due to the relative smaller non-specific [^{3}H]DA uptake and the specific [^{3}H]DA that was very close to the V_{max}. The time points at which VMAT2C and VMAT2M vesicles were saturated by 0.3 µM [^{3}H]DA during the first incubation in the vesicular [^{3}H]DA release study was determined in the following time course study. The study was performed as above time course study except that the experiment was performed in the presence of 0.3 µM [^{3}H]DA. The time at which VMAT2C and VMAT2M vesicles were saturated by 0.3 µM [^{3}H]DA at 30 °C was 5 and 3 min, respectively (Figure 3.12).

The same temperature and time of incubation as the above time course study using 0.3 µM [^{3}H]DA was used in the first incubation in the vesicular [^{3}H]DA release study. After the first incubation with 0.3 µM [^{3}H]DA for 5 min at 30 °C, VMAT2C associated vesicles were centrifuged at 100,000 g, and the resulting pellet was resuspended in a final volume of 4.2 ml of ice-cold assay buffer. VMAT2M-associated vesicle was incubated with 0.3 µM [^{3}H]DA at 30 °C for 3 min, and samples containing the VMAT2M-associated vesicle suspension were centrifuged (20,000g for 20 min at 4 °C), and the resulting pellet was resuspended in a final volume of 4.2 ml of ice-cold assay buffer. [^{3}H]DA-preloaded vesicles containing VMAT2C or VMAT2M (180 µl) were added to duplicate tubes containing methamphetamine (100 nM-1 mM) in the absence and presence of (R)-GZ-924 (3-300 nM). Samples were incubated in a final volume of 200 µl for 5 min using VMAT2C and 3 min using VMAT2M, respectively, at 30 ºC, and processed as previously described.

3.2.8 [^{3}H]Dofetilide Binding Assay to HERG Channels Expressed in HEK-293 Cells Membranes

The HEK-293 cell line stably expressing the human ERG (ether-a-go-go related gene) potassium channel (accession number U04270) was obtained at passage 11 (P11) from Millipore (CYL3006, lot 2, Billerica, MA). hERG-HEK cells were cultured according to the pr

Cell membrane were prepared based on previously described methods (Erickson et al., 1990; Fieber and Adams, 1991; Finlayson et al., 2001; Nooney et al., 1992) using cells grown from two different batches provided by Millipore. Cells were rinsed with pre-warmed (37 °C) HBSS (Life Technologies, Carlsbad, CA). Cells were then collected by scraping the 150 mm dishes using 13 ml plus 5 mL ice-cold 0.32 M sucrose with a Corning® cell scrapers blade L 1.8 cm (Sigma-Aldrich, St. Louis, MO). Harvested cell suspensions were poured into centrifuge tubes and homogenized on ice with a Teflon pestle using a Maximal Digital homogenizer (Fisher Scientific). Cells were then pelleted by centrifugation at 300 g and 800 g for 4 min each at 4 °C. Pellets were resuspended in 9 mL of ice-cold Milli-Q water. Osmolarity was restored by the addition of 1 mL of 500 mM Tris buffer (pH 7.4) and homogenization. Cellular suspensions were centrifuged again at 20,000 g for 30 min at 4 °C. Resulting pellets were homogenized in ~2 mL assay buffer composed of 50 mM Tris, 10 mM KCl, 1 mM $MgCl_2$ (pH 7.4), prepared the day prior to plasma membrane preparation and kept at 4 °C. Homogenization was performed using Pasteur glass pipettes and 2 ml tissue grinders (Kimble Chase, Vineland, NJ), and aliquots of cell membranes were stored at -80 °C. Cell membranes were thawed prior to assay, and protein content was determined using a Bradford Protein Assay (Bradford, 1976) and albumin from bovine serum (Sigma, St. Louis, MO, A2153) as the standard.

The potassium channel I_{Kr} coded by hERG plays a major role in phase 3 repolarization of ventricular myocytes by opposing the depolarizing Ca^{2+} influx during the plateau phase (Sanguinetti et al., 1995). Analogs with high affinity for

this channel have potential to possess cardiac toxicity. Dofetilide, an antiarryhtmic agent, has been shown to preferentially block open (or activated) hERG transfected in HEK-293 cells (Snyders and Chaudhary, 1996). [^{3}H]Dofetilide binding assays were utilized to determine the affinity of analogs for this channel. [^{3}H]Dofetilide binding assays were performed at room temperature in a Tris buffer (50 mM Tris, 10 mM KCl, 1 mM $MgCl_2$; pH 7.4) as previously reported (Nooney et al., 1992). Buffer was prepared less than 48 h before the assay and kept at 4 °C. The reaction protocol was as follows: cell membrane suspension (4-10 µg) was added to tubes containing assay buffer, 25 µl of test compound or the corresponding vehicle and 25 µl of [^{3}H]dofetilide (5 nM, final concentration) for a final volume of 250 µl. Nonspecific binding was determined in the presence of amitriptyline (1 mM). Amitriptyline has been reported to induce QT prolongation by blocking the current of heterologously expressed hERG potassium channels (Jo et al., 2000; Teschemacher et al., 1999). Assays were performed in duplicate. Reactions proceeded for 60 min at room temperature and were terminated by rapid filtration in a Brandel M-48 cell/membrane harvester using GF/B Glass Fiber FP-105 filters (Brandel Inc., Gaithersburg, MD) pre-soaked in 0.25% polyethylenimine solution (PEI, Fluka/Sigma-Aldrich, St. Louis, M) overnight. Filters were then washed three times with ~1 ml of ice-cold assay buffer. Filter discs that match the filter grids of the Brandel harvester were transferred into vials, and 5 ml scintillation cocktail (Research Products International Corporation, Mount Prospect, IL) was added. Radioactivity was determined by liquid scintillation spectrometry.

3.2.9 Inhibition of Methamphetamine-Evoked Endogenous and [^{3}H]DA Release from Striatal Slices

To determine if (R)-GZ-924 inhibition of methamphetamine-induced DA release from vesicles translated to inhibition of methamphetamine-induced DA release from the intact striatal slice preparation, a previously described slice superfusion methodology was employed and modified (Gerhardt et al., 1989). [^{3}H]DA was used to determine the ability of (R)-GZ-924 to inhibit methamphetamine-evoked DA release from synaptic vesicles, while endogenous DA was measured to determine the ability of (R)-GZ-924 to inhibit methamphetamine -evoked DA release from striatal slice. To preclude the influence of different label between those two studies, [^{3}H]DA was also measured to determine the ability of (R)-GZ-924 to inhibit methamphetamine evoked DA release from striatal slice.

In the endogenous release study, striatal slices (0.5 mm thickness) were prepared and incubated for 60 min in Krebs' buffer (118 mM NaCl, 4.7 mM KCl, 1.2 mM $MgCl_2$, 1.0 mM NaH_2PO_4, 1.3 mM $CaCl_2$, 11.1 mM α-D-glucose, 25 mM $NaHCO_3$, 0.11 mM L-ascorbic acid, and 0.004 mM EDTA, pH 7.4, saturated with 95% O_2/5% CO_2) at 34 °C in a metabolic shaker. Each slice was transferred to a glass superfusion chamber and superfused with Krebs' buffer at 1 ml/min for 60 min prior to sample collection. Samples (1 ml) were collected for 1 min every 5 min during the 80 min superfusion period. Initially, two samples were collected in the absence of analog to determine basal DA outflow. Each slice was superfused

for 30 min with a single concentration (0, 0.3-30 μM) of (R)-GZ-924 to determine analog-evoked fractional release. Then, methamphetamine (5 μM) was added to the buffer with (R)-GZ-924 for 15 min, followed by an additional 25 min of superfusion with (R)-GZ-924 alone. In each experiment, duplicate control slices were superfused with methamphetamine in the absence of (R)-GZ-924. Methamphetamine concentration (5 μM) and exposure time (15 min) were chosen to provide reliable DA release of sufficient quantity to allow evaluation of inhibition by (R)-GZ-924 (Horton et al., 2011b). Samples (1 ml) were kept on ice. Perchloric acid (0.1 M; 50 μl) was added to each sample. Upon assay, 20 μl ascorbate oxidase (168 U/mg reconstituted to 81 U/ml) was added to a 500 μl aliquot of each sample. Samples were vortexed for 30 s and an aliquot (100 μl) was injected into the HPLC-EC system to determine amounts of DA and DOPAC in the superfusate samples.

The HPLC-EC system consisted of a pump (model 126; Beckman Coulter, Fullerton, CA), autosampler (model 508; Beckman Coulter), an ODS Ultrasphere C18 reverse-phase 80 × 4.6 mm, 3 μm column, and a Coulometric-II detector with guard cell (model 5020) maintained at + 0.60 V and analytical cell (model 5011) with E1 and E2 set at −150 mV and +350 mV, respectively (ESA Inc., Chelmsford, MA). HPLC mobile phase (flow rate, 1.2 ml/min) consisted of 0.07 M citrate/0.1 M acetate buffer, containing 175 mg/L octylsulfonic acid sodium salt and 650 mg/L NaCl (pH 4.2) and 7% methanol. Separations were performed at room temperature, and 5 to 6 min was required to process each sample. Retention times of DA and DOPAC standards were used to identify respective

peaks. Peak heights were used to quantify the detected amounts of DA and DOPAC based on standard curves. Detection limit for DA and DOPAC was 1 to 2 pg/100 µl.

In the [^{3}H]DA release study, each slice was incubated as above except that slices were incubated for 30 min with Krebs' buffer followed by incubation for 30 min with 0.1 µM [^{3}H]DA (final concentration). Each slice was transferred to a glass superfusion chamber as above, but superfused with the Krebs' buffer at 1 ml/min for 60 min in the absence or presence of 10 µM pargyline, a MAO inhibitor. Superfusion experiments were conducted in the absence and presence of pargyline using a within-subject design in order to evaluate the effects of methamphetamine and (R)-GZ-924 with and without, respectively, metabolism of the [^{3}H]DA. Samples were collected the same way as in the endogenous DA release study except that 5 ml of samples were collected every 5 min. [^{3}H]-content in the superfusate samples were determined by liquid β-scintillation spectrometry.

3.2.10 Inhibition of Nicotine-Evoked [^{3}H]DA Overflow Assay

To determine if (R)-GZ-924 inhibition of methamphetamine-evoked DA release from striatal slices was specific, the ability of the analog to inhibit nicotine-evoked [^{3}H]DA release from rat striatal slices was evaluated using a previously described method (Smith et al., 2010). Rat striatal slices (0.5 mm thickness) were incubated as previously described in the [^{3}H]DA release study. Slices were transferred to an automated superfusion system maintained at 34 °C

(Brandel Suprafusion system 2500, Biomedical Research & Development Laboratories, Inc., Gaithersburg, MD) and superfused for 60 min with Krebs' buffer at 0.6 ml/min flow rate. Buffer contained 10 μM nomifensine (a DA uptake inhibitor) to prevent reuptake of [^{3}H]DA and 10 μM pargyline (a MAO inhibitor) to prevent metabolism of [^{3}H]DA, assuring that the superfusate [^{3}H] primarily represents parent neurotransmitter (Mantle et al., 1976; Smith et al., 2010). Superfusate samples were collected every 4 min (2.4 ml/sample). The first two samples were collected in the absence of (R)-GZ-924 to determine basal [^{3}H]DA outflow. Each slice was superfused for 36 min in the absence (control) or presence of a single concentration of (R)-GZ-924 (0, 0.01 nM-10 μM), followed by addition of nicotine (10 μM) to the buffer and superfusion for 36 min. Nicotine concentration and exposure time were chosen based on a previous report, in which 10 μM nicotine evoked [^{3}H]DA release from striatal slices during the 36 min period (Smith et al., 2010). A control slice in each experiment was superfused for 36 min in the absence of (R)-GZ-924, followed by addition of 10 μM nicotine to the buffer to determine nicotine-evoked [^{3}H]DA overflow. (R)-GZ-924 remained in the buffer throughout the superfusion period. At the end of each experiment, slices were solubilized, and [^{3}H]-content remaining in the tissue and [^{3}H] in the superfusate samples were determined by liquid β-scintillation spectrometry.

3.2.11 [^{3}H]Nicotine and [^{3}H]MLA Binding Assays

Analog-induced inhibition of [^{3}H]nicotine and [^{3}H]MLA binding was determined using published methods (Miller et al., 2004). Whole brain, excluding cortex and cerebellum, was homogenized using a Tekmar polytron (Tekmar-Dohrmann, Mason, OH) in 20 volumes of ice-cold modified Krebs'-HEPES buffer containing 2 mM HEPES, 14.4 mM NaCl, 0.15 mM KCl, 0.2 mM $CaCl_2$, and 0.1 mM MgSO4, pH 7.5. Homogenates were centrifuged at 31,000g for 17 min at 4 °C (Avanti J-301 centrifuge; Beckman Coulter, Fullerton, CA). Pellets were resuspended by sonication (Vibra Cell; Sonics and Materials Inc., Danbury, CT) in 20 volumes of Krebs'-HEPES buffer and incubated at 37 °C for 10 min (Reciprocal Shaking Bath model 50; Precision Scientific, Chicago, IL). Suspensions were centrifuged using the above conditions. Resulting pellets were resuspended by sonication in 20 volumes buffer and centrifuged at 31,000g for 17 min at 4°C. Final pellets were stored in incubation buffer containing 40 mM HEPES, 288 mM NaCl, 3.0 mM KCl, 4.0 mM $CaCl_2$, and 2.0 mM $MgSO_4$, pH 7.5. Membrane suspensions (100–140 µg of protein/100 µl) were added to duplicate wells containing 50 µl of analog (7-9 concentrations, 1 nM-0.1 mM, final concentration), 50 µl of buffer, and 50 µl of [^{3}H]nicotine or [^{3}H]MLA (3 nM; final concentration) for a final volume of 250 µl and incubated for 1 h at room temperature. Nonspecific binding was determined in the presence of 10 µM cytisine or 10 µM nicotine for the [^{3}H]nicotine and [^{3}H]MLA assays, respectively. Reactions were terminated by harvesting samples on Unifilter-96 GF/B filter plates presoaked in 0.5% PEI using a Packard Filter Mate Harvester

(PerkinElmer Life and Analytical Sciences). Samples were washed three times with 350 µl of ice-cold buffer. Filter plates were dried for 60 min at 45 °C and bottom-sealed, and each well was filled with 40 µl of Microscint 20 cocktail. Bound radioactivity was determined via liquid scintillation spectrometry (TopCount NXT scintillation counter; PerkinElmer Life and Analytical Sciences).

3.2.12 Methamphetamine Self-Administration

To determine whether (R)-GZ-924 decreases methamphetamine self-administration, behavioral experiments were conducted as described previously in Dr. Bardo's lab (Neugebauer et al., 2007). Operant conditioning chambers (ENV-008; MED Associates, St. Albans, VT) were enclosed within sound-attenuating compartments (ENV-018M; MED Associates). Each chamber was connected to a personal computer interface (SG-502; MED Associates), and was operated using MED-PC software. A recessed food tray (5 × 4.2 cm) was located on the response panel of each chamber. Two retractable response levers were mounted on either side of the recessed food tray (7.3 cm above the metal rod floor). A white cue light (28-V and 3-cm diameter) was mounted 6 cm above each response lever.

Rats were trained briefly to respond on a lever for food reinforcement. Immediately after food training, rats were allowed free access to food for 3 days. Then, rats were anesthetized (100 mg/kg ketamine and 5 mg/kg diazepam, i.p.), and catheters were implanted into the right jugular vein, exiting through a dental acrylic head mount affixed to the skull via jeweler screws. Methamphetamine

infusions were administered (i.v., 0.1 ml over 5.9 s) via a syringe pump (PHM-100; MED Associates) through a water-tight swivel attached to a 10 ml syringe via catheter tubing, which was attached to the cannula mounted to the head of the rat. A 1-week recovery period from surgery was allowed, and then, rats were trained to press one of two levers for an infusion of methamphetamine (0.05 mg/kg/infusion). A 20 s timeout signaled by illumination of both lever lights was initiated after each infusion. The response requirement was gradually increased to a terminal fixed ratio (FR) 5 schedule of reinforcement. Each session was 60 min duration. Training continued until responding stabilized across sessions. Stable responding was defined as less than 20% variability in the number of infusions earned across 3 successive sessions, a minimum of a 2:1 ratio of active (methamphetamine) lever responding to inactive (no drug) lever responding, and at least 10 infusions per session. After stability was reached, an acute dose (0, 1-30 mg/kg, s.c.) of (R)-GZ-924 was administered 15 min before the session according to a within-subject Latin square design. Dose range of (R)-GZ-924 was chosen based on the dose of lobeline and lobelane (3.0 and 5.6 mk/kg, s.c.) that inhibited methamphetamine self-administration in rats (Harrod et al., 2001; Neugebauer et al., 2007). Two maintenance sessions (i.e., no pretreatment) were included between each test session to ensure stable responding throughout the experiment.

3.2.13 Food-Maintained Responding

To determine the specificity of (R)-GZ-924 effect on responding for methamphetamine, the ability of (R)-GZ-924 to decrease responding for food was determined as described previously (Neugebauer et al., 2007). Drug naïve rats were trained to respond on one lever (active lever) for food pellet reinforcement (45 mg pellets; BIO-SERV, Frenchtown, NJ), while responding on the other lever (inactive lever) had no programmed consequence. Locations (left or right) of the active and inactive levers were counterbalanced across rats. The response requirement was gradually increased, terminating at FR 5. After lever training, a 20 s signaled timeout (illumination of both lever lights) was initiated after each pellet delivery. Timeout after each pellet delivery was included to be consistent with the methamphetamine self-administration procedure. Each food-reinforced session lasted 60 min. Training continued until responding stabilized across sessions. Stable responding was defined as less than 20% variability in the number of pellets earned across 3 successive sessions, and a minimum of a 2:1 ratio of active lever responding to inactive lever responding. After the stability criteria were met, an acute dose of (R)-GZ-924 (1 or 15 mg/kg, s.c.) was administered 15 min before the 60 min session. Dose was chosen base on the dose response of (R)-GZ-924 to inhibit methamphetamine self-administration in rats. Two maintenance sessions (i.e., no pretreatment) were included between test sessions to ensure stable responding throughout the experiment. In addition, to assess the effect of repeated (R)-GZ-924 on food responding, rats were pretreated with(R)-GZ-924 (10 mg/kg, s.c., a dose from the dose response of

(R)-GZ-924 to inhibit methamphetamine self-administration in rats) for 9 sessions.

3.2.14 Data Analysis

For studies using vesicles, synaptosomes, and hERG-HEK-293 cell membranes, specific [^{3}H]DTBZ binding, [^{3}H]DA uptake, [^{3}H]nicotine binding, [^{3}H]MLA binding, and [^{3}H]dofetilide binding were determined by subtracting the nonspecific binding or uptake from the total. Non-specific [^{3}H]DTBZ binding and vesicular [^{3}H]DA uptake were determined in the presence of RO4-1284. Nonspecific [^{3}H]nicotine and [^{3}H]MLA binding was determined in the presence of cytisine or nicotine, respectively. Non-specific synaptosomal [^{3}H]DA uptake and [^{3}H]dofetilide binding were determined in the presence of nomifensine and amitriptyline, respectively. Concentrations of analogs that produced 50% inhibition of maximal binding or uptake (IC_{50} values) or evoked 50% of [^{3}H]DA release (EC_{50} values) were determined from the concentration-response curves via an iterative curve-fitting program (Prism 5.0; GraphPad Software Inc., San Diego, CA). Inhibition constants (K_i values) were determined using the Cheng-Prusoff equation (Cheng and Prusoff, 1973). To determine if the structural changes to the lobelane molecule increased affinity for the VMAT2C binding site, the VMAT2C uptake site and for DAT, two-tailed t tests were performed to compare the log K_i value for each analog to lobelane, the parent compound, in each assay. For kinetic analyses of [^{3}H]DA uptake at VMAT2C, K_m and V_{max} values were determined from concentration-response curves. To determine the

mechanism of analog-induced inhibition of [^{3}H]DA uptake at VMAT2C, two-tailed t-tests were performed on the arithmetic V_{max} and the log K_m values obtained in the presence of analog compared to those under control conditions in the absence of analog. To assess if analog affinity at the DTBZ site on VMAT2C was associated with analog affinity at the [^{3}H]DA uptake on VMAT2C, Spearman correlation of the K_i values for the [^{3}H]DTBZ binding assays and K_i values for the vesicular [^{3}H]DA uptake assays for all analog was conducted. For vesicular [^{3}H]DA release assay, F test was performed to compare the fits of two equations, the one-site binding model and the two-site binding model. (R)-GZ-924 inhibition of methamphetamine-evoked vesicular [^{3}H]DA release was analyzed by two-way repeated-measures ANOVA, with (R)-GZ-924 and methamphetamine concentration as repeated measures factors. If a significant (R)-GZ-924 x methamphetamine interaction was found, one-way ANOVAs followed by Dunnetts's tests were performed at each methamphetamine concentration to determine the (R)-GZ-924 concentrations that decreased methamphetamine-evoked [^{3}H]DA release. To further elucidate the mechanism of (R)-GZ-924 inhibition of methamphetamine-evoked [^{3}H]DA release, a Lew and Angus plot of the pEC_{50} values as a function of log (R)-GZ-924 concentration was generated, and the data underwent linear regression using Prism 5.0 (GraphPad Software Inc.). Difference from unity of the regression slope (95% confidence intervals) determined if the interaction was orthosteric or allosteric (Kenakin, 2006b). inhibition of methamphetamine-evoked

For the methamphetamine-evoked endogenous and radiolabeled DA release, DA, DOPAC and [^{3}H]DA concentrations in each superfusate sample were divided by the respective striatal slice weight to obtain fractional release. For nicotine-evoked [^{3}H]DA overflow study, amount of [^{3}H] was divided by the total tissue [^{3}H] at the time of sample collection to obtain the fractional release. Basal endogenous DA and DOPAC, and [^{3}H]DA outflow were determined as the average fractional release in the two superfusate samples collected just before addition of (R)-GZ-924 to the buffer. To determine if (R)-GZ-924 in a concentration and time dependent manner evoked fractional DA, DOPAC, and [^{3}H]DA release, two-way repeated-measures ANOVA was performed on release in samples obtained prior to addition of either methamphetamine or nicotine to the buffer. If concentration × time interactions were found, one-way ANOVAs were performed at each time point to determine the (R)-GZ-924 concentrations that evoked fractional DA and DOPAC release, and that evoked [^{3}H]DA release. To determine if (R)-GZ-924 in a concentration and time dependent manner inhibited the effect of methamphetamine on fractional DA and DOPAC release and inhibited the effect of nicotine on fractional [^{3}H]DA release, two-way repeated-measures ANOVA was performed on release data in samples after the addition of methamphetamine or nicotine to the buffer. If concentration × time interactions were found, one-way ANOVAs were performed at each time point to determine the (R)-GZ-924 concentrations that inhibited methamphetamine-evoked or nicotine-evoked release. To determine if the effect of (R)-GZ-924 to

evoke [^{3}H]DA release was altered by pargyline, three-way repeated-measures ANOVA was performed.

Endogenous DA and DOPAC overflow, and [^{3}H]DA overflow were determined by summing the fractional release data to obtain the total overflow across time and subtracting basal outflow for that same amount of time. One-way ANOVAs were performed to determine if (R)-GZ-924 in a concentration-dependent manner evoked DA, DOPAC, or [^{3}H]DA overflow. One-way ANOVAs also determined if (R)-GZ-924 inhibited methamphetamine-evoked DA and DOPAC overflow, and nicotine-evoked [^{3}H]DA overflow in a concentration-dependent manner. Dunnett's post hoc tests were used to compare treatment to control conditions when appropriate. When analyzing (R)-GZ-924-induced DA, DOPAC, and [^{3}H]DA overflow, control represents overflow in the absence of the analog. When analyzing the ability of (R)-GZ-924 to inhibit the effect of methamphetamine or nicotine, control represents overflow in the presence of methamphetamine or nicotine alone. Overflow data were fit to concentration-response curves via Prism 5.0 (GraphPad Software Inc.). IC_{50} and I_{max} values for (R)-GZ-924 were determined from the inhibition curves.

For the behavioral experiments, to determine whether (R)-GZ-924 decreased methamphetamine self-administration and food-maintained responding, one-way ANOVAs with dose as a within-subject factor were performed. Dunnett's post hoc tests were used to compare the (R)-GZ-924

treatment to the saline control condition when appropriate. Statistical significance was defined at $p < 0.05$.

3.3 Results

3.3.1 Inhibition of [^{3}H]DTBZ Binding at VMAT2C

In order to determine analogs affinity for the DTBZ site on VMAT2C, [^{3}H]DTBZ binding inhibition assay was performed. Concentration-response curves for the series of racemic, acyclic lobelane analogs, the pure enantiomers, and for the standards lobelane, lobeline, and RO4-1284 to inhibit [^{3}H]DTBZ binding to whole brain membranes are illustrated in Figure 3.2. K_i and I_{max} values from the concentration-response curves are provided in Table 3.1 and Table 3.2. The standard compounds, RO4-1284, lobelane and lobeline had K_i values of 0.016 ± 0.0013, 0.97 ± 0.19 and 3.5 ± 1.0 μM, whici have been shown in Table 2.1. At the highest concentration evaluated, the majority of the racemic analogs completely inhibited [^{3}H]DTBZ binding; however, all of the analogs inhibited binding by at least 70% of control. A wide range of K_i values (96 nM to 17 μM) was obtained for the racemic analogs.

Analogs incorporating a homoamphetamine scaffold and a 2-3-carbon linker exhibited affinity either not different from or lower than that for lobelane (Figure 3.2, top left panel). Of note, (±)-GZ-813B and (±)-GZ-814B, the N-methylated analogs with a 3-carbon linker and a 2-carbon linker respectively, exhibited affinity for the [^{3}H]DTBZ binding site (K_i = 17 ± 6.3 μM and 30 ± 11 μM,

respectively) that was18- and 31-fold lower than that for lobelane [$t_{(4)}$ = 7.15, p < 0.01; $t_{(4)}$ = 8.77, p < 0.001, respectively].

Generally, racemic analogs incorporating an amphetamine scaffold and a 2, 4, 5 or 6-carbon linker exhibited affinity for the [^{3}H]DTBZ binding site either not different from or lower than that for lobelane, with the exception of (±)-GZ-893A (see below) (Figure 3.2, top right panel). As examples, (±)-GZ-861B and (±)-GZ-816B, which incorporates a 2-carbon linker, the absence or presence of an N-methyl substituent, and an amine or methoxy R_2-subtituent on the phenyl ring of the amphetamine side of the molecule, exhibited affinity (K_i = 17 ± 6.6 µM and 12 ± 1.8 µM, respectively) for the [^{3}H]DTBZ binding site, which was 18- and 13-fold, respectively, lower than lobelane [$t_{(4)}$ = 18.9, p < 0.0001; $t_{(4)}$ = 12.0, p < 0.001, respectively]. The exception, (±)-GZ-893A, a nor-analog with a 4-carbon linker and a bromo R_2-substituent on the amphetamine phenyl ring, exhibited a 10-fold higher affinity [K_i = 0.096 ± 0.043 µM; $t_{(4)}$ = 4.97, p < 0.01] for the [^{3}H]DTBZ binding site compared to lobelane. (±)-GZ-893A was the most potent analog for the [^{3}H]DTBZ binding site in the acyclic lobelane analog series.

Racemic analogs incorporating an amphetamine scaffold and a 3-carbon linker exhibited affinity for the [^{3}H]DTBZ binding site either not different from or lower than that for lobelane, with the exception of (±)-GZ-865G (Figure 3.2, bottom left panel). Analogs within the range of affinities include (±)-GZ-815A, (±)-GZ-819A and (±)-GZ-819B, with K_i values of 1.3 ± 0.086, 0.43 ± 0.047, 2.6 ± 0.47 µM, respectively. The exception, (±)-GZ-865G, a nor-analog with a hydroxyl R_2

and a methoxy R_3-substituent, had 3-fold higher affinity [K_i = 0.28 ± 007 μM; $t_{(4)}$ = 3.20, $p < 0.05$] than that for lobelane.

Concentration-response curves for inhibition of [^{3}H]DTBZ binding for (R)-GZ-878A and (S)-GZ-878B, which are pure enantiomers of (±)-GZ-815A, for (R)-GZ-880A and (S)-GZ-880B, which are pure enantiomers of (±)-GZ-819A, and for (R)-GZ-924 and (S)-GZ-925, which are pure enantiomers of (±)-GZ-819B, are illustrated in Figure 3.2 (bottom right panel). K_i and I_{max} values for the pure enantiomers are provided in Table 3.2. All of the pure enantiomers inhibited [^{3}H]DTBZ binding by at least 90%, with K_i values ranging from 0.75 to 1.1 μM. Enantioselectivity for the [^{3}H]DTBZ binding site was not observed. Furthermore, K_i values for the enantiomers were not different from that for lobelane.

3.3.2 Inhibition of [^{3}H]DA Uptake at VMAT2C

In order to determine analogs affinity for the DA translocation site on VMAT2C, vesicular [^{3}H]DA uptake inhibition assay was performed. Concentration-response curves of racemic, acyclic lobelane analogs, the pure enantiomers and the standards lobelane, lobeline, and RO4-1284 are illustrated in Figure 3.3. K_i and I_{max} values are provided in Tables 3.1 and 3.2. The standard compounds, RO4-1284, lobelane and lobeline had K_i values for inhibition of [^{3}H]DA uptake of 41 ± 8.1, 40 ± 3.5, and 563 ± 30 nM, respectively, consistent with previous results (Nickell et al., 2010). At the highest concentration, all racemic analogs inhibited VMAT2C function by at least 90%. The range of K_i values for the series of racemic analogs was 3 to 510 nM. Within this series, (±)-

GZ-814B, (±)-GZ-813B, (±)-GZ-819C, (±)-GZ-815B, (±)-GZ-816B, and (±)-GZ-820C, exhibited affinities (K_i = 84-512 nM) lower than that for lobelane [$t_{(5)}$ = 6.56, $p < 0.01$; $t_{(5)}$ = 17.1, $p < 0.0001$; $t_{(5)}$ = 8.21, $p < 0.001$; $t_{(5)}$ = 11.5, $p < 0.0001$; $t_{(5)}$ = 13.1, $p < 0.0001$; $t_{(5)}$ = 13.1, $p < 0.0001$, respectively] and had a common structural feature of an N-methyl R_1 substituent.

For racemic analogs incorporating the homoamphetamine scaffold, (±)-GZ-854B, a nor-analog with a methoxy R_2, a bromo R_3-substituent and a 2-carbon linker, exhibited 4-fold higher affinity (K_i = 9.7 ± 4.4 nM) than lobelane [$t_{(5)}$ = 2.69, $p < 0.05$] for inhibition of VMAT2C function (Figure 3.3, top left panel). Similarly, (±)-GZ-865A, a nor-analog with methoxy R_3-substituent and a 3-carbon linker, had 2-fold higher affinity (K_i = 26 ± 2.3 nM) compared to lobelane [$t_{(5)}$ = 3.43, $p < 0.05$]. The remaining racemic analogs in this homoamphetamine subgroup exhibited affinities for DA uptake not different from or lower than that for lobelane.

Racemic analogs incorporating an amphetamine scaffold and a 2, 4, 5 or 6-carbon linker exhibited a wide range of affinity (K_i = 3-512 nM) for the DA translocation site on VMAT2C (Figure 3.3, top right panel). nor-Analogs or N-methylated analogs with a 2-carbon linker and various R_2 substituents exhibited affinity that were not different from or were lower than that for lobelane. nor-Analogs with a 4-carbon linker and including a R_2 bromo substituent [(±)-GZ-893A] or not including this substituent [(±)-GZ-893B] had 12-fold higher affinities (K_i = 3.3 ± 0.26 and 3.3 ± 1.7 nM, respectively) than lobelane [$t_{(5)}$ = 20.2, $p <$

0.001; $p < 0.05$; $t_{(5)} = 6.19$, $p < 0.01$, respectively]. nor-Analogs with a 5 or 6-carbon linker and no R_2 substituent [(±)-GZ-909, and (±)-GZ-908] exhibited 3- and 4-fold higher affinities (K_i = 14 ± 0.82, and 9.3 ± 1.8 nM respectively) than lobelane [$t_{(6)} = 9.78$, $p < 0.0001$; $t_{(6)} = 6.07$, $p < 0.0001$, respectively].

Racemic analogs incorporating the amphetamine scaffold and a 3-carbon linker also exhibited a wide range of affinity (K_i = 6.9-272 nM) for the DA translocation site on VMAT2C (Figure 3.3, bottom left panel). The majority of the nor-analogs in this amphetamine subgroup had higher affinity (K_i = 6.9-20 nM) than that for lobelane ($p < 0.05$). (±)-GZ-819B, a nor-analog incorporating an amphetamine scaffold, a 3-carbon linker and no R_2 and R_3 substituents, had the highest affinity (K_i = 6.9 ± 1.8 nM) for the DA translocation site on VMAT2C, and a 6-fold higher affinity than lobelane [$t_{(6)} = 6.50$, $p < 0.001$].

Concentration-response curves for inhibition of [^{3}H]DA uptake by VMAT2C for the three pairs of enantiomers [(R)-GZ-878A and (S)-GZ-878B, (R)-GZ-880A and (S)-GZ-880B, and (R)-GZ-924 and (S)-GZ-925] are illustrated in Figure 3.3 (bottom right panel); K_i and I_{max} values are provided in Table 3.2. K_i values ranged from 5.6 to 65 nM and [^{3}H]DA uptake was inhibited completely by each pure enantiomer. Enantioselectivity was observed between (R)-GZ-924 and (S)-GZ-925, the nor-enantiomers incorporating an amphetamine scaffold and a 3-carbon linker [K_i = 5.9 ± 1.0 and 65 ± 3.6 nM, respectively; $t_{(8)} = 9.65$, $p < 0.0001$], and between (R)-GZ-880A and (S)-GZ-880B, the nor-enantiomers incorporating a 4-bromo-amphetamine scaffold and a 3-carbon linker (K_i = 5.6 ±

0.95 and 32 ± 4.4 nM, respectively; $t_{(5)} = 7.42$, $p < 0.001$]. Enantioselectivity was not found for (R)-GZ-878A and (S)-GZ-878B, the nor-enantiomers incorporating a 4-methoxy-amphetamine scaffold and a 3-carbon linker. In addition, (R)-GZ-924 and (R)-GZ-880A exhibited 7-fold higher affinity for the [^{3}H]DA uptake site compared to lobelane [$t_{(8)} = 7.60$, $p < 0.0001$; $t_{(6)} = 10.2$, $p < 0.001$, respectively].

3.3.3 Correlation of K_i Values for the [^{3}H]DTBZ Binding and [^{3}H]DA Uptake at VMAT2C

In order to determine the relationship between affinity for the DTBZ site and affinity for the DA translocation site on VMAT2C, correlation of affinity for both sites was performed. With respect to the standard compounds, RO4-1284 exhibited 2-fold higher affinity for the binding site compared to the uptake site on VMAT2C, although not significantly different. Interestingly, lobeline and lobelane had 7- and 24-fold higher affinity for the uptake site relative to the binding site on VMAT2C. (±)-GZ-865G, the nor-analog incorporating an amphetamine scaffold, a 3-carbon linker, a hydroxyl R_2, and a methoxy R_3-substituent was an exception among the analogs, in that this analog was equipotent at VMAT2C binding and uptake sites. In contrast, all racemic analogs and enantiomers in the acyclic lobelane series exhibited affinity 12-650-fold higher at the uptake site relative to the binding site, and a positive correlation between the affinity for the binding site and uptake site for this series of compounds was found (Spearman r = 0.62; $p < 0.001$, Figure 3.4).

3.3.4 Mechanism of Inhibition of [^{3}H]DA Uptake at VMAT2C

In order to determine the mechanism of inhibition of [^{3}H]DA uptake at VMAT2C, kinetic studies were performed. Mechanism of action was evaluated for lobelane and the three pairs of enantiomers, (R)-GZ-787A and (S)-GZ-787B, (R)-GZ-880A and (S)-GZ-880B, and (R)-GZ-924 and (S)-GZ-925. Kinetic analyses of enantiomer inhibition of DA uptake were conducted using concentrations obtained for the respective K_i values from their inhibition curves (Figure 3.5). K_m and V_{max} values are provided in Table 3.3. Lobelane increased the K_m value for DA uptake by 9-fold [$t_{(10)} = 13.7$, $p < 0.0001$], with no change in V_{max}, consistent with a previous results (Nickell et al., 2011b). The enantiomers increased the K_m value for DA by 3-9-fold compared to control [$t_{(8)} = 9.25$ for (R)-GZ-924, $p < 0.0001$; $t_{(11)} = 2.42$ for (S)-GZ-925, $p < 0.05$; $t_{(8)} = 13.1$ for (R)-GZ-880A, $p < 0.0001$; $t_{(8)} = 4.61$ for (S)-GZ-880B, $p < 0.001$; $t_{(8)} = 13.9$ for (R)-GZ-878A, $p < 0.0001$; $t_{(8)} = 3.69$ for (S)-GZ-878B, $p < 0.01$], with no change in V_{max}, indicating competitive inhibition of VMAT2C function.

3.3.5 Inhibition of [^{3}H]Dofetilide Binding to HERG Channels

In order to determine analogs selectivity at VMAT2C over hERG channels, [^{3}H]dofetilide binding inhibition assay was performed. Potential for cardiac toxicity was evaluated using the [^{3}H]dofetilide binding assay. The standard compound, amitriptyline, had an IC_{50} value of 12 ± 4.8 μM, consistent with previous reports (Diaz et al., 2004). Lobelane and the three pairs of enantiomers were evaluated for inhibition of [^{3}H]dofetilide binding to hERG channels. IC_{50} values for lobelane

and the enantiomers are provided in Table 3.2. IC_{50} values for the enantiomers ranged from 0.78 to 8.5 μM and the selectivity of the enantiomers for VMAT2C function over hERG channels ranged from 35 to 510 fold. The most selective enantiomer, (R)-GZ-924, exhibited 510-fold higher inhibitory potency for VMAT2C function compared to hERG channels.

3.3.6 Inhibition of [^{3}H]DA Uptake at DAT

In order to determine analogs selectivity at VMAT2C over DAT, DAT [^{3}H]DA uptake inhibition assay was performed. Concentration-response curves for the pairs of pure enantiomers and the standards, lobelane and lobeline, are illustrated in Figure 3.6. K_i and I_{max} values are provided in Table 3.4. Lobelane and lobeline had K_i values for inhibition of [^{3}H]DA uptake of 1.3 ± 0.16 and 18 ± 0.76 μM, respectively, consistent with previous results (Nickell et al., 2010). At the highest concentrations, all of the enantiomers completely inhibited [^{3}H]DA uptake by DAT. The range of K_i values for the enantiomers was 1.0 to 5.8 μM. (R)-GZ-878A and (S)-GZ-878B, the pair of enantiomers incorporating a 4-methoxy-amphetamine scaffold and a 3-carbon linker, exhibited 4-fold lower affinity [K_i = 5.6 ± 1.3 and 5.2 ± 0.18 μM, respectively; $t_{(6)} = 5.74$, $p < 0.01$; $t_{(6)} = 11.2$, $p < 0.0001$, respectively] than lobelane inhibiting [^{3}H]DA uptake into synaptosomes. No significant difference in affinity for DAT was observed between (R)-GZ-878A and (S)-GZ-878B. The affinity for DAT of (R)-GZ-880A and (S)-GZ-880B, enantiomers incorporating a 4-bromo-amphetamine scaffold and a 3-carbon linker, were not different from that for lobelane. No significant

difference in affinity for DAT was observed between (R)-GZ-880A and (S)-GZ-880B as well. (S)-GZ-925, the compound incorporating an amphetamine scaffold and a 3-carbon linker, exhibited a 2-fold lower affinity (K_i = 2.6 ± 0.14 μM) than lobelane [$t_{(5)} = 4.79$, $p < 0.01$]. Enantiomeric selectivity was found for (R)-GZ-924 and (S)-GZ-925, with (S)-GZ-925 exhibiting 2-fold higher affinity than (R)-GZ-924 [$t_{(4)} = 11.6$, $p < 0.001$].

3.3.7 Release of [^{3}H]DA from Synaptic Vesicles

In order to determine analogs ability to redistribute DA from synaptic vesicles to cytosol, vesicular [^{3}H]DA release assay was performed. Concentration-response curves and EC_{50} and E_{max} values for lobelane, lobeline, methamphetamine, and the enantiomers to evoke [^{3}H]DA release from synaptic vesicles are provided in Figure 3.7. EC_{50} values of lobelane, lobeline, and methamphetamine were 0.26 ± 0.031, 13 ± 7.4, and 19 ± 4.1 μM, respectively (top left panel in Fig 3.7), as shown in top panel in Figure 2.7. The EC_{50} value for lobelane was 50-fold lower than that for lobeline [$t_{(6)} = 3.86$, $p < 0.01$], and 35-fold lower than that for methamphetamine [$t_{(6)} = 11.1$, $p < 0.001$]. All enantiomers released [^{3}H]DA from the synaptic vesicles in a biphasic manner [$F_{(2, 77)} = 71.3$ for (R)-GZ-924, $p < 0.0001$; $F_{(2, 50)} = 6.43$ for (S)-GZ-925, $p < 0.05$; $F_{(2, 29)} = 6.45$ for (R)-GZ-880A, $p < 0.05$, $F_{(2, 34)} = 14.1$ for (S)-GZ-880B, $p < 0.0001$; $F_{(2, 39)} = 5.98$ for (R)-GZ-878A, $p < 0.05$, $F_{(2, 48)} = 14.2$ for (S)-GZ-878B, $p < 0.001$]. Enantioselectivity was found between (R)-GZ-924 and (S)-GZ-925, the pair of enantiomers incorporating the amphetamine scaffold and the 3-carbon

linker. High EC_{50} value (96 ± 51 nM) of (S)-GZ-925 was 26-fold greater than that for (R)-GZ-924 [3.7 ± 0.64 nM, $t_{(9)} = 2.49$, $p < 0.05$]. No difference in the Low EC_{50} values was found between the two enantiomers. No enantioselectivity was found between (R)-GZ-880A and (S)-GZ-880B, or between (R)-GZ-878A and (S)-GZ-878B, the two pairs of enantiomers incorporating the 4-bromoamphetamine and the 4-methoxyamphetamine scaffold and the 3-carbon linker.

To determine whether the effect of (R)-GZ-924, the most potent and selective analog for VMAT2C, on vesicular DA release was due to the interaction with TBZ or reserpine binding site on VMAT2C, classical VMAT2 inhibitors, TBZ and reserpine (Scherman and Henry, 1984) was used to block the effect of the analog. The concentrations utilized were 30 nM for TBZ and 50 nM for reserpine. At these concentrations, the two compounds did not elicit [^{3}H]DA release from the synaptic vesicles (Horton et al., 2013; Nickell et al., 2011b). The concentration-response curves for (R)-GZ-924 to release [^{3}H]DA in the presence of TBZ and reserpine are illustrated in Figure 3.8. Both TBZ and reserpine inhibited the (R)-GZ-924-induced high affinity release, but not release associated with the low affinity site. In the presence of TBZ and reserpine, (R)-GZ-924-evoked [^{3}H]DA release best fit a one-site model [$F_{(2, 43)} = 1.79$ and $F_{(2, 43)} = 2.75$, respectively, $p > 0.05$].

3.3.8 (R)-GZ-924 Inhibition of Methamphetamine-Evoked [^{3}H]DA Release from Synaptic Vesicles via VMAT2C and VMAT2M

To determine the ability of (R)-GZ-924 to inhibit effect of methamphetamine at synaptic vesicles, methamphetamine-evoked vesicular [^{3}H]DA release was determined in the presence of the analog. Initially, the inhibition assay using VMAT2C was performed at 37 °C. The concentration response for methamphetamine-evoked vesicular [^{3}H]DA release in the absence and presence of (R)-GZ-924 via VMAT2C is illustrated in Figure 3.9. Two-way repeated-measures ANOVA revealed main effects of methamphetamine [$F_{(10, 132)}$ = 1190, $p < 0.0001$], (R)-GZ-924 [$F_{(3, 132)}$ = 222, $p < 0.0001$], and methamphetamine × (R)-GZ-924 interaction [$F_{(30, 132)}$ = 13.9, $p < 0.0001$]. (R)-GZ-924 inhibited methamphetamine at 10 µM [$F_{(3, 12)}$ = 99.7, $p < 0.0001$], at 30 µM [$F_{(3, 12)}$ = 226, $p < 0.0001$], at 100 µM [$F_{(3, 12)}$ = 258, $p < 0.0001$], at 200 µM [$F_{(3, 12)}$ = 40.6, $p < 0.0001$], at 500 µM [$F_{(3, 12)}$ = 42.5, $p < 0.0001$], and at 1000 µM [$F_{(3, 12)}$ = 18.6, $p < 0.0001$]. (R)-GZ-924 at 3, 30 and 300 nM inhibited [^{3}H]DA release evoked by methamphetamine at 10-100, 10-1000 and 10-1000 µM concentration ranges, respectively.

From the methamphetamine concentration-response curves at 37 °C, EC_{50} and E_{max} values in the absence and presence of (R)-GZ-924 via VMAT2C were generated and provided in Table 3.5. EC_{50} and E_{max} values for methamphetamine alone using VMAT2C were 11.9 ± 0.769 µM and 82.4 ± 0.614%, respectively, consistent with a previous study (Nickell et al., 2010).

Increasing concentrations of (R)-GZ-924 shifted the methamphetamine concentration-response curve to the right. (R)-GZ-924 (30 and 300 nM) increased [$F_{(3,12)}$ = 62.0, $p < 0.0001$] the log EC_{50} values by 5- and 14-fold in VMAT2C, whereas no changes in E_{max} values were found. Lew and Angus analysis revealed a linear fit (R^2 = 0.67, $p < 0.05$) with a slope of -0.44 and a 95% confidence interval of -0.51 and -0.36 in VMAT2C (Figure 3.9., inset). No overlap of the 95% confidence interval with unity indicate that (R)-GZ-924 inhibited methamphetamine-evoked [^{3}H]DA release in a surmountable allosteric manner in VMAT2C at 37 °C.

In the previous vesicular [^{3}H]DA release study in Chapter 2 (Section 2.2.6), the vesicles collected was VMAT2C vesicles. In the slice release, both VMAT2C and VMAT2M vesicles existed in each intact slice (Figure 3.21). The lead analog in Chapter 2 [(±)-GZ-730B] inhibited methamphetamine-evoked [^{3}H]DA release from synaptic vesicles but endogenous DA release from striatal slices. The incomplete vesicular VMAT2 preparation in the vesicular [^{3}H]DA release study might be responsible for the conflict between those studies. In the current study, the ability of (R)-GZ-924 to inhibit methamphetamine-evoked [^{3}H]DA release from vesicles via VMAT2C and VMAT2M was determined in a within subject design. Studies on VMAT2M uptake was done at 30 °C in the literature instead of 37 °C (Chu et al., 2010). Thus, all the studies on VMAT2M in this chapter were performed at 30 °C. In order to compare the results between studies using VMAT2C and VMAT2M, inhibition of methamphetamine-evoked [^{3}H]DA release by (R)-GZ-924 via VMAT2C was performed at 30 °C as well.

At a different temperature, function of the transporter might be different and the experiment condition needed to be optimized. Before performing the inhibition assay at 30 °C, the concentration of [^{3}H]DA and time points at which VMAT2C and VMAT2M vesicles was saturated during the first incubation in the vesicular [^{3}H]DA release study needed to be determined. In order to determine the concentration of [^{3}H]DA utilized in the first incubation in the VMAT2C and VMAT2M [^{3}H]DA release study, [^{3}H]DA uptake kinetic study was performed. Furthermore, to perform the above [^{3}H]DA uptake kinetic study, an optimal incubation time needed to be determined by a time course study. Thus, the time points at which VMAT2C and VMAT2M was saturated by 0.1 µM [^{3}H]DA at 30 °C was determined first. 0.1 µM [^{3}H]DA was chosen since the affinity of [^{3}H]DA for VMAT2C was around 0.1 µM (Chu et al., 2010; Nickell et al., 2011b). The time at which VMAT2C and VMAT2M vesicles were saturated by 0.1 µM [^{3}H]DA was 8 and 2 min, respectively (Figure 3.10). Thus, [^{3}H]DA uptake kinetics at VMAT2C and VMAT2M were performed using the respective optimal incubation time at 30 °C to determine the optimal concentration of [^{3}H]DA in the first incubation of the vesicular [^{3}H]DA release study (Figure 3.11). V_{max} and K_m values for VMAT2C was 42 ± 1.6 pmol/min/mg and 0.22 ± 0.030 µM, respectively. V_{max} and K_m values for VMAT2M was 15 ± 1.3 pmol/min/mg and 0.27 ± 0.039 µM, respectively. No difference of K_m between VMAT2M and VMAT2C was found. V_{max} for VMAT2M was lower compared to that for VMAT2C [$t_{(4)} = 13.1$, $p < 0.001$]. The concentration of [^{3}H]DA at which VMAT2C and VMAT2M vesicles was saturated under respective incubation time at 30 °C was 0.5 µM. However, great

non-specific [^{3}H]DA uptake was found at 0.5 µM. 0.3 µM was chosen due to the relative smaller non-specific [^{3}H]DA uptake and the specific [^{3}H]DA uptake that was very close to the V_{max}. The time points at which VMAT2C and VMAT2M vesicles was saturated by 0.3 µM [^{3}H]DA during the first incubation in the vesicular [^{3}H]DA release study was determined in the time course study. The time at which VMAT2C and VMAT2M vesicles were saturated by 0.3 µM [^{3}H]DA at 30 °C was 5 and 3 min, respectively (Figure 3.12).

The concentration response for methamphetamine-evoked vesicular [^{3}H]DA release at 30 °C in the absence and presence of (R)-GZ-924 via VMAT2C is illustrated in the top panel in Figure 3.13. Two-way repeated-measures ANOVA revealed main effects of methamphetamine [$F_{(10, 132)} = 167$, $p < 0.0001$], (R)-GZ-924 [$F_{(3, 132)} = 90.6$, $p < 0.0001$], and a methamphetamine × (R)-GZ-924 interaction [$F_{(30, 132)} = 2.83$, $p < 0.0001$]. (R)-GZ-924 inhibited methamphetamine at 0.1 µM [$F_{(3, 12)} = 8.83$, $p < 0.01$], at 1 µM [$F_{(3, 12)} = 8.98$, $p < 0.01$], at 3 µM [$F_{(3, 12)} = 36.4$, $p < 0.0001$], at 10 µM [$F_{(3, 12)} = 35.4$, $p < 0.0001$], at 30 µM [$F_{(3, 12)} = 34.3$, $p < 0.0001$], at 100 µM [$F_{(3, 12)} = 18.6$, $p < 0.0001$], at 200 µM [$F_{(3, 12)} = 12.5$, $p < 0.001$], and at 500 µM [$F_{(3, 12)} = 4.34$, $p < 0.05$]. (R)-GZ-924 at 3, 30 and 300 nM inhibited [^{3}H]DA release evoked by methamphetamine at 3-100, 0.1-500 and 0.1-500 µM concentration ranges, respectively.

From the methamphetamine concentration-response curves at 30 °C, EC_{50} and E_{max} values in the absence and presence of (R)-GZ-924 via VMAT2C were generated and provided in Table 3.6. EC_{50} and E_{max} values for

methamphetamine alone using VMAT2C were 10.3 ± 3.18 μM and 61.0 ± 5.56%, respectively, not different from that at 37 °C (11.9 ± 0.769 μM and 82.4 ± 0.614%). Increasing concentrations of (R)-GZ-924 shifted the methamphetamine concentration-response curve to the right in VMAT2C. (R)-GZ-924 (3, 30 and 300 nM) increased [$F_{(3,12)} = 29.5$, $p < 0.0001$] the log EC_{50} values by 11, 15 and 59-fold with no alteration of the E_{max} values for VMAT2C. Lew and Angus analysis revealed a linear fit ($R^2 = 0.68$, $p < 0.01$) with a slope of -0.37 and a 95% confidence interval of -0.55 and -0.19 for VMAT2C (top panel in Figure 3.13, inset). Similar to the study using VMAT2C at 37 °C, No overlap of the 95% confidence interval with unity indicated that (R)-GZ-924 inhibited methamphetamine-evoked [^{3}H]DA release in a surmountable allosteric manner when evaluating VMAT2C at 30 °C.

The concentration response for methamphetamine-evoked vesicular [^{3}H]DA release at 30 °C in the absence and presence of (R)-GZ-924 via VMAT2M is illustrated in the bottom panel in Figure 3.13. Two-way repeated-measures ANOVA revealed main effects of methamphetamine [$F_{(10, 132)} = 40.4$, $p < 0.0001$] and (R)-GZ-924 [$F_{(3, 132)} = 27.9$, $p < 0.0001$]. The methamphetamine × (R)-GZ-924 interaction was not significant. (R)-GZ-924 inhibited methamphetamine at 10 μM [$F_{(3, 12)} = 7.10$, $p < 0.01$], at 30 μM [$F_{(3, 12)} = 14.2$, $p < 0.001$], at 100 μM [$F_{(3, 12)} = 9.97$, $p < 0.01$], and at 200 μM [$F_{(3, 12)} = 5.35$, $p < 0.05$]. (R)-GZ-924 at 30 and 300 nM inhibited [^{3}H]DA release evoked by methamphetamine at 30 and 10-200 μM concentration ranges, respectively.

From the methamphetamine concentration-response curves at 30 °C, EC_{50} and E_{max} values in the absence and presence of (R)-GZ-924 via VMAT2M were generated and provided in Table 3.6. EC_{50} and E_{max} values for methamphetamine alone using VMAT2M were 5.28 ± 1.48 µM and 28.9 ± 4.39%, respectively. E_{max} for VMAT2M was significantly low compared to E_{max} for VMAT2C [$t_{(6)} = 4.53$, $p < 0.01$] at 30 °C. Increasing concentrations of (R)-GZ-924 shifted the methamphetamine concentration-response curve to the right in VMAT2M. (R)-GZ-924 (30 and 300 nM) increased [$F_{(3,12)} = 29.4$, $p < 0.0001$] the log EC_{50} values by 14 and 110-fold, respectively, with no alteration of the E_{max} values for VMAT2M. Lew and Angus analysis revealed a linear fit ($R^2 = 0.89$, $p < 0.0001$) with a slope of -0.75 and a 95% confidence interval of -0.94 and -0.55 for VMAT2M (bottom panel in Figure 3.13, inset). Similar to the VMAT2C study at 30 °C, no overlap of the 95% confidence interval with unity indicated that (R)-GZ-924 inhibited methamphetamine-evoked [^{3}H]DA release in a surmountable allosteric manner when evaluating VMAT2M at 30 °C.

3.3.9 Lack of (R)-GZ-924 Inhibition of Methamphetamine-Evoked Endogenous Fractional DA Release from Striatal Slices

To determine the ability of (R)-GZ-924 to inhibit effect of methamphetamine at striatal slices, methamphetamine-evoked endogenous DA release from striatal slices was determined in the presence of the analog. The time course of the concentration-dependent effect of (R)-GZ-924 alone on fractional DA release across the first 15-40 min of superfusion is illustrated in

Figure 3.14, and the results are presented as DA overflow in Table 3.7. The main effect of (R)-GZ-924 concentration, time, and the interaction of concentration × time were not significant. Thus, (R)-GZ-924 alone did not evoke fractional DA release. Consistently, (R)-GZ-924 did not evoke DA overflow (Table 3.7).

Analysis of fractional DA release following the addition of methamphetamine to the superfusion buffer during 45-55 min in the absence and presence of (R)-GZ-924 revealed that the concentration effect and the concentration × time interaction were not significant; however a main effect of time [$F_{(2, 29)} = 11.3$; $p < 0.05$] was found. Consistent with these observations, methamphetamine-evoked DA overflow was not different in the absence and presence of (R)-GZ-924 across a range of concentrations (Table 3.8). Thus, methamphetamine increased fractional DA release from superfused striatal slices across the 15 min exposure period in both the absence and presence of (R)-GZ-924; however, (R)-GZ-924 did not inhibit the effect of methamphetamine to release DA.

3.3.10 (R)-GZ-924-Evoked Fractional Release of DOPAC, DOPAC Overflow from Striatal Slices and Interaction with Methamphetamine

To determine the effect of (R)-GZ-924 on DOPAC release, the ability of (R)-GZ-924 to evoke DOPAC release from striatal slices was determined. The time course of the concentration-dependent effect of (R)-GZ-924 alone on fractional release of DOPAC across the first 15-40 min of superfusion is illustrated in the top panel of Figure 3.15, and the results presented as DOPAC

overflow are illustrated in the bottom panel of Figure 3.15. The main effect of (R)-GZ-924 and time were significant [$F_{(5, 18)} = 11.5$, $p < 0.001$; $F_{(5, 20)} = 2.75$, $p < 0.05$, respectively], and the interaction of concentration × time was not significant. (R)-GZ-924 (30 µM) increased fractional release of DOPAC at 35 min [$F_{(4, 19)} = 3.56$, $p < 0.05$] and 40 min [$F_{(4, 18)} = 3.54$, $p < 0.05$]. Consistently, (R)-GZ-924 (10 and 30 µM) increased DOPAC overflow [$F_{(4, 19)} = 18.0$, $p < 0.05$; bottom panel of Figure 3.15].

The time course of the concentration-dependent effect of (R)-GZ-924 on fractional release of DOPAC across 45-50 min of superfusion in the presence of methamphetamine is illustrated in top panel of Figure 3.15 as well. The main effect of (R)-GZ-924 was significant [$F_{(5, 22)} = 4.28$, $p < 0.01$], and the main effect of time and the interaction of concentration × time were not significant. (R)-GZ-924 increased fractional release of DOPAC at 45 min [$F_{(4, 19)} = 5.03$, $p < 0.01$], 50 min [$F_{(4, 23)} = 6.69$, $p < 0.01$], and 55 min [$F_{(4, 23)} = 4.09$, $p < 0.05$]. (R)-GZ-924 at 3, 10, and 30 µM increased the release of DOPAC at 50-55 min, 45-55 min, and 50-55 min, respectively.

3.3.11 (R)-GZ-924-Induced Alteration of Methamphetamine-Evoked Fractional [^{3}H]-Release from Striatal Slices in the Absence and Presence of Pargyline

Contradictory results using (R)-GZ-924 between [^{3}H]DA release from synaptic vesicles and endogenous DA release from striatal slices was found. To determine whether different label, [^{3}H]DA versus endogenous DA, was

responsible for such contradictory results, the ability of (R)-GZ-924 to inhibit methamphetamine-evoked [^{3}H]DA release from striatal slices was determined. Using a within-subject design, the time course of the concentration-dependent effect of (R)-GZ-924 to inhibit the effect of methamphetamine was determined on fractional [^{3}H]-release from superfused striatal slices in the absence and presence of pargyline (Figure 3.16, top and bottom panels, respectively). Three-way repeated-measures ANOVA was conducted on the data prior to the addition of methamphetamine to the superfusion buffer to evaluate the time course of the concentration-dependent effects of (R)-GZ-924 in the absence and presence of pargyline. Main effects of (R)-GZ-924 [$F_{(4, 27)} = 4.81$, $p < 0.01$], pargyline [$F_{(1, 27)} = 37.9$, $p < 0.001$], and time [$F_{(2, 27)} = 11.8$, $p < 0.001$], as well as interactions of (R)-GZ-924 × time [$F_{(9, 27)} = 4.12$, $p < 0.01$] and pargyline × time [$F_{(2, 27)} = 6.66$, $p < 0.01$] were obtained. To further evaluate the significant interactions, post hoc analyses were performed and revealed that 10 µM (R)-GZ-924 increased fractional [^{3}H]-release from 30-40 min in the absence of pargyline, but not in the presence of pargyline.

With respect to the (R)-GZ-924-induced inhibition of methamphetamine on fractional [^{3}H]-release in the absence and presence of pargyline, main effects of (R)-GZ-924 [$F_{(4, 8)} = 3.08$, $p < 0.05$] and time [$F_{(2, 8)} = 103$, $p < 0.001$], as well as two-way interactions of (R)-GZ-924 × pargyline [$F_{(4, 8)} = 4.24$, $p < 0.05$] and pargyline × time [$F_{(2, 8)} = 7.93$, $p < 0.01$], and the three-way interaction of (R)-GZ-924 × pargyline × time [$F_{(8, 8)} = 7.85$, $p < 0.001$] were found. Post hoc analyses revealed that in the presence of pargyline from 50-60 min of superfusion, the

high concentration (10 μM) of (R)-GZ-924 plus methamphetamine increased fractional [^{3}H]-release above methamphetamine alone. Thus, (R)-GZ-924 did not alter methamphetamine-evoked fractional [^{3}H]-release in the absence of pargyline, whereas in the presence of pargyline, (R)-GZ-924 (10 μM) increased methamphetamine-evoked fractional [^{3}H]-release.

3.3.12 Inhibition of Nicotine-Evoked [^{3}H]DA Overflow from Rat Striatal Slices

To determine the specificity of (R)-GZ-924 on methamphetamine, the ability of (R)-GZ-924 to inhibit nicotine-evoked [^{3}H]DA overflow from striatal slices was determined. The concentration-response curve and K_i and I_{max} values are illustrated in Figure 3.17. (R)-GZ-924 inhibited nicotine-evoked [^{3}H]DA overflow from rat striatal slices (I_{max} = 85 ± 2%; IC_{50} = 0.98 ± 0.33 nM). A main effect of concentration was revealed by one-way ANOVA [$F_{(5, 30)} = 7.25$, $p < 0.05$]. Dunnett's post hoc test revealed that (R)-GZ-924 at 10 and 100 nM significantly decreased nicotine-evoked [^{3}H]DA overflow from striatal slices.

3.3.13 Inhibition of [^{3}H]MLA and [^{3}H]Nicotine Binding

To determine whether (R)-GZ-924 inhibition of nicotine-evoked [^{3}H]DA overflow was due to binding to the nicotinic receptors, the ability of (R)-GZ-924 to inhibit [^{3}H]MLA and [^{3}H]nicotine binding was determined. Concentration-response curves for (±)-GZ-819B (the racemic analog containing (R)-GZ-924), and the standards lobeline, MLA, and nicotine, and K_i values are illustrated in Figure 3.18. The standard compounds lobeline and MLA exhibited K_i values of 10 ± 1.0

and 1.8 ± 0.22 μM (top panel in Figure 3.18), respectively, for the [^{3}H]MLA binding site. Lobeline and nicotine exhibited K_i values of 12 ± 1.5 and 2.9 ± 0.3 μM (bottom panel in Figure 3.18), respectively, for the [^{3}H]nicotine binding site, consistent with previous results (Miller et al., 2004). (±)-GZ-819B did not inhibit [^{3}H]MLA or [^{3}H]nicotine binding within the concentrations range evaluated.

3.3.14 (R)-GZ-924-Induced Decreases in Methamphetamine Self-Administration and Food-Maintained Responding

To determine whether (R)-GZ-924 inhibition of methamphetamine-evoked [^{3}H]DA release from synaptic vesicles translate to the study using live animals, the ability of (R)-GZ-924 to inhibit methamphetamine self-administration in rats was determined. The dose-response for (R)-GZ-924 to decrease methamphetamine self-administration and responding for food is illustrated in Figure 3.19 (top and middle panel, respectively). (R)-GZ-924 dose-dependently decreased the number of methamphetamine infusions [$F_{(3,15)} = 36.9$, $p < 0.0001$]. The effect of (R)-GZ-924 was significant at 10 and 30 mg/kg. However, (R)-GZ-924 also dose-dependently decreased the number of food pellets obtained [$F_{(2,13)} = 37.3$; $p < 0.0001$], with 1 and 15 mg/kg producing significant effects. In addition, the inhibitory effect of (R)-GZ-924 (10 mg/kg) on food was not tolerated after repeated treatment (bottom panel in Figure 3.19). Thus, (R)-GZ-924 decreased methamphetamine self-administration in rats; however, this effect was not specific.

3.4 Discussion

Removing the C-3 and C-4 carbons in the central piperidine ring of lobelane afforded racemic acyclic analogs. The most potent racemic analogs that inhibited VMAT2 function were identified and the corresponding enantiomers of these racemic compounds were synthesized. All of the enantiomers inhibited [^{3}H]DA uptake at VMAT2 competitively and released [^{3}H]DA from the synaptic vesicles in a biphasic manner. The lead compound, (R)-GZ-924, the analog incorporating the amphetamine scaffold and the 3-carbon linker, released vesicular [^{3}H]DA in a biphasic manner, with the high affinity component being TBZ- and reserpine-sensitive. Also, (R)-GZ-924 inhibited methamphetamine-evoked [^{3}H]DA release from striatal synaptic vesicles, but did not inhibit methamphetamine-evoked [^{3}H]DA or endogenous DA release from striatal slices. (R)-GZ-924 evoked DOPAC overflow from striatal slices, indicating that (R)-GZ-924-redistributed DA was metabolized by MAO. Interestingly, (R)-GZ-924 inhibited nicotine-evoked [^{3}H]DA release from striatal slices, revealing a lack of selectivity for methamphetamine. Furthermore, (R)-GZ-924 decreased methamphetamine self-administration and food-maintained responding, revealing a similar lack of specificity for decreasing methamphetamine reinforcement in rats.

The [^{3}H]DTBZ binding assay provides information about the affinity of the analogs for the DTBZ site on VMAT2. For all the racemic analogs, either increasing or decreasing the linker length, or adding substituents to the

amphetamine or homoamphetamine N or phenyl rings did not increase analog affinity for this binding site. Two exceptions were (±)-GZ-893A, a nor-analog incorporating the 4-bromoamphetamine scaffold and 4-carbon linkers, and (±)-GZ-865G, a nor-analog incorporating a 4-hydroxyamphetamine scaffold and the N-3-methoxyphenylpropyl substituent, which exhibited 10 and 3-fold, respectively, higher affinity than lobelane for the DTBZ site on VMAT2. In addition, replacing the homoamphetamine with an amphetamine moiety resulted in 1.5-11 fold increase in affinity for the VMAT2 binding site. The majority of the nor-analogs exhibited higher affinity for the DTBZ binding site on VMAT2 compared to the corresponding N-methylated analogs. However, two nor-analogs, (±)-GZ-819B and (±)-GZ-820B, analogs incorporating the amphetamine scaffold and the 3 and 2-carbon linkers, respectively, exhibited comparable affinity relative to their N-methylated analogs, (±)-GZ-819C and (±)-GZ-820C. Evaluation of the (R)- and (S)-analogs of three of the racemic analogs in the series revealed no enantiomeric effect on affinity for the DTBZ binding site on VMAT2.

[^{3}H]DA uptake at VMAT2 provides information about analog inhibition of transporter function. Racemic analogs with 3-4 carbons in the linkers between the phenyl ring and the amphetamine or homoamphetamine N-atom had the highest affinity for the [^{3}H]DA uptake site on VMAT2. Replacing the homoamphetamine with an amphetamine moiety resulted in a 1.9 to 13-fold increase in affinity for the substrate site on VMAT2. Racemic nor-analogs exhibited a 1.7 to 24-fold increase in affinity for the substrate site on VMAT2

compared to the corresponding N-methylated analogs. Enantiomers of three potent racemic analogs (±)-GZ-819B, (±)-GZ-819A and (±)-GZ-815A, including (R)-GZ-924 and (S)-GZ-925, (R)-GZ-880A and (S)-GZ-880B, and (R)-GZ-878A and (S)-GZ-878B, respectively, were synthesized and evaluated. Of the enantiomers, (R)-GZ-924 and (S)-GZ-925, analogs incorporating an amphetamine scaffold, a 3-carbon linker and no substituents on the phenyl rings, exhibited a 10-fold difference in affinity for the VMAT2 substrate site.

A positive correlation between affinity for VMAT2 binding and uptake was revealed, indicating that the inhibition of VMAT2 function was due to binding at the DTBZ site on VMAT2. A similar result was found for analogs in Chapter 2 (Section 2.4). Similar to the analogs in Chapter 2, this series of analogs bound to the DTBZ binding site on VMAT2 and inhibit DA uptake (VMAT2 function) through an allosteric effect. A 10-fold greater affinity for the uptake site relative to the binding sites was found for this series of analogs. A similar result was also found for analogs in Chapter 2 (Section 2.4). In general, compounds interacting with VMAT2 can be classified as either uptake inhibitors or substrates. In terms of substrates, higher potencies were observed in VMAT2 functional assays relative to binding assays, while equivalent potencies were observed in both assays for uptake inhibitors (Andersen, 1987; Nickell et al., 2011a; Partilla et al., 2006). Similar to the analogs in Chapter 2, all the analogs in this study exhibited higher affinities in the VMAT2 functional assay in relative to the binding assay, suggesting that they are substrates for VMAT2. Evaluation of the mechanism of inhibition at the VMAT2 uptake site revealed a competitive interaction, indicating

that analog inhibition of VMAT2 function was surmountable by DA, consistent with the results found in our previous series of analogs that interacted with VMAT2 (Horton et al., 2011b; Nickell et al., 2010).

Inhibition of DAT has been associated with abuse liability (Howell and Wilcox, 2001). To select a lead compound, selectivity for VMAT2 versus DAT was determined. The range of selectivity of the enantiomers for VMAT2 over DAT was 40-260-fold, indicating that all the enantiomers likely would not possess abuse liability. The most potent and selective enantiomers for VMAT2 over DAT were (R)-GZ-924 (183-fold) and (R)-GZ-880A (167-fold). Subsequently, the selectivity of (R)-GZ-924 and (R)-GZ-880A for VMAT2 over hERG channels was determined to be 510 and 84-fold, indicating that (R)-GZ-924 and (R)-GZ-880A likely would not possess cardiac toxicity. The most potent and selective enantiomer at VMAT2 over DAT and hERG was (R)-GZ-924, which assumed lead compound status.

All enantiomers evoked [^{3}H]DA release from VMAT2C-associated synaptic vesicles biphasically, indicating an interaction of the analogs with two different sites (a high-affinity site and a low-affinity site) on VMAT2C. In addition, (R)-GZ-924-evoked release from the high affinity site was TBZ- and reserpine-sensitive, consistent with a previous report on another series of analogs (Horton et al., 2013). This result suggested that (R)-GZ-924-evoked high affinity DA release was through VMAT2C, while the low affinity release was not. (R)-GZ-924-evoked low affinity DA release might be due to its non-specific effect on vesicular DA

release. For instance, methamphetamine released DA from synaptic vesicles by decreasing the proton gradient (Sulzer and Rayport, 1990). (R)-GZ-924 might release DA from synaptic vesicles by decreasing the proton gradient like methamphetamine.

Furthermore, our group suggested that inhibition of methamphetamine self-administration could be caused by the inhibition of methamphetamine-evoked [^{3}H]DA release from presynaptic vesicles (Horton et al., 2013). However, in the previous vesicular [^{3}H]DA release study in Chapter 2 (Section 2.2.6), the vesicles collected was VMAT2C vesicles. In the slice release study, both VMAT2C and VMAT2M vesicles existed in each intact slice (Figure 3.21). The lead analog in Chapter 2 [(±)-GZ-730B] inhibited methamphetamine-evoked [^{3}H]DA release from synaptic vesicles but not endogenous DA release from striatal slices. A similar contradictory result using (R)-GZ-924 was also found between the studies using striatal VMAT2C and striatal slices. The incomplete vesicular VMAT2 preparation in the vesicular [^{3}H]DA release study might be responsible for the conflict between those studies. In the current study, the ability of (R)-GZ-924 to inhibit methamphetamine-evoked [^{3}H]DA release from vesicles via VMAT2M and VMAT2C was determined in a within subject design.

The optimal concentration of [^{3}H]DA to incubate VMAT2M and VMAT2C at 30 °C was 0.3 μM determined by the kinetic study. Affinity of DA for VMAT2M and VMAT2C at 30 °C was obtained from the kinetic study and was not different, consistent with studies in the literature (Chu et al., 2010), indicating that the

structure of VMAT2M and VMAT2C was not different. In both time course studies to determine the optimal incubation time at 30 °C, VMAT2M vesicles were saturated faster than VMAT2C vesicles, indicating the uptake rate of VMAT2M was faster than that for VMAT2C. However, V_{max} for VMAT2M was 2-fold lower than that for VMAT2C in the [^{3}H]DA uptake kinetic study at 30 °C. Such a contradictory result could be caused by the means to calculate V_{max} in our study. V_{max} was normalized by protein amount. Large amount of protein was found in the VMAT2M suspension. Since VMAT2M vesicles were associated with the broken synaptosome membranes, it was reasonable that the VMAT2M suspension contained large amount of synaptosome membranes. In contrast, VMAT2C suspension did not contain the broken synaptosome membranes due to more and higher speed spins. Thus, V_{max} for VMAT2M, normalized by protein contaminated by the synaptosome membranes, might not be accurate. Interestingly, Fleckenstein's lab found that VMAT2M uptake rate was higher than that for VMAT2C using rotating disk electrode voltammetry (Volz et al., 2007). The velocity of DA transportation by VMAT2M was also normalized by protein contaminated by the broken synaptosome membranes in their study. Thus, the contradictory results might not due to the normalization of uptake rate by protein, and might be due to the different technique used to measure velocity of DA transportation.

After the optimal incubation time and concentration of [^{3}H]DA was determined, VMAT2C and VMAT2M vesicles were used to determine the ability of (R)-GZ-924 to inhibit methamphetamine-evoked release of [^{3}H]DA. (R)-GZ-924

(30 and 300 nM) produced a rightward shift of the concentration-response of methamphetamine-evoked [^{3}H]DA release at both 30 °C and 37 °C via VMAT2C, with no influence on the maximal release induced by methamphetamine. Thus, the mechanism of (R)-GZ-924 inhibition on methamphetamine-evoked [^{3}H]DA release via VMAT2C was not altered by temperature. In addition, (R)-GZ-924 (30 and 300 nM) produced a rightward shift of the concentration-response of methamphetamine via both VMAT2M and VMAT2C at 30 °C, with no influence on the maximal release induced by methamphetamine. The method of Lew and Angus revealed a slope different from unity in the release study using both VMAT2M and VMAT2C. Thus, (R)-GZ-924 was determined to be a surmountable allosteric inhibitor for both VMAT2M and VMAT2C (Horton et al., 2013; Kenakin, 2006b). Based on the characteristic of allosteric inhibitors, binding of (R)-GZ-924 to a site different from the methamphetamine binding site on VMAT2M and VMAT2C resulted in a conformational change in the transporter to decrease affinity for methamphetamine, but did not alter the efficacy of methamphetamine to release DA. Four different sites on VMAT2C have been reported by our lab: an extravesicular DTBZ binding site, an extravesicular DA uptake site and two intravesicular high and low affinity DA release sites (Horton et al., 2013). Methamphetamine interacts with the low affinity intravesicular site to evoke vesicular DA release (Horton et al., 2012). Thus, as an allosteric inhibitor, (R)-GZ-924 may interact with the extravesicular DTBZ binding site, the extravesicular DA uptake site and the intravesicular high affinity DA release site on VMAT2C to inhibit methamphetamine effect (Figure 3.20). No study has been reported on

binding or release site on VMAT2M. Further study on defining binding and release site on VMAT2M needed to be done to allow to investigate the mechanism of interaction of (R)-GZ-924 and lead analogs from other series with VMAT2M.

However, methamphetamine in the absence or presence of (R)-GZ-924 only released around 30% of the [^{3}H]DA via VMAT2M, but around 70% of the [^{3}H]DA via VMAT2C. VMAT2M containing vesicles were associated with the presynaptic membrane and undergoing exocytosis. The release of DA through exocytosis may be initiated before final incubation in the vesicular [^{3}H]DA release study. Such release via exocytosis likely leads to less [^{3}H]DA release via VMAT2M in the current release study relative to VMAT2C.

Interestingly, in the absence of (R)-GZ-924 and methamphetamine, the [^{3}H]DA left in the vesicles associated with membranes was more than that left in the vesicles in the cytosol. However, only less than 10% of total vesicles were reported to associate with the presynaptic membrane (Rizzoli and Betz, 2005). Such results could be due to the different endogenous DA content in the two different isolated vesicles. Prior to incubation with [^{3}H]DA, due to less amount, vesicles associated with membranes contained much less endogenous DA compared to the vesicles in the cytosol. After incubation with same concentration of [^{3}H]DA, total DA including [^{3}H]DA and endogenous DA were less for vesicles associated with membranes compared to vesicles in the cytosol. However, only [^{3}H]DA can be determined and the amount of [^{3}H]DA determined may not be

capable of representing the total vesicular DA content in the two pools of vesicles.

The next critical step in our drug discovery approach was to determine whether the lead analog, (R)-GZ-924, inhibited methamphetamine-evoked endogenous DA release from striatal slices. Despite inhibiting methamphetamine-evoked [^{3}H]DA release from synaptic vesicles, this analog did not inhibit methamphetamine-evoked endogenous DA release from striatal slices, but increased DOPAC overflow significantly. Such increase of DOPAC overflow suggested the metabolism of the cytosol DA into DOPAC, however, it was not fully understood why methamphetamine-evoked DA release was not inhibited simultaneously. Furthermore, the ability of (R)-GZ-924 to inhibit methamphetamine-evoked [^{3}H]DA release from striatal slices was determined in the presence and absence of the MAO inhibitor pargyline. Consistent with the study measuring endogenous DA, methamphetamine-evoked [^{3}H]DA release was not inhibited by (R)-GZ-924 in the presence or absence of pargyline. Interestingly, in the presence of pargyline, (R)-GZ-924 did not release [^{3}H]DA by itself, while in the absence of pargyline (R)-GZ-924 released [^{3}H] in a concentration dependent manner. It was not a surprise to see this result since in the absence of pargyline. [^{3}H]DA would be metabolized by MAO into [^{3}H]DOPAC or other [^{3}H]metabolites. The [^{3}H]metabolites would diffuse across the membrane into the extracellular space following concentration gradient. In such a case, (R)-GZ-924-evoked [^{3}H]metabolites release was measured, indicating lack of MAO inhibition of the analog. In addition, in the presence of pargyline, [^{3}H]DA could not

be metabolized due to MAO inhibition. In such case, redistributed [^{3}H]DA was not capable of diffusing across the membrane like DOPAC, and were trapped in the presynaptic terminal. Thus, subsequent exposure of methamphetamine reversed DAT and released more [^{3}H]DA compared to methamphetamine alone.

Unexpectedly, (R)-GZ-924 inhibited nicotine-evoked [^{3}H]DA overflow from striatal slices. Interestingly, at the same concentration range, (R)-GZ-924 released [^{3}H]DA from synaptic vesicles. Since nicotine-evoked release of [^{3}H]DA was originally from presynaptic vesicles, it is possible that nicotine-evoked and (R)-GZ-924 redistributed [^{3}H]DA were the same. Thus, the vesicular DA for nicotine-evoked release was not available probably due to the (R)-GZ-924 induced redistribution of DA form synaptic vesicles to cytosol. Alternatively, (R)-GZ-924 could be a nAChR antagonist and inhibit the neurochemical effect of nicotine. Nicotine bound and activated α4- and α6-containing nAChRs to evoke DA release from presynaptic terminals (Pivavarchyk et al., 2011). Current study showed that same amount of (R)-GZ-924 and (S)-GZ-925 mixed as racemic did not bind α4-containing or α7 nAChRs. Thus, these compounds are not likely acting as an α4-containing or α7 nAChR antagonist. However, the analog could inhibit nicotine-evoked [^{3}H]DA release as an α6-containing nAChR antagonist. However, around 80% nicotine-evoked [^{3}H]DA release was inhibited by (R)-GZ-924 in the current study, while α-4 and α-6 containing nicotinic receptors mediated ~50% of the total nicotine-evoked [^{3}H]DA release, respectively (Pivavarchyk et al., 2011). Thus, (R)-GZ-924 might not act as a specific nAChR subtype antagonist to inhibit nicotine-evoked [^{3}H]DA overflow. In addition,

nicotine-evoked DA release could be blocked completely by the channel block mecamylamine (Smith et al., 2009; Varanda et al., 1985). Thus, (R)-GZ-924 might acted as a channel blocker in a manner similar to mecamylamine to inhibit nicotine-evoked [^{3}H]DA release from presynaptic terminals.

(R)-GZ-924, in a dose dependent manner, inhibited methamphetamine self-administration in rats, with no concurrent inhibition of methamphetamine-evoked DA release from striatal slices. However, other brain regions, including prefrontal cortex and nucleus accumbens, involved in the mesocorticolimbic pathway have not been studied and (R)-GZ-924 might inhibit methamphetamine-evoked DA release into extracellular space in such brain regions. In addition, serotonin and norepinephrine transporter inhibitors have been reported to inhibit the neurochemical and behavioral effect of methamphetamine (Berigan and Russell, 2001; Shoptaw et al., 2008). Since serotonin and norepinephrine are also transported by VMAT2 into vesicles, (R)-GZ-924 inhibition of VMAT2 function might affect neurochemical and behavioral effect of methamphetamine by regulating those two monoamines. In addition, local infusion of an α3β4* nicotinic receptor antagonist into medial habenula, the interpeduncular area or the basolateral amygdala decreased methamphetamine self-administration by indirectly regulating the dopaminergic mesolimbic pathway (Glick et al., 2008). Thus, (R)-GZ-924, as a potential nAChR antagonist, might also antagonize α3β4 nAChRs, which could lead to the inhibition of methamphetamine self-administration in rats. Unfortunately, food-maintained responding was inhibited by (R)-GZ-924 and the inhibitory effect on food was not tolerated after repeated

treatment. The inhibitory effect of (R)-GZ-924 on food responding demonstrated that the effect was not specific for methamphetamine. The nicotinic receptor channel blocker mecamylamine inhibited food self-administration in rats by inhibiting the neurochemical effects of nicotine (Levin et al., 2000). Thus, the effect of (R)-GZ-924 on food-maintained responding could be due to the inhibition of the neurochemical effects of nicotine. In addition, since (R)-GZ-924 might bind nicotinic receptors, the analog could inhibit food-maintained responding by interacting with peripheral nicotinic receptors, leading to undesirable gastric side effects that might be reflected by the food-maintained responding data.

In conclusion, the potent and selective VMAT2 inhibitor, (R)-GZ-924, inhibited methamphetamine-evoked vesicular [^{3}H]DA release, inhibited methamphetamine self-administration and food-maintained responding in rats. The lack of specificity for decreasing methamphetamine reinforcement in rats might be due to the lack of selectivity of this analog for the neurochemical effect of methamphetamine. Further study will be performed by modifying (R)-GZ-924 to afford potent and selective analogs for VMAT2 with specific neurochemical and behavioral effect for methamphetamine.

Table 3.1. K_i and I_{max} values in the [^{3}H]DTBZ binding and vesicular [^{3}H]DA uptake assays, binding/uptake K_i ratio for RO4-1284, lobeline, lobelane, acyclic lobelane racemic analogs.

	[^{3}H]DTBZ binding		VMAT2 [^{3}H]DA uptake		Binding/Uptake K_i Ratio
Analog [a]	K_i (μM)	I_{max} (%)	K_i (nM)	I_{max} (%)	
Ro4-1284	0.016 ± 0.0013 [b,*]	93 ± 7 [b]	41 ± 8.1	100	0.39
Lobeline	3.5. ± 1.0 *	91 ± 0.3	583 ± 30 *	100	7
Lobelane	0.97 ± 0.19	98 ± 2	40 ± 3.5	100	24
Racemic analogs incorporating homoamphetamine scaffold					
(±)-GZ-854B	0.87 ± 0.026	93 ± 4	9.7 ± 4.4 *	100	87
(±)-GZ-865B	1.5 ± 0.072	99 ± 1	24 ± 5.8	93 ± 6	63
(±)-GZ-865A	3.2 ± 0.11 *	100	26 ± 2.3 *	98 ± 2	123
(±)-GZ-853A	4.7 ± 0.41 *	100	30 ± 2.4	100	157
(±)-GZ-814A	1.6 ± 0.33	96 ± 3	50 ± 4.2	100	32
(±)-GZ-813A	4.8 ± 1.1 *	100	51 ± 12	100	96
(±)-GZ-854A	1.5 ± 0.19	96 ± 4	60 ± 7.2	100	25
(±)-GZ-853B	2.4 ± 0.055 *	98 ± 1	62 ± 29	99 ± 0.3	39
(±)-GZ-814B	30 ± 11 *	87 ± 5	84 ± 4.6 *	100	357
(±)-GZ-813B	17 ± 6.3 *	90 ± 3	362 ± 34 *	97 ± 0.4	47
Racemic analogs incorporating amphetamine scaffold and 2, 4, 5 and 6 carbon linkers					
(±)-GZ-893A	0.096 ± 0.043 *	100	3.3 ± 0.26 *	100	32
(±)-GZ-893B	0.79 ± 0.30	100	3.3 ± 1.7 *	100	263
(±)-GZ-908	0.91 ± 0.59	96 ± 4	9.3 ± 1.8 *	95 ± 3	101
(±)-GZ-909	0.67 ± 0.071	97 ± 2	14 ± 0.82 *	93 ± 4	49
(±)-GZ-820A	1.2 ± 0.13	99 ± 1	34 ± 6.2	96 ± 3	36
(±)-GZ-859B	2.6 ± 0.40 *	95 ± 2	47 ± 6.1	100	55
(±)-GZ-860B	5.1 ± 1.2 *	100	60 ± 6.9 *	100	85
(±)-GZ-820B	7.7 ± 1.3 *	97 ± 1	63 ± 5.4 *	100	122
(±)-GZ-852B	2.5 ± 1.6	95 ± 2	69 ± 9.0 *	99 ± 0.4	36
(±)-GZ-816A	3.8 ± 0.99 *	96 ± 4	74 ± 2.2 *	100	51
(±)-GZ-861B	17 ± 6.6 *	71 ± 5	206 ± 75 *	99 ± 1	81
(±)-GZ-816B	12 ± 1.8 *	90 ± 2	459 ± 79 *	97 ± 1	26
(±)-GZ-820C	7.5 ± 2.2 *	78 ± 1	512 ± 106 *	98 ± 2	15
Racemic analogs incorporating amphetamine scaffold and 3 carbon linkers					
(±)-GZ-819B	2.6 ± 0.47 *	99 ± 1	6.9 ± 1.8 *	100	650
(±)-GZ-819A	0.43 ± 0.047	99 ± 0.3	8.7 ± 1.4 *	100	54
(±)-GZ-865F	1.4 ± 0.40	100	7.5 ± 2.2 *	96 ± 2	175
(±)-GZ-852A	1.3 ± 0.31	96 ± 1	10 ± 0.22 *	99 ± 0.2	130
(±)-GZ-865C	0.41 ± 0.14	95 ± 5	12 ± 2.7 *	100	37
(±)-GZ-865D	0.46 ± 0.083	100	12 ± 3.4 *	100	38
(±)-GZ-860A	2.0 ± 0.28 *	95 ± 2	13 ± 0.43 *	100	154
(±)-GZ-888	2.2 ± 0.097 *	100	14 ± 2.8 *	100	157
(±)-GZ-865E	1.7 ± 0.39	100	17 ± 3.4 *	97 ± 3	100
(±)-GZ-815A	1.3 ± 0.086	100	20 ± 3.6 *	99 ± 0.2	59
(±)-GZ-859A	0.82 ± 0.27	95 ± 2	33 ± 8.3	93 ± 5	25
(±)-GZ-861A	2.8 ± 0.75 *	94 ±1	36 ± 2.5	100	78
(±)-GZ-865G	0.28 ± 0.072 *	100	72 ± 30	96 ± 2	4
(±)-GZ-819C	1.6 ± 0.47	99 ± 1	102 ± 6.1 *	100 ± 0.3	17
(±)-GZ-815B	7.1 ± 0.82 *	94 ± 3	272 ± 38 *	97 ± 2	26

[a] The order of analogs is based on scaffold, carbon linker lengths, and affinity for VMAT2C [^{3}H]DA uptake. [b] K_i and I_{max} values are mean (± SEM). * $p < 0.05$ different from lobelane. n = 3-4 rats/analog.

Table 3.2. IC_{50} and I_{max} values in the [^{3}H]DTBZ binding, [^{3}H]Dofetilide binding, and vesicular [^{3}H]DA uptake assays, binding/uptake IC_{50} ratio for three pairs of enantiomers.

	[^{3}H]DTBZ binding		VMAT2 [^{3}H]DA uptake		[^{3}H]Dofetilide binding		[^{3}H]DTBZ binding/Uptake IC_{50} ratio	[^{3}H]Dofetilide binding/Uptake IC_{50} ratio
Analog [a]	IC_{50} (μM)	I_{max} (%)	IC_{50} (nM)	I_{max} (%)	IC_{50} (μM)	I_{max} (%)		
Lobelane	1.6 ± 0.24 [b]	98 ± 2 [b]	67 ± 5.9	100	0.20 ± 0.015	90 ± 2.7	24	3
(R)-GZ-924	1.8 ± 1.2	98 ± 1.1	9.8 ± 1.7 *	100	5.0 ± 3.0 *	95 ± 7.3	184	510
(S)-GZ-925	1.5 ± 0.28	100	108 ± 5.9	100	8.5 ± 1.7 *	100	14	79
(R)-GZ-880A	1.9 ± 0.15	100	9.3 ± 1.6 *	99 ± 0.82	0.78 ± 0.23 *	100	204	84
(S)-GZ-880B	1.5 ± 0.18	100	54 ± 7.4	100	1.9 ± 058 *	100	28	35
(R)-GZ-878A	2.1 ± 0.75	99 ± 0.57	75 ± 6.0	100	3.1 ± 1.2 *	87 ± 5.9	28	41
(S)-GZ-878B	2.2 ± 0.26	100	34 ± 2.4	100	2.2 ± 0.49 *	96 ± 4.6	65	65

[a] Analogs are arranged with each pair of enantiomers next to each other. [b] IC_{50} and I_{max} values are mean (± SEM); * $p < 0.05$ different from lobelane. n = 3-4 rats/analog.

Table 3.3. K_m and V_{max} values from kinetic analysis of [^{3}H]DA uptake at VMAT2C for lobelane and three pairs of enantiomers.

Compound	K_m (μM)	V_{max} (pm/min/mg)
Control [b]	0.10 ± 0.0070 [c]	42 ± 5.9
Lobelane	0.93 ± 0.12 *	59 ± 12
(R)-GZ-878A	0.68 ± 0.089 *	44 ± 1.4
(S)-GZ-878B	0.25 ± 0.065 *	33 ± 5.1
(R)-GZ-880A	0.90 ± 0.15 *	54 ± 12
(S)-GZ-880B	0.53 ± 0.18 *	40 ± 8.4
(R)-GZ-924	0.35 ± 0.043 *	36 ± 12
(S)-GZ-925	0.44 ± 0.15 *	68 ± 27

[a] Concentrations of enantiomers utilized for kinetic analyses were the K_i values from the inhibition curves in Fig. 3 [lobelane (40 nM), (R)-GZ-878A (45 nM), (S)-GZ-878B (20 nM), (R)-GZ-880A (6 nM), (S)-GZ-880B (32 nM), (R)-GZ-924 (6 nM), (S)-GZ-925 (65 nM)]. [b] Control represents V_{max} and K_m values in the absence of analogs. [c] Data are mean (± SEM) for K_m and V_{max} values. * $p < 0.05$ different from K_m values in control. n = 4-7 rats/analog.

Table 3.4. K_i and I_{max} values of lobeline, lobelane and three pairs of enantiomers in DAT uptake assays.

Compound	K_i (μM)	I_{max} (%)
Lobeline	18 ± 0.76 [a]	99 ± 0.6
Lobelane	1.3 ± 0.16	98 ± 1
(R)-GZ-924	1.1 ± 0.049	99 ± 1
(S)-GZ-925	2.6 ± 0.14 *, #	99 ± 0.2
(R)-GZ-878A	5.6 ± 1.3 *	100
(S)-GZ-878B	5.2 ± 0.2 *	99 ± 0.2
(R)-GZ-880A	1.0 ± 0.12	100
(S)-GZ-880B	1.8 ± 0.18	100

[a] Data are expressed as mean ± SEM. * $p < 0.05$ different from K_i value of lobelane. # $p < 0.05$ different from K_i value of (R)-GZ-924. n = 3-4 rats/analog.

Table 3.5. EC_{50} and E_{max} values for methamphetamine-evoked [^{3}H]DA release via VMAT2C in the absence and presence of (R)-GZ-924 at 37 °C.

(R)-GZ-924 (nM)	VMAT2C	
	EC_{50}	E_{max}
0	11.9 ± 0.769 [a]	82.4 ± 0.614
3	22.9 ± 1.85	81.9 ± 1.09
30	59.0 ± 7.82 *	79.0 ± 2.36
300	171 ± 16.7 *	80.4 ± 1.87

[a] Data are expressed as mean ± SEM. * $p < 0.05$ different from [^{3}H]DA release in the presence of methamphetamine alone. n = 4/experiment.

Table 3.6. EC_{50} and E_{max} values for methamphetamine-evoked [^{3}H]DA release via VMAT2M and VMAT2C in the absence and presence of (R)-GZ-924 at 30 °C.

(R)-GZ-924 (nM)	VMAT2M		VMAT2C	
	EC_{50}	E_{max}	EC_{50}	E_{max}
0	5.28 ± 1.48 [a]	28.9 ± 4.39	10.3 ± 3.18	61.0 ± 5.56
3	17.6 ± 8.90	25.9 ± 1.47	119 ± 28.9 *	65.5 ± 1.83
30	74.9 ± 17.3 *	27.1 ± 2.78	164 ± 36.5 *	66.0 ± 6.28
300	583 ± 77.8 *	37.4 ± 2.91	613 ± 134 *	78.7 ± 3.17

[a] Data are expressed as mean ± SEM. * $p < 0.05$ different from [^{3}H]DA release in the presence of methamphetamine alone. n = 4/experiment.

Table 3.7. (R)-GZ-924-induced DA overflow from rat striatal slices.

(R)-GZ-924 (μM)	0 [a]	0.3	1	3	10	30
DA overflow (pg/40ml/mg)	18 ± 3.4 [b]	20 ± 9.8	24 ± 5.7	27 ± 8.7	23 ± 4.9	17 ± 5.0

Data are the DA overflow during the 30 min period before the addition of methamphetamine. [a] represents buffer control. [b] Data are expressed as pg/30ml/mg (mean ± SEM). n = 7 rats.

Table 3.8. Methamphetamine-evoked DA overflow from rat striatal slices in the presence of (R)-GZ-924.

(R)-GZ-924 (μM)	0 [a]	0.3	1	3	10	30
DA overflow (pg/30ml/mg)	0.45 ±0.089 [b]	2.3 ± 1.2	1.7 ± 0.77	2.2 ± 1.2	4.4 ± 2.1	5.4 ± 3.1

Data are the DA overflow during the 15 min with methamphetamine and (R)-GZ-924 and the 25 min period with the analog after the removing methamphetamine. [a] 0 represents buffer control. [b] Data are expressed as pg/40 ml/mg (mean ± SEM). n = 7 rats.

Lobeline and lobelane

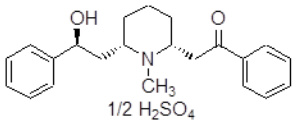

Lobeline

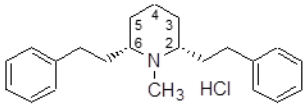

Lobelane

Reserpine, TBZ and RO4-1284

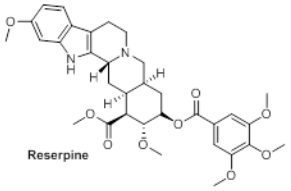

Reserpine

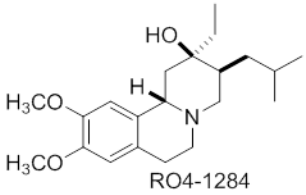

RO4-1284

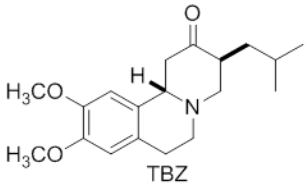

TBZ

Racemic analogs incorporating homoamphetamine scaffold

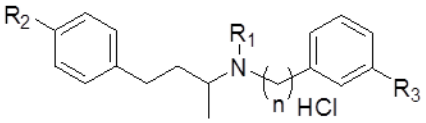

	n	R_1	R_2	R_3
(±)-GZ-854B	2	H	OCH_3	Br
(±)-GZ-854A	2	H	OCH_3	OCH_3
(±)-GZ-814A	2	H	H	H
(±)-GZ-853B	2	H	OCH_3	H
(±)-GZ-814B	2	CH_3	H	H
(±)-GZ-813B	3	CH_3	H	H
(±)-GZ-813A	3	H	H	H
(±)-GZ-865B	3	H	OCH_3	OCH_3
(±)-GZ-865A	3	H	H	OCH_3
(±)-GZ-853A	3	H	OCH_3	H

Racemic analogs incorporating amphetamine scaffold and 3 carbon linkers

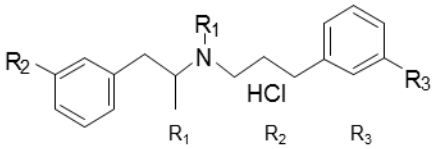

	R_1	R_2	R_3
(±)-GZ-819C	CH_3	H	H
(±)-GZ-819B	H	H	H
(±)-GZ-865G	H	OH	OCH_3
(±)-GZ-865C	H	OCH_3	OCH_3
(±)-GZ-819A	H	Br	H
(±)-GZ-865D	H	Br	OCH_3
(±)-GZ-859A	H	OH	H
(±)-GZ-815A	H	OCH_3	H
(±)-GZ-852A	H	F	H
(±)-GZ-865F	H	NO_2	OCH_3
(±)-GZ-865E	H	F	OCH_3
(±)-GZ-860A	H	NO_2	H
(±)-GZ-888	H	H	OCH_3
(±)-GZ-861A	H	NH_3	H
(±)-GZ-815B	CH_3	OCH_3	H

Racemic analogs incorporating amphetamine scaffold and 2, 4, 5 and 6 carbon linkers

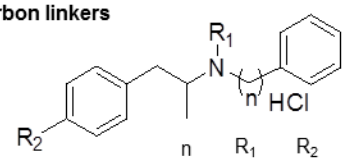

	n	R_1	R_2
(±)-GZ-820C	2	CH_3	H
(±)-GZ-820B	2	H	H
(±)-GZ-820A	2	H	Br
(±)-GZ-852B	2	H	F
(±)-GZ-859B	2	H	OH
(±)-GZ-816A	2	H	OCH_3
(±)-GZ-860B	2	H	NO_2
(±)-GZ-816B	2	CH_3	OCH_3
(±)-GZ-861B	2	H	NH_2
(±)-GZ-893B	4	H	H
(±)-GZ-893A	4	H	Br
(±)-GZ-909	5	H	H
(±)-GZ-908	6	H	H

Enantiomers incorporating amphetamine scaffold and 3 carbon linkers

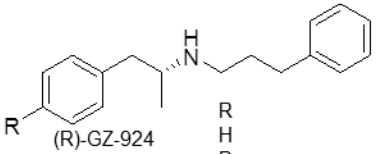

	R
(R)-GZ-924	H
(R)-GZ-880A	Br
(R)-GZ-878A	OCH_3

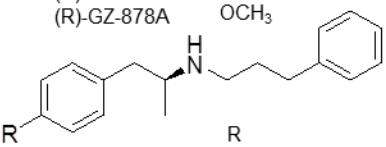

	R
(S)-GZ-925	H
(S)-GZ-880B	Br
(S)-GZ-878B	OCH_3

Figure 3.1. Chemical structures of lobeline, lobelane, reserpine, TBZ, RO4-1284, and acyclic lobelane analogs.

Lobeline is the principal alkaloid from *lobelia inflata*. Lobelane is a defunctionalized, saturated analog of lobeline. TBZ and RO4-1284 are benzoquinolizine compounds and VMAT2 inhibitors that bind a site distinct from the DA uptake site on VMAT2. Reserpine is an indole alkaloid and VMAT2 inhibitor that binds the DA uptake site on VMAT2. Acyclic racemic analogs are grouped according to structural similarity: Analogs incorporating a homoamphetamine scaffold; analogs incorporating an amphetamine scaffold and a 2, 4, 5 or 6-carbon linker; analogs incorporating an amphetamine scaffold and a 3-carbon linker; three pairs of enantiomers incorporating an amphetamine scaffold and the 3-carbon linker: (R)-GZ-924 and (S)-GZ-925 are the enantiomers in (±)-GZ-819B; (R)-GZ-880A and (S)-GZ-880B are the enantiomers in (±)-GZ-819A, (R)-GZ-878A and (S)-GZ-878B are the enantiomers in (±)-GZ-815A.

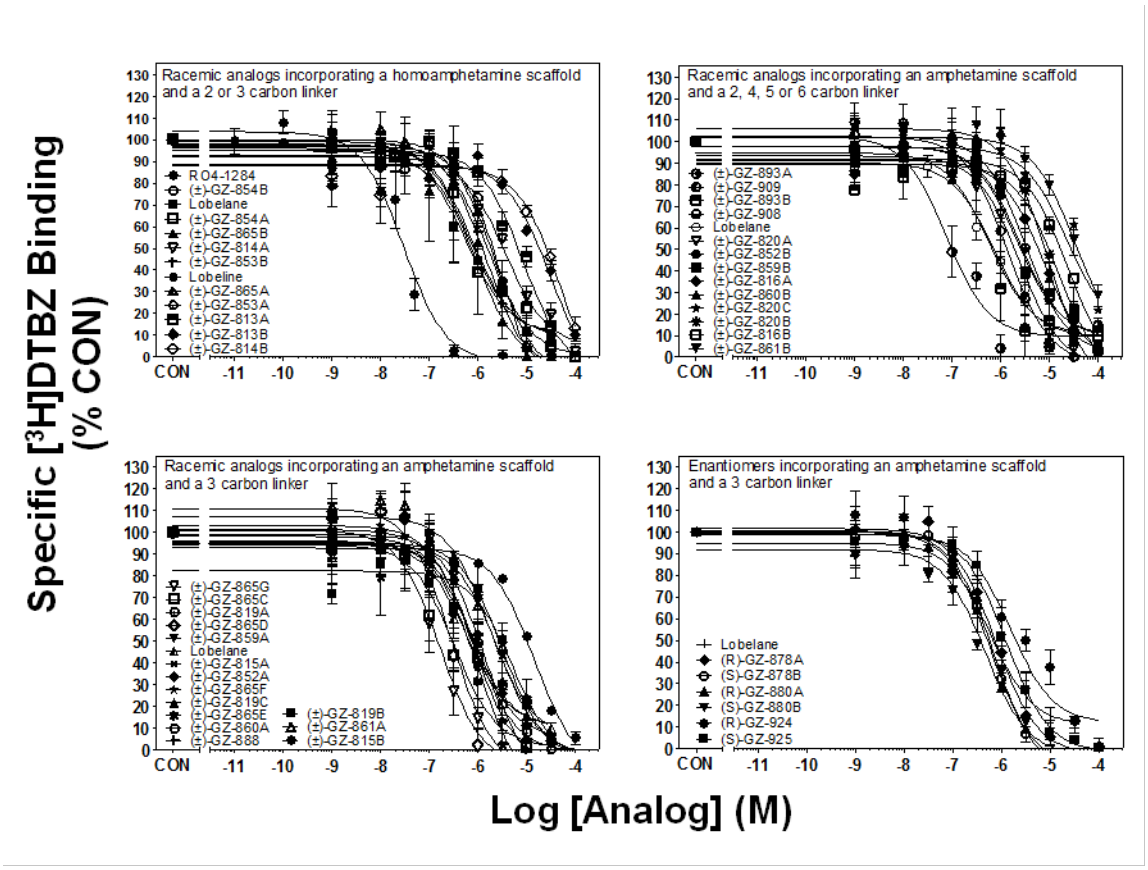

Figure 3.2. Acyclic lobelane analogs inhibit [^{3}H]DTBZ binding at VMAT2C.

Analogs are divided into groups based on structural similarity: RO4-1284, lobeline, lobelane, acyclic lobelane racemic analogs incorporating a homoamphetamine scaffold (top left); acyclic lobelane racemic analogs incorporating an amphetamine scaffold and a 2, 4, 5 or 6-carbon linker (top right); acyclic lobelane racemic analogs incorporating an amphetamine scaffold and a 3-carbon linker (bottom left); three pairs of enantiomers incorporating an amphetamine scaffold and the 3-carbon linker (bottom right). All racemic analogs are presented in the legend in order from the most potent to the least potent from top to bottom and left to right. Three pairs of enantiomers are presented next to each other in the legend. Control represents specific [^{3}H]DTBZ binding in the absence of analogs. Binding values in the curves are mean (± SEM) specific

[^{3}H]DTBZ binding represented as a percentage of the respective control (1.35 ± 0.04 pmol/mg, n = 3-4 rats/analogs).

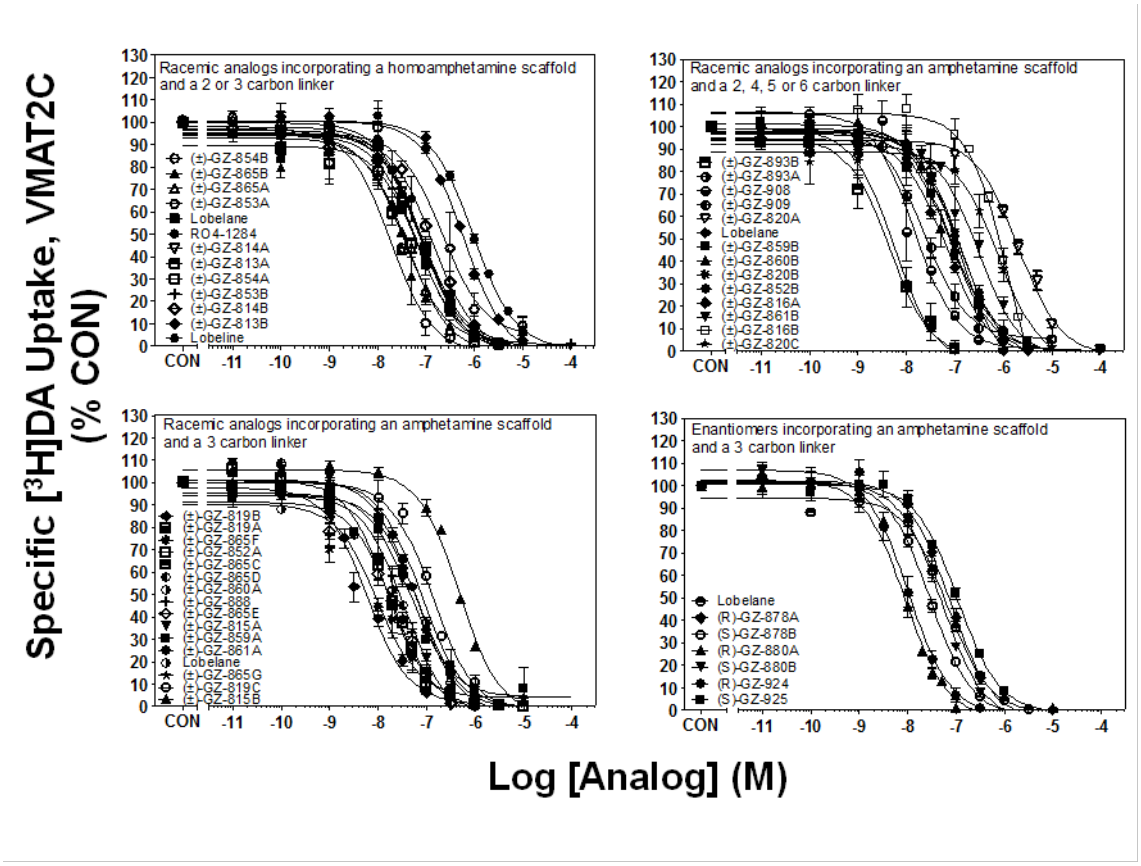

Figure 3.3. Acyclic lobelane analogs inhibit [^{3}H]DA uptake into rat striatal synaptic vesicles.

Analogs are divided into groups based on structural similarity: RO4-1284, lobeline, lobelane, acyclic lobelane racemic analogs incorporating a homoamphetamine scaffold (top left); acyclic lobelane racemic analogs incorporating an amphetamine scaffold and a 2, 4, 5 or 6-carbon linker (top right); acyclic lobelane racemic analogs incorporating an amphetamine scaffold and a 3-carbon linker (bottom left); three pairs of enantiomers incorporating an amphetamine scaffold and the 3-carbon linker (bottom right). All racemic analogs are presented in the legend in order from the most potent to the least potent. Three pairs of enantiomers are presented next to each other in the legend. Control represents specific [^{3}H]DA uptake in the absence of analogs. Uptake values in the curves are mean (± SEM) specific [^{3}H]DA uptake presented as a

percentage of the respective control (32.1 ± 1.8 pmol/min/mg, n =3-4 rats/analog).

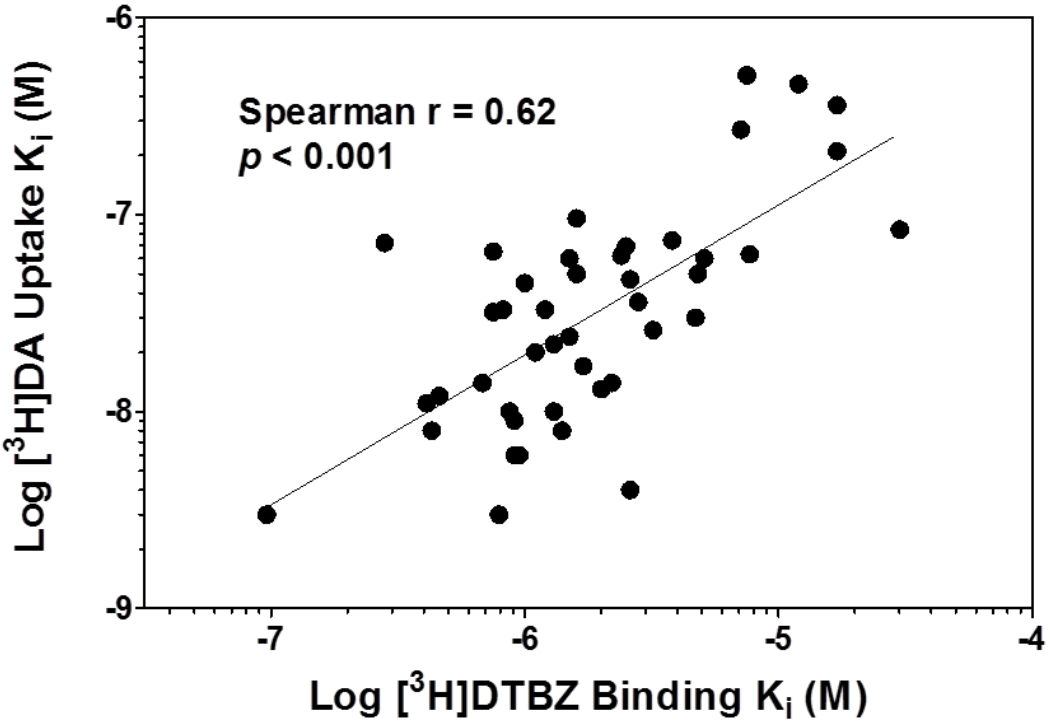

Figure 3.4. Vesicular [^{3}H]DA uptake and [^{3}H]DTBZ binding affinity correlation.

Affinity for [^{3}H]DTBZ binding site on VMAT2C and affinity for inhibition of VMAT2C function are positively correlated (Spearman r = 0.62; $p < 0.001$). K_i values are obtained from concentration-response curves in the [^{3}H]DTBZ binding and [^{3}H]DA uptake assays (Fig. 2 and 3, and Table 3.1 and 3.2).

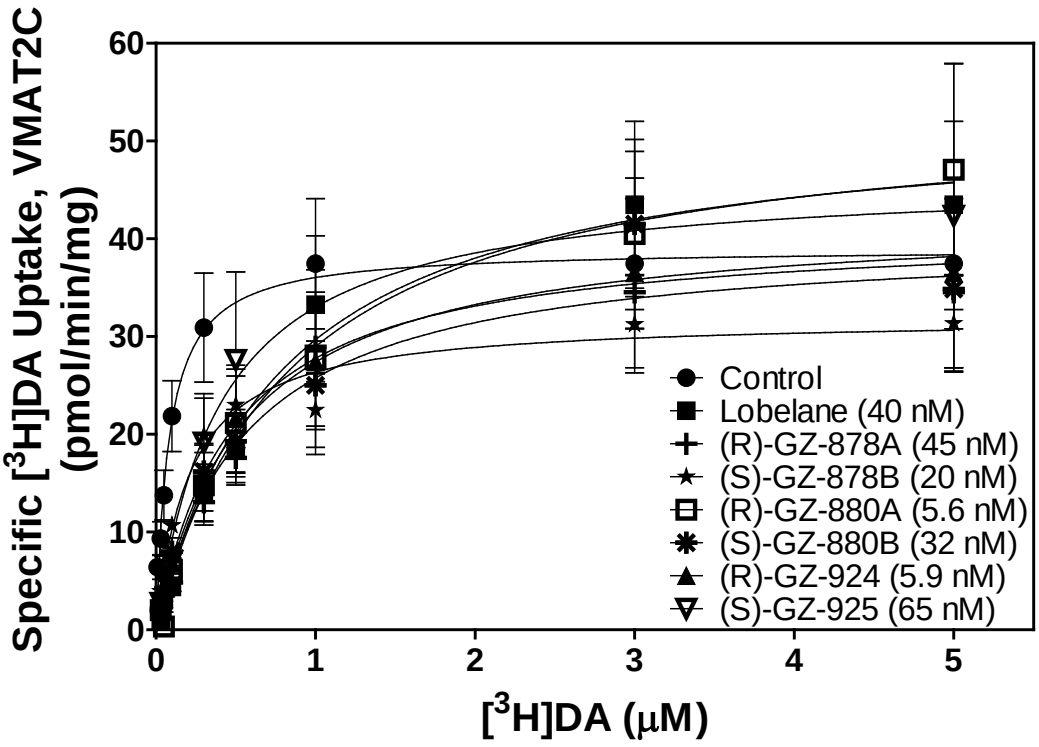

Figure 3.5. Kinetic analysis of VMAT2C [^{3}H]DA uptake in presence of lobelane, (R)-GZ-924, (S)-GZ-925, (R)-GZ-880A, (S)-GZ-880B, (R)-GZ-878A and (S)-GZ-878B.

Concentrations of analogs, the values included in parentheses adjacent to the name of the enantiomers, are the respective K_i values from the concentration response curves in Fig. 3. V_{max} and K_m values (± SEM) are presented in Table 3.3. n = 4-7 rats/analog.

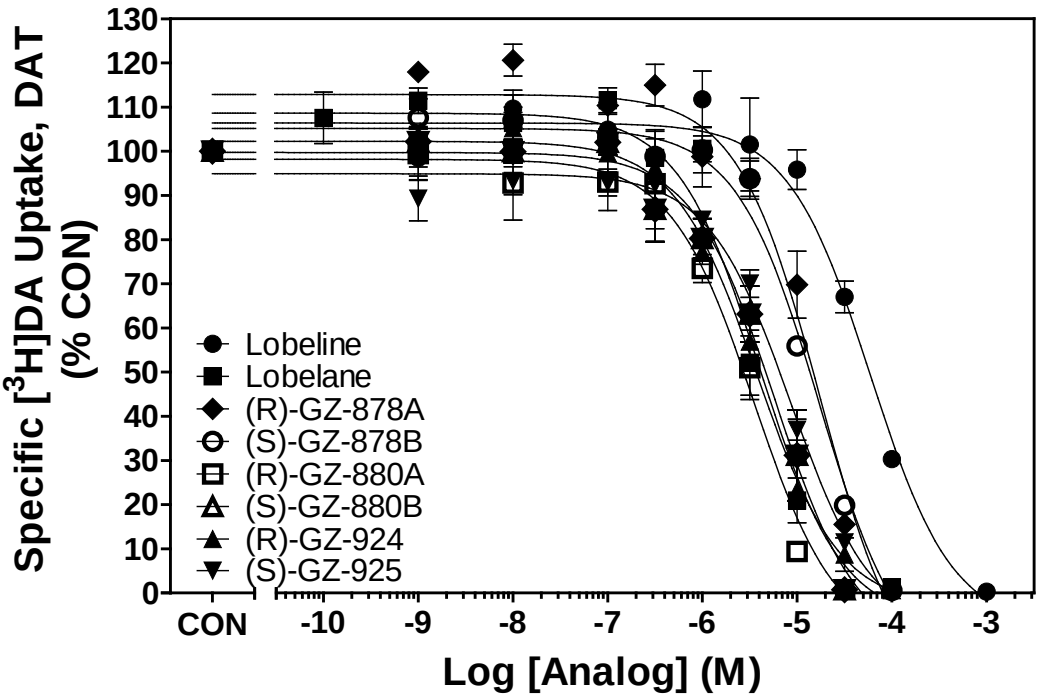

Figure 3.6. (R)-GZ-924, (S)-GZ-925, (R)-GZ-880A, (S)-GZ-880B, (R)-GZ-878A and (S)-GZ-878B inhibit [^{3}H]DA uptake into rat striatal synaptosomes.

The corresponding two enantiomers are presented next to each other in the legend. Control represents specific [^{3}H]DA uptake in the absence of analogs. Uptake values in the curves are mean (± SEM) specific [^{3}H]DA uptake presented as a percentage of the respective control (35.8 ± 6.7 pmol/min/mg, n =3-4 rats/analog).

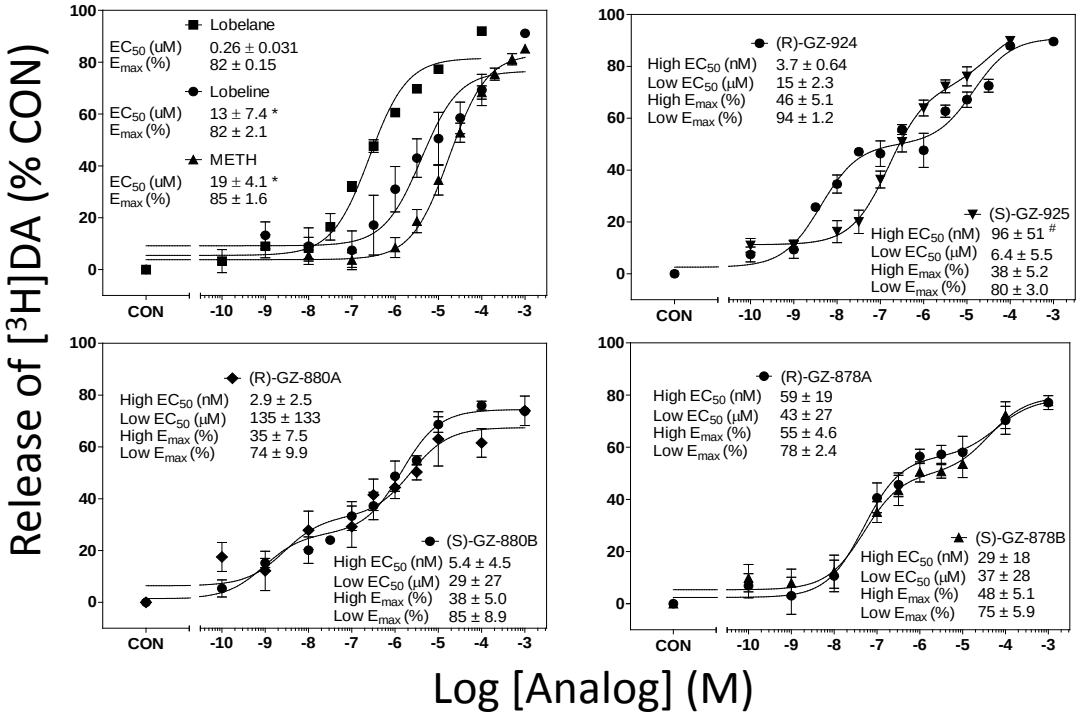

Figure 3.7. (R)-GZ-924, (S)-GZ-925, (R)-GZ-880A, (S)-GZ-880B, (R)-GZ-878A and (S)-GZ-878B evoke [^{3}H]DA release from synaptic vesicles.

Concentration-response curves and EC_{50} and E_{max} values for standards (lobelane, lobeline, methamphetamine), (R)-GZ-924 and (S)-GZ-925, (R)-GZ-880A and (S)-GZ-880B, (R)-GZ-878A and (S)-GZ-878B to evoke [^{3}H]DA release from synaptic vesicles are provided in top left, top right, bottom left, and bottom right panels, respectively, in Fig. 7. Control represents [^{3}H]DA release in the absence of enantiomers. METH represents methamphetamines. Release values in the curves are mean (± SEM) [^{3}H]DA release as a percentage of the respective control (3369 ± 399 disintegrations per minute (DPM), n = 4 rats/analog).

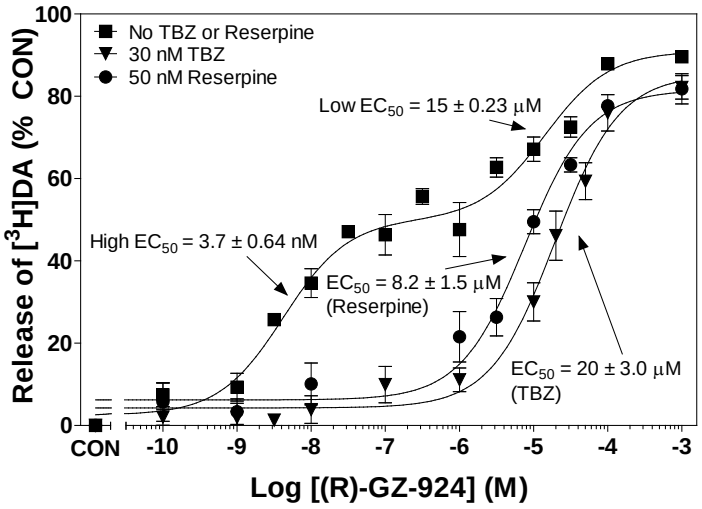

Figure 3.8. TBZ and reserpine eliminate (R)-GZ-924-evoked high affinity [^{3}H]DA release.

Concentration-response curves of (R)-GZ-924-evoked [^{3}H]DA release in the presence of TBZ and reserpine are illustrated. Control represents [^{3}H]DA release in the absence of drugs. Release values in the curves are mean (± SEM) [^{3}H]DA release as a percentage of the respective control (3345 ± 751 DPM, n = 4-7 rats/analog).

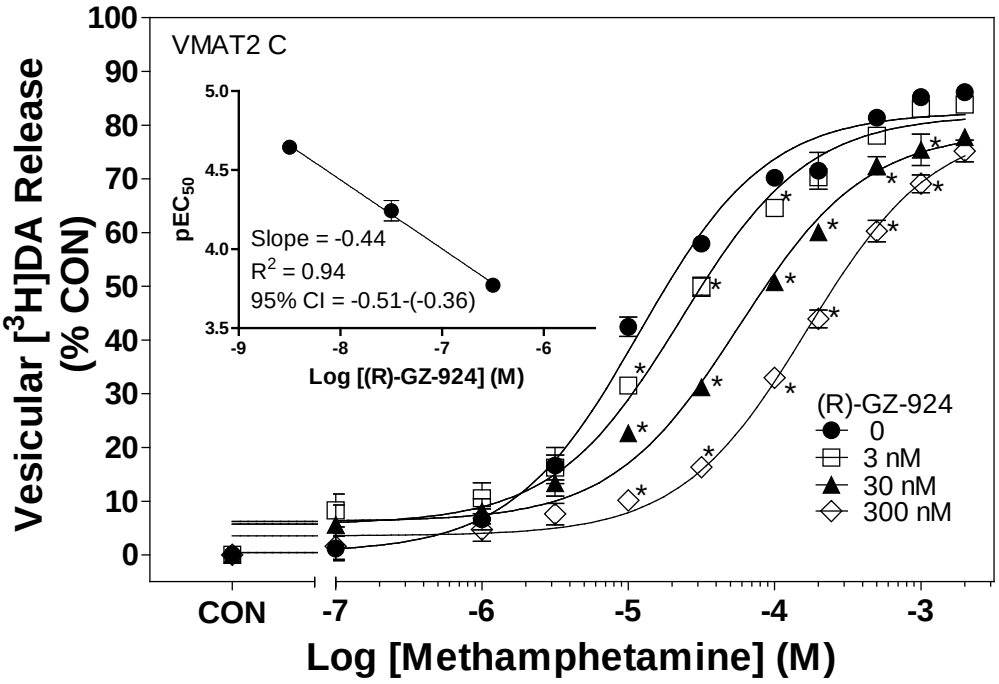

Figure 3.9. (R)-GZ-924 inhibits methamphetamine-evoked [^{3}H]DA release from striatal synaptic vesicles via VMAT2C at 37 °C.

Control represents [^{3}H]DA release in the absence of methamphetamine and (R)-GZ-924. Release values in the curves are mean (± SEM) [^{3}H]DA release as a percentage of the respective control (3162 ± 73 DPM, n = 4/experiment). Inset shows the Lew and Angus method. pEC_{50} values are plotted as a function of log value of (R)-GZ-924 concentration. * $p < 0.05$ compared to methamphetamine.

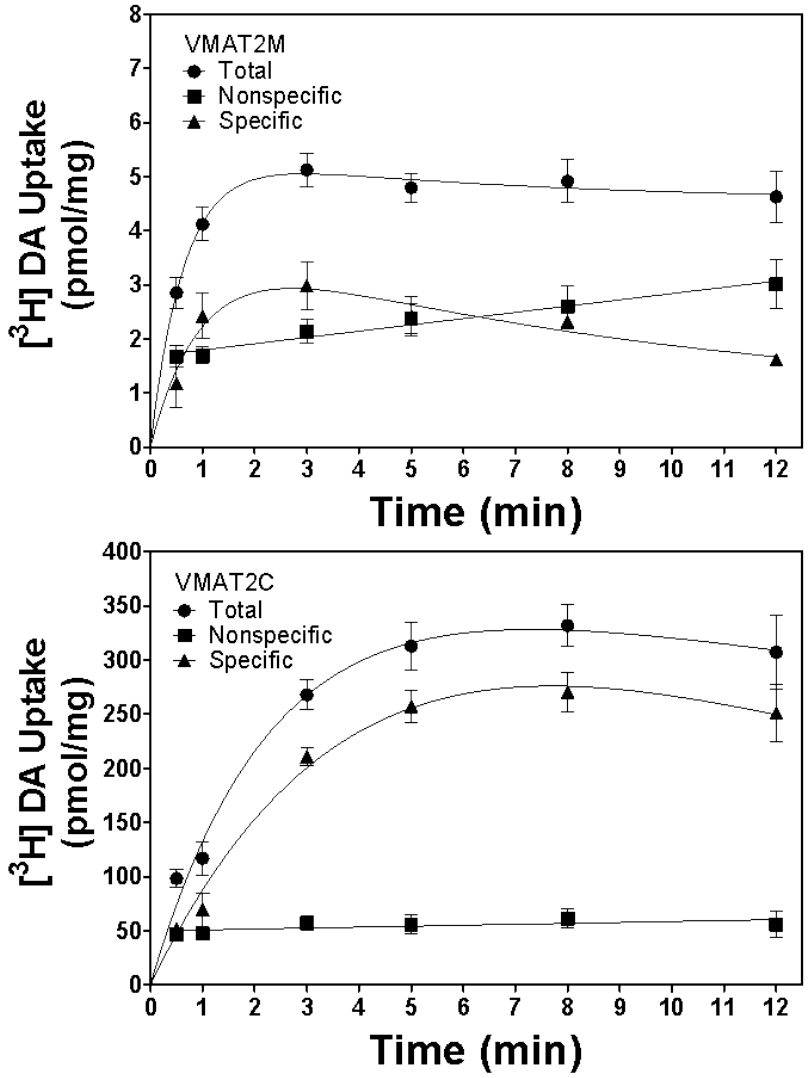

Figure 3.10. VMAT2M and VMAT2C [^{3}H]DA uptake reach maximum at 2 and 8 min, respectively, in the presence of 0.1 μM [^{3}H]DA at 30 °C.

Uptake values in the curves are mean (± SEM) [^{3}H]DA uptake (pmol/mg), n = 3 rats.

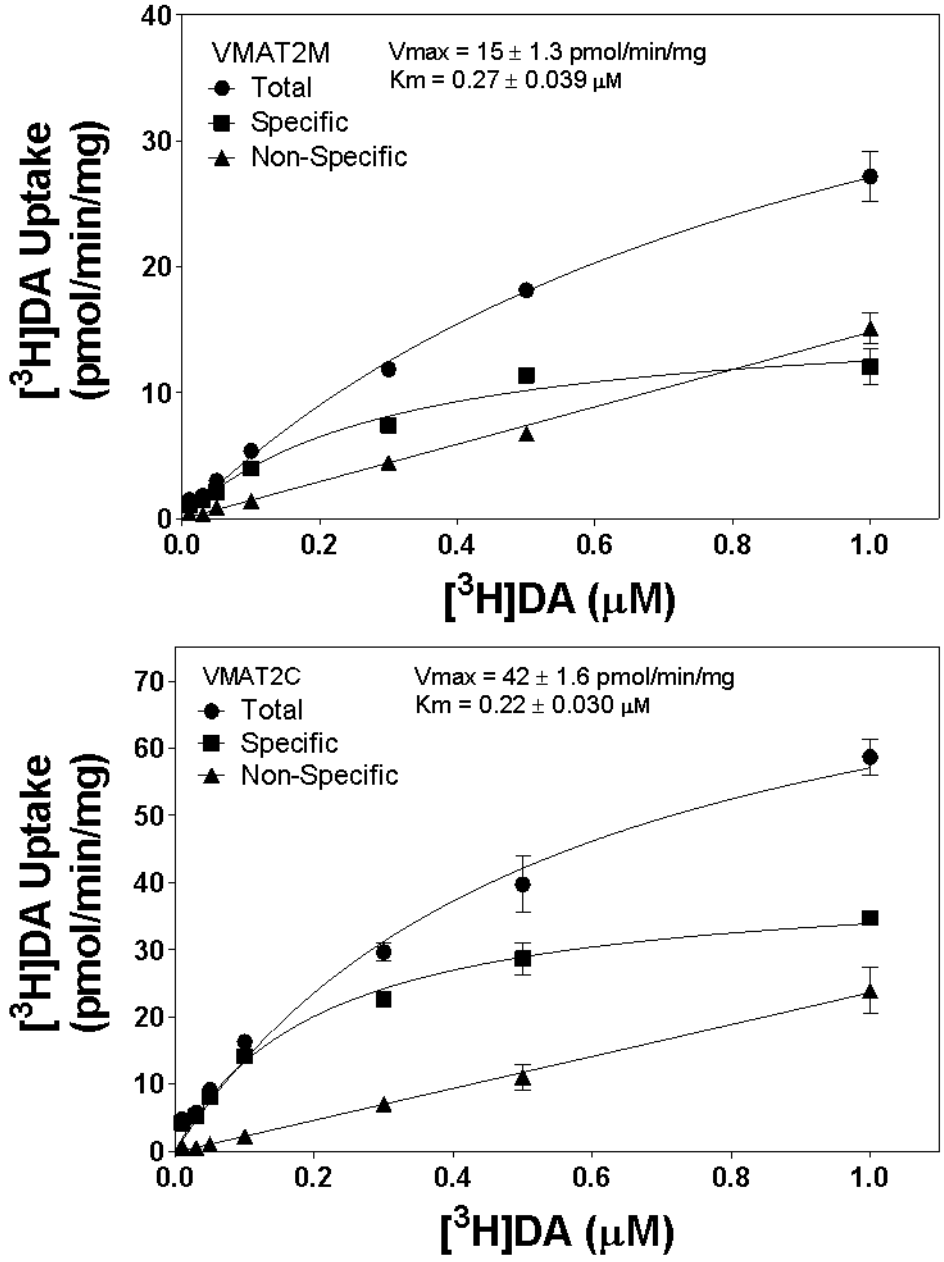

Figure 3.11. Kinetic analysis of VMAT2M and VMAT2C [^{3}H]DA uptake at 30 °C.

Uptake values in the curves are mean (± SEM) [^{3}H]DA uptake (pmol/mg), n = 3 rats.

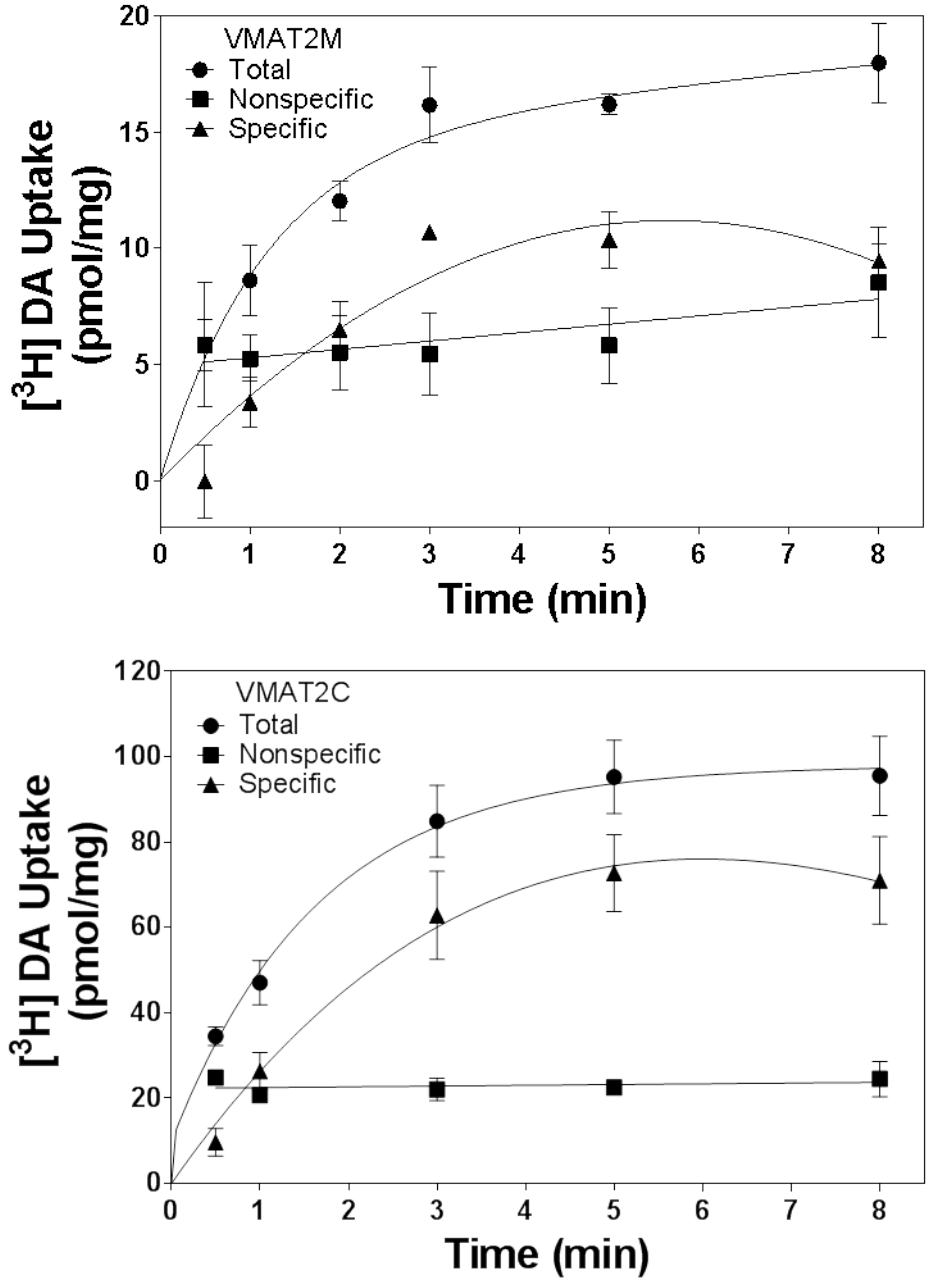

Figure 3.12. VMAT2M and VMAT2C [^{3}H]DA uptake reach maximum at 3 and 5 min, respectively, in the presence of 0.3 µM [^{3}H]DA at 30 °C.

Uptake values in the curves are mean (± SEM) specific [^{3}H]DA uptake (pmol/mg), n = 3 rats.

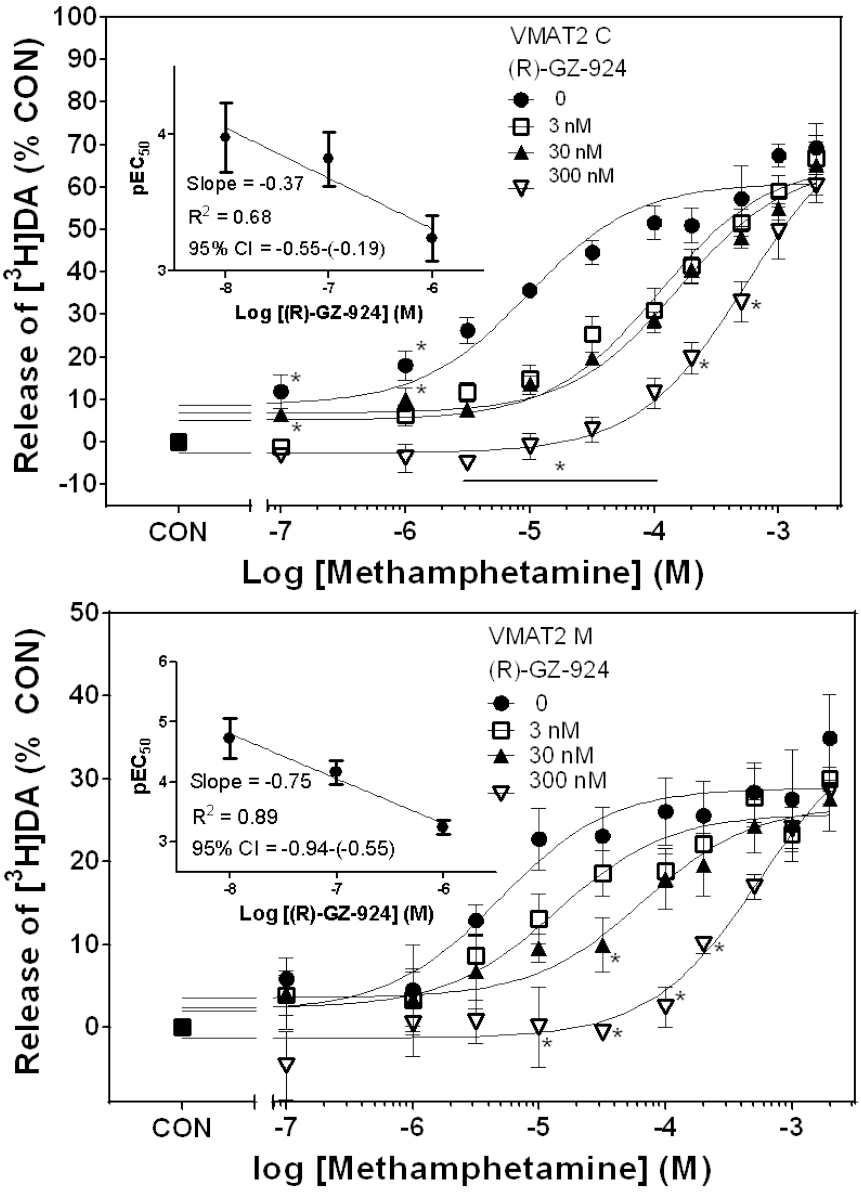

Figure 3.13. (R)-GZ-924 inhibits methamphetamine-evoked [^{3}H]DA release from striatal synaptic vesicles via VMAT2M and VMAT2C at 30 °C.

The concentration response of methamphetamine-evoked vesicular [^{3}H]DA release in the presence of (R)-GZ-924 via VMAT2M and VMAT2C are illustrated in top and bottom panels, respectively. Control represents [^{3}H]DA release in the absence of methamphetamine and (R)-GZ-924. Release values in the curves are mean (± SEM) [^{3}H]DA release as a percentage of the respective

control (5524 ± 294 DPM for VMAT2M and 4443 ± 141 DPM for VMAT2C, n = 4/experiment). Inset shows the Lew and Angus method. pEC_{50} values are plotted as a function of log value of (R)-GZ-924 concentration. * $p < 0.05$ compared to methamphetamine.

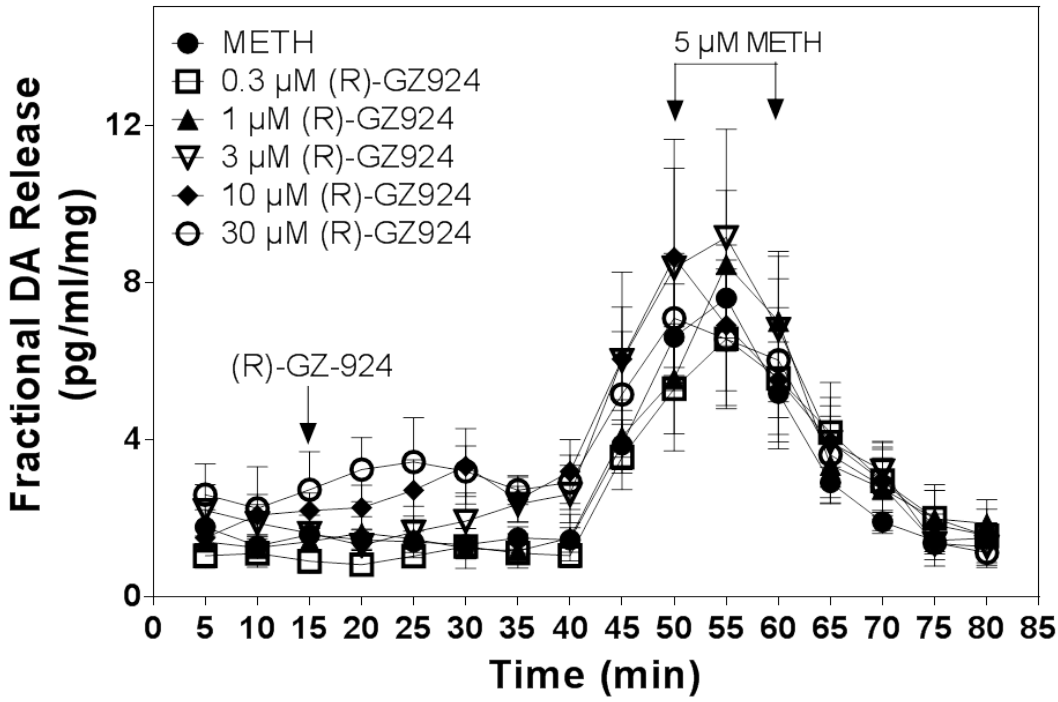

Figure 3.14. (R)-GZ-924 does not inhibit methamphetamine-evoked endogenous DA release from striatal slices.

Striatal slices were superfused with a range of concentrations of (R)-GZ-924 (0.3-30 µM). Fractional DA releases are amount of DA released in each min sample. (R)-GZ-924 was added to the buffer following 10 min basal sample collection, indicated by the arrow, and the analog remained in the buffer until the end of the experiment. METH represents methamphetamines. Methamphetamine (5 µM) was added to the buffer for 15 min, indicated by the horizontal bar with two arrows. Fractional release values are expressed as mean (± SEM) pg/ml/mg of the slice weight. n = 7 rats.

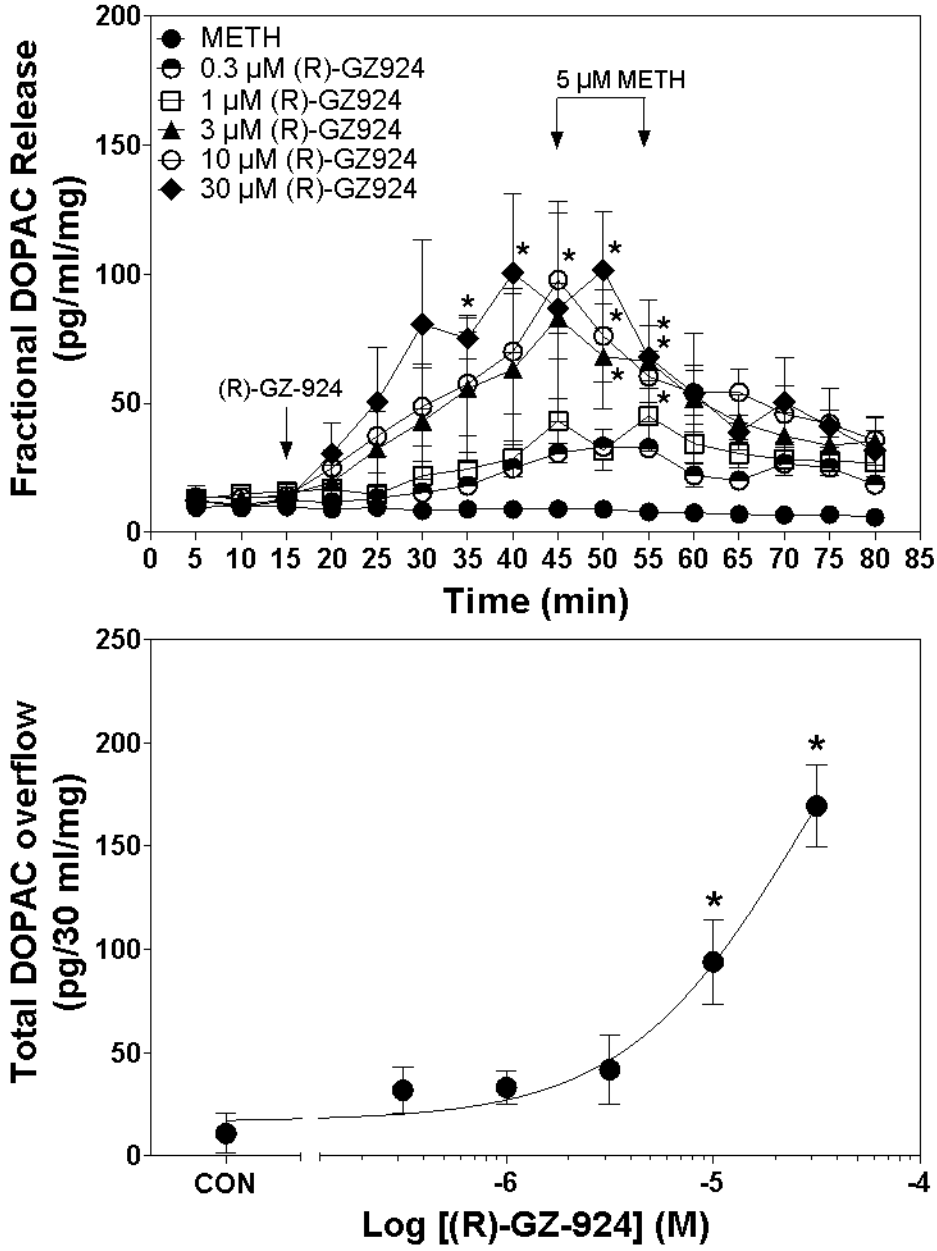

Figure 3.15. (R)-GZ-924 evokes fractional release of DOPAC and DOPAC overflow from striatal slices.

Striatal slices were superfused with a range of concentrations of (R)-GZ-924 (0.3-30 μM). Fractional DOPAC releases (top panel) are amount of DOPAC released in each min sample. (R)-GZ-924 was added to the buffer following 10 min basal sample collection, indicated by the arrow, and the analog remained in

the buffer until the end of the experiment. METH represents methamphetamines. Methamphetamine (5 μM) was added to the buffer for 15 min, indicated by the horizontal bar with two arrows. Fractional release values are expressed as mean (± SEM) pg/ml/mg of the slice weight. n = 7 rats. Overflow data (bottom panel) represent the release of DOPAC during the 30 min period of superfusion in the presence or absence (control) of the analog before the addition of methamphetamine. Control represents the total overflow from slices in the absence of the analog. n = 7 rats. * $p < 0.05$ compared to control.

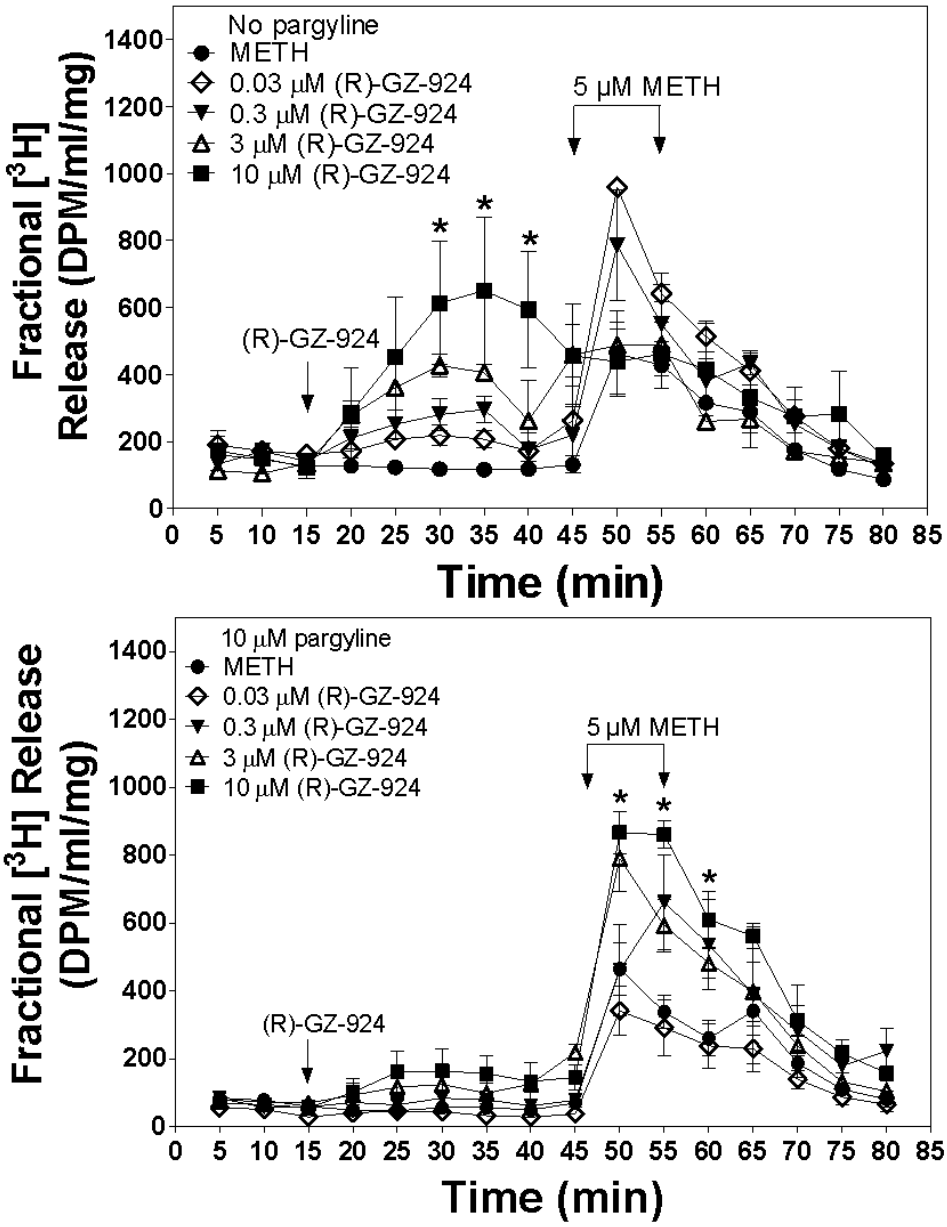

Figure 3.16. (R)-GZ-924 increases [^{3}H] release in the absence of methamphetamine and pargyline, and methamphetamine-evoked [^{3}H] release in the presence of pargyline from striatal slices.

Striatal slices were superfused with a range of concentrations of (R)-GZ-924 (0.3-10 μM). Fractional [^{3}H] releases in the absence or presence of 10 μM pargyline are amount of [^{3}H] released in each 5 min sample. (R)-GZ-924 was added to the buffer following 10 min basal sample collection, indicated by the

arrow, and the analog remained in the buffer until the end of the experiment. METH represents methamphetamines. Methamphetamine (5 μM) was added to the buffer for 15 min, indicated by the horizontal bar with two arrows. Fractional release values are expressed as mean (± SEM) pg/ml/mg of the slice weight. n = 3 rats. * $p < 0.05$ compared with buffer control.

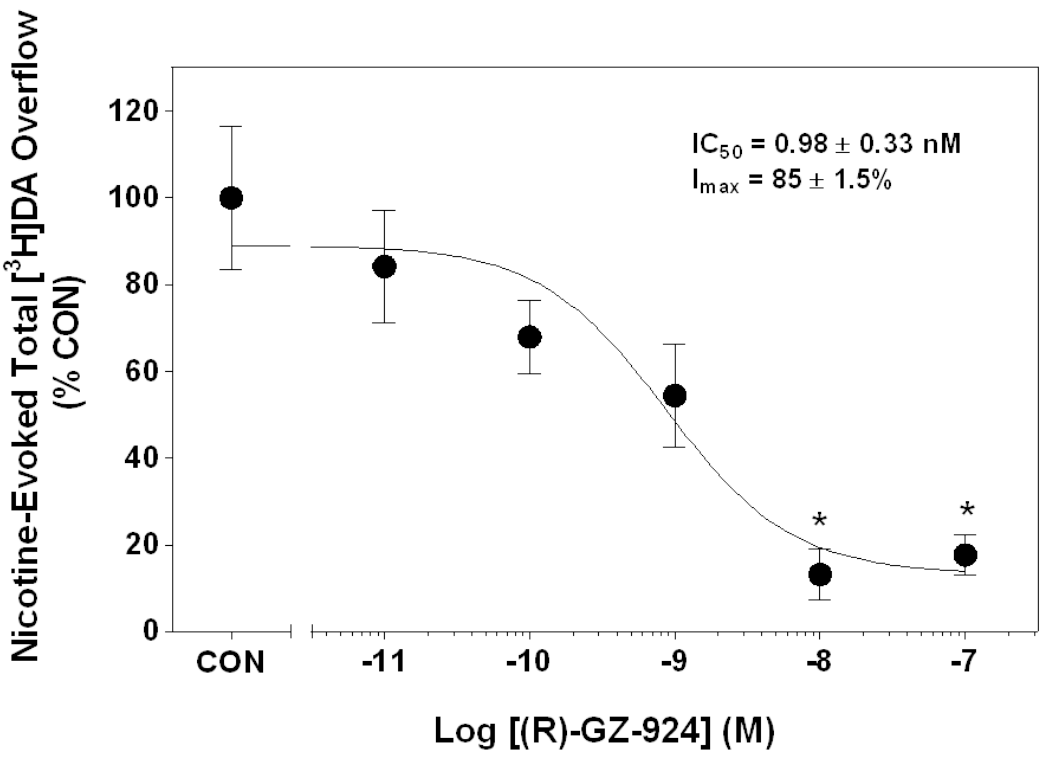

Figure 3.17. (R)-GZ-924 inhibits nicotine-evoked [^{3}H]DA release from rat striatal slices.

Control represents total nicotine-evoked [^{3}H]DA overflow in the absence of (R)-GZ-924. Overflow values in the curve are mean (± SEM) [^{3}H]DA overflow represented as a percentage of the control values (2.2 ± 0.36, n = 6 rats). *, $p < 0.05$ compared to control

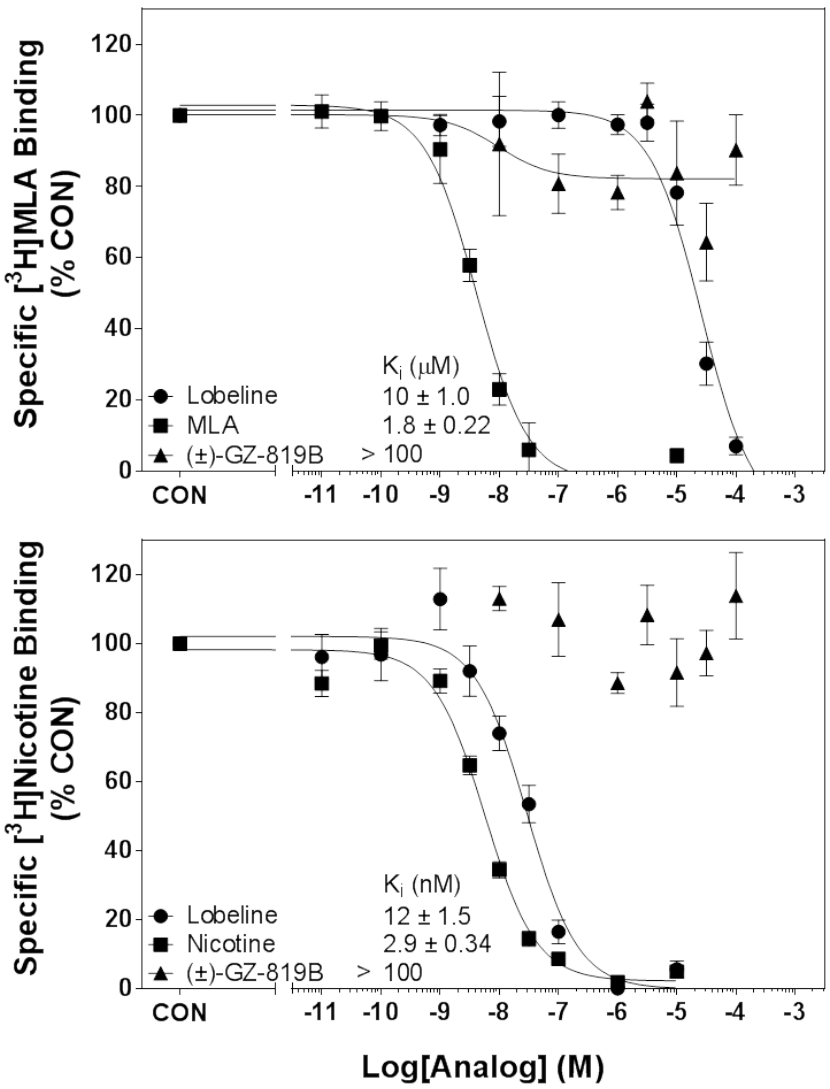

Figure 3.18. (±)-GZ-819B does not inhibit [^{3}H]MLA and [^{3}H]nicotine binding.

(±)-GZ-819B is the racemic analog and contains the same amount of (R)-GZ-924 and (S)-GZ-925. Control represents specific [^{3}H]nicotine (top panel) and specific [^{3}H]MLA (bottom panel) binding. Binding values in the curves are mean (± SEM) specific [^{3}H]nicotine and [^{3}H]MLA binding represented as a percentage of the respective control (36.7 ± 0.8 fmol/mg for [^{3}H]MLA and 65.4 ± 3.1 fmol/mg for [^{3}H]nicotine, n = 3-5 rats/analog).

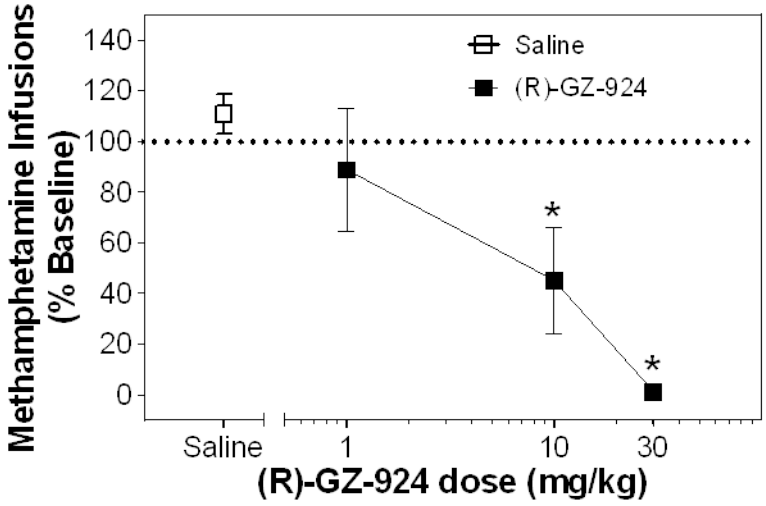
Methamphetamine Infusions (% Baseline)
140
120
100
80
60
40
20
0
Saline
(R)-GZ-924
*
*
Saline
1
10
30
(R)-GZ-924 dose (mg/kg)

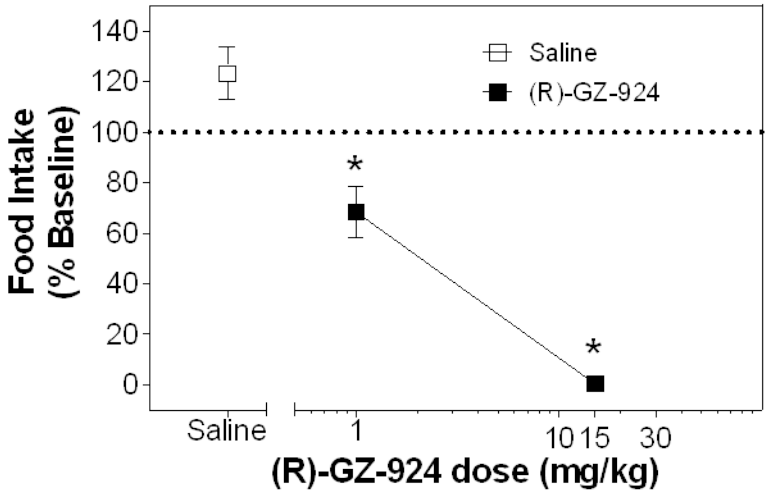
Food Intake (% Baseline)
140
120
100
80
60
40
20
0
Saline
(R)-GZ-924
*
*
Saline
1
10
15
30
(R)-GZ-924 dose (mg/kg)

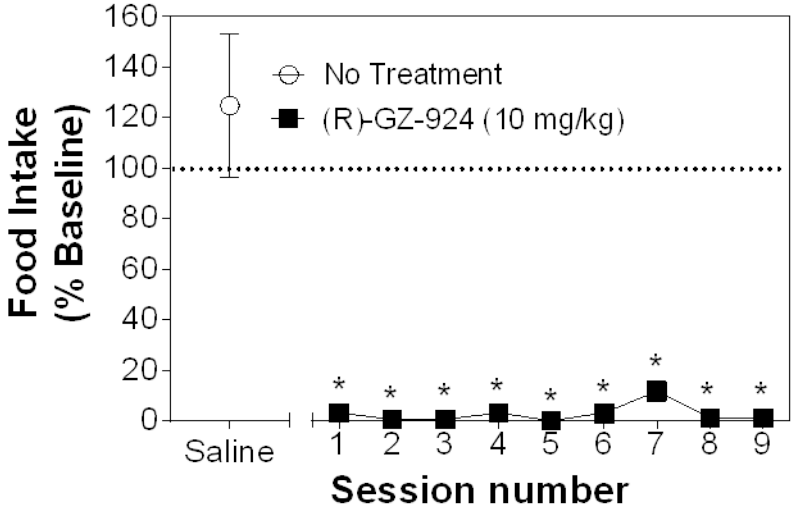
Food Intake (% Baseline)
160
140
120
100
80
60
40
20
0
No Treatment
(R)-GZ-924 (10 mg/kg)
*
*
*
*
*
*
*
*
*
Saline
1
2
3
4
5
6
7
8
9
Session number

Figure 3.19. (R)-GZ-924 inhibits methamphetamine self-administration nonspecifically.

(R)-GZ-924 dose-dependently decreases methamphetamine self-administration (top panel). Food-maintained responding is also reduced (bottom panel). Data points in the figure are expressed as mean (± SEM) number of methamphetamine infusions (0.05 mg/kg/infusion) or number of pellets as percentage of the baseline responding (16 ± 1.4 for methamphetamine self-administration; 33 ± 3.1 for food-maintained responding, n = 6 rats). * $p < 0.05$ compared with saline control.

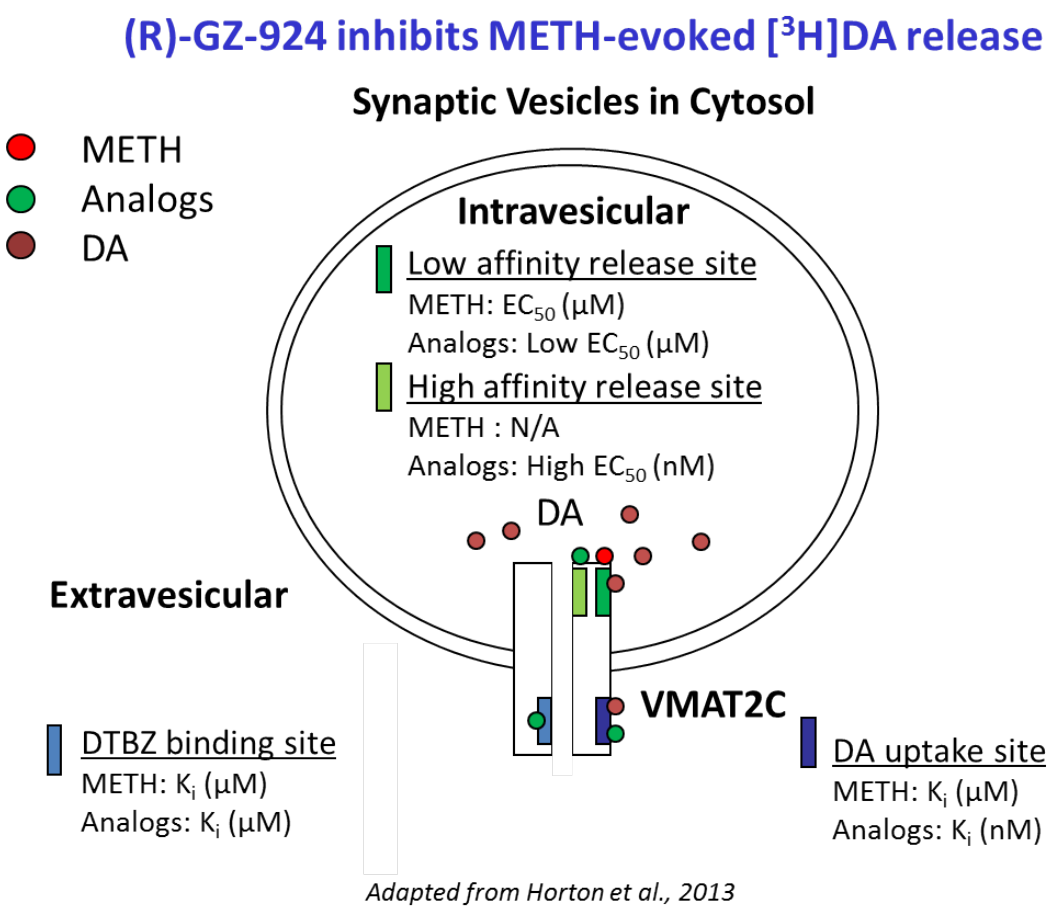

Figure 3.20. (R)-GZ-924 interacts with the extravesicular [^{3}H]DTBZ binding site, the extravesicular [^{3}H]DA uptake site, and the intravesicular high affinity [^{3}H]DA release site on VMAT2C to inhibit methamphetamine-evoked vesicular [^{3}H]DA release.

METH represents methamphetamine.

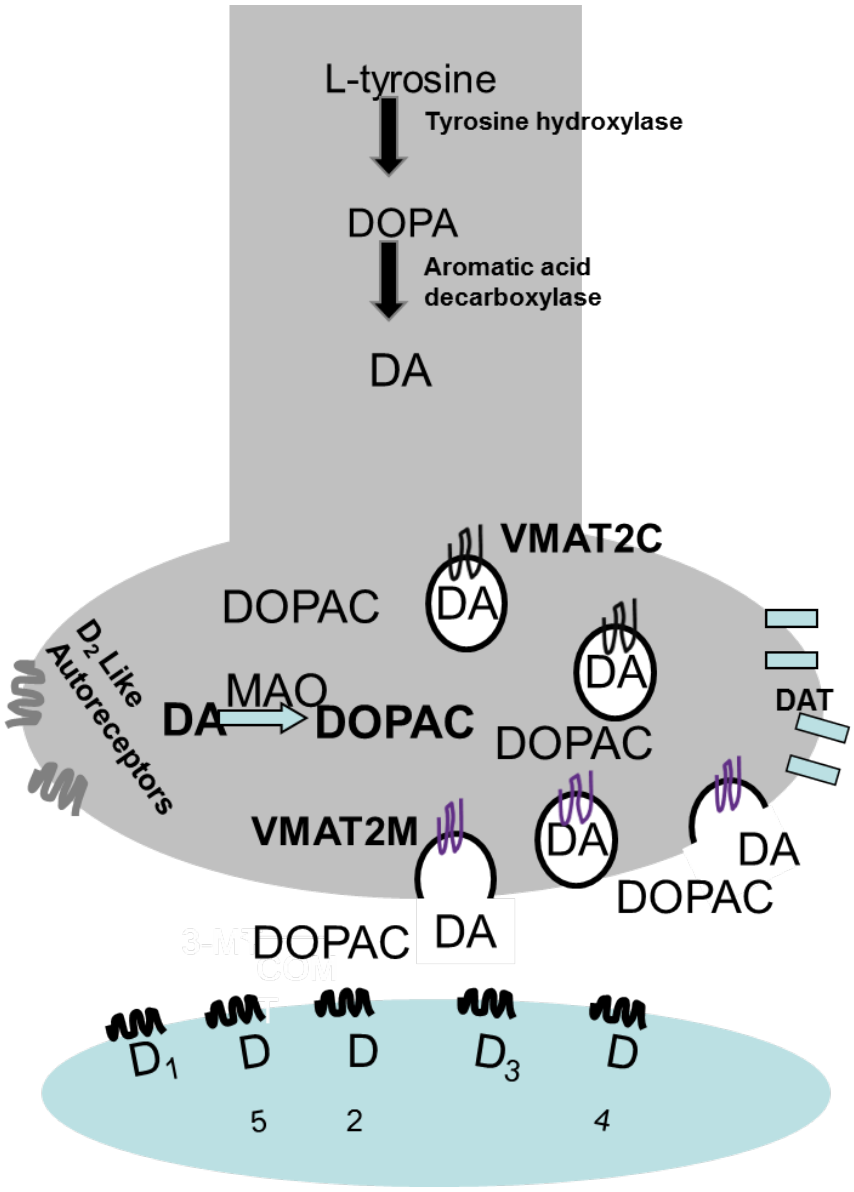

Figure 3.21. VMAT2C-containing vesicles are in the cytosol and VMAT2M-containing vesicles are associated the presynaptic membrane.

Black circle represents VMAT2C-containing vesicles in the cytosol. Semi-circle represents VMAT2M-containing vesicles associated with the presynaptic membrane.

CHAPTER 4 Discussion

4.1 Review

Methamphetamine inhibits DA uptake and promotes DA release from presynaptic vesicles by interacting with VMAT2, contributing to increased DA within presynaptic terminals (Brown et al., 2000; Pifl et al., 1995; Sulzer et al., 1995). Cytosolic DA concentrations were further increased by methamphetamine-induced inhibition of MAO, the mitochondrial enzyme that is responsible for the metabolism of cytosolic DA (Mantle et al., 1976). The elevated cytosolic DA is released into synaptic cleft by methamphetamine-induced reverse transport of DAT (Sulzer et al., 1995). Interaction of methamphetamine with DAT and VMAT2 leads to elevated extracellular DA concentrations that contribute to the reward and reinforcing effects. Currently, no efficacious medicinal treatments are available for methamphetamine abuse. Recently, VMAT2 has been suggested as a promising target and studies focusing on VMAT2 as the therapeutic target have been performed (Dwoskin and Crooks, 2002; Zheng et al., 2006).

Lobeline, a major alkaloid from *Lobelia inflata*, has been evaluated in phase 1b clinical trials as a novel therapeutic for the treatment of methamphetamine abuse (Jones, 2007). Lobeline inhibits vesicular DA uptake and promotes vesicular DA release, resulting in redistributed cytosolic DA that is metabolized by MAO intraneuronally (Dwoskin and Crooks, 2002). Lobeline inhibits methamphetamine-induced release of DA from rat striatal slices. However,

lobeline does not alter the effects of methamphetamine on DA using *in vivo* microdialysis. Interestingly, a more selective VMAT2 inhibitor, N-(1,2R-dihydroxylpropyl)-2,6-cis-di(4-methoxyphenethyl) piperidine hydrochloride (GZ-793A), decreases the duration of methamphetamine-evoked elevation of extracellular DA. Both Lobeline and GZ-793A augment the methamphetamine-induced decrease in extracellular DOPAC (Meyer et al., 2013).

Methamphetamine alone increases extracellular DA by methamphetamine-induced DAT reverse transport, and decreases extracellular DOPAC by inhibiting MAO function which decreases metabolism of DA into DOPAC (Sulzer et al., 2005). However, low dose of methamphetamine (0.5 mg/kg, s.c.) may not be able to inhibit MAO function (Mantle et al., 1976; Robinson, 1985). Thus, methamphetamine-induced DAT reverse transport might reduce cytosolic DA available for MAO metabolism without affect MAO function, which leads to the decrease of extracellular DOPAC (Meyer et al., 2013; Zetterstrom et al., 1988). In addition, methamphetamine-induced decrease of cytosolic DA might attenuate DA-mediated end production inhibition of tyrosine hydroxylase (TH) activity (Gordon et al., 2008; Meyer et al., 2013). In contrast, lobeline and GZ-793A redistribute DA into cytosol and the cytosolic DA will be metabolized into DOPAC, observed as increase of extracellular DOPAC (Meyer et al., 2013). In addition, the redistributed DA in the cytosol might lead to end product inhibition of TH activity (Gordon et al., 2008). Thus, lobeline and GZ-793A pretreatment inhibit TH activity and subsequent DA synthesis, which results in a reduction of DA available for subsequent methamphetamine-induced reverse

transport and also an enhancement of methamphetamine-induced decrease in extracellular DOPAC (Meyer et al., 2013).

In addition, lobeline inhibits methamphetamine-induced hyperactivity and methamphetamine self-administration in rats (Harrod et al., 2001; Miller et al., 2001; Nickell et al., 2010). Meanwhile lobeline does not support self-administration in rats, indicating a lack of abuse liability (Harrod et al., 2003). Above results indicate that lobeline is a potential treatment candidate for methamphetamine abuse. VMAT2 is responsible for the uptake of cytosolic DA into synaptic vesicles for storage and subsequent release (Dwoskin and Crooks, 2002). *In vitro* studies indicate that lobeline decreases methamphetamine-evoked DA release from presynaptic terminals via an interaction with VMAT2 at the DTBZ binding site (Teng et al., 1998; Zheng et al., 2007). However, previous studies have shown that lobeline can bind α4β2* and α7 nicotinic receptors as well, which generates both central and peripheral side effects (Damaj et al., 1997; Miller et al., 2004).

In order to increase the selectivity of lobeline at VMAT2, lobelane, a defunctionalized, saturated analog of lobeline has been generated. Lobelane shows higher affinity for VMAT2, lower affinity for α4β2* and α7 nicotinic receptors, and higher affinity to inhibit vesicular DA uptake in comparison to lobeline (Miller et al., 2004). Furthermore, lobelane decreases methamphetamine-evoked DA release from striatal slices and methamphetamine self-administration without influencing sucrose-maintained responding

(Neugebauer et al., 2007; Nickell et al., 2010). However, the effect of lobelane is tolerated after repeated treatment (Neugebauer et al., 2007). Thus, additional structure activity relationship studies have been performed to discover drug candidates for the treatment of methamphetamine abuse. In the current study, lobelane analogs with varying methylene linker lengths and acyclic lobelane analogs have been evaluated as potential therapeutic candidates.

The objective of Chapter 2 was to modify the length of the methylene linkers of lobelane molecule to afford a series of analogs in the search of potent ligands for VMAT2 function, and to determine their ability to inhibit methamphetamine-evoked [^{3}H]DA release from synaptic vesicles and endogenous DA release from rat striatal slices. It is important to point out that all of the non-symmetrical analogs in this series were racemic and that the enantiomers could exhibit different affinities. The results indicate that the linkers between the central piperidine and the phenyl rings of the lobelane analogs that contain one methylene units at the C-6 position and one or three methylene units at the C-2 position of the piperidine ring maintain high affinity at VMAT2 to inhibit binding and function. Introducing a cyclohexane substituent at the C-6 position of the piperidine ring improved affinity of one analog [(±)-GZ-725A], the analog with 0,2 methylene units in the linkers, in the VMAT2 binding and uptake assay. (±)-GZ-729C, the non-symmetrical lobelane analog with 1,2 methylene units in the linkers, and (±)-GZ-730B, the nor-analog with 1,3 methylene units in the linkers, were the two most potent analogs to inhibit VMAT2 function (Figure 4.1).

A positive correlation was found between the K_i values in the [^{3}H]DTBZ binding and [^{3}H]DA uptake assays, as would be expected if inhibition of VMAT2 function was due to binding to the DTBZ site on VMAT2. Furthermore, (±)-GZ-729C and (±)-GZ-730B inhibited methamphetamine-evoked [^{3}H]DA release via VMAT2 through a surmountable allosteric mechanism. However, those two analogs did not inhibit methamphetamine-evoked endogenous DA release from rat striatal slices, but increased DOPAC release significantly. Such increases in DOPAC release suggested that cytosolic DA was metabolized into DOPAC. However, it was not fully understood why methamphetamine-evoked DA release was not inhibited simultaneously. VMAT2 localized on vesicles that co-fractionate with synaptosomal membranes are defined as VMAT2M, while vesicles that do not co-fractionate with synaptosomal membranes are defined as VMAT2C (Volz et al., 2007). In the vesicular [^{3}H]DA release study, the vesicles collected were VMAT2C vesicles. In the slice release study, both VMAT2C and VMAT2M vesicles existed in each intact slice. The incomplete vesicular VMAT2 preparation in the vesicular [^{3}H]DA release study might be responsible for the conflict between those studies. In addition, different tissue preparation, striatal synaptic vesicles versus slices, and different label, [^{3}H]DA versus endogenous DA, might contribute to the contradictory results. No further investigation in rats was performed due to the poor water solubility of (±)-GZ-729C and (±)-GZ-730B.

The objective of Chapter 3 was to modify the lobelane molecule to afford acyclic lobelane analogs in search of potent and selective ligands for VMAT2 with better water solubility. Racemic-acyclic lobelane analogs inhibited [^{3}H]DTBZ

binding and [^{3}H]DA uptake at VMAT2. A positive correlation for K_i values was found between the [^{3}H]DTBZ binding and [^{3}H]DA uptake assays, suggesting that inhibition of VMAT2 function might be due to binding to the DTBZ site on VMAT2. Both homoamphetamine and N methyl substituents have detrimental effect on analogs affinity for [^{3}H]DTBZ binding and [^{3}H]DA uptake at VMAT2. Racemic nor-analogs with 3-4 carbons in the linkers between the phenyl ring and the amphetamine N-atom had the highest affinity for the [^{3}H]DA uptake site on VMAT2. Enantiomers of the most potent racemic analogs for VMAT2 [^{3}H]DA uptake site were synthesized, and evaluated in inhibition of [^{3}H]DTBZ binding and [^{3}H]DA uptake at VMAT2, DAT, and for interaction at the hERG channel. The most potent and selective enantiomer for VMAT2 was (R)-GZ-924 (Figure 4.2), with 3 carbons in the linker between the phenyl ring and the amphetamine N atom. (R)-GZ-924 showed 11-fold greater affinity for VMAT2 and 2-fold lower affinity for DAT compared to its S-enantiomer GZ-925. Thus, stereochemistry of the N-2-phenylpropyl substituent at the amphetamine N-atom was an important factor in the design of acyclic analogs with regards to VMAT2 inhibition. Kinetic analyses of [^{3}H]DA uptake at VMAT2 revealed competitive inhibition by the enantiomers. The incomplete vesicular VMAT2 preparation in the vesicular [^{3}H]DA release study in Chapter 2 might be responsible for the conflict between studies using striatal vesicles and slices. Thus, the ability of (R)-GZ-924 to inhibit methamphetamine-evoked [^{3}H]DA release from vesicles via both VMAT2C and VMAT2M was determined in a within subject design. However, (R)-GZ-924 similarly inhibited methamphetamine-evoked [^{3}H]DA release via VMAT2M and

VMAT2C in a surmountable allosteric mechanism. Thus, the contradictory results using striatal VMAT2M and VMAT2C between striatal slices were not due to the different pools of vesicles in the *in vitro* preparations. Interestingly, methamphetamine only released around 30% of the [^{3}H]DA in the vesicles associated with the presynaptic membranes, but more than 70% of the [^{3}H]DA in the vesicles in the cytosol. VMAT2 inhibitors such as TBZ and reserpine only released about 50% and 30%, respectively, of DA from vesicles (Horton et al., 2013; Nickell et al., 2011b), while VMAT2 releaser such as methamphetamine released more than 80% of the DA from the vesicles in the cytosol (Horton et al., 2013; Nickell et al., 2011b). Thus, instead of as a releaser, methamphetamine might act as an inhibitor at membrane-associated vesicles and only partially release [^{3}H]DA from the vesicles. Such different release of DA could be caused by a change of the transporter function due to a conformational change in VMAT2M protein structure upon association of the vesicles with the presynaptic membranes. Alternatively, since membrane-associated vesicles were undergoing exocytosis, release of DA from membrane-associated vesicles might be initiated before incubation with methamphetamine in the vesicular [^{3}H]DA release assay. Release via exocytosis would be predicted to lead to the less [^{3}H]DA release from the membrane-associated vesicles in the current study.

Although (R)-GZ-924 inhibited methamphetamine-evoked [^{3}H]DA release at VMAT2C and VMAT2M, this analog did not inhibit methamphetamine-evoked [^{3}H]DA or endogenous DA release from striatal slices. (R)-GZ-924 evoked the overflow of DOPAC from striatal slices, indicating that (R)-GZ-924-redistributed

DA was metabolized by MAO and appeared extracellularly as DOPAC. Interestingly, (R)-GZ-924 inhibited nicotine-evoked [^{3}H]DA release from striatal slices at the same concentration range that (R)-GZ-924 released [^{3}H]DA from synaptic vesicles. Thus, the vesicular DA for nicotine-evoked release was not available probably due to the (R)-GZ-924 induced redistribution of DA form synaptic vesicles to cytosol. Furthermore, (R)-GZ-924 decreased methamphetamine self-administration and food-maintained responding, revealing a similar lack of specificity for decreasing methamphetamine reinforcement in rats.

4.2 Comparisons between Lobelane Analogs with Various Methylene Linker Lengths and the Corresponding Acyclic Lobelane Analogs

The objective of Chapter 2 was to change the methylene linker length of lobelane molecule to generate a series of analogs in the search of potent ligands for VMAT2. However, the most potent analogs, (±)-GZ-729C and (±)-GZ-730B, in this series only had affinity that was twice that of lobelane. To generate compounds with higher affinity for VMAT2, acyclic lobelane analogs, afforded by removing the C-3 and C-4 carbons in the central piperidine ring, were evaluated in Chapter 2. By removing the C-3 and C-4 carbons from the lobelane molecule, (±)-GZ-813B was generated. The [^{3}H]DTBZ binding affinity of (±)-GZ-813B was 17 times lower and the [^{3}H]DA uptake affinity was 9 times lower compared to lobelane. Removing the C-3 and C-4 carbon appeared to have detrimental effect on VMAT2 affinity of lobelane. However, removing the methyl substituent at the

homoamphetamine N atom in (±)-GZ-813B afforded (±)-GZ-813A, with 3- and 7-fold increased affinity at the [^{3}H]DTBZ binding site and [^{3}H]DA uptake site, respectively. Thus, removing the methyl substituent on the homoamphetamine N atom in the acyclic lobelane analogs had a beneficial effect on VMAT2 binding and function.

Since removing the methyl substituent at the N atom increased analog affinity at VMAT2, the, acyclic nor-analogs [(±)-GZ-893B and (±)-GZ-893A] were generated and found to be the most potent VMAT2 inhibitors in this series. However, these two analogs proved toxic in animals killing >50% of the rats following administration. (±)-GZ-819B, an acyclic analog afforded by removing C-3 and C-4 carbons of the piperidine of (±)-GZ-729C and subsequent removal of the methyl substituent from the N atom, was the most potent analog that was not toxic. Since (±)-GZ-819B was racemic, the corresponding enantiomers, (R)-GZ-924 and (S)-GZ-925, were synthesized and (R)-GZ-924 was the most potent and selective enantiomer and was selected as the lead from this series. Comparing to (±)-GZ-729C and (±)-GZ-730B (leads among lobelane analogs with the piperidine ring), (R)-GZ-924 (lead among acyclic lobelane analogs) was 4-fold more potent inhibiting VMAT2 function. In addition, the selectivity of (R)-GZ-924 on VMAT2 over DAT was 183-fold, while the selectivity of (±)-GZ-729C and (±)-GZ-730B on VMAT2 over DAT were 14 and 67-fold, respectively. Thus, the acyclic lobelane enantiomer (R)-GZ-924 was more potent and more selective for VMAT2 compared to (±)-GZ-729C and (±)-GZ-730B. These results suggest that

the less rigid molecule structure of the acyclic analog contributed to improved affinity for VMAT2.

Compounds interacting with VMAT2 can be classified as either uptake inhibitors or substrates. In terms of substrates, higher potencies were observed in functional assays in relative to binding assays; while equivalent potencies were observed in both assays for uptake inhibitors (Andersen, 1987; Nickell et al., 2011a; Partilla et al., 2006). All the analogs in this study exhibited higher affinities in the VMAT2 functional assay relative to the binding assay, and were suggested to be substrates for VMAT2. Since the analogs redistribute DA within the presynaptic terminals, the ability of analog to release [^{3}H]DA from synaptic vesicles was determined. Interestingly, two different intravesicular sites (a high-affinity site and a low-affinity site) on VMAT2 to which analogs bind have been reported by our lab. In addition, the lead N-1,2-dihydroxypropyl lobelane analog (GZ-793A)-evoked high affinity DA release was TBZ and reserpine sensitive (Horton et al., 2012). Similarly, (±)-GZ-729C and (±)-GZ-730B (leads among lobelane analogs with the piperidine ring), and (R)-GZ-924 (lead among acyclic lobelane analogs) released vesicular [^{3}H]DA in a biphasic manner. High EC_{50} values of (±)-GZ-729C and (±)-GZ-730B-induced release were 3 times greater than that of (R)-GZ-924, while no differences of Low EC_{50} values were found. These results showed that the affinity of the lead lobelane analogs, with the intact central piperidine ring, such as (±)-GZ-729C and (±)-GZ-730B, for the high affinity release site on VMAT2 was less than that for the acyclic lobelane lead enantiomer (R)-GZ-924.

The next critical step in our drug discovery approach was to determine whether the analogs inhibited methamphetamine-evoked endogenous DA release from striatal slices. We hypothesized that our analogs redistributed the cytosolic DA that would be metabolized by MAO and not available for methamphetamine-induced reverse transport through DAT. Thus, (±)-GZ-729C, (±)-GZ-730B, and (R)-GZ-924, the more potent and selective inhibitors at VMAT2 compared to lobelane, were predicted to redistribute cytosolic DA more efficiently and inhibit methamphetamine-evoked endogenous DA release at lower concentration. However, none of the analogs inhibited the effect of methamphetamine to release DA from the slice preparation. In addition, our group has suggested that inhibition of methamphetamine self-administration could be an outcome of the inhibition of methamphetamine-evoked DA release from presynaptic vesicles (Horton et al., 2012). Thus, further investigation of the inhibition of methamphetamine-induced vesicular [^{3}H]DA release was performed. All analogs produced a rightward shift of the concentration-response for methamphetamine-evoked [^{3}H]DA release, with no alteration in maximal effect. (R)-GZ-924 was more potent at inhibiting methamphetamine-evoked vesicular [^{3}H]DA release compared to (±)-GZ-729C and (±)-GZ-730B. These results were consistent with the finding that (R)-GZ-924 was more potent in inhibiting VMAT2 function and releasing vesicular [^{3}H]DA. To determine the mechanism of inhibition, Lew and Angus analysis was performed by plotting pE_{50} values against the log concentration of the inhibitors, and a slope different from unity was found for all three analogs. Thus, (±)-GZ-729C, (±)-GZ-730B, and (R)-GZ-924 were

determined to be surmountable allosteric inhibitors of methamphetamine-evoked vesicular [^{3}H]DA release similar to our previous analogs (Horton et al., 2012; Kenakin, 2006a). Based on the characteristics of a surmountable allosteric inhibitor, binding of (±)-GZ-729C, (±)-GZ-730B, and (R)-GZ-924 could cause a conformational change in VMAT2 to decrease the affinity of methamphetamine for the transporter, not affecting the efficacy of methamphetamine to release [^{3}H]DA (Kenakin, 2006a).

4.3 Mechanisms Underlying (±)-GZ-729C, (±)-GZ-730B, and (R)-GZ-924-induced Inhibition of Methamphetamine-evoked [^{3}H]DA Release from Synaptic Vesicles

Interpretations of the Lew and Angus analyses applied in the characterization of antagonists are straightforward in studies on interaction of receptors and ligands (Kenakin, 2006b). In the current study, the effect of methamphetamine and the antagonist response was determined using transporter VMAT2. It was ambiguous to apply receptor-based models to interpret mechanism of inhibition in experiments measuring transporter mediated release. However, DA flux through VMAT2 was accompanied by ion flow, as observed in other transporters as well, suggesting a similar function between transporters and the ligand-gated ion channel receptors (Galli et al., 1998; Sonders and Amara, 1996; Sonders et al., 1997). Thus, Interpretations of the Lew and Angus analyses was used in this dissertation study to evaluate interaction of transporters and ligands.

The analog inhibition of methamphetamine-induced vesicular [^{3}H]DA release was first reported by Dr. Horton from our lab using GZ-793A (Horton et al., 2013). In order to determine mechanism of GZ-793A-induced inhibition of methamphetamine-evoked [^{3}H]DA release from synaptic vesicles, it was assumed that methamphetamine bound an intravesicular site on VMAT2 to evoke DA release from the vesicles (Horton et al., 2013). The other release site on VMAT2 has been suggested by our lab and determined to be a high affinity site relative to the site that methamphetamine binds (Horton et al., 2013). Two extravesicular sites, including TBZ site and reserpine site, have been demonstrated on VMAT2 (Scherman and Henry, 1984). Thus, four sites, including the intravesicular high and low affinity DA release sites, and extravesicular DTBZ and reserpine binding sites, exist on VMAT2 (Horton et al., 2013). GZ-793A interacted with the high affinity DA release site and the DA uptake site on VAMT2 to inhibit methamphetamine-induced vesicular [^{3}H]DA release. The same assumptions were used in the studies in this dissertation and a similar manner of inhibition was found using (±)-GZ-729C, (±)-GZ-730B and (R)-GZ-924.

In the studies in this dissertation, the ability and mechanism of (±)-GZ-729C, (±)-GZ-730B and (R)-GZ-924 to inhibit methamphetamine-induced vesicular [^{3}H]DA release were determined. (±)-GZ-729C, (±)-GZ-730B and (R)-GZ-924 evoked [^{3}H]DA release from synaptic vesicles in a biphasic manner, and such release has been reported in the study using GZ-793A (Horton et al., 2013). This result suggested that, similar to GZ-793A, (±)-GZ-729C, (±)-GZ-730B and

(R)-GZ-924 bound both high and low affinity intravesicular DA release sites on VMAT2. In addition, (±)-GZ-729C, (±)-GZ-730B and (R)-GZ-924 were determined to be surmountable allosteric inhibitors of methamphetamine-evoked vesicular [^{3}H]DA release (Kenakin, 2006a). Thus, similar to GZ-793A, (±)-GZ-729C, (±)-GZ-730B and (R)-GZ-924 may bind to the high affinity release site different from that which methamphetamine binds, and binding of the analogs could produce a conformational change in VMAT2 to decrease the affinity of methamphetamine for the transporter (Kenakin, 2006a). Interestingly, EC_{50} values of (±)-GZ-729C, (±)-GZ-730B and (R)-GZ-924 for the high affinity release site on VMAT2 to release DA were about 10-fold less than the concentration of the respective analog to inhibit methamphetamine-evoked [^{3}H]DA release from synaptic vesicles. Methamphetamine in the above inhibition study might contribute to this difference. Specifically, methamphetamine appeared to inhibit analogs-induced [^{3}H]DA release at low concentration. A similar inhibition of methamphetamine on analog-induced high affinity release has been indicated in a previous study using GZ-793A (Horton et al., 2013). This was not a complete surprise considering the characterization of allosteric inhibition, which was mutual between two ligands inhibiting each other (Kenakin, 2006b). Thus, at low concentrations, the analogs and methamphetamine might bind the respective intravesicular release sites on VMAT2 and inhibit the ability of each other to release vesicular [^{3}H]DA release through allosteric inhibition.

In addition, (±)-GZ-729C, (±)-GZ-730B, and (R)-GZ-924 also displaced [^{3}H]DTBZ binding from VMAT2, suggesting that those analogs bound the TBZ

site to inhibit VMAT2 function. TBZ was capable of inhibiting methamphetamine-evoked vesicular [^{3}H]DA release (Horton et al., 2013). Thus, analogs-induced inhibition of methamphetamine-evoked [^{3}H]DA release could be due to the interaction with the TBZ site on VMAT2. However, the affinity of (±)-GZ-729C, (±)-GZ-730B, and (R)-GZ-924 for TBZ site on VMAT2 were at micromolar range, while methamphetamine-evoked [^{3}H]DA release was inhibited at nanomolar range by those analogs. Inhibition of methamphetamine effect occurred at concentrations at which binding to the TBZ site was not involved. Thus, interaction of (±)-GZ-729C, (±)-GZ-730B, and (R)-GZ-924 with the TBZ site on VMAT2 is not likely responsible for inhibition of methamphetamine-evoked [^{3}H]DA release. However, different vesicular membrane preparation in those two experiments should be considered and might affect the results. Another explanation is that (±)-GZ-729C, (±)-GZ-730B, and (R)-GZ-924, as VMAT2 substrates, might interact with the reserpine binding site on VMAT2 to inhibit methamphetamine-evoked vesicular [^{3}H]DA release. (±)-GZ-729C, (±)-GZ-730B, and (R)-GZ-924 exhibited high affinity at nanomolar range for the [^{3}H]DA uptake site on VMAT2. The analogs may produce a conformational change in VMAT2 protein decreasing methamphetamine affinity for the intravesicular DA release site, without influencing efficacy. Alternatively, interaction of (±)-GZ-729C, (±)-GZ-730B, and (R)-GZ-924 with the substrate site on VMAT2 may have inhibited the uptake of methamphetamine into vesicles, since methamphetamine acts as a substrate and could be transported into vesicles by VMAT2 (Partilla et al., 2006). Such inhibition will prevent the methamphetamine-induced conformational

change of VMAT2, the exposure of DA binding sites on VMAT2 inside vesicles, and the subsequent release of the neurotransmitter. In addition, analog-induced inhibition of transport of methamphetamine into vesicles might also prevent the weak base effect of methamphetamine and subsequent DA release.

At high concentration, methamphetamine-induced [^{3}H]DA release was not inhibited by any of the analogs. The VMAT2 inhibitor TBZ did not inhibit the effect of methamphetamine to evoked [^{3}H]DA release as well (Horton et al., 2013). These results suggest that high concentrations of methamphetamine evoke [^{3}H]DA release from vesicles not via VMAT2. This suggestion was supported by previous studies in which methamphetamine, as a lipophilic weak base, could diffuse across the vesicular membrane to alkalize the vesicular lumen, abolish the pH gradient and release vesicular DA (Peter et al., 1995; Sulzer et al., 2005). Thus, high concentration methamphetamine-evoked [^{3}H]DA release, not sensitive to VMAT2 inhibitors, could be due to diffusion across the membrane and the weak base effect. Such diffusion of methamphetamine only occurred at relative high concentration. Such high concentrations of methamphetamine can only be utilized in *in vitro* studies and would not be realized in vivo. These *in vitro* studies were performed to evaluate the mechanism of action of the drug.

The synaptic vesicle with four binding sites in Horton's study (Horton et al., 2013) and the above studies in this dissertation was a model of VMAT2C-

contianing vesicles. In addition, inhibition studies using VMAT2M-containing vesicles were also performed to determine whether the contradictory results in the slice and vesicular release study was due to the effect of methamphetamine and (R)-GZ-924 on the VMAT2M-containing vesicles. Similar to the study using VMAT2C, (R)-GZ-924 inhibited methamphetamine-evoked [^{3}H]DA release via VMAT2M in the surmountable allosteric manner. Thus, VMAT2M-containing vesicles are not responsible for the contradictory results. Based on the characteristics of allosteric inhibitors, (R)-GZ-924 bond a different site from methamphetamine site on VMAT2M and inhibited the methamphetamine-evoked vesicular [^{3}H]DA release. Further studies exploring the binding sites on VMAT2M are needed to investigate the mechanism of interaction of methamphetamine and (R)-GZ-924 with VMAT2M.

4.4 Mechanisms Underlying (R)-GZ-924 Effect on Methamphetamine and Nicotine-evoked DA Release from Striatal Slices

Activation of nicotinic receptors in the brain leads to DA release from presynaptic terminals via vesicle fusion to the presynaptic terminal membrane and release of vesicular DA. Methamphetamine redistributes DA from the vesicular component to the cytosolic component in presynaptic terminals. Both nicotine and methamphetamine-evoked DA release originated from synaptic vesicles. In the current study, (R)-GZ-924 evoked DOPAC overflow from rat striatal slices, indicating that DA in vesicles was redistributed to cytoplasm and metabolized by MAO. However, it was not fully understood why

methamphetamine-evoked DA release was not inhibited. In addition, (R)-GZ-924 inhibited nicotine-evoked [^{3}H]DA overflow from striatal slices, and at the same concentration range, released vesicular [^{3}H]DA by reducing vesicular content. Since nicotine-evoked release of [^{3}H]DA was from synaptic vesicles, it was possible that nicotine-evoked and (R)-GZ-924 redistributed [^{3}H]DA were the same. Thus, (R)-GZ-924 might inhibit nicotine-evoked [^{3}H]DA overflow by redistributing DA from synaptic vesicles into cytosol. Alternatively, (R)-GZ-924 might inhibit the neurochemical effect of nicotine by acting as nicotinic receptor antagonist.

The interpretation that (R)-GZ-924 did not inhibit MAO function was based upon the observation that (R)-GZ-924 in a dose dependent manner increased DOPAC overflow, and a similar analog-induced DOPAC overflow was reported in in Horton's study (Horton et al., 2011b). This interpretation was further supported by the experiment in this dissertation to determine the ability of (R)-GZ-924 to inhibit methamphetamine-evoked [^{3}H]DA release from striatal slices in the presence and absence of the MAO inhibitor pargyline. Pargyline increased DA content in striatal tissue and vesicles by inhibiting the metabolism of DA (Buu and Lussier, 1989; Fekete et al., 1979), and pargyline pretreatment exacerbated methamphetamine depletion of DA content (Kita et al., 1995). Thus, pargyline would be predicted to facilitate methamphetamine-evoked [^{3}H]DA release since pargyline-induced inhibition of MAO would increase cytosolic DA available for methamphetamine-induced reverse transport via DAT. Consistent with the study using endogenous DA, methamphetamine-evoked [^{3}H]DA release was not

inhibited by (R)-GZ-924 in the presence or absence of pargyline. Interestingly, in the presence of pargyline (R)-GZ-924 did not release [^{3}H] by itself, while in the absence of pargyline (R)-GZ-924 released [^{3}H] in a concentration dependent manner. This result was not a surprise since in the absence of pargyline [^{3}H]DA would be metabolized by MAO into [^{3}H]DOPAC or other [^{3}H]metabolites. The [^{3}H]metabolites then diffuse across the membrane following the concentration gradient. Thus, (R)-GZ-924-evoked [^{3}H]metabolites release was measured instead of [^{3}H]DA, indicating a lack of MAO inhibition by the analog. In addition, in the presence of pargyline, (R)-GZ-924 redistributed DA from vesicles to cytosol and the redistributed DA would not be metabolized due to pargyline inhibition of MAO. The redistributed [^{3}H]DA appeared to be trapped in the presynaptic terminals and did not appear in the extracellular fluid. Thus, the subsequently exposure to methamphetamine released a greater amount of [^{3}H]DA compared with exposure to methamphetamine alone. Although methamphetamine-evoked [^{3}H]DA release was not inhibited by (R)-GZ-924 in the presence or absence of pargyline, the lack of MAO inhibition by (R)-GZ-924 was further supported by the above study.

In addition, (R)-GZ-924 inhibited nicotine-evoked [^{3}H]DA release from rat striatal slices, indicating a possible interaction of the drug with nicotinic receptors. Such interaction with nicotinic receptors was reported for lobeline which interacts with both α4β2* and α7 nicotinic receptors. In addition, lobeline inhibited nicotinic receptors mediating nicotine-evoked [^{3}H]DA release (Miller et al., 2000; Miller et al., 2001). Although defunctionalization of the lobeline molecule afforded

lobelane analogs with no interaction at nicotinic receptors (Miller et al., 2004), removing the C-3 and C-4 carbons in the central piperidine ring afforded acyclic lobelane analogs which may have had affinity for nicotinic receptors. An extraordinary diversity of nicotinic receptors are expressed in brain (Dani and Bertrand, 2007). Among all the subtypes of nicotinic receptors, six heteromeric nicotinic receptor subtypes expressed on dopaminergic nerve terminals mediate nicotine-evoked DA release. Four of these subtypes included α6 subunits (α6β2β3*, α4α6β2β3*, α6β2*, α4α6β2*) and are sensitive to α-conotoxin MII (α-CtxMII). The other two subunits (α4β2* and α4α5β2*) without α6 subunit do not show high affinity/sensitivity for α-CtxMII. (R)-GZ-924 is predicted to not act as an antagonist at α4-containing nicotinic receptors due to the finding that (±)-GZ-819B, which includes (R)-GZ-924, did not bind to α4-containing nicotinic receptors. Thus, the analog may inhibit nicotine-evoked [^{3}H]DA release as an antagonist at α6-containing nicotinic receptors. However, nicotine-evoked [^{3}H]DA release was inhibited by ~80% in the current study, while α-4 and α-6 containing nicotinic receptors mediate ~50% of the total nicotine-evoked DA release, respectively (Pivavarchyk et al., 2011). An explanation for the greater inhibition is that (R)-GZ-924 may not be selective for specific nicotinic receptor subtypes, thus providing greater inhibition of the effect of nicotine. Additionally, a channel blocker, mecamylamine, has been reported to inhibit nicotine-evoked DA release completely by blocking the ion channel. Thus, (R)-GZ-924 may act as a channel blocker in a manner similar to mecamylamine to inhibit nicotine-evoked [^{3}H]DA release from presynaptic terminals (Smith et al., 2009; Varanda et al., 1985)

4.5 Mechanisms Underlying (R)-GZ-924 Inhibition on Methamphetamine Self-administration in Rats

(R)-GZ-924, in a dose-dependent manner, inhibited methamphetamine self-administration in rats, without inhibition of methamphetamine-evoked endogenous and [^{3}H]DA release from striatal slices. However, (R)-GZ-924 might inhibit the neurochemical effect of methamphetamine in other brain regions involved in the mesocorticolimbic DA pathway such as the frontal cortex and NAc. In addition, VMAT2 transports monoamines including NE and 5-HT into vesicles in the presynaptic terminals as well and modulates the transmission of NE and 5-HT in brain. Furthermore, bupropion, a NET and DAT inhibitor, decreased the craving for methamphetamine in early abstinence and prevented relapse by inhibiting the reinforcing effects of methamphetamine (Berigan and Russell, 2001). Pre-treatment with the serotonin reuptake inhibitor fluoxetine inhibited methamphetamine-induced locomotor sensitization in mice (Takamatsu et al., 2006). Thus, (R)-GZ-924 may inhibit methamphetamine self-administration by modulating NE and 5-HT interactions. Interestingly, (R)-GZ-924 inhibited nicotine-evoked [^{3}H]DA release from rat striatal slices, indicating a possible interaction of the drug with nicotinic receptors. Nicotinic receptor ligands are capable of regulating the neurochemical and behavioral effect of methamphetamine. Inhibition of the behavioral effect of methamphetamine by nicotinic receptor ligands was first reported by Glick et al in 2008. Specifically, local infusion of an α3β4 nicotinic receptor antagonist into medial habenula, the interpeduncular area or the basolateral amygdala decreased methamphetamine

self-administration by indirectly regulating the dopaminergic mesolimbic pathway (Glick et al., 2008). Thus, possible interactions of (R)-GZ-924 with nicotinic receptors led to the suggestion that the analog could also inhibit α3β4 nicotinic receptors to inhibit methamphetamine self-administration in rats.

Unfortunately, food-maintained responding was inhibited by (R)-GZ-924 and the inhibitory effect was not tolerated after repeated treatment, demonstrating that the effect of the analog was not specific for methamphetamine. The nicotinic receptor channel blocker mecamylamine inhibited food self-administration in rats by inhibiting the neurochemical effects of nicotine (Levin et al., 2000). Thus, the effect of (R)-GZ-924 on food-maintained responding could be due to the inhibition of the neurochemical effects of nicotine. In addition, since (R)-GZ-924 may bind nicotinic receptors, the analog could inhibit food-maintained responding by interacting with peripheral nicotinic receptors, leading to undesirable gastric side effects reflected by the food-maintained responding results.

4.6 Limitations

The *in vitro* models were utilized to determine the potency and selectivity of lobelane analogs at VMAT2 and the ability to inhibit methamphetamine-evoked DA release from rat striatal vesicles and slices. When comparing potency of analogs across different experiments using different tissue preparations, it was assumed that analogs had universal access to the protein targets. For instance analogs were assumed to have equal access to DAT between striatal

synaptosomal preparations and slice preparations, while in fact analogs would have greater access to DAT in the synaptosomal preparations. In the case of systemic treatment, assumptions were made that the analogs were capable of reaching the pharmacological targets as the *in vitro* studies. However, *in vitro* studies such as the vesicular DA release assays were performed in which high concentrations of methamphetamine were used. In addition, affinities of analogs for the transporters were obtained via *in vitro* models and the intact physiological systems were not utilized. Lack of druglikeness and poor water solubility was a characteristic of some of the analogs in the first series and the physical chemical properties of the analogs should be considered before conducting the structure activity relationship studies.

4.7 Conclusion

The research in this dissertation has been focused on discovering VMAT2 selective lobelane analogs as treatments for methamphetamine abuse. A lead analog, (R)-GZ-924, was discovered and inhibited methamphetamine-evoked vesicular [^{3}H]DA release. Furthermore, (R)-GZ-924 inhibited both methamphetamine self-administration and food-maintained responding in rats, indicating that the decrease in responding for methamphetamine was nonspecific. The lack of specificity for methamphetamine in rats prevented potential pharmacotherapeutic benefits. Further evaluation of the pharmacophore is needed to discover VMAT2 ligands which specifically inhibit the neurochemical and behavioral effect of methamphetamine.

4.8 Future direction

More analogs will be generated and evaluated for VMAT2 activity and selectivity. Current SAR studies in our lab indicate that an analog with a central piperazine ring (JPC-141) exhibited potential as a clinical candidate to treat methamphetamine abuse. The lead piperazine analog did not possess potential cardiac toxicity and inhibited methamphetamine-self administration in rats with an effect on food which was tolerated after repeated treatment (our unpublished observations). In the current study in this dissertation, removing the C-3 and C-4 carbon in the central piperidine ring in lobelane analogs afforded acyclic lobelane analogs with increased affinity for VMAT2. Thus, structure modification of the central piperazine to afford acyclic JPC analogs could be performed in the future SAR studies. Before synthesis of the analogs, the cardiac and liver toxicity of the designed analogs will be predicted in silico. Analogs with great chance to possess cardiac and liver toxicity will be avoided. The predicted non-toxic analogs will be synthesized and analogs with a 30-fold selectivity for VMAT2 over DAT, hERG, and nicotinic receptors will be evaluated in the endogenous DA release assays using striatal slices. Analogs inhibiting methamphetamine-evoked endogenous DA release will be synthesized in larger quantities and evaluated in methamphetamine-induced locomotor sensitization study, providing initial efficacy data in rats. Analogs decreasing methamphetamine-induced locomotor sensitization will be evaluated in striatal DA content study in combination with

methamphetamine. Analogs without exacerbation of methamphetamine-induced DA depletion will be evaluated in the methamphetamine self-administration and reinstatement using both peripheral and oral administration. In addition, analogs passing the above screen will be further evaluated in pharmacokinetics, including absorption, distribution, metabolism, elimination, and toxicity, to determine their potential as a clinical candidate.

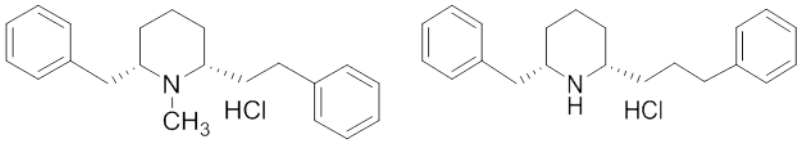

(±)-GZ-729C (±)-GZ-730B

Figure 4.1. Chemical structure of (±)-GZ-729C and (±)-GZ-730B.

(±)-GZ-729C is a non-symmetrical lobelane analog with 1,2 methylene units in the linkers and (±)-GZ-730B is a lobelane nor-analog with 1,3 methylene units in the linkers.

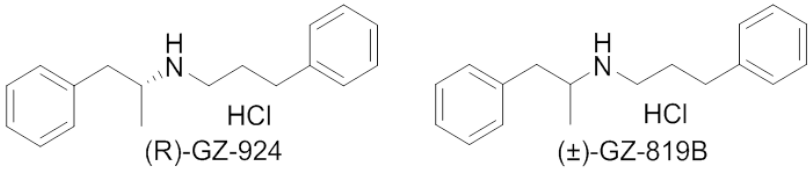

(R)-GZ-924 (±)-GZ-819B

Figure 4.2. Chemical structure of (R)-GZ-924 and (±)-GZ-819B.

(R)-GZ-924 is one of the enantiomers of (±)-GZ-819B, an acyclic nor-analog incorporating an amphetamine scaffold, a 3-carbon linker and with no substituents on the phenyl rings.

Reference

Afonso-Oramas, D., Cruz-Muros, I., Alvarez de la Rosa, D., Abreu, P., Giraldez, T., Castro-Hernandez, J., Salas-Hernandez, J., Lanciego, J. L., Rodriguez, M., and Gonzalez-Hernandez, T. (2009). Dopamine transporter glycosylation correlates with the vulnerability of midbrain dopaminergic cells in Parkinson's disease. Neurobiology of disease *36*, 494-508.

Ago, Y., Nakamura, S., Uda, M., Kajii, Y., Abe, M., Baba, A., and Matsuda, T. (2006). Attenuation by the 5-HT1A receptor agonist osemozotan of the behavioral effects of single and repeated methamphetamine in mice. Neuropharmacology *51*, 914-922.

Akhondzadeh, S., Tavakolian, R., Davari-Ashtiani, R., Arabgol, F., and Amini, H. (2003). Selegiline in the treatment of attention deficit hyperactivity disorder in children: a double blind and randomized trial. Prog Neuropsychopharmacol Biol Psychiatry *27*, 841-845.

Anand, R., Conroy, W. G., Schoepfer, R., Whiting, P., and Lindstrom, J. (1991). Neuronal nicotinic acetylcholine receptors expressed in Xenopus oocytes have a pentameric quaternary structure. J Biol Chem *266*, 11192-11198.

Andersen, P. H. (1987). Biochemical and pharmacological characterization of [3H]GBR 12935 binding in vitro to rat striatal membranes: labeling of the dopamine uptake complex. J Neurochem *48*, 1887-1896.

Anglin, M. D., Burke, C., Perrochet, B., Stamper, E., and Dawud-Noursi, S. (2000). History of the methamphetamine problem. J Psychoactive Drugs *32*, 137-141.

Arbuthnott, G. W., Fairbrother, I. S., and Butcher, S. P. (1990). Dopamine release and metabolism in the rat striatum: an analysis by 'in vivo' brain microdialysis. Pharmacol Ther *48*, 281-293.

Auta, J., Longone, P., Guidotti, A., and Costa, E. (1999). The regulation of hippocampal nicotinic acetylcholine receptors (nAChRs) after a protracted treatment with selective or nonselective nAChR agonists. J Mol Neurosci *13*, 31-45.

Babcock, T., Dirks, B., Adeyi, B., and Scheckner, B. (2012). Efficacy of lisdexamfetamine dimesylate in adults with attention-deficit/hyperactivity disorder previously treated with amphetamines: analyses from a randomized, double-blind, multicenter, placebo-controlled titration study. BMC pharmacology & toxicology *13*, 18.

Bagchi, S. P., Smith, T. M., and Bagchi, P. (1980). Divergent reserpine effects on amfonelic acid and amphetamine stimulation of synaptosomal dopamine formation from phenylalanine. Biochem Pharmacol *29*, 2957-2962.

Barrett, S. P., Darredeau, C., and Pihl, R. O. (2006). Patterns of simultaneous polysubstance use in drug using university students. Hum Psychopharmacol *21*, 255-263.

Batki, S. L., Moon, J., Delucchi, K., Bradley, M., Hersh, D., Smolar, S., Mengis, M., Lefkowitz, E., Sexe, D., Morello, L.*, et al.* (2000). Methamphetamine

quantitative urine concentrations during a controlled trial of fluoxetine treatment. Preliminary analysis. Ann N Y Acad Sci *909*, 260-263.
Battaglia, G., Fornai, F., Busceti, C. L., Aloisi, G., Cerrito, F., De Blasi, A., Melchiorri, D., and Nicoletti, F. (2002). Selective blockade of mGlu5 metabotropic glutamate receptors is protective against methamphetamine neurotoxicity. J Neurosci *22*, 2135-2141.
Beckett, A. H., and Rowland, M. (1965). Urinary excretion kinetics of amphetamine in man. J Pharm Pharmacol *17*, 628-639.
Benwell, M. E., and Balfour, D. J. (1998). The influence of lobeline on nucleus accumbens dopamine and locomotor responses to nicotine in nicotine-pretreated rats. Br J Pharmacol *125*, 1115-1119.
Benyamin, R., Trescot, A. M., Datta, S., Buenaventura, R., Adlaka, R., Sehgal, N., Glaser, S. E., and Vallejo, R. (2008). Opioid complications and side effects. Pain Physician *11*, S105-120.
Berigan, T. R., and Russell, M. L. (2001). Treatment of Methamphetamine Cravings With Bupropion: A Case Report. Prim Care Companion J Clin Psychiatry *3*, 267-268.
Bhat, R. V., Turner, S. L., Selvaag, S. R., Marks, M. J., and Collins, A. C. (1991). Regulation of brain nicotinic receptors by chronic agonist infusion. J Neurochem *56*, 1932-1939.
Boileau, I., Payer, D., Houle, S., Behzadi, A., Rusjan, P. M., Tong, J., Wilkins, D., Selby, P., George, T. P., Zack, M.*, et al.* (2012). Higher binding of the dopamine D3 receptor-preferring ligand [11C]-(+)-propyl-hexahydro-naphtho-oxazin in methamphetamine polydrug users: a positron emission tomography study. J Neurosci *32*, 1353-1359.
Bonisch, H. (1984). The transport of (+)-amphetamine by the neuronal noradrenaline carrier. Naunyn Schmiedebergs Arch Pharmacol *327*, 267-272.
Booth, B. M., Leukefeld, C., Falck, R., Wang, J., and Carlson, R. (2006). Correlates of rural methamphetamine and cocaine users: results from a multistate community study. J Stud Alcohol *67*, 493-501.
Bradford, M. M. (1976). A rapid and sensitive method for the quantitation of microgram quantities of protein utilizing the principle of protein-dye binding. Analytical biochemistry *72*, 248-254.
Briggs, C. A., and McKenna, D. G. (1998). Activation and inhibition of the human alpha7 nicotinic acetylcholine receptor by agonists. Neuropharmacology *37*, 1095-1102.
Brodie, J. D., Figueroa, E., Laska, E. M., and Dewey, S. L. (2005). Safety and efficacy of gamma-vinyl GABA (GVG) for the treatment of methamphetamine and/or cocaine addiction. Synapse *55*, 122-125.
Brouwer, K. C., Case, P., Ramos, R., Magis-Rodriguez, C., Bucardo, J., Patterson, T. L., and Strathdee, S. A. (2006). Trends in production, trafficking, and consumption of methamphetamine and cocaine in Mexico. Subst Use Misuse *41*, 707-727.

Brown, J. M., Hanson, G. R., and Fleckenstein, A. E. (2000). Methamphetamine rapidly decreases vesicular dopamine uptake. J Neurochem *74*, 2221-2223.

Brown, J. M., Quinton, M. S., and Yamamoto, B. K. (2005). Methamphetamine-induced inhibition of mitochondrial complex II: roles of glutamate and peroxynitrite. J Neurochem *95*, 429-436.

Budygin, E. A., Brodie, M. S., Sotnikova, T. D., Mateo, Y., John, C. E., Cyr, M., Gainetdinov, R. R., and Jones, S. R. (2004). Dissociation of rewarding and dopamine transporter-mediated properties of amphetamine. Proc Natl Acad Sci U S A *101*, 7781-7786.

Burn, J. H., and Rand, M. J. (1958). The action of sympathomimetic amines in animals treated with reserpine. J Physiol *144*, 314-336.

Burrows, K. B., Gudelsky, G., and Yamamoto, B. K. (2000). Rapid and transient inhibition of mitochondrial function following methamphetamine or 3,4-methylenedioxymethamphetamine administration. Eur J Pharmacol *398*, 11-18.

Buu, N. T., and Lussier, C. (1989). Consequences of monoamine oxidase inhibition: increased vesicular accumulation of dopamine and norepinephrine and increased metabolism by catechol-O-methyltransferase and phenolsulfotransferase. Prog Neuropsychopharmacol Biol Psychiatry *13*, 563-568.

Caine, S. B., and Koob, G. F. (1993). Modulation of cocaine self-administration in the rat through D-3 dopamine receptors. Science *260*, 1814-1816.

Callaway, C. W., Kuczenski, R., and Segal, D. S. (1989). Reserpine enhances amphetamine stereotypies without increasing amphetamine-induced changes in striatal dialysate dopamine. Brain Res *505*, 83-90.

Carroll, K. M., and Onken, L. S. (2005). Behavioral therapies for drug abuse. Am J Psychiatry *162*, 1452-1460.

Carroll, K. M., Rounsaville, B. J., Gordon, L. T., Nich, C., Jatlow, P., Bisighini, R. M., and Gawin, F. H. (1994). Psychotherapy and pharmacotherapy for ambulatory cocaine abusers. Arch Gen Psychiatry *51*, 177-187.

Chen, N., Ferrer, J. V., Javitch, J. A., and Justice, J. B., Jr. (2000). Transport-dependent accessibility of a cytoplasmic loop cysteine in the human dopamine transporter. J Biol Chem *275*, 1608-1614.

Chen, N., Vaughan, R. A., and Reith, M. E. (2001). The role of conserved tryptophan and acidic residues in the human dopamine transporter as characterized by site-directed mutagenesis. J Neurochem *77*, 1116-1127.

Chio, C. L., Drong, R. F., Riley, D. T., Gill, G. S., Slightom, J. L., and Huff, R. M. (1994a). D4 dopamine receptor-mediated signaling events determined in transfected Chinese hamster ovary cells. J Biol Chem *269*, 11813-11819.

Chio, C. L., Lajiness, M. E., and Huff, R. M. (1994b). Activation of heterologously expressed D3 dopamine receptors: comparison with D2 dopamine receptors. Mol Pharmacol *45*, 51-60.

Chiu, C. T., Ma, T., and Ho, I. K. (2005). Attenuation of methamphetamine-induced behavioral sensitization in mice by systemic administration of naltrexone. Brain Res Bull *67*, 100-109.

Chiu, V. M., and Schenk, J. O. (2012). Mechanism of action of methamphetamine within the catecholamine and serotonin areas of the central nervous system. Current drug abuse reviews *5*, 227-242.
Cho, A. K. (1990). Ice: a new dosage form of an old drug. Science *249*, 631-634.
Chu, P. W., Hadlock, G. C., Vieira-Brock, P., Stout, K., Hanson, G. R., and Fleckenstein, A. E. (2010). Methamphetamine alters vesicular monoamine transporter-2 function and potassium-stimulated dopamine release. J Neurochem *115*, 325-332.
Chu, P. W., Seferian, K. S., Birdsall, E., Truong, J. G., Riordan, J. A., Metcalf, C. S., Hanson, G. R., and Fleckenstein, A. E. (2008). Differential regional effects of methamphetamine on dopamine transport. Eur J Pharmacol *590*, 105-110.
Ciliax, B. J., Heilman, C., Demchyshyn, L. L., Pristupa, Z. B., Ince, E., Hersch, S. M., Niznik, H. B., and Levey, A. I. (1995). The dopamine transporter: immunochemical characterization and localization in brain. J Neurosci *15*, 1714-1723.
Clarke, P. B., and Kumar, R. (1983). The effects of nicotine on locomotor activity in non-tolerant and tolerant rats. Br J Pharmacol *78*, 329-337.
Collins, A. C., Romm, E., and Wehner, J. M. (1990). Dissociation of the apparent relationship between nicotine tolerance and up-regulation of nicotinic receptors. Brain Res Bull *25*, 373-379.
Comer, S. D., Hart, C. L., Ward, A. S., Haney, M., Foltin, R. W., and Fischman, M. W. (2001). Effects of repeated oral methamphetamine administration in humans. Psychopharmacology (Berl) *155*, 397-404.
Cook, C. E., Jeffcoat, A. R., Sadler, B. M., Hill, J. M., Voyksner, R. D., Pugh, D. E., White, W. R., and Perez-Reyes, M. (1992). Pharmacokinetics of oral methamphetamine and effects of repeated daily dosing in humans. Drug Metab Dispos *20*, 856-862.
Corrigall, W. A., Coen, K. M., and Adamson, K. L. (1994). Self-administered nicotine activates the mesolimbic dopamine system through the ventral tegmental area. Brain Res *653*, 278-284.
Cousins, M. S., Stamat, H. M., and de Wit, H. (2001). Acute doses of d-amphetamine and bupropion increase cigarette smoking. Psychopharmacology (Berl) *157*, 243-253.
Coyle, J. T., and Snyder, S. H. (1969). Antiparkinsonian drugs: inhibition of dopamine uptake in the corpus striatum as a possible mechanism of action. Science *166*, 899-901.
Crime, U. N. O. o. D. a. (2007). World Drug Report Volume 1. Analysis. United Nations Office on Drugs and Crime, Vienna.
Cruickshank, C. C., and Dyer, K. R. (2009). A review of the clinical pharmacology of methamphetamine. Addiction *104*, 1085-1099.
Cruickshank, C. C., Montebello, M. E., Dyer, K. R., Quigley, A., Blaszczyk, J., Tomkins, S., and Shand, D. (2008). A placebo-controlled trial of mirtazapine for the management of methamphetamine withdrawal. Drug Alcohol Rev *27*, 326-333.

Damaj, M. I., Patrick, G. S., Creasy, K. R., and Martin, B. R. (1997). Pharmacology of lobeline, a nicotinic receptor ligand. J Pharmacol Exp Ther *282*, 410-419.

Dani, J. A., and Bertrand, D. (2007). Nicotinic acetylcholine receptors and nicotinic cholinergic mechanisms of the central nervous system. Annu Rev Pharmacol Toxicol *47*, 699-729.

Daniels, G. M., and Amara, S. G. (1999). Regulated trafficking of the human dopamine transporter. Clathrin-mediated internalization and lysosomal degradation in response to phorbol esters. J Biol Chem *274*, 35794-35801.

Daniels, J. R., Wessinger, W. D., Hardwick, W. C., Li, M., Gunnell, M. G., Hall, C. J., Owens, S. M., and McMillan, D. E. (2006). Effects of anti-phencyclidine and anti-(+)-methamphetamine monoclonal antibodies alone and in combination on the discrimination of phencyclidine and (+)-methamphetamine by pigeons. Psychopharmacology (Berl) *185*, 36-44.

Dar, D. E., Thiruvazhi, M., Abraham, P., Kitayama, S., Kopajtic, T. A., Gamliel, A., Slusher, B. S., Carroll, F. I., and Uhl, G. R. (2005). Structure-activity relationship of trihexyphenidyl analogs with respect to the dopamine transporter in the on going search for a cocaine inhibitor. Eur J Med Chem *40*, 1013-1021.

Davison, G. C., and Rosen, R. C. (1972). Lobeline and reduction of cigarette smoking. Psychol Rep *31*, 443-456.

De La Garza, R., 2nd, Mahoney, J. J., 3rd, Culbertson, C., Shoptaw, S., and Newton, T. F. (2008). The acetylcholinesterase inhibitor rivastigmine does not alter total choices for methamphetamine, but may reduce positive subjective effects, in a laboratory model of intravenous self-administration in human volunteers. Pharmacol Biochem Behav *89*, 200-208.

Delgado, R., Maureira, C., Oliva, C., Kidokoro, Y., and Labarca, P. (2000). Size of vesicle pools, rates of mobilization, and recycling at neuromuscular synapses of a Drosophila mutant, shibire. Neuron *28*, 941-953.

Di Chiara, G., and Imperato, A. (1988). Drugs abused by humans preferentially increase synaptic dopamine concentrations in the mesolimbic system of freely moving rats. Proc Natl Acad Sci U S A *85*, 5274-5278.

Diaz, G. J., Daniell, K., Leitza, S. T., Martin, R. L., Su, Z., McDermott, J. S., Cox, B. F., and Gintant, G. A. (2004). The [3H]dofetilide binding assay is a predictive screening tool for hERG blockade and proarrhythmia: Comparison of intact cell and membrane preparations and effects of altering [K+]o. J Pharmacol Toxicol Methods *50*, 187-199.

Drug Enforcement Administration, J. (2002). Implementation of the Comprehensive Methamphetamine Control Act of 1996; regulation of pseudoephedrine, phenylpropanolamine, and combination ephedrine drug products and reports of certain transactions to nonregulated persons. Final rule. Fed Regist *67*, 14853-14862.

Dwoskin, L. P., and Crooks, P. A. (2002). A novel mechanism of action and potential use for lobeline as a treatment for psychostimulant abuse. Biochem Pharmacol *63*, 89-98.

Egana, L. A., Cuevas, R. A., Baust, T. B., Parra, L. A., Leak, R. K., Hochendoner, S., Pena, K., Quiroz, M., Hong, W. C., Dorostkar, M. M.*, et al.* (2009). Physical and functional interaction between the dopamine transporter and the synaptic vesicle protein synaptogyrin-3. J Neurosci *29*, 4592-4604.

Eglen, R. M. (2006). Muscarinic receptor subtypes in neuronal and non-neuronal cholinergic function. Autonomic & autacoid pharmacology *26*, 219-233.

Eisch, A. J., O'Dell, S. J., and Marshall, J. F. (1996). Striatal and cortical NMDA receptors are altered by a neurotoxic regimen of methamphetamine. Synapse *22*, 217-225.

Elia, J., Ambrosini, P. J., and Rapoport, J. L. (1999). Treatment of attention-deficit-hyperactivity disorder. N Engl J Med *340*, 780-788.

Erickson, J. D., and Eiden, L. E. (1993). Functional identification and molecular cloning of a human brain vesicle monoamine transporter. J Neurochem *61*, 2314-2317.

Erickson, J. D., Eiden, L. E., and Hoffman, B. J. (1992). Expression cloning of a reserpine-sensitive vesicular monoamine transporter. Proc Natl Acad Sci U S A *89*, 10993-10997.

Erickson, J. D., Masserano, J. M., Barnes, E. M., Ruth, J. A., and Weiner, N. (1990). Chloride ion increases [3H]dopamine accumulation by synaptic vesicles purified from rat striatum: inhibition by thiocyanate ion. Brain research *516*, 155-160.

Erickson, J. D., Schafer, M. K., Bonner, T. I., Eiden, L. E., and Weihe, E. (1996). Distinct pharmacological properties and distribution in neurons and endocrine cells of two isoforms of the human vesicular monoamine transporter. Proc Natl Acad Sci U S A *93*, 5166-5171.

Everitt, B. J., and Robbins, T. W. (2005). Neural systems of reinforcement for drug addiction: from actions to habits to compulsion. Nat Neurosci *8*, 1481-1489.

Eyerman, D. J., and Yamamoto, B. K. (2005). Lobeline attenuates methamphetamine-induced changes in vesicular monoamine transporter 2 immunoreactivity and monoamine depletions in the striatum. J Pharmacol Exp Ther *312*, 160-169.

Eyerman, D. J., and Yamamoto, B. K. (2007). A rapid oxidation and persistent decrease in the vesicular monoamine transporter 2 after methamphetamine. J Neurochem *103*, 1219-1227.

Fasano, C., Poirier, A., DesGroseillers, L., and Trudeau, L. E. (2008). Chronic activation of the D2 dopamine autoreceptor inhibits synaptogenesis in mesencephalic dopaminergic neurons in vitro. Eur J Neurosci *28*, 1480-1490.

Fekete, M. I., Herman, J. P., Kanyicska, B., and Palkovits, M. (1979). Dopamine, noradrenaline and 3,4-dihydroxyphenylacetic acid (DOPAC) levels of individual brain nuclei, effects of haloperidol and pargyline. J Neural Transm *45*, 207-218.

Ferrer, J. V., and Javitch, J. A. (1998). Cocaine alters the accessibility of endogenous cysteines in putative extracellular and intracellular loops of

the human dopamine transporter. Proc Natl Acad Sci U S A *95*, 9238-9243.

Fieber, L. A., and Adams, D. J. (1991). Acetylcholine-evoked currents in cultured neurones dissociated from rat parasympathetic cardiac ganglia. J Physiol *434*, 215-237.

Finlayson, K., McLuckie, J., Hern, J., Aramori, I., Olverman, H. J., and Kelly, J. S. (2001). Characterisation of [(125)I]-apamin binding sites in rat brain membranes with HE293 cells transfected with SK channel subtypes. Neuropharmacology *41*, 341-350.

Fischer, J. F., and Cho, A. K. (1979). Chemical release of dopamine from striatal homogenates: evidence for an exchange diffusion model. J Pharmacol Exp Ther *208*, 203-209.

Fitzgerald, J. L., and Reid, J. J. (1993). Interactions of methylenedioxymethamphetamine with monoamine transmitter release mechanisms in rat brain slices. Naunyn Schmiedebergs Arch Pharmacol *347*, 313-323.

Fleckenstein, A. E., Metzger, R. R., Gibb, J. W., and Hanson, G. R. (1997). A rapid and reversible change in dopamine transporters induced by methamphetamine. Eur J Pharmacol *323*, R9-10.

Fleckenstein, A. E., Volz, T. J., and Hanson, G. R. (2009). Psychostimulant-induced alterations in vesicular monoamine transporter-2 function: neurotoxic and therapeutic implications. Neuropharmacology *56 Suppl 1*, 133-138.

Fleckenstein, A. E., Volz, T. J., Riddle, E. L., Gibb, J. W., and Hanson, G. R. (2007). New insights into the mechanism of action of amphetamines. Annu Rev Pharmacol Toxicol *47*, 681-698.

Floor, E., and Meng, L. (1996). Amphetamine releases dopamine from synaptic vesicles by dual mechanisms. Neurosci Lett *215*, 53-56.

Florin, S. M., Kuczenski, R., and Segal, D. S. (1995). Effects of reserpine on extracellular caudate dopamine and hippocampus norepinephrine responses to amphetamine and cocaine: mechanistic and behavioral considerations. J Pharmacol Exp Ther *274*, 231-241.

Fon, E. A., Pothos, E. N., Sun, B. C., Killeen, N., Sulzer, D., and Edwards, R. H. (1997). Vesicular transport regulates monoamine storage and release but is not essential for amphetamine action. Neuron *19*, 1271-1283.

Fudala, P. J., and Iwamoto, E. T. (1986). Further studies on nicotine-induced conditioned place preference in the rat. Pharmacol Biochem Behav *25*, 1041-1049.

Fudala, P. J., Teoh, K. W., and Iwamoto, E. T. (1985). Pharmacologic characterization of nicotine-induced conditioned place preference. Pharmacol Biochem Behav *22*, 237-241.

Fukami, G., Hashimoto, K., Koike, K., Okamura, N., Shimizu, E., and Iyo, M. (2004). Effect of antioxidant N-acetyl-L-cysteine on behavioral changes and neurotoxicity in rats after administration of methamphetamine. Brain Res *1016*, 90-95.

Fumagalli, F., Gainetdinov, R. R., Valenzano, K. J., and Caron, M. G. (1998). Role of dopamine transporter in methamphetamine-induced neurotoxicity: evidence from mice lacking the transporter. J Neurosci *18*, 4861-4869.

Fung, Y. K., and Uretsky, N. J. (1982). The importance of calcium in the amphetamine-induced stimulation of dopamine synthesis in mouse striata in vivo. J Pharmacol Exp Ther *223*, 477-482.

Gainetdinov, R. R. (2008). Dopamine transporter mutant mice in experimental neuropharmacology. Naunyn Schmiedebergs Arch Pharmacol *377*, 301-313.

Galli, A., Blakely, R. D., and DeFelice, L. J. (1996). Norepinephrine transporters have channel modes of conduction. Proc Natl Acad Sci U S A *93*, 8671-8676.

Galli, A., Blakely, R. D., and DeFelice, L. J. (1998). Patch-clamp and amperometric recordings from norepinephrine transporters: channel activity and voltage-dependent uptake. Proc Natl Acad Sci U S A *95*, 13260-13265.

Garcia-Rates, S., Camarasa, J., Escubedo, E., and Pubill, D. (2007). Methamphetamine and 3,4-methylenedioxymethamphetamine interact with central nicotinic receptors and induce their up-regulation. Toxicol Appl Pharmacol *223*, 195-205.

Gatch, M. B., Flores, E., and Forster, M. J. (2008). Nicotine and methamphetamine share discriminative stimulus effects. Drug Alcohol Depend *93*, 63-71.

Geller, I., Hartmann, R., and Blum, K. (1971). Effects of nicotine, nicotine monomethiodide, lobeline, chlordiazepoxide, meprobamate and caffeine on a discrimination task in laboratory rats. Psychopharmacologia *20*, 355-365.

Gentry, W. B., Ghafoor, A. U., Wessinger, W. D., Laurenzana, E. M., Hendrickson, H. P., and Owens, S. M. (2004). (+)-Methamphetamine-induced spontaneous behavior in rats depends on route of (+)METH administration. Pharmacol Biochem Behav *79*, 751-760.

Gerasimov, M. R., Ashby, C. R., Jr., Gardner, E. L., Mills, M. J., Brodie, J. D., and Dewey, S. L. (1999). Gamma-vinyl GABA inhibits methamphetamine, heroin, or ethanol-induced increases in nucleus accumbens dopamine. Synapse *34*, 11-19.

Gerhardt, G. A., Dwoskin, L. P., and Zahniser, N. R. (1989). Outflow and overflow of picogram levels of endogenous dopamine and DOPAC from rat striatal slices: improved methodology for studies of stimulus-evoked release and metabolism. J Neurosci Methods *26*, 217-227.

Giorguieff-Chesselet, M. F., Kemel, M. L., Wandscheer, D., and Glowinski, J. (1979). Regulation of dopamine release by presynaptic nicotinic receptors in rat striatal slices: effect of nicotine in a low concentration. Life Sci *25*, 1257-1262.

Giros, B., Jaber, M., Jones, S. R., Wightman, R. M., and Caron, M. G. (1996). Hyperlocomotion and indifference to cocaine and amphetamine in mice lacking the dopamine transporter. Nature *379*, 606-612.

Glick, S. D., Sell, E. M., and Maisonneuve, I. M. (2008). Brain regions mediating alpha3beta4 nicotinic antagonist effects of 18-MC on methamphetamine and sucrose self-administration. Eur J Pharmacol *599*, 91-95.
Glover, E. D., Rath, J. M., Sharma, E., Glover, P. N., Laflin, M., Tonnesen, P., Repsher, L., and Quiring, J. (2010). A multicenter phase 3 trial of lobeline sulfate for smoking cessation. Am J Health Behav *34*, 101-109.
Gnegy, M. E. (2003). The effect of phosphorylation on amphetamine-mediated outward transport. Eur J Pharmacol *479*, 83-91.
Gong, W., Neill, D. B., and Justice, J. B., Jr. (1998). GABAergic modulation of ventral pallidal dopamine release studied by in vivo microdialysis in the freely moving rat. Synapse *29*, 406-412.
Gonzalez, A. M., Walther, D., Pazos, A., and Uhl, G. R. (1994). Synaptic vesicular monoamine transporter expression: distribution and pharmacologic profile. Brain Res Mol Brain Res *22*, 219-226.
Gordon, S. L., Quinsey, N. S., Dunkley, P. R., and Dickson, P. W. (2008). Tyrosine hydroxylase activity is regulated by two distinct dopamine-binding sites. J Neurochem *106*, 1614-1623.
Grabowski, J., Roache, J. D., Schmitz, J. M., Rhoades, H., Creson, D., and Korszun, A. (1997). Replacement medication for cocaine dependence: methylphenidate. Journal of clinical psychopharmacology *17*, 485-488.
Graham, D. L., Noailles, P. A., and Cadet, J. L. (2008). Differential neurochemical consequences of an escalating dose-binge regimen followed by single-day multiple-dose methamphetamine challenges. J Neurochem *105*, 1873-1885.
Griffiths, J., and Marley, P. D. (2001). Ca2+ -dependent activation of tyrosine hydroxylase involves MEK1. Neuroreport *12*, 2679-2683.
Gu, H., Caplan, M. J., and Rudnick, G. (1998). Cloned catecholamine transporters expressed in polarized epithelial cells: sorting, drug sensitivity, and ion-coupling stoichiometry. Adv Pharmacol *42*, 175-179.
Guan, X. M., and McBride, W. J. (1989). Serotonin microinfusion into the ventral tegmental area increases accumbens dopamine release. Brain Res Bull *23*, 541-547.
Gygi, M. P., Gygi, S. P., Johnson, M., Wilkins, D. G., Gibb, J. W., and Hanson, G. R. (1996). Mechanisms for tolerance to methamphetamine effects. Neuropharmacology *35*, 751-757.
Haddad, P. M., and Anderson, I. M. (2002). Antipsychotic-related QTc prolongation, torsade de pointes and sudden death. Drugs *62*, 1649-1671.
Hansson, S. R., Mezey, E., and Hoffman, B. J. (1998). Ontogeny of vesicular monoamine transporter mRNAs VMAT1 and VMAT2. II. Expression in neural crest derivatives and their target sites in the rat. Brain Res Dev Brain Res *110*, 159-174.
Harris, D. S., Boxenbaum, H., Everhart, E. T., Sequeira, G., Mendelson, J. E., and Jones, R. T. (2003). The bioavailability of intranasal and smoked methamphetamine. Clin Pharmacol Ther *74*, 475-486.

Harris, J. E., and Baldessarini, R. J. (1975). Amphetamine-induced inhibition of tyrosine hydroxylation in homogenates of rat corpus striatum. Neuropharmacology *14*, 457-471.
Harrod, S. B., Dwoskin, L. P., and Bardo, M. T. (2004). Lobeline produces conditioned taste avoidance in rats. Pharmacol Biochem Behav *78*, 1-5.
Harrod, S. B., Dwoskin, L. P., Crooks, P. A., Klebaur, J. E., and Bardo, M. T. (2001). Lobeline attenuates d-methamphetamine self-administration in rats. J Pharmacol Exp Ther *298*, 172-179.
Harrod, S. B., Dwoskin, L. P., Green, T. A., Gehrke, B. J., and Bardo, M. T. (2003). Lobeline does not serve as a reinforcer in rats. Psychopharmacology (Berl) *165*, 397-404.
Hayashi, T., Justinova, Z., Hayashi, E., Cormaci, G., Mori, T., Tsai, S. Y., Barnes, C., Goldberg, S. R., and Su, T. P. (2010). Regulation of sigma-1 receptors and endoplasmic reticulum chaperones in the brain of methamphetamine self-administering rats. J Pharmacol Exp Ther *332*, 1054-1063.
Heidbreder, C. A., and Newman, A. H. (2010). Current perspectives on selective dopamine D(3) receptor antagonists as pharmacotherapeutics for addictions and related disorders. Ann N Y Acad Sci *1187*, 4-34.
Heinzerling, K. G., Shoptaw, S., Peck, J. A., Yang, X., Liu, J., Roll, J., and Ling, W. (2006). Randomized, placebo-controlled trial of baclofen and gabapentin for the treatment of methamphetamine dependence. Drug Alcohol Depend *85*, 177-184.
Henningfield, J. E., and Griffiths, R. R. (1981). Cigarette smoking and subjective response: effects of d-amphetamine. Clin Pharmacol Ther *30*, 497-505.
Henry, J. P., Sagne, C., Bedet, C., and Gasnier, B. (1998). The vesicular monoamine transporter: from chromaffin granule to brain. Neurochem Int *32*, 227-246.
Herrold, A. A., Shen, F., Graham, M. P., Harper, L. K., Specio, S. E., Tedford, C. E., and Napier, T. C. (2009). Mirtazapine treatment after conditioning with methamphetamine alters subsequent expression of place preference. Drug Alcohol Depend *99*, 231-239.
Hettema, J., Steele, J., and Miller, W. R. (2005). Motivational interviewing. Annu Rev Clin Psychol *1*, 91-111.
Higgins, S. T., Delaney, D. D., Budney, A. J., Bickel, W. K., Hughes, J. R., Foerg, F., and Fenwick, J. W. (1991). A behavioral approach to achieving initial cocaine abstinence. Am J Psychiatry *148*, 1218-1224.
Higley, A. E., Kiefer, S. W., Li, X., Gaal, J., Xi, Z. X., and Gardner, E. L. (2011). Dopamine D(3) receptor antagonist SB-277011A inhibits methamphetamine self-administration and methamphetamine-induced reinstatement of drug-seeking in rats. Eur J Pharmacol *659*, 187-192.
Hiranita, T., Nawata, Y., Sakimura, K., Anggadiredja, K., and Yamamoto, T. (2006). Suppression of methamphetamine-seeking behavior by nicotinic agonists. Proc Natl Acad Sci U S A *103*, 8523-8527.
Hogan, K. A., Staal, R. G., and Sonsalla, P. K. (2000). Analysis of VMAT2 binding after methamphetamine or MPTP treatment: disparity between homogenates and vesicle preparations. J Neurochem *74*, 2217-2220.

Hooks, M. S., Jones, D. N., Justice, J. B., Jr., and Holtzman, S. G. (1992). Naloxone reduces amphetamine-induced stimulation of locomotor activity and in vivo dopamine release in the striatum and nucleus accumbens. Pharmacol Biochem Behav *42*, 765-770.

Horti, A., Scheffel, U., Stathis, M., Finley, P., Ravert, H. T., London, E. D., and Dannals, R. F. (1997). Fluorine-18-FPH for PET imaging of nicotinic acetylcholine receptors. J Nucl Med *38*, 1260-1265.

Horton, D. B., Nickell, J. R., Zheng, G., Crooks, P. A., and Dwoskin, L. P. (2013). GZ-793A, a lobelane analog, interacts with the vesicular monoamine transporter-2 to inhibit the effect of methamphetamine. J Neurochem *127*, 177-186.

Horton, D. B., Siripurapu, K. B., Norrholm, S. D., Culver, J. P., Hojahmat, M., Beckmann, J. S., Harrod, S. B., Deaciuc, A. G., Bardo, M. T., Crooks, P. A., and Dwoskin, L. P. (2011a). meso-Transdiene analogs inhibit vesicular monoamine transporter-2 function and methamphetamine-evoked dopamine release. J Pharmacol Exp Ther *336*, 940-951.

Horton, D. B., Siripurapu, K. B., Zheng, G., Crooks, P. A., and Dwoskin, L. P. (2011b). Novel N-1,2-dihydroxypropyl analogs of lobelane inhibit vesicular monoamine transporter-2 function and methamphetamine-evoked dopamine release. J Pharmacol Exp Ther *339*, 286-297.

Horton, D. B., Zheng, G., Crooks, P. A., and Dwoskin, L. P. (2012). GZ-793A interacts with the vesicular monoamine transporter-2 to inhibit the effect of methamphetamine. J Neurochem in press.

Hotchkiss, A. J., and Gibb, J. W. (1980). Long-term effects of multiple doses of methamphetamine on tryptophan hydroxylase and tyrosine hydroxylase activity in rat brain. J Pharmacol Exp Ther *214*, 257-262.

Hotchkiss, A. J., Morgan, M. E., and Gibb, J. W. (1979). The long-term effects of multiple doses of methamphetamine on neostriatal tryptophan hydroxylase, tyrosine hydroxylase, choline acetyltransferase and glutamate decarboxylase activities. Life Sci *25*, 1373-1378.

Howell, L. L., Carroll, F. I., Votaw, J. R., Goodman, M. M., and Kimmel, H. L. (2007). Effects of combined dopamine and serotonin transporter inhibitors on cocaine self-administration in rhesus monkeys. J Pharmacol Exp Ther *320*, 757-765.

Howell, L. L., and Wilcox, K. M. (2001). The dopamine transporter and cocaine medication development: drug self-administration in nonhuman primates. J Pharmacol Exp Ther *298*, 1-6.

Howell, M., Shirvan, A., Stern-Bach, Y., Steiner-Mordoch, S., Strasser, J. E., Dean, G. E., and Schuldiner, S. (1994). Cloning and functional expression of a tetrabenazine sensitive vesicular monoamine transporter from bovine chromaffin granules. FEBS Lett *338*, 16-22.

Hoyer, D., Clarke, D. E., Fozard, J. R., Hartig, P. R., Martin, G. R., Mylecharane, E. J., Saxena, P. R., and Humphrey, P. P. (1994). International Union of Pharmacology classification of receptors for 5-hydroxytryptamine (Serotonin). Pharmacol Rev *46*, 157-203.

Human, D. o. H. a. (2012). Results from the 2011 National Survey on Drug Use and Health: Summary of National Findings.
Hurley, M. J., and Jenner, P. (2006). What has been learnt from study of dopamine receptors in Parkinson's disease? Pharmacol Ther *111*, 715-728.
Ichikawa, J., Kuroki, T., Kitchen, M. T., and Meltzer, H. Y. (1995). R(+)-8-OH-DPAT, a 5-HT1A receptor agonist, inhibits amphetamine-induced dopamine release in rat striatum and nucleus accumbens. Eur J Pharmacol *287*, 179-184.
Indarte, M., Madura, J. D., and Surratt, C. K. (2008). Dopamine transporter comparative molecular modeling and binding site prediction using the LeuT(Aa) leucine transporter as a template. Proteins *70*, 1033-1046.
Itzhak, Y., and Ali, S. F. (1996). The neuronal nitric oxide synthase inhibitor, 7-nitroindazole, protects against methamphetamine-induced neurotoxicity in vivo. J Neurochem *67*, 1770-1773.
Jacobs, B. L., and Azmitia, E. C. (1992). Structure and function of the brain serotonin system. Physiol Rev *72*, 165-229.
Jardetzky, O. (1966). Simple allosteric model for membrane pumps. Nature *211*, 969-970.
Jayaram-Lindstrom, N., Wennberg, P., Hurd, Y. L., and Franck, J. (2004). Effects of naltrexone on the subjective response to amphetamine in healthy volunteers. J Clin Psychopharmacol *24*, 665-669.
Jo, S. H., Youm, J. B., Lee, C. O., Earm, Y. E., and Ho, W. K. (2000). Blockade of the HERG human cardiac K(+) channel by the antidepressant drug amitriptyline. Br J Pharmacol *129*, 1474-1480.
Jones, R. (2007). Double-blind, placebo-controlled, cross-over assessment of intravenous methamphetamine and sublingual lobeline interactions. NCT00439504 Clinical Trialsgov.
Jones, S. R., Gainetdinov, R. R., Jaber, M., Giros, B., Wightman, R. M., and Caron, M. G. (1998a). Profound neuronal plasticity in response to inactivation of the dopamine transporter. Proc Natl Acad Sci U S A *95*, 4029-4034.
Jones, S. R., Gainetdinov, R. R., Wightman, R. M., and Caron, M. G. (1998b). Mechanisms of amphetamine action revealed in mice lacking the dopamine transporter. J Neurosci *18*, 1979-1986.
Jones, S. R., Joseph, J. D., Barak, L. S., Caron, M. G., and Wightman, R. M. (1999). Dopamine neuronal transport kinetics and effects of amphetamine. J Neurochem *73*, 2406-2414.
Justice, D. o. (2008). National Drug Threat Assessment 2008.
Jutkiewicz, E. M., Nicolazzo, D. M., Kim, M. N., and Gnegy, M. E. (2008). Nicotine and amphetamine acutely cross-potentiate their behavioral and neurochemical responses in female Holtzman rats. Psychopharmacology (Berl) *200*, 93-103.
Kahlig, K. M., Binda, F., Khoshbouei, H., Blakely, R. D., McMahon, D. G., Javitch, J. A., and Galli, A. (2005). Amphetamine induces dopamine efflux

through a dopamine transporter channel. Proc Natl Acad Sci U S A *102*, 3495-3500.
Kalisker, A., Waymire, J. C., and Rutledge, C. O. (1975). Effects of 6-hydroxydopamine and reserpine on amphetamine-induced release of norepinephrine in rat cerebral cortex. J Pharmacol Exp Ther *193*, 64-72.
Kenakin, T. P. (2006a). A Pharmacology Primer, Second Edition: Theory, Application, and Methods. 2nd Edition. Academic Press, San Diego.
Kenakin, T. P. (2006b). A Pharmacology Primer, Second Edition: Theory, Application, Methods. 2nd Edition. Academic Press, San Diego.
Kiluk, B. D., Nich, C., Babuscio, T., and Carroll, K. M. (2010). Quality versus quantity: acquisition of coping skills following computerized cognitive-behavioral therapy for substance use disorders. Addiction *105*, 2120-2127.
Kirshner, N. (1962). Uptake of catecholamines by a particulate fraction of the adrenal medulla. J Biol Chem *237*, 2311-2317.
Kita, T., Wagner, G. C., Philbert, M. A., King, L. A., and Lowndes, H. E. (1995). Effects of pargyline and pyrogallol on the methamphetamine-induced dopamine depletion. Mol Chem Neuropathol *24*, 31-41.
Kitayama, S., Shimada, S., Xu, H., Markham, L., Donovan, D. M., and Uhl, G. R. (1992). Dopamine transporter site-directed mutations differentially alter substrate transport and cocaine binding. Proc Natl Acad Sci U S A *89*, 7782-7785.
Klitenick, M. A., DeWitte, P., and Kalivas, P. W. (1992). Regulation of somatodendritic dopamine release in the ventral tegmental area by opioids and GABA: an in vivo microdialysis study. J Neurosci *12*, 2623-2632.
Knoth, J., Isaacs, J. M., and Njus, D. (1981a). Amine transport in chromaffin granule ghosts. pH dependence implies cationic form is translocated. J Biol Chem *256*, 6541-6543.
Knoth, J., Zallakian, M., and Njus, D. (1981b). Stoichiometry of H+-linked dopamine transport in chromaffin granule ghosts. Biochemistry *20*, 6625-6629.
Kosten, T., and Owens, S. M. (2005). Immunotherapy for the treatment of drug abuse. Pharmacol Ther *108*, 76-85.
Krantz, D. E., Peter, D., Liu, Y., and Edwards, R. H. (1997). Phosphorylation of a vesicular monoamine transporter by casein kinase II. J Biol Chem *272*, 6752-6759.
Krasnova, I. N., and Cadet, J. L. (2009). Methamphetamine toxicity and messengers of death. Brain research reviews *60*, 379-407.
Krueger, B. K. (1990). Kinetics and block of dopamine uptake in synaptosomes from rat caudate nucleus. J Neurochem *55*, 260-267.
Kuffler, S. W., and Edwards, C. (1958). Mechanism of gamma aminobutyric acid (GABA) action and its relation to synaptic inhibition. J Neurophysiol *21*, 589-610.

Kuhn, D. M., Aretha, C. W., and Geddes, T. J. (1999). Peroxynitrite inactivation of tyrosine hydroxylase: mediation by sulfhydryl oxidation, not tyrosine nitration. J Neurosci *19*, 10289-10294.

Kuhn, D. M., Sadidi, M., Liu, X., Kreipke, C., Geddes, T., Borges, C., and Watson, J. T. (2002). Peroxynitrite-induced nitration of tyrosine hydroxylase: identification of tyrosines 423, 428, and 432 as sites of modification by matrix-assisted laser desorption ionization time-of-flight mass spectrometry and tyrosine-scanning mutagenesis. J Biol Chem *277*, 14336-14342.

Kuribara, H. (1999). Does nicotine modify the psychotoxic effect of methamphetamine? Assessment in terms of locomotor sensitization in mice. J Toxicol Sci *24*, 55-62.

Kuroki, T., Meltzer, H. Y., and Ichikawa, J. (1999). Effects of antipsychotic drugs on extracellular dopamine levels in rat medial prefrontal cortex and nucleus accumbens. J Pharmacol Exp Ther *288*, 774-781.

Lamb, R. J., and Henningfield, J. E. (1994). Human d-amphetamine drug discrimination: methamphetamine and hydromorphone. J Exp Anal Behav *61*, 169-180.

Laqueille, X., Dervaux, A., El Omari, F., Kanit, M., and Bayle, F. J. (2005). Methylphenidate effective in treating amphetamine abusers with no other psychiatric disorder. Eur Psychiatry *20*, 456-457.

Larsen, K. E., Fon, E. A., Hastings, T. G., Edwards, R. H., and Sulzer, D. (2002). Methamphetamine-induced degeneration of dopaminergic neurons involves autophagy and upregulation of dopamine synthesis. J Neurosci *22*, 8951-8960.

Lee, S. H., Kang, S. S., Son, H., and Lee, Y. S. (1998). The region of dopamine transporter encompassing the 3rd transmembrane domain is crucial for function. Biochem Biophys Res Commun *246*, 347-352.

Leonard, B. E. (2004). Sigma receptors and sigma ligands: background to a pharmacological enigma. Pharmacopsychiatry *37 Suppl 3*, S166-170.

Levin, E. D., Mead, T., Rezvani, A. H., Rose, J. E., Gallivan, C., and Gross, R. (2000). The nicotinic antagonist mecamylamine preferentially inhibits cocaine vs. food self-administration in rats. Physiology & behavior *71*, 565-570.

Liang, N. Y., and Rutledge, C. O. (1982). Comparison of the release of [3H]dopamine from isolated corpus striatum by amphetamine, fenfluramine and unlabelled dopamine. Biochem Pharmacol *31*, 983-992.

Lile, J. A., Stoops, W. W., Vansickel, A. R., Glaser, P. E., Hays, L. R., and Rush, C. R. (2005). Aripiprazole attenuates the discriminative-stimulus and subject-rated effects of D-amphetamine in humans. Neuropsychopharmacology *30*, 2103-2114.

Lin, L. Y., Di Stefano, E. W., Schmitz, D. A., Hsu, L., Ellis, S. W., Lennard, M. S., Tucker, G. T., and Cho, A. K. (1997). Oxidation of methamphetamine and methylenedioxymethamphetamine by CYP2D6. Drug Metab Dispos *25*, 1059-1064.

Lineberry, T. W., and Bostwick, J. M. (2006). Methamphetamine abuse: a perfect storm of complications. Mayo Clin Proc *81*, 77-84.
Lipinski, C. A., Lombardo, F., Dominy, B. W., and Feeney, P. J. (2001). Experimental and computational approaches to estimate solubility and permeability in drug discovery and development settings. Advanced drug delivery reviews *46*, 3-26.
Lipton, S. A., and Rosenberg, P. A. (1994). Excitatory amino acids as a final common pathway for neurologic disorders. N Engl J Med *330*, 613-622.
Liu, P. S., Liaw, C. T., Lin, M. K., Shin, S. H., Kao, L. S., and Lin, L. F. (2003). Amphetamine enhances Ca2+ entry and catecholamine release via nicotinic receptor activation in bovine adrenal chromaffin cells. Eur J Pharmacol *460*, 9-17.
Logan, B. K. (2002). Methamphetamine Effects on Human Performance and Behavior. Forensic Sci Rev *14*.
Loland, C. J., Norregaard, L., Litman, T., and Gether, U. (2002). Generation of an activating Zn(2+) switch in the dopamine transporter: mutation of an intracellular tyrosine constitutively alters the conformational equilibrium of the transport cycle. Proc Natl Acad Sci U S A *99*, 1683-1688.
MacKenzie, R. G., and Heischober, B. (1997). Methamphetamine. Pediatr Rev *18*, 305-309.
Mager, S., Min, C., Henry, D. J., Chavkin, C., Hoffman, B. J., Davidson, N., and Lester, H. A. (1994). Conducting states of a mammalian serotonin transporter. Neuron *12*, 845-859.
Mahar Doan, K. M., Humphreys, J. E., Webster, L. O., Wring, S. A., Shampine, L. J., Serabjit-Singh, C. J., Adkison, K. K., and Polli, J. W. (2002). Passive permeability and P-glycoprotein-mediated efflux differentiate central nervous system (CNS) and non-CNS marketed drugs. J Pharmacol Exp Ther *303*, 1029-1037.
Manchikanti, L. (2007). National drug control policy and prescription drug abuse: facts and fallacies. Pain Physician *10*, 399-424.
Manepalli, S., Surratt, C. K., Madura, J. D., and Nolan, T. L. (2012). Monoamine transporter structure, function, dynamics, and drug discovery: a computational perspective. AAPS J *14*, 820-831.
Mantle, T. J., Tipton, K. F., and Garrett, N. J. (1976). Inhibition of monoamine oxidase by amphetamine and related compounds. Biochem Pharmacol *25*, 2073-2077.
Masuoka, D. T., Alcaraz, A. F., and Schott, H. F. (1982). [3H]Dopamine release by d-amphetamine from striatal synaptosomes of reserpinized rats. Biochem Pharmacol *31*, 1969-1974.
Matsumoto, T. K., A.; Miyakawa, T.; Endo, K.;Yabana, T.; Kishimoto, H.; Okudaira, K.; Iseki, E.; Sakai, T.; Kosaka, K. (2002). Methamphetamine in Japan: the consequences of methamphetamine abuse as a function of route of administration. Addiction *97*, 809–817.
Matthews, R. T., and German, D. C. (1984). Electrophysiological evidence for excitation of rat ventral tegmental area dopamine neurons by morphine. Neuroscience *11*, 617-625.

McCann, U. D., Wong, D. F., Yokoi, F., Villemagne, V., Dannals, R. F., and Ricaurte, G. A. (1998). Reduced striatal dopamine transporter density in abstinent methamphetamine and methcathinone users: evidence from positron emission tomography studies with [11C]WIN-35,428. J Neurosci *18*, 8417-8422.

McDaid, J., Tedford, C. E., Mackie, A. R., Dallimore, J. E., Mickiewicz, A. L., Shen, F., Angle, J. M., and Napier, T. C. (2007). Nullifying drug-induced sensitization: behavioral and electrophysiological evaluations of dopaminergic and serotonergic ligands in methamphetamine-sensitized rats. Drug Alcohol Depend *86*, 55-66.

McFadden, L. M., Carter, S., and Matuszewich, L. (2012a). Juvenile exposure to methamphetamine attenuates behavioral and neurochemical responses to methamphetamine in adult rats. Behav Brain Res *229*, 118-122.

McFadden, L. M., Hunt, M. M., Vieira-Brock, P. L., Muehle, J., Nielsen, S. M., Allen, S. C., Hanson, G. R., and Fleckenstein, A. E. (2012b). Prior methamphetamine self-administration attenuates serotonergic deficits induced by subsequent high-dose methamphetamine administrations. Drug Alcohol Depend *126*, 87-94.

McGregor, C., Srisurapanont, M., Jittiwutikarn, J., Laobhripatr, S., Wongtan, T., and White, J. M. (2005). The nature, time course and severity of methamphetamine withdrawal. Addiction *100*, 1320-1329.

McMillan, D. E., Hardwick, W. C., Li, M., Gunnell, M. G., Carroll, F. I., Abraham, P., and Owens, S. M. (2004). Effects of murine-derived anti-methamphetamine monoclonal antibodies on (+)-methamphetamine self-administration in the rat. J Pharmacol Exp Ther *309*, 1248-1255.

Meyer, A. C., Neugebauer, N. M., Zheng, G., Crooks, P. A., Dwoskin, L. P., and Bardo, M. T. (2013). Effects of VMAT2 inhibitors lobeline and GZ-793A on methamphetamine-induced changes in dopamine release, metabolism and synthesis in vivo. J Neurochem *127*, 187-198.

Michel, P. P., and Hefti, F. (1990). Toxicity of 6-hydroxydopamine and dopamine for dopaminergic neurons in culture. J Neurosci Res *26*, 428-435.

Millar, N. S., and Gotti, C. (2009). Diversity of vertebrate nicotinic acetylcholine receptors. Neuropharmacology *56*, 237-246.

Miller, D. K., Crooks, P. A., and Dwoskin, L. P. (2000). Lobeline inhibits nicotine-evoked [(3)H]dopamine overflow from rat striatal slices and nicotine-evoked (86)Rb(+) efflux from thalamic synaptosomes. Neuropharmacology *39*, 2654-2662.

Miller, D. K., Crooks, P. A., Teng, L., Witkin, J. M., Munzar, P., Goldberg, S. R., Acri, J. B., and Dwoskin, L. P. (2001). Lobeline inhibits the neurochemical and behavioral effects of amphetamine. J Pharmacol Exp Ther *296*, 1023-1034.

Miller, D. K., Crooks, P. A., Zheng, G., Grinevich, V. P., Norrholm, S. D., and Dwoskin, L. P. (2004). Lobeline analogs with enhanced affinity and selectivity for plasmalemma and vesicular monoamine transporters. J Pharmacol Exp Ther *310*, 1035-1045.

Miller, W. R. (2005). Motivational interviewing and the incredible shrinking treatment effect. Addiction *100*, 421.
Millspaugh, C. F. (1974). American Medicinal Plants: An Illustrated and Descriptive Guide to Plants Indigenous to and Naturalized in the United States Which Are Used in Medicine. New York: Dover. p.385-8.).
Miranda, M., Dionne, K. R., Sorkina, T., and Sorkin, A. (2007). Three ubiquitin conjugation sites in the amino terminus of the dopamine transporter mediate protein kinase C-dependent endocytosis of the transporter. Mol Biol Cell *18*, 313-323.
Mitler, M. M., Hajdukovic, R., and Erman, M. K. (1993). Treatment of narcolepsy with methamphetamine. Sleep *16*, 306-317.
Moeller, F. G., Schmitz, J. M., Herin, D., and Kjome, K. L. (2008). Use of stimulants to treat cocaine and methamphetamine abuse. Curr Psychiatry Rep *10*, 385-391.
Mosharov, E. V., Gong, L. W., Khanna, B., Sulzer, D., and Lindau, M. (2003). Intracellular patch electrochemistry: regulation of cytosolic catecholamines in chromaffin cells. J Neurosci *23*, 5835-5845.
Muller, C. P., Carey, R. J., Huston, J. P., and De Souza Silva, M. A. (2007). Serotonin and psychostimulant addiction: focus on 5-HT1A-receptors. Prog Neurobiol *81*, 133-178.
Mundorf, M. L., Hochstetler, S. E., and Wightman, R. M. (1999). Amine weak bases disrupt vesicular storage and promote exocytosis in chromaffin cells. J Neurochem *73*, 2397-2405.
Munzar, P., Laufert, M. D., Kutkat, S. W., Novakova, J., and Goldberg, S. R. (1999). Effects of various serotonin agonists, antagonists, and uptake inhibitors on the discriminative stimulus effects of methamphetamine in rats. J Pharmacol Exp Ther *291*, 239-250.
NACO (2006). National Association of Counties reports
Nakanishi, N., Onozawa, S., Matsumoto, R., Kurihara, K., Ueha, T., Hasegawa, H., and Minami, N. (1995). Effects of protein kinase inhibitors and protein phosphatase inhibitors on cyclic AMP-dependent down-regulation of vesicular monoamine transport in pheochromocytoma PC12 cells. FEBS Lett *368*, 411-414.
Narayanan, S., Bhat, R., Mesangeau, C., Poupaert, J. H., and McCurdy, C. R. (2011). Early development of sigma-receptor ligands. Future Med Chem *3*, 79-94.
NDTS (2008). National Drug Threat Survey
Neisewander, J. L., Fuchs, R. A., Tran-Nguyen, L. T., Weber, S. M., Coffey, G. P., and Joyce, J. N. (2004). Increases in dopamine D3 receptor binding in rats receiving a cocaine challenge at various time points after cocaine self-administration: implications for cocaine-seeking behavior. Neuropsychopharmacology *29*, 1479-1487.
Network, D. A. W. (2010). National Estimates of Drug-Related Emergency Department Visits.

Neugebauer, N. M., Harrod, S. B., Stairs, D. J., Crooks, P. A., Dwoskin, L. P., and Bardo, M. T. (2007). Lobelane decreases methamphetamine self-administration in rats. Eur J Pharmacol *571*, 33-38.

Newman, A. H., Blaylock, B. L., Nader, M. A., Bergman, J., Sibley, D. R., and Skolnick, P. (2012). Medication discovery for addiction: translating the dopamine D3 receptor hypothesis. Biochem Pharmacol *84*, 882-890.

Newton, T. F., Roache, J. D., De La Garza, R., 2nd, Fong, T., Wallace, C. L., Li, S. H., Elkashef, A., Chiang, N., and Kahn, R. (2005). Safety of intravenous methamphetamine administration during treatment with bupropion. Psychopharmacology (Berl) *182*, 426-435.

Newton, T. F., Roache, J. D., De La Garza, R., 2nd, Fong, T., Wallace, C. L., Li, S. H., Elkashef, A., Chiang, N., and Kahn, R. (2006). Bupropion reduces methamphetamine-induced subjective effects and cue-induced craving. Neuropsychopharmacology *31*, 1537-1544.

Nguyen, T. T., and Amara, S. G. (1996). N-linked oligosaccharides are required for cell surface expression of the norepinephrine transporter but do not influence substrate or inhibitor recognition. J Neurochem *67*, 645-655.

Nichols, D. E., and Nichols, C. D. (2008). Serotonin receptors. Chem Rev *108*, 1614-1641.

Nickell, J. R., Krishnamurthy, S., Norrholm, S., Deaciuc, G., Siripurapu, K. B., Zheng, G., Crooks, P. A., and Dwoskin, L. P. (2010). Lobelane inhibits methamphetamine-evoked dopamine release via inhibition of the vesicular monoamine transporter-2. J Pharmacol Exp Ther *332*, 612-621.

Nickell, J. R., Zheng, G., Deaciuc, A. G., Crooks, P. A., and Dwoskin, L. P. (2011a). Phenyl ring-substituted lobelane analogs: inhibition of [3H]dopamine uptake at the vesicular monoamine transporter-2. J Pharmacol Exp Ther *336*, 724-733.

Nickell, J. R., Zheng, G., Deaciuc, A. G., Crooks, P. A., and Dwoskin, L. P. (2011b). Phenyl ring-substituted lobelane analogs: inhibition of [(3)H]dopamine uptake at the vesicular monoamine transporter-2. J Pharmacol Exp Ther *336*, 724-733.

Niddam, R., Arbilla, S., Scatton, B., Dennis, T., and Langer, S. Z. (1985). Amphetamine induced release of endogenous dopamine in vitro is not reduced following pretreatment with reserpine. Naunyn Schmiedebergs Arch Pharmacol *329*, 123-127.

Nooney, J. M., Peters, J. A., and Lambert, J. J. (1992). A patch clamp study of the nicotinic acetylcholine receptor of bovine adrenomedullary chromaffin cells in culture. J Physiol *455*, 503-527.

Norinder, U., and Haeberlein, M. (2002). Computational approaches to the prediction of the blood-brain distribution. Advanced drug delivery reviews *54*, 291-313.

NSDUH (2011). Results from the 2011 National Survey on Drug Use and Health.

Numachi, Y., Ohara, A., Yamashita, M., Fukushima, S., Kobayashi, H., Hata, H., Watanabe, H., Hall, F. S., Lesch, K. P., Murphy, D. L.*, et al.* (2007). Methamphetamine-induced hyperthermia and lethal toxicity: role of the dopamine and serotonin transporters. Eur J Pharmacol *572*, 120-128.

Olive, M. F., Koenig, H. N., Nannini, M. A., and Hodge, C. W. (2001). Stimulation of endorphin neurotransmission in the nucleus accumbens by ethanol, cocaine, and amphetamine. J Neurosci *21*, RC184.

Pace, C. J., Glick, S. D., Maisonneuve, I. M., He, L. W., Jokiel, P. A., Kuehne, M. E., and Fleck, M. W. (2004). Novel iboga alkaloid congeners block nicotinic receptors and reduce drug self-administration. Eur J Pharmacol *492*, 159-167.

Parker, E. M., and Cubeddu, L. X. (1986). Effects of d-amphetamine and dopamine synthesis inhibitors on dopamine and acetylcholine neurotransmission in the striatum. II. Release in the presence of vesicular transmitter stores. J Pharmacol Exp Ther *237*, 193-203.

Parker, E. M., and Cubeddu, L. X. (1988). Comparative effects of amphetamine, phenylethylamine and related drugs on dopamine efflux, dopamine uptake and mazindol binding. J Pharmacol Exp Ther *245*, 199-210.

Parker, M. J., Beck, A., and Luetje, C. W. (1998). Neuronal nicotinic receptor beta2 and beta4 subunits confer large differences in agonist binding affinity. Mol Pharmacol *54*, 1132-1139.

Parsons, L. H., and Justice, J. B., Jr. (1993). Perfusate serotonin increases extracellular dopamine in the nucleus accumbens as measured by in vivo microdialysis. Brain Res *606*, 195-199.

Parsons, S. M. (2000). Transport mechanisms in acetylcholine and monoamine storage. FASEB J *14*, 2423-2434.

Partilla, J. S., Dempsey, A. G., Nagpal, A. S., Blough, B. E., Baumann, M. H., and Rothman, R. B. (2006). Interaction of amphetamines and related compounds at the vesicular monoamine transporter. J Pharmacol Exp Ther *319*, 237-246.

Pasinetti, G. M., Morgan, D. G., Johnson, S. A., Millar, S. L., and Finch, C. E. (1990). Tyrosine hydroxylase mRNA concentration in midbrain dopaminergic neurons is differentially regulated by reserpine. J Neurochem *55*, 1793-1799.

Paterson, S. J., Robson, L. E., and Kosterlitz, H. W. (1983). Classification of opioid receptors. Br Med Bull *39*, 31-36.

Perez-Reyes, M., White, W. R., McDonald, S. A., Hicks, R. E., Jeffcoat, A. R., Hill, J. M., and Cook, C. E. (1991a). Clinical effects of daily methamphetamine administration. Clin Neuropharmacol *14*, 352-358.

Perez-Reyes, M., White, W. R., McDonald, S. A., Hill, J. M., Jeffcoat, A. R., and Cook, C. E. (1991b). Clinical effects of methamphetamine vapor inhalation. Life Sci *49*, 953-959.

Peter, D., Jimenez, J., Liu, Y., Kim, J., and Edwards, R. H. (1994). The chromaffin granule and synaptic vesicle amine transporters differ in substrate recognition and sensitivity to inhibitors. J Biol Chem *269*, 7231-7237.

Peter, D., Liu, Y., Sternini, C., de Giorgio, R., Brecha, N., and Edwards, R. H. (1995). Differential expression of two vesicular monoamine transporters. J Neurosci *15*, 6179-6188.

Pierce, R. C., and Kumaresan, V. (2006). The mesolimbic dopamine system: the final common pathway for the reinforcing effect of drugs of abuse? Neuroscience and biobehavioral reviews *30*, 215-238.
Pifl, C., Drobny, H., Reither, H., Hornykiewicz, O., and Singer, E. A. (1995). Mechanism of the dopamine-releasing actions of amphetamine and cocaine: plasmalemmal dopamine transporter versus vesicular monoamine transporter. Mol Pharmacol *47*, 368-373.
Pivavarchyk, M., Smith, A. M., Zhang, Z., Zhou, D., Wang, X., Toyooka, N., Tsuneki, H., Sasaoka, T., McIntosh, J. M., Crooks, P. A., and Dwoskin, L. P. (2011). Indolizidine (-)-235B' and related structural analogs: discovery of nicotinic receptor antagonists that inhibit nicotine-evoked [3H]dopamine release. Eur J Pharmacol *658*, 132-139.
Pothos, E. N., Mosharov, E., Liu, K. P., Setlik, W., Haburcak, M., Baldini, G., Gershon, M. D., Tamir, H., and Sulzer, D. (2002). Stimulation-dependent regulation of the pH, volume and quantal size of bovine and rodent secretory vesicles. J Physiol *542*, 453-476.
Prinzmetal, M., Bloomberg, W. (1935). The use of benzedrine for treatment of narcolepsy. JAMA *105*, 2051–2054.
Pulvirenti, L., Balducci, C., Piercy, M., and Koob, G. F. (1998). Characterization of the effects of the partial dopamine agonist terguride on cocaine self-administration in the rat. J Pharmacol Exp Ther *286*, 1231-1238.
Quinton, M. S., and Yamamoto, B. K. (2006). Causes and consequences of methamphetamine and MDMA toxicity. AAPS J *8*, E337-347.
Raiteri, M., Cerrito, F., Cervoni, A. M., and Levi, G. (1979). Dopamine can be released by two mechanisms differentially affected by the dopamine transport inhibitor nomifensine. J Pharmacol Exp Ther *208*, 195-202.
Rauhut, A. S., Neugebauer, N., Dwoskin, L. P., and Bardo, M. T. (2003). Effect of bupropion on nicotine self-administration in rats. Psychopharmacology (Berl) *169*, 1-9.
Rawson, R. A., Marinelli-Casey, P., Anglin, M. D., Dickow, A., Frazier, Y., Gallagher, C., Galloway, G. P., Herrell, J., Huber, A., McCann, M. J.*, et al.* (2004). A multi-site comparison of psychosocial approaches for the treatment of methamphetamine dependence. Addiction *99*, 708-717.
Reith, M. E., and Coffey, L. L. (1994). Structure-activity relationships for cocaine congeners in inhibiting dopamine uptake into rat brain synaptic vesicles and bovine chromaffin granule ghosts. J Pharmacol Exp Ther *271*, 1444-1452.
Ricaurte, G. A., Schuster, C. R., and Seiden, L. S. (1980). Long-term effects of repeated methylamphetamine administration on dopamine and serotonin neurons in the rat brain: a regional study. Brain Res *193*, 153-163.
Richards, D. A., Guatimosim, C., Rizzoli, S. O., and Betz, W. J. (2003). Synaptic vesicle pools at the frog neuromuscular junction. Neuron *39*, 529-541.
Richards, J. B., Sabol, K. E., and de Wit, H. (1999). Effects of methamphetamine on the adjusting amount procedure, a model of impulsive behavior in rats. Psychopharmacology (Berl) *146*, 432-439.

Riddle, E. L., Topham, M. K., Haycock, J. W., Hanson, G. R., and Fleckenstein, A. E. (2002). Differential trafficking of the vesicular monoamine transporter-2 by methamphetamine and cocaine. Eur J Pharmacol *449*, 71-74.

Rizzoli, S. O., and Betz, W. J. (2005). Synaptic vesicle pools. Nat Rev Neurosci *6*, 57-69.

Robertson, G. S., and Robertson, H. A. (1989). Evidence that L-dopa-induced rotational behavior is dependent on both striatal and nigral mechanisms. J Neurosci *9*, 3326-3331.

Robinson, J. B. (1985). Stereoselectivity and isoenzyme selectivity of monoamine oxidase inhibitors. Enantiomers of amphetamine, N-methylamphetamine and deprenyl. Biochem Pharmacol *34*, 4105-4108.

Romano, C., and Goldstein, A. (1980). Stereospecific nicotine receptors on rat brain membranes. Science *210*, 647-650.

Ronen, T. (2004). Cognitive-Behavioral Therapy with Children and Families, chapter 4in Dorfman, R., Meyer, P., & Morgan, M. (2004).

Ross, S. B., and Renyi, A. L. (1964). Blocking Action of Sympathomimetic Amines on the Uptake of Tritiated Noradrenaline by Mouse Cerebral Cortex Tissues in Vitro. Acta pharmacologica et toxicologica *21*, 226-239.

Ross, S. B., and Renyi, A. L. (1966). In vitro inhibition of noradrenaline-3H uptake by reserpine and tetrabenazine in mouse cerebral cortex tissues. Acta pharmacologica et toxicologica *24*, 73-88.

Rothman, R. B., and Baumann, M. H. (2003). Monoamine transporters and psychostimulant drugs. Eur J Pharmacol *479*, 23-40.

Rudnick, G. (2006). Structure/function relationships in serotonin transporter: new insights from the structure of a bacterial transporter. Handb Exp Pharmacol, 59-73.

Rudnick, G., Steiner-Mordoch, S. S., Fishkes, H., Stern-Bach, Y., and Schuldiner, S. (1990). Energetics of reserpine binding and occlusion by the chromaffin granule biogenic amine transporter. Biochemistry *29*, 603-608.

Ruf, M., Lovitt, C., and Imrie, J. (2006). Recreational drug use and sexual risk practice among men who have sex with men in the United Kingdom. Sex Transm Infect *82*, 95-97.

Sager, J. J., and Torres, G. E. (2011). Proteins interacting with monoamine transporters: current state and future challenges. Biochemistry *50*, 7295-7310.

Sai, Y., Wu, Q., Le, W., Ye, F., Li, Y., and Dong, Z. (2008). Rotenone-induced PC12 cell toxicity is caused by oxidative stress resulting from altered dopamine metabolism. Toxicology in vitro : an international journal published in association with BIBRA *22*, 1461-1468.

Sanguinetti, M. C., Jiang, C., Curran, M. E., and Keating, M. T. (1995). A mechanistic link between an inherited and an acquired cardiac arrhythmia: HERG encodes the IKr potassium channel. Cell *81*, 299-307.

Sattar, S. P., Bhatia, S. C., and Petty, F. (2004). Potential benefits of quetiapine in the treatment of substance dependence disorders. J Psychiatry Neurosci *29*, 452-457.
Sattler, R., and Tymianski, M. (2000). Molecular mechanisms of calcium-dependent excitotoxicity. Journal of molecular medicine *78*, 3-13.
Schechter, M. D., and Rosecrans, J. A. (1972). Nicotine as a discriminative cue in rats: inability of related drugs to produce a nicotine-like cueing effect. Psychopharmacologia *27*, 379-387.
Schep, L. J., Slaughter, R. J., and Beasley, D. M. (2010). The clinical toxicology of metamfetamine. Clin Toxicol (Phila) *48*, 675-694.
Scherman, D., and Henry, J. P. (1984). Reserpine binding to bovine chromaffin granule membranes. Characterization and comparison with dihydrotetrabenazine binding. Mol Pharmacol *25*, 113-122.
Schmidt, H. H., Hofmann, H., Schindler, U., Shutenko, Z. S., Cunningham, D. D., and Feelisch, M. (1996). No .NO from NO synthase. Proc Natl Acad Sci U S A *93*, 14492-14497.
Schoffelmeer, A. N., De Vries, T. J., Wardeh, G., van de Ven, H. W., and Vanderschuren, L. J. (2002). Psychostimulant-induced behavioral sensitization depends on nicotinic receptor activation. J Neurosci *22*, 3269-3276.
Seiden, L. S., Sabol, K. E., and Ricaurte, G. A. (1993). Amphetamine: effects on catecholamine systems and behavior. Annu Rev Pharmacol Toxicol *33*, 639-677.
Seminerio, M. J., Hansen, R., Kaushal, N., Zhang, H. T., McCurdy, C. R., and Matsumoto, R. R. (2013). The evaluation of AZ66, an optimized sigma receptor antagonist, against methamphetamine-induced dopaminergic neurotoxicity and memory impairment in mice. Int J Neuropsychopharmacol *16*, 1033-1044.
Seminerio, M. J., Robson, M. J., Abdelazeem, A. H., Mesangeau, C., Jamalapuram, S., Avery, B. A., McCurdy, C. R., and Matsumoto, R. R. (2012). Synthesis and pharmacological characterization of a novel sigma receptor ligand with improved metabolic stability and antagonistic effects against methamphetamine. AAPS J *14*, 43-51.
Shirvan, A., Laskar, O., Steiner-Mordoch, S., and Schuldiner, S. (1994). Histidine-419 plays a role in energy coupling in the vesicular monoamine transporter from rat. FEBS Lett *356*, 145-150.
Shoblock, J. R., Maisonneuve, I. M., and Glick, S. D. (2003a). Differences between d-methamphetamine and d-amphetamine in rats: working memory, tolerance, and extinction. Psychopharmacology (Berl) *170*, 150-156.
Shoblock, J. R., Sullivan, E. B., Maisonneuve, I. M., and Glick, S. D. (2003b). Neurochemical and behavioral differences between d-methamphetamine and d-amphetamine in rats. Psychopharmacology (Berl) *165*, 359-369.
Shoptaw, S., Heinzerling, K. G., Rotheram-Fuller, E., Steward, T., Wang, J., Swanson, A. N., De La Garza, R., Newton, T., and Ling, W. (2008).

Randomized, placebo-controlled trial of bupropion for the treatment of methamphetamine dependence. Drug Alcohol Depend *96*, 222-232.
Shoptaw, S., Huber, A., Peck, J., Yang, X., Liu, J., Jeff, D., Roll, J., Shapiro, B., Rotheram-Fuller, E., and Ling, W. (2006a). Randomized, placebo-controlled trial of sertraline and contingency management for the treatment of methamphetamine dependence. Drug Alcohol Depend *85*, 12-18.
Shoptaw, S., Klausner, J. D., Reback, C. J., Tierney, S., Stansell, J., Hare, C. B., Gibson, S., Siever, M., King, W. D., Kao, U., and Dang, J. (2006b). A public health response to the methamphetamine epidemic: the implementation of contingency management to treat methamphetamine dependence. BMC Public Health *6*, 214.
Sievert, M. K., and Ruoho, A. E. (1997). Peptide mapping of the [125I]Iodoazidoketanserin and [125I]2-N-[(3'-iodo-4'-azidophenyl)propionyl]tetrabenazine binding sites for the synaptic vesicle monoamine transporter. J Biol Chem *272*, 26049-26055.
Simon, H., Scatton, B., and Moal, M. L. (1980). Dopaminergic A10 neurones are involved in cognitive functions. Nature *286*, 150-151.
Skau, K. A., and Gerald, M. C. (1978). Inhibition of alpha-bungarotoxin binding to rat and mouse diaphragms by amphetamine and related nonquaternary compounds. J Pharmacol Exp Ther *205*, 69-76.
Slotkin, T. A., Seidler, F. J., Whitmore, W. L., Lau, C., Salvaggio, M., and Kirksey, D. F. (1978). Rat brain synaptic vesicles: uptake specificities of [3H]norepinephrine and [3H]serotonin in preparations from whole brain and brain regions. J Neurochem *31*, 961-968.
Smith, A. M., Dhawan, G. K., Zhang, Z., Siripurapu, K. B., Crooks, P. A., and Dwoskin, L. P. (2009). The novel nicotinic receptor antagonist, N,N'-dodecane-1,12-diyl-bis-3-picolinium dibromide (bPiDDB), inhibits nicotine-evoked [(3)H]norepinephrine overflow from rat hippocampal slices. Biochem Pharmacol *78*, 889-897.
Smith, A. M., Pivavarchyk, M., Wooters, T. E., Zhang, Z., Zheng, G., McIntosh, J. M., Crooks, P. A., Bardo, M. T., and Dwoskin, L. P. (2010). Repeated nicotine administration robustly increases bPiDDB inhibitory potency at alpha6beta2-containing nicotinic receptors mediating nicotine-evoked dopamine release. Biochem Pharmacol *80*, 402-409.
Snyder, S. H. (1986). Drugs and the Brain. Scientific American Books, 130-131.
Snyders, D. J., and Chaudhary, A. (1996). High affinity open channel block by dofetilide of HERG expressed in a human cell line. Mol Pharmacol *49*, 949-955.
Sofuoglu, M. (2010). Cognitive enhancement as a pharmacotherapy target for stimulant addiction. Addiction *105*, 38-48.
Sofuoglu, M., DeVito, E. E., Waters, A. J., and Carroll, K. M. (2013). Cognitive enhancement as a treatment for drug addictions. Neuropharmacology *64*, 452-463.
Sokoloff, P., and Schwartz, J. C. (1995). Novel dopamine receptors half a decade later. Trends Pharmacol Sci *16*, 270-275.

Sonders, M. S., and Amara, S. G. (1996). Channels in transporters. Curr Opin Neurobiol *6*, 294-302.
Sonders, M. S., Zhu, S. J., Zahniser, N. R., Kavanaugh, M. P., and Amara, S. G. (1997). Multiple ionic conductances of the human dopamine transporter: the actions of dopamine and psychostimulants. J Neurosci *17*, 960-974.
Stall, R. D., Hays, R. B., Waldo, C. R., Ekstrand, M., and McFarland, W. (2000). The Gay '90s: a review of research in the 1990s on sexual behavior and HIV risk among men who have sex with men. AIDS *14 Suppl 3*, S101-114.
Statistics, M. I. N. (2009). The METH Project.
Stead, L. F., and Hughes, J. R. (2012). Lobeline for smoking cessation. Cochrane Database Syst Rev *2*, CD000124.
Steiner-Mordoch, S., Shirvan, A., and Schuldiner, S. (1996). Modification of the pH profile and tetrabenazine sensitivity of rat VMAT1 by replacement of aspartate 404 with glutamate. J Biol Chem *271*, 13048-13054.
Stephans, S. E., and Yamamoto, B. K. (1994). Methamphetamine-induced neurotoxicity: roles for glutamate and dopamine efflux. Synapse *17*, 203-209.
Sulzer, D., Chen, T. K., Lau, Y. Y., Kristensen, H., Rayport, S., and Ewing, A. (1995). Amphetamine redistributes dopamine from synaptic vesicles to the cytosol and promotes reverse transport. J Neurosci *15*, 4102-4108.
Sulzer, D., Maidment, N. T., and Rayport, S. (1993). Amphetamine and other weak bases act to promote reverse transport of dopamine in ventral midbrain neurons. J Neurochem *60*, 527-535.
Sulzer, D., and Pothos, E. N. (2000). Regulation of quantal size by presynaptic mechanisms. Rev Neurosci *11*, 159-212.
Sulzer, D., and Rayport, S. (1990). Amphetamine and other psychostimulants reduce pH gradients in midbrain dopaminergic neurons and chromaffin granules: a mechanism of action. Neuron *5*, 797-808.
Sulzer, D., Sonders, M. S., Poulsen, N. W., and Galli, A. (2005). Mechanisms of neurotransmitter release by amphetamines: a review. Prog Neurobiol *75*, 406-433.
Sulzer, D., St Remy, C., and Rayport, S. (1996). Reserpine inhibits amphetamine action in ventral midbrain culture. Mol Pharmacol *49*, 338-342.
Sweeney, C. T., Sembower, M. A., Ertischek, M. D., Shiffman, S., and Schnoll, S. H. (2013). Nonmedical use of prescription ADHD stimulants and preexisting patterns of drug abuse. J Addict Dis *32*, 1-10.
Tabet, N. (2006). Acetylcholinesterase inhibitors for Alzheimer's disease: anti-inflammatories in acetylcholine clothing! Age Ageing *35*, 336-338.
Takahashi, N., Miner, L. L., Sora, I., Ujike, H., Revay, R. S., Kostic, V., Jackson-Lewis, V., Przedborski, S., and Uhl, G. R. (1997). VMAT2 knockout mice: heterozygotes display reduced amphetamine-conditioned reward, enhanced amphetamine locomotion, and enhanced MPTP toxicity. Proc Natl Acad Sci U S A *94*, 9938-9943.
Takamatsu, Y., Yamamoto, H., Ogai, Y., Hagino, Y., Markou, A., and Ikeda, K. (2006). Fluoxetine as a potential pharmacotherapy for methamphetamine dependence: studies in mice. Ann N Y Acad Sci *1074*, 295-302.

Tamargo, J. (2000). Drug-induced torsade de pointes: from molecular biology to bedside. Japanese journal of pharmacology *83*, 1-19.

Tanda, G., Newman, A. H., and Katz, J. L. (2009). Discovery of drugs to treat cocaine dependence: behavioral and neurochemical effects of atypical dopamine transport inhibitors. Adv Pharmacol *57*, 253-289.

Tate, C. G., and Blakely, R. D. (1994). The effect of N-linked glycosylation on activity of the Na(+)- and Cl(-)-dependent serotonin transporter expressed using recombinant baculovirus in insect cells. J Biol Chem *269*, 26303-26310.

Teng, L., Crooks, P. A., and Dwoskin, L. P. (1998). Lobeline displaces [3H]dihydrotetrabenazine binding and releases [3H]dopamine from rat striatal synaptic vesicles: comparison with d-amphetamine. J Neurochem *71*, 258-265.

Teng, L., Crooks, P. A., Sonsalla, P. K., and Dwoskin, L. P. (1997). Lobeline and nicotine evoke [3H]overflow from rat striatal slices preloaded with [3H]dopamine: differential inhibition of synaptosomal and vesicular [3H]dopamine uptake. J Pharmacol Exp Ther *280*, 1432-1444.

Teschemacher, A. G., Seward, E. P., Hancox, J. C., and Witchel, H. J. (1999). Inhibition of the current of heterologously expressed HERG potassium channels by imipramine and amitriptyline. Br J Pharmacol *128*, 479-485.

Tetko, I. V., Gasteiger, J., Todeschini, R., Mauri, A., Livingstone, D., Ertl, P., Palyulin, V. A., Radchenko, E. V., Zefirov, N. S., Makarenko, A. S.*, et al.* (2005). Virtual computational chemistry laboratory--design and description. Journal of computer-aided molecular design *19*, 453-463.

Tidey, J. W., O'Neill, S. C., and Higgins, S. T. (2000). d-amphetamine increases choice of cigarette smoking over monetary reinforcement. Psychopharmacology (Berl) *153*, 85-92.

Tiihonen, J., Kuoppasalmi, K., Fohr, J., Tuomola, P., Kuikanmaki, O., Vorma, H., Sokero, P., Haukka, J., and Meririnne, E. (2007). A comparison of aripiprazole, methylphenidate, and placebo for amphetamine dependence. Am J Psychiatry *164*, 160-162.

Torres, G. E., Carneiro, A., Seamans, K., Fiorentini, C., Sweeney, A., Yao, W. D., and Caron, M. G. (2003a). Oligomerization and trafficking of the human dopamine transporter. Mutational analysis identifies critical domains important for the functional expression of the transporter. J Biol Chem *278*, 2731-2739.

Torres, G. E., Gainetdinov, R. R., and Caron, M. G. (2003b). Plasma membrane monoamine transporters: structure, regulation and function. Nat Rev Neurosci *4*, 13-25.

Trudeau, M. C., Warmke, J. W., Ganetzky, B., and Robertson, G. A. (1995). HERG, a human inward rectifier in the voltage-gated potassium channel family. Science *269*, 92-95.

Trujillo, K. A., Belluzzi, J. D., and Stein, L. (1991). Naloxone blockade of amphetamine place preference conditioning. Psychopharmacology (Berl) *104*, 265-274.

Varanda, W. A., Aracava, Y., Sherby, S. M., VanMeter, W. G., Eldefrawi, M. E., and Albuquerque, E. X. (1985). The acetylcholine receptor of the neuromuscular junction recognizes mecamylamine as a noncompetitive antagonist. Mol Pharmacol *28*, 128-137.

Vaughan, R. A., Huff, R. A., Uhl, G. R., and Kuhar, M. J. (1997). Protein kinase C-mediated phosphorylation and functional regulation of dopamine transporters in striatal synaptosomes. J Biol Chem *272*, 15541-15546.

Volz, T. J., Farnsworth, S. J., King, J. L., Riddle, E. L., Hanson, G. R., and Fleckenstein, A. E. (2007). Methylphenidate administration alters vesicular monoamine transporter-2 function in cytoplasmic and membrane-associated vesicles. J Pharmacol Exp Ther *323*, 738-745.

Von Bohlen und Halbach, O., and Dermietzel, R. (2002). Neurotransmitters and Neuromodulators: Handbook of Receptors and Biological Effects. pp: 53-63).

Wachtel, S. R., Ortengren, A., and de Wit, H. (2002). The effects of acute haloperidol or risperidone on subjective responses to methamphetamine in healthy volunteers. Drug Alcohol Depend *68*, 23-33.

Wagner, G. C., Ricaurte, G. A., Seiden, L. S., Schuster, C. R., Miller, R. J., and Westley, J. (1980). Long-lasting depletions of striatal dopamine and loss of dopamine uptake sites following repeated administration of methamphetamine. Brain Res *181*, 151-160.

Wang, Y. M., Gainetdinov, R. R., Fumagalli, F., Xu, F., Jones, S. R., Bock, C. B., Miller, G. W., Wightman, R. M., and Caron, M. G. (1997). Knockout of the vesicular monoamine transporter 2 gene results in neonatal death and supersensitivity to cocaine and amphetamine. Neuron *19*, 1285-1296.

White, R. (2000). Dexamphetamine substitution in the treatment of amphetamine abuse: an initial investigation. Addiction *95*, 229-238.

Williams, B. R., Nazarians, A., and Gill, M. A. (2003). A review of rivastigmine: a reversible cholinesterase inhibitor. Clin Ther *25*, 1634-1653.

Wimalasena, D. S., and Wimalasena, K. (2004). Kinetic evidence for channeling of dopamine between monoamine transporter and membranous dopamine-beta-monooxygenase in chromaffin granule ghosts. J Biol Chem *279*, 15298-15304.

Wimalasena, K. (2011). Vesicular monoamine transporters: structure-function, pharmacology, and medicinal chemistry. Med Res Rev *31*, 483-519.

Wise, R. A. (1978). Catecholamine theories of reward: a critical review. Brain Res *152*, 215-247.

Wise, R. A. (2009). Roles for nigrostriatal--not just mesocorticolimbic--dopamine in reward and addiction. Trends in neurosciences *32*, 517-524.

Woody, G. E. (2003). Research findings on psychotherapy of addictive disorders. Am J Addict *12 Suppl 2*, S19-26.

Woolverton, W. L., Ricaurte, G. A., Forno, L. S., and Seiden, L. S. (1989). Long-term effects of chronic methamphetamine administration in rhesus monkeys. Brain Res *486*, 73-78.

Xi, Z. X., Gilbert, J. G., Pak, A. C., Ashby, C. R., Jr., Heidbreder, C. A., and Gardner, E. L. (2005). Selective dopamine D3 receptor antagonism by SB-

277011A attenuates cocaine reinforcement as assessed by progressive-ratio and variable-cost-variable-payoff fixed-ratio cocaine self-administration in rats. Eur J Neurosci *21*, 3427-3438.

Xu, Y. T., Robson, M. J., Szeszel-Fedorowicz, W., Patel, D., Rooney, R., McCurdy, C. R., and Matsumoto, R. R. (2012). CM156, a sigma receptor ligand, reverses cocaine-induced place conditioning and transcriptional responses in the brain. Pharmacol Biochem Behav *101*, 174-180.

Yakel, J. L. (2013). Cholinergic receptors: functional role of nicotinic ACh receptors in brain circuits and disease. Pflugers Arch *465*, 441-450.

Yamada, S., Isogai, M., Kagawa, Y., Takayanagi, N., Hayashi, E., Tsuji, K., and Kosuge, T. (1985). Brain nicotinic acetylcholine receptors. Biochemical characterization by neosurugatoxin. Mol Pharmacol *28*, 120-127.

Yamamoto, B. K., Moszczynska, A., and Gudelsky, G. A. (2010). Amphetamine toxicities: classical and emerging mechanisms. Ann N Y Acad Sci *1187*, 101-121.

Yamashita, A., Singh, S. K., Kawate, T., Jin, Y., and Gouaux, E. (2005). Crystal structure of a bacterial homologue of Na+/Cl--dependent neurotransmitter transporters. Nature *437*, 215-223.

Yelin, R., and Schuldiner, S. (2002). Vesicular neurotransmitter transporters: Pharmacology, Biochemistry and Molecular Analysis. In: Reith MEA, editor Neurotransmitter Transporters: Structure, Function, and Regulation Totowa, NJ: Humana Press; , 313–354.

Yelin, R., Steiner-Mordoch, S., Aroeti, B., and Schuldiner, S. (1998). Glycosylation of a vesicular monoamine transporter: a mutation in a conserved proline residue affects the activity, glycosylation, and localization of the transporter. J Neurochem *71*, 2518-2527.

Zaczek, R., Culp, S., and De Souza, E. B. (1991). Interactions of [3H]amphetamine with rat brain synaptosomes. II. Active transport. J Pharmacol Exp Ther *257*, 830-835.

Zapata, A., Kivell, B., Han, Y., Javitch, J. A., Bolan, E. A., Kuraguntla, D., Jaligam, V., Oz, M., Jayanthi, L. D., Samuvel, D. J.*, et al.* (2007). Regulation of dopamine transporter function and cell surface expression by D3 dopamine receptors. J Biol Chem *282*, 35842-35854.

Zetterstrom, T., Sharp, T., Collin, A. K., and Ungerstedt, U. (1988). In vivo measurement of extracellular dopamine and DOPAC in rat striatum after various dopamine-releasing drugs; implications for the origin of extracellular DOPAC. Eur J Pharmacol *148*, 327-334.

Zheng, F., Zheng, G., Deaciuc, A. G., Zhan, C. G., Dwoskin, L. P., and Crooks, P. A. (2007). Computational neural network analysis of the affinity of lobeline and tetrabenazine analogs for the vesicular monoamine transporter-2. Bioorg Med Chem *15*, 2975-2992.

Zheng, G., Dwoskin, L. P., and Crooks, P. A. (2006). Vesicular monoamine transporter 2: role as a novel target for drug development. AAPS J *8*, E682-692.

Zheng, G., Dwoskin, L. P., Deaciuc, A. G., and Crooks, P. A. (2008). Synthesis and evaluation of a series of homologues of lobelane at the vesicular monoamine transporter-2. Bioorg Med Chem Lett *18*, 6509-6512.
Zhou, J. (2004). Norepinephrine transporter inhibitors and their therapeutic potential. Drugs Future *29*, 1235-1244.

VITA

Zheng Cao

Current Position

Doctoral Candidate in the Department of Pharmaceutical Sciences
College of Pharmacy
University of Kentucky
Lexington, KY 40536

Education

2007-2014	Graduate student, College of Pharmacy, University of Kentucky
	Advisor: Dr. Linda P. Dwoskin
2002-2007	B.S., Shenyang Pharmaceutical University, Shenyang, P.R. China

Honors and Awards

Fall 2011	University of Kentucky Student Travel Support
Fall 2012	University of Kentucky Student Travel Support

Memberships in Professional Organizations

Member of the American Association of Pharmaceutical Scientists (AAPS)
Member of the Society for Neuroscience (SfN)
Member of Bluegrass Chapter- SfN

Published Abstract/Presentation

1. **Cao Z.**, Zheng G., Deaciuc A. G., Crooks P. A., Dwoskin L. P. Lobelane analogs interact with vesicular monoamine transporter-2 to inhibit the effect of methamphetamine. *Bluegrass Chapter of the Society for Neuroscience-Spring Neuroscience Day. 2013*.
2. **Cao Z.**, Zheng G., Deaciuc A. G., Crooks P. A., Dwoskin L. P. Lobelane analogs interact with vesicular monoamine transporter-2 to inhibit the effect of methamphetamine. *Society for Neuroscience. 2012.*
3. **Cao Z.**, Zheng G., Nickell, J. R., Deaciuc A. G., Crooks P. A., Dwoskin L. P. Acyclic lobelane analogs as potential pharmacotherapies for methamphetamine abuse. *University of Kentucky, College of Pharmacy, Annual Symposium on Drug Discovery and Development. 2012.*
4. **Cao Z.**, Zheng G., Horton D. B., Deaciuc A. G., Crooks P. A., Dwoskin L. P. Acyclic lobelane analogs as novel inhibitors of vesicular monoamine transporter-2 function. *The Center for Clinical and Translational Science 7th Annual Spring Conference. 2012.*

5. **Cao Z.**, Zheng G., Horton D. B., Deaciuc A. G., Crooks P. A., Dwoskin L. P. Acyclic lobelane analogs as novel inhibitors of vesicular monoamine transporter-2 function. *Society for Neuroscience. 2011.*
6. **Cao Z.**, Zheng G., Horton D. B., Deaciuc A. G., Crooks P. A., Dwoskin L. P. Acyclic lobelane analogs as novel inhibitors of vesicular monoamine transporter-2. *Bluegrass Chapter of the Society for Neuroscience-Spring Neuroscience Day. 2011*.
7. **Cao Z.**, Zheng G., Horton D. B., Deaciuc A. G., Crooks P. A., Dwoskin L. P. Acyclic lobelane analogs as novel inhibitors of vesicular monoamine transporter-2. *The Center for Clinical and Translational Science 6th Annual Spring Conference. 2011.*
8. Danford E., **Cao Z**., Nickell J. R., Siripurapu K. B., Zheng G., Crooks P. A., Dwoskin L. P. Acyclic lobelane analogs as new therapeutics for methamphetamine addiction. *University of Kentucky, July 2010.*
9. **Cao Z.**, Zheng G., Deaciuc A. G., Crooks P. A., and Dwoskin L. P. Acyclic lobelane analogs as novel ligands for the vesicular monoamine transporter-2. *Pharmaceutics Graduate Student Research Meeting. 2010.*
10. **Cao Z.**, Zheng G., Deaciuc A. G., Crooks P. A., Dwoskin L. P. Lobelane analogs with varying methylene linker lengths as novel ligands for the vesicular monoamine transproter-2. *Bluegrass Chapter of the Society for Neuroscience-Spring Neuroscience Day. 2009*;
11. **Cao Z.**, Zheng G., Deaciuc A. G., Crooks P. A., Dwoskin L. P. Lobelane analogs with varying methylene linker lengths as novel ligands for the vesicular monoamine transproter-2. *Pharmaceutics Graduate Student Research Meeting. 2009.*

Manuscript in progress

1. **Cao Z.**, Zheng G., Nickell J. R., Crooks P. A., Dwoskin L. P. Lobelane analogs with varying methylene linker lengths as novel ligands for vesicular monoamine transporter-2. To be submitted to *J Pharmacol Exp Ther.*
2. **Cao Z.**, Zheng G., Nickell J. R., Siripurapu K. B., Smith A. M., Horton D. B., Deaciuc A. G., Crooks P. A., Dwoskin L. P. Acyclic lobelane analogs inhibit vesicular monoamine transporter-2 function and methamphetamine-evoked dopamine release. To be submitted to *J Pharmacol Exp Ther.*